The mononuclear phagocyte system in Graft-versus-Host-Disease

Laura Jardine

Submitted in partial fulfillment of the requirements for the degree of Doctor of Philosophy

Institute of Cellular Medicine
Newcastle University
UK

April 2016

Dedication

For patients at the Northern Centre for Cancer Care

Abstract: The mononuclear phagocyte system in Graft-versus-Host-Disease

The human mononuclear phagocyte system of monocytes, macrophages and dendritic cells participates in both innate and adaptive immune responses. However, the accurate identities, functions and inter-relationships of these crucial immune cells during inflammation are poorly defined. Two inflammatory settings were examined in this work: the skin in acute Graft-versus-Host Disease and the lung during experimental inflammation induced by LPS inhalation. The purpose of this enquiry was to characterize inflammatory mononuclear phagocytes in tissue, investigate their origins and explore their contribution to disease pathogenesis.

In the skin GvHD study, shave biopsies were obtained from 73 individuals on presentation with acute rash following bone marrow transplantation (BMT). Controls were obtained from 19 BMT recipients at matched time points without rash and 26 healthy individuals undergoing plastic surgery. Tissue was digested and the leukocyte composition analysed by flow cytometry/ sorting. Sorted populations were used in functional assays or in gene expression experiments performed using NanoString technology. An *in vitro* equivalent of CD14-expressing mononuclear phagocytes (MPs) was developed using HLA-matched mixed leukocyte reactions. Gene expression was measured and the function of these equivalents in a skin explant model of GvHD was tested. GvHD lesional skin was characterized by expansion of CD14-expressing MPs (GVH14) and a reduction in CD1c-expressing MPs. GVH14 were identified as donor monocyte-derived macrophages. Functionally, GVH14 could produce chemokines to recruit T lymphocytes to lesions. They were capable of activating and expanding T lymphocytes *in vitro*. GVH14 equivalents could damage basal keratinocytes of the epidermis without the presence of T cells. This characterization has identified a novel pathogeneic role for macrophages in acute GvHD.

In the LPS inhalation study, 13 healthy individuals received saline (0.9% sodium chloride) and 13 received LPS (0.9% sodium chloride with 2mg LPS from *E.coli* 026:B6) by dosimeter nebulizer. Blood samples were obtained at 2, 4, 6 and 24 hours following inhalation. Between 7 and 8 hours post-inhalation, bronchoalveolar

lavage (BAL) of a sub-segment of the right middle lobe was performed. BAL fluid supernatant chemokines and cytokines were analysed by multiplexed ELISA. The cellular component of BAL was analysed by flow cytometry/ sorting. Sorted populations were used in functional assays or in gene expression experiments performed using NanoString technology. Seven distinct MPs were identified in steady state (i.e. following saline inhalation). Following LPS inhalation, neutrophils, CD14-expressing MPs and CD1c-expressing MPs were expanded. Phenotypically, CD1c expressing MPs resembled blood cDC2. Both subsets of blood cDC2 were recruited to the airspace but their distinct functions and gene expression profiles converged upon recruitment. This analysis provides the first detailed characterization of BAL fluid MPs. As such it provides a foundation for studying MPs in human lung diseases, including the Idiopathic Pneumonia Syndrome occurring after BMT. It detailed the surprising observation that blood cDC2 can be recruited to tissue in inflammation, challenging the dogma that inflammatory MPs must be monocyte-derived.

Acknowledgements

This work was supported by a Wellcome Trust Clinical Research Training Fellowship (WT097941).

First, I would like to acknowledge those who have contributed data for analysis in this thesis: Rachel Dickinson, Kile Green and Gary Reynolds for NanoString data and Merry Gunawan for flow cytometry data.

None of this work would have been possible without a well-equipped and well-managed flow cytometry core facility. Andy Filby and Ian Dimmick deserve credit for this. For their wisdom, patience and good company during the pursuit of flow cytometry data, I thank David MacDonald and Andrew Fuller. The microscopy core facility run by Alex Laude has been valuable. Trevor Booth and Xiao Nong Wang deserve thanks for their microscopy assistance. Assistance with NanoString experiments was expertly given by Kile Green. Martin Howell kindly provided access to a Luminex instrument.

For the skin GvHD project, sincere thanks are given to the patients who provide samples for research during a challenging time in their lives. GvHD research would not be possible without the thriving BMT programme run by Matthew Collin and supported by Graham Jackson, Venetia Bigley, Erin Hurst, Smeera Nair, Arian Lawrence, Steven Fox, Susan Paskar and Sue Munro. Thanks are given to Smeera Nair, Erin Hurst and Amy Publicover for performing skin biopsies and to Tara Shrestha for maintaining the flow of samples across the city.

Running Group 4 of the LPS inhalation study was an introduction to the challenges of experimental medicine. Sarah Wiscombe deserves much credit for establishing the ethical approvals for this study, maintaining an enviable standard of organization and being so amenable to sharing samples. Ian Forrest and the RVI endoscopy suite were instrumental to acquiring BAL samples. Considering the pressure of clinical demands, their efforts to help with this study were particularly valued. The Clinical Research Facility, the volunteers and the principal investigator, John Simpson, were

vital to the success of this work. I would like to thank Andy Filby for sparing his own time to provide flow cytometry assistance out-of-hours on this project.

I would like to thank members of the Human Dendritic Cell Lab past and present- with a particular mention for Sarah Pagan, Venetia Bigley and Naomi McGovern- for passing on vital practical skills.

Matthew Collin deserves thanks for allowing me into his lab as a naïve recent-graduate and providing both freedom and opportunity to learn about science. Muzz Haniffa requires thanks for support and encouragement, sharing unpublished observations and sending me copious references to contextualize my work. John Kirby and Catharien Hilkens deserve thanks for reviewing progression of this work and providing valuable feedback. All three supervisors have provided important perspectives and valuable opportunities. Their patience with a stubborn pupil is not underestimated.

Finally, I would like to thank Mum and Oliver for providing the childcare essential to completing this work, and thank Robyn for providing a new perspective on life and the place of work within it.

Table of Contents

List of abbreviations

Abbreviations introduced in the text are listed below. To improve readability, the full names of transcription factors and intracellular adaptor proteins are not introduced in the text. A separate list is provided below.

AM	alveolar macrophage
AF	autofluorescnece
ALL	acute lymphoblastic leukaemia
AML	acute myeloid leukemia
APC	antigen presenting cell
APC	allophycocyanin
ATG	anti-thymocyte globulin
BAL	bronchoalveolar lavage
BMT	bone marrow or haematopoietic stem cell transplantation
BOOP	bronchiolitis obliterans organizing pneumonia
BOS	bronchiolitis obliterans syndrome
BTLA	B and T lymphocyte attenuator
CBA	cytokine bead array
CCR/L	CC group chemokine receptor/ligand
CD	cluster of differentiation
CD14 MDM	CD14-positive monocyte-derived macrophage
cDC1	classical DC 1
cDC2	classical DC 2
CDP	common dendritic cell precursor
CLL	chronic lymphocytic leukemia
CML	chronic myeloid leukemia
cMOP	common monocyte precursor
COP	cryptogenic organizing pneumonia
CRP	C reactive protein
CTL	cytotoxic T lymphocyte
CX3CR/L	CX3C group chemokine receptor/ligand
CXCR/L	CXC group chemokine receptor/ligand
DAMP	damage-associated molecular patterns
DC	dendritic cell
DETCs	dendritic epidermal T cells
DLI	donor lymphocyte infusion
DMSO	dimethyl sulphoxide
DPX	distyrene, plasticizer and xylene mountant
EDTA	ethylenediaminetetraacetic acid
ELISA	enzyme-linked immunosorbant assay
FACS	fluorescence activated cell sorting
FCS	fetal calf serum
FISH	fluorescence in situ hybridization
FITC	fluorescein isothiocyantate
FLC	foetal liver chimera

FSC	forward scatter
FXIIIa	factor thirteen A
G-CSF	granulocyte colony stimulating factor
GM-CSF	granulocyte macrophage colony stimulating factor
GMP	granulocyte monocyte precursor
GvHD	graft-versus-host disease
GvL	graft-versus-leukemia effect
HUVEC	human umbilical vein endothelial cells
IDEC	inflammatory dendritic epidermal cells
IDO	indoleamine 2,3-dioxygenase
IFN	interferon
IL	interleukin
iNOS	inducible nitric oxide synthase
IPS	Idiopathic Pneumonia Syndrome
IRF	interferon regulatory factors
ISW	immunosuppression withdrawal
LBP	lipopolysaccharide binding protein
LC	Langerhans cell
LPS	lipopolysaccharide
LTR	lichenoid tissue reaction
Ly6C	lymphocyte antigen 6 complex, locus C1
M-CSF	macrophage colony stimulating factor
M-MDSC	mononuclear myeloid derived suppressor cells
MCP1/CCL2	monocyte chemoattractant protein-1
MDM	monocyte-derived macrophage
MDP	macrophage and DC progenitor
MDS	myelodysplastic syndromes
MHC	major histocompatibility complex
MM	multiple myeloma
moDC	monocyte-derived DC (refers to *in vitro* only in this text)
MP	mononuclear phagocyte
MRD	matched related donor
mRNA	messenger ribonucleic acid
MUD	matched unrelated donor
NIH	National institutes of health
NK	natural killer lymphocyte
NOD2	nucleotide binding oligomerization domain containing 2
PAMP	pathogen associated molecular pattern
PBMC	peripheral blood mononuclear cell
PBS	phosphate buffered saline
PCA	principal components analysis
PCR	polymerase chain reaction
pDC	plasmacytoid DC
PE	phycoerythrin
PMA	phorbol 12-myristate 13-acetate
pre-DC	precursor dendritic cell
PRR	pattern recognition receptor
RBC	red blood cell

RIC	reduced intensity conditioning
ROC	receiver operating characteristic
SEM	standard error of the mean
SD	standard deviation
SLAN	6-Sulfo LacNac
SLAN-DC	MP with 6-Sulfo LacNac modification of P-selectin
SSC	side scatter
TCD	T cell depleted
Th1	T helper cell type 1
Th2	T helper cell type 2
Th17	T helper cell type 17
TIP-DC	TNFα and iNOS producing DC
TLR	toll-like receptor
TNF	tumour necrosis factor
TR	T cell replete
Treg	regulatory T cell
TRM	transplant related mortality
XCR/L	XC group chemokine receptor/ligand

Transcription factors and intracellular adaptor proteins

AP-1	Activator protein 1
ATF3	Activating transcription factor 3
Batf3	Basic leucine zipper transcription factor ATF-like 3
C/EBPδ	CCAAT-enhancer binding protein delta
Flt3	Fms-related tyrosine kinase 3
GATA-2	GATA binding protein 2
Klf4	Kruppel-like factor 4
MyD88	Myeloid differentiation primary response gene 88
NF-κB	Nuclear factor kappa-light-chain-enhancer of activated B cells)
TRIF	TIR domain-containing adaptor inducing interferon-β
ZBTB46	Zinc finger and BTB domain containing 46

List of tables and figures

Chapter 1. Introduction

This chapter will begin with an introduction to the concepts in immunology most relevant to mononuclear phagocyte (MP) biology. An overview of the mononuclear phagocyte system (MPS) will follow, structured by detailing its cell subsets, their functions and origins. Following a summary of the steady state MPS, features in inflammation will be explored. Tissue specific considerations of the MPS will be discussed for the two organs examined in this work: skin and lung. Graft-versus-host disease (GvHD) will be introduced, before summarizing the hypotheses and general aims of this thesis.

1.1 Relevant concepts in immunology

1.1.1 Innate and adaptive immunity

To protect an organism against damage from infectious or harmful agents, the immune system must provide a rapid response. This ability is termed the innate immune response and is shared by all multicellular organisms, from nematodes to humans. At its most primitive, the innate immune system comprises receptors that bind pathogen-associated molecules, signaling cascades and antimicrobial effector molecules (Schulenburg et al., 2008). Cells capable of engulfing foreign particles (phagocytes) were initially discovered in starfish larvae and have evolved into a critical aspect of innate immunity in vertebrates (Tauber, 2003). Non-phagocytic cells (basophils, mast cells, innate lymphoid cells) contribute to innate responses via release of effector and signaling molecules (Murphy, 2011).

Dogma that the innate immune system responds without memory of prior events has been challenged in recent years (Saeed et al., 2014), (Cheng et al., 2014). However, the principal repository of immune memory in vertebrates is the adaptive immune system. Lymphocytes of the adaptive immune system have vast diversity of antigen-specific receptors, can persist long-term and can respond rapidly to antigen re-challenge via population expansion, cytokine and antibody production and cytotoxic function. MPs of the innate immune system are pivotal regulators of adaptive immunity via antigen presentation (Steinman and Hemmi, 2006).

1.1.2 Antigen presentation

To initiate an adaptive immune response, a naïve T cell must receive three signals from an antigen-presenting cell (APC). First, an antigenic peptide is presented via a major histocompatibility complex (MHC) protein specific for the T cell receptor. Second, an activation signal (e.g. CD80 and CD86 binding CD28) promotes T cell survival and proliferation. Third, a cytokine signal activates a specific differentiation program in the T cell (Murphy, 2011). In situations where signal 1 is provided in isolation, anergic (non-responsive) T cells result (Quill and Schwartz, 1987).

While most somatic cells express MHC proteins, only macrophages, dendritic cells (DCs) and B-lymphocytes are competent APCs. Naïve T cell stimulation is a specialized function of DCs and occurs primarily in lymphoid tissue (Steinman and Witmer, 1978). Memory T cells encounter both macrophages and DCs in non-lymphoid tissues and antigen presentation in this context may contribute to lymphocyte responses (Wakim et al., 2008). B cells present antigen to enlist T cell help for antibody production.

Proteins within cytosolic and endocytic compartments are processed and presented differently. Cytosolic proteins are presented on MHC class I proteins (HLA-A, B and C in humans) to CD8 T cells. Endocytic proteins are presented on MHC class II proteins (HLA-DR, DQ, DP in humans) to CD4 T cells. Phagocytosis by macrophages and DCs delivers pathogenic/ immunogenic antigens to the endocytic compartment, but not all antigens are capable of entering the cytosolic compartment. For example, viruses that do not directly infect a DC/ macrophage, solid tumour-associated antigens and vaccine-delivered antigens cannot become cytosolic in the APC. Some DCs are capable of presenting exogenous antigen on MHC class I to CD8 T cells: a process termed cross-presentation. Transfer of entire MHC-peptide complexes to the surface of APCs may also occur, and is referred to as cross-dressing (Wakim and Bevan, 2011).

1.1.3 Non-self and danger recognition

Matzinger's Danger model is the most comprehensive explanation of how the immune system responds to cells from another individual or species. The model is

based on Janeway's theory that APCs require stimulation to generate an adaptive immune response (Matzinger, 2002). While APCs continually ingest dying or damaged tissue cells in addition to pathogens, auto-immunity is not ubiquitous. Janeway proposed that productive immunity only occurs when pattern recognition receptors (PRRs) on APCs are stimulated. Conserved pathogen associated molecular patterns (PAMPs) provide this stimulus. Matzinger added the refinement that stimuli do not have to be pathogen-associated (Matzinger, 1994). 'Danger signals' or damage-associated molecular patterns (DAMPs) are released by tissue necrosis. Recognized danger signals include heat shock proteins and uric acid. DAMPs and PAMPs together are referred to as 'alarmins' (Oppenheim and Yang, 2005).

1.1.4 Acute inflammation

Activation of alarmins must induce rapid local changes to contain foreign antigen. Three of the clinical signs of acute inflammation described by Celsus two thousand years ago (calor/ heat, rubor/ redness and tumor/ swelling) indicate that a vascular response is critical. Reduced vascular flow rate, increased endothelial permeability and endothelial activation permit leukocyte entry to tissue. Neutrophils are recruited first, initiating a cellular innate immune response. Monocytes follow within hours (Shi and Pamer, 2011). In addition to leukocytes, plasma proteins, such as complement, are key effectors. Tissue resident leukocytes, including macrophages, contribute by producing cytokines such as interleukin-6 (IL-6) and tumour necrosis factor alpha (TNFα) and chemokines that recruit other leukocytes to the inflamed site (Davies et al., 2013).

1.2 The mononuclear phagocyte system

A scheme of the human MPS is depicted in Figure 1.1. The following sections discuss the foundation for classifying these cells as a system and review the defining features of each member. Figure 1.1 contextualizes how each member fits within the organization of the MPS.

Figure 1.1 Organization of the human MPS

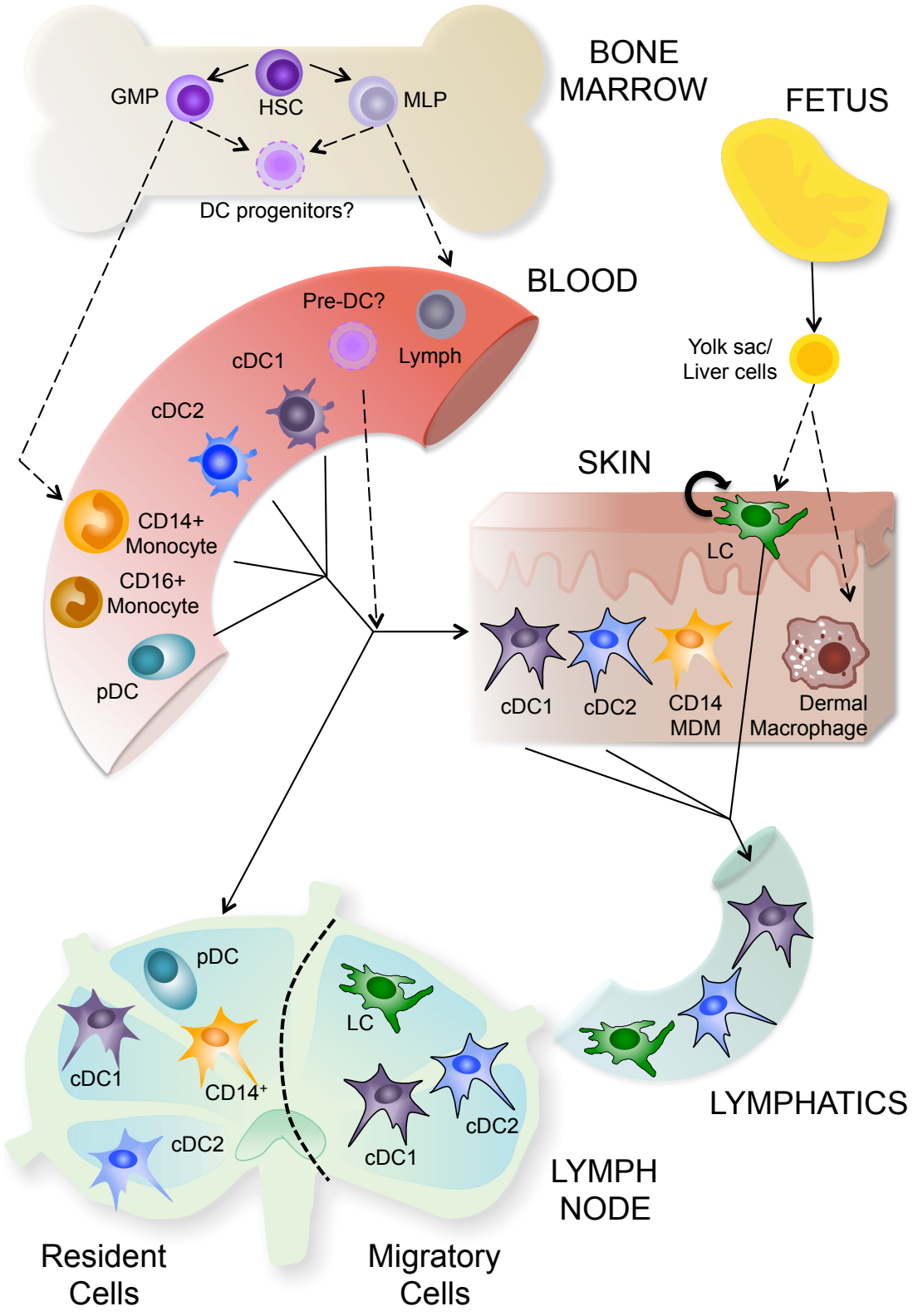

Figure 1.1 Organization of the human MPS
Image modified from (Haniffa et al., 2015a). HSC= haematopoietic stem cell, GMP= Granulocyte macrophage precursor, MLP= Multi-lymphoid progenitor. Dashed arrows indicate possible precursor-progeny relationships

1.2.1 Historical description

The MPS was proposed in 1972 in order to describe phagocytic cells sharing similar phenotype and function (van Furth et al., 1972). The system recognized bone marrow precursors, circulating monocytes and tissue specific macrophages as a continuum that was distinct from polymorphonuclear phagocytes (granulocytes/ neutrophils). In contrast to earlier attempts at classification, van Furth and colleagues excluded non-immune cells such as fibroblasts and endothelial cells. When Steinman and Cohn isolated a novel cell type from mouse spleen in 1973-79, the DC was added to the MPS, even thought it had limited capacity for phagocytosis and properties that clearly distinguished it from macrophages (Steinman and Cohn, 1973), (Steinman and Cohn, 1974). Ongoing support for classifying monocytes, macrophages and DCs as part of a unified system is mixed (Geissmann et al., 2010). In the past decade, clear differences in the origins of monocytes, macrophages and DCs have been identified (Naik et al., 2007), (Ginhoux et al., 2010), (Hettinger et al., 2013), (Lee et al., 2015), (Breton et al., 2015). Developmental relationships between cells are still being dissected, particularly in inflammation. The “MPS” has been used in this thesis as a synonym for monocytes, macrophages and DCs. Applying false identifiers to cell populations can be highly misleading, and MP is a useful moniker in the absence of a definite identity.

1.2.2 Dendritic cell subsets and functions

DCs are rare leukocytes with innate immune functions. They are distinct from monocytes and macrophages in their ability to bridge innate and adaptive immunity by migrating from tissue to draining lymph node and priming naïve antigen-specific T cells (Steinman and Witmer, 1978). Numerous subsets of DCs exist, which are stable over time and conserved across species (Robbins et al., 2008), (Haniffa et al., 2012), (Satpathy et al., 2013), (McGovern et al., 2014). Subsets can perform specific functions in the immune response and, while there is some overlap and plasticity, it is likely that a full complement of subsets is required for normal immune function (Merad et al., 2013).

DC subsets were originally defined by expression patterns of surface antigens. However, antigen expression patterns vary between tissues and species making it

difficult to identify lineage similarity (Vu Manh et al., 2015). A recent system of nomenclature categorizes DCs into three subsets based on evidence for distinct developmental pathways in the mouse. The nomenclature has been extended to human subsets through cross-species gene expression profiling (Guilliams et al., 2014). Phenotype and reported functions of the three subsets- plasmacytoid DC (pDC), classical DC 1 (cDC1) and classical DC 2 (cDC2)- are summarized in Table 1.1. Langerhans cells (LCs) are APCs found in epithelia, particularly the epidermis of the skin. While they exhibit DC functions, LCs have developmental similarities with macrophages: they are seeded during embryonic development and are maintained independently of adult haematopoiesis during steady state (Hoeffel et al., 2012), (Bigley et al., 2011). For this reason, current nomenclature does not include them as a DC subset.

While this system of nomenclature has brought clarity, it conceals certain points of complexity. Subsets were defined by transcription factor dependence, based on studies in gene-targeted mice but this dependence is neither as exclusive nor absolute as the nomenclature implies. For example, the transcription factor Batf3 is required for cDC1 development in steady state. During inflammation, cDC1 develop in Batf3-/- mice due to compensation by related transcription factors (Tussiwand et al., 2012). Subsets defined by the nomenclature are not entirely homogeneous. For example, a proportion of cDC2 in mouse is dependent on the transcription factor Klf4 (Tussiwand et al., 2015). When deleted, Th2 responses are diminished but Th1 and Th17 responses are maintained. In humans, cDC2 can be split into two subsets based on expression of surface antigen B and T lymphocyte attenuator (BTLA) (Reynolds G, personal communication). BTLA+ cDC2 support regulatory T cell (Treg) induction whereas BTLA- cDC2 support types 1 and 17 T helper cell (Th1/ Th17) induction. Finally, the nomenclature implies cross-species homology. The functional specialization of subsets may be subtly different between mice and humans. Teasing apart genuine differences from those introduced by experimental approaches (*in vivo* in mice versus *in vitro* in humans) is challenging. Antigen cross-presentation capacity, for example, is focused in cDC1 in mouse but may be seen in LCs and cDC2 in humans (Haniffa et al., 2015a), (Malissen et al., 2014).

Table 1.1 Dendritic cell subsets and functions

Group	Species	Subset	Surface antigens	Pattern recognition receptors	Key functions
cDC1	Mouse	CD8+ (lymphoid tissue) CD103+ (non-lymphoid tissue)	MHC II+, CD11c+, Flt3+ XCR1+ CLEC9A+ CADM1+	TLR 3 TLR 8	Induction of CD8 T cell immunity Cross-presentation Th1 polarization (some studies)
	Human	CD141++	MHC II+, CD11c^{lo} CD103+, SIRPa- (gut) XCR1+ CLEC9A+ CADM1+		
cDC2	Mouse	CD11b+	MHC II+, CD11c+ CD103+ (in gut) SIRPa+	TLR 1-8	Activation of CD4 T cells Peripheral Treg induction Th2 and Th17 induction
	Human	CD1c+	MHC II+, CD11c+ CD103+SIRPa+ (gut) SIRPa+		
pDC	Mouse	pDC	CD11c^{lo} MHC II^{lo} B220+ Siglec H+	TLR 7 TLR 9	Abundant IFN-α secretion Antigen presenting capacity (upon activation)
	Human	pDC	CD11c^{lo} MHC II+ CD123+ BDCA-2+ BDCA-4+		

Table 1.1 Dendritic cell subsets and functions
References: cDC1 (Bachem et al., 2010), (Crozat et al., 2010), (Poulin et al., 2010), (Jongbloed et al., 2010); cDCs (Merad et al., 2013), (Reynolds and Haniffa, 2015); pDCs (Reizis et al., 2011); gut DCs (Watchmaker et al., 2014)

1.2.3 Dendritic cell origins and mobilization

DC populations are bone marrow-dependent in that they require ongoing haematopoiesis to survive (Steinman et al., 1974). In mice, DCs share a common precursor with monocytes: the macrophage and DC progenitor (MDP) (Fogg et al., 2006). The more proximal precursors- common dendritic cell precursor (CDP) and precursor dendritic cell (pre-DC) are DC-restricted (Naik et al., 2007), (Onai et al., 2007). Recent evidence from single cell precursor analysis suggests that commitment to cDC1 or cDC2 lineage occurs in the bone marrow at the CDP stage (Schlitzer et al., 2013). In humans, a bone marrow precursor common to both monocytes and DCs can also be identified (Doulatov et al., 2010), (Lee et al., 2015). A precursor with DC commitment, (the hCDP) has been proposed to remain the in the bone marrow and a precursor with cDC1 and cDC2 potential (hpre-CDC) has been identified in the periphery (Breton et al., 2015).

Extrapolation from mouse to human would suggest that human tissue DCs are maintained by circulating DC precursors (Bogunovic et al., 2009). Humans have a larger blood DC complement than mice (Haniffa et al., 2015a). Blood and tissue DCs share similarities in gene expression (Robbins et al., 2008). Comparison of surface phenotype fits with a sequential acquisition of activation markers and lymph-node migratory function between blood and tissue (Haniffa et al., 2012). However, the relative contribution of DC precursors and blood DCs to tissue in humans remains uncertain.

In steady state, DCs are concentrated beneath host-environment interfaces and in lymphoid tissues (Merad et al., 2013). This location permits immediate response to immunogenic stimuli without a mobilization phase. DCs in non-lymphoid tissue respond to PRR ligation by migrating to draining lymph nodes through up-regulation of CC chemokine receptor 7 (CCR7) and response to a CC chemokine ligand 19/21 (CCL19/21) gradient. They prepare for T cell interactions by up-regulating co-stimulatory ligands and MHC class II (Inaba et al., 1990). However, tissue DC populations may appear unchanged or expanded during inflammation (Lowes et al., 2005), (Tamoutounour et al., 2013). Monocyte-derived DCs can be identified in inflamed tissue but the precise contributions of resident and recruited, classical and monocyte-derived DCs to the inflamed tissue pool and the immune response have been poorly characterized.

1.2.4 Macrophage diversity and functions

Macrophages are tissue-resident MPs with important functions in tissue homeostasis and the innate immune response. Specific immune functions include phagocytosis, microbial killing, cytokine production, effector T cell re-stimulation and organization of DC-T cell interactions (Takemura and Werb, 1984), (Natsuaki et al., 2014). The diversity of macrophages is underpinned by niche requirements of specific tissues. Therefore, nomenclature follows site of residency rather than developmental origin, phenotype or function (Guilliams et al., 2014).

To provide an example of niche specialization, alveolar macrophages (AM) are the resident macrophage of the lung alveolar space. They are required to protect the respiratory epithelium from inhaled insults, such as particulates and pathogens,

without triggering inflammation that may impair gas exchange or damage the epithelium (Lambrecht, 2006). To fit this niche, AM phagocytose material without producing pro-inflammatory cytokines and may directly suppress DC activation of T cells (Lambrecht, 2006). AM also clear and catabolize pulmonary surfactant (Trapnell and Whitsett, 2002), required for maintaining physiological surface tension and lung compliance. The specialization of AM is detectable at the transcriptional and epigenetic level. Only monocytes or yolk sac macrophages can fully colonize an empty AM niche, faithfully reproduce AM gene expression and protect from alveolar proteinosis (van de Laar et al., 2016). However, mature peritoneal macrophages transferred into the airway adopt many features of an AM-specific signature, emphasizing the importance of tissue education in defining macrophage identity (Lavin et al., 2014), (Lavin et al., 2015).

1.2.4 Macrophage origins and activation

Macrophage populations in many murine tissues are bone marrow-independent, in that they persist and self-renew without input from circulating monocytes or from any adult haematopoiesis (Yona et al., 2013), (Ginhoux et al., 2010), (Hashimoto et al., 2013). These macrophage populations, for example microglia of the brain and AM of the lung, are embryonically derived, either from primitive haematopoiesis (yolk sac macrophages) or from transient definitive haematopoiesis (fetal liver monocytes) depending on the tissue (Ginhoux and Guilliams, 2016). Macrophages in the gut and heart have ongoing input from circulating monocytes (Epelman et al., 2014a), (Bain et al., 2014).

The differences in macrophage origin between tissues have been proposed to result from whether a tissue niche remains open or closed to competition from circulating monocytes (Scott et al., 2014), (Ginhoux and Guilliams, 2016). Brain microglia, for example, are isolated behind the blood brain barrier and are the archetypal embryonically derived, self-renewing macrophage (Ginhoux et al., 2010). Gut and lung however are equally exposed to circulating monocytes, but retain different levels of embryonic macrophages. Additional factors that determine macrophage composition are unknown at present.

Macrophages with distinct kinetics have also been demonstrated in humans. In the

dermis, CD14+ monocyte-derived macrophages (CD14 MDM) exist along side factor thirteen A-positive (FXIIIa+) dermal macrophages (McGovern et al., 2014). Bone marrow transplantation restores CD14 MDM from donor haematopoiesis, but recipient FXIIIa+ dermal macrophages can persist for months to years (Haniffa et al., 2009). Patients with prolonged monocytopaenia (up to 10 years in one case) have been reported who lack CD14 MDM but retain dermal macrophages in their skin (Bigley et al., 2011).

The importance of ontogeny in ultimate macrophage function is unclear. While AM derive from fetal liver monocytes (Guilliams et al., 2013), yolk sac macrophages and adult monocytes are equally capable of colonizing an empty AM niche with no discernible differences in gene expression or function (van de Laar et al., 2016). Further, the ability of mature macrophages to adopt new tissue identities suggests nurture may be a stronger factor than nature (Lavin et al., 2014).

Unlike DCs and monocytes, macrophages do not mobilize in response to inflammatory stimuli. They remain within their tissue, but undergo a change in activation state, depending on the combinations of stimuli they receive from pathogens, host and other leukocytes. The concept of macrophage activation arose from observations that pathogen-exposed macrophages adopted more potent (but not antigen-specific) effector functions (Mackaness, 1962), (Martinez and Gordon, 2014). Different immune stimuli were noted to produce contrasting activation states *in vitro*, and the M1/ M2 paradigm was proposed to explain these contrasts, mirroring the Th1/ Th2 nomenclature for T helper cells (Figure 1.2) (Mantovani et al., 2004). It is increasingly recognized that M1 and M2 represent two poles, between which stimuli and combinations of stimuli can produced a spectrum of activation states (Xue et al., 2014). M1/ M2 macrophage activation states have been observed *in vivo*, but the majority of disease states exhibit mixed profiles (Sica and Mantovani, 2012). As highlighted by Martinez and Gordon, M1/ M2 was based upon macrophage response to individual immune signals (e.g. IL-4), removed from the context of a physiological immune response (Martinez and Gordon, 2014). In reality, macrophages are exposed to a wide range of stimuli including combinations of M1 and M2 stimuli simultaneously. Micro-geographical variations in these stimuli and cryptogenic heterogeneity amongst macrophages result in gradations of activation in a given tissue (Pettersen et al., 2011).

Figure 1.2 Models of macrophage activation

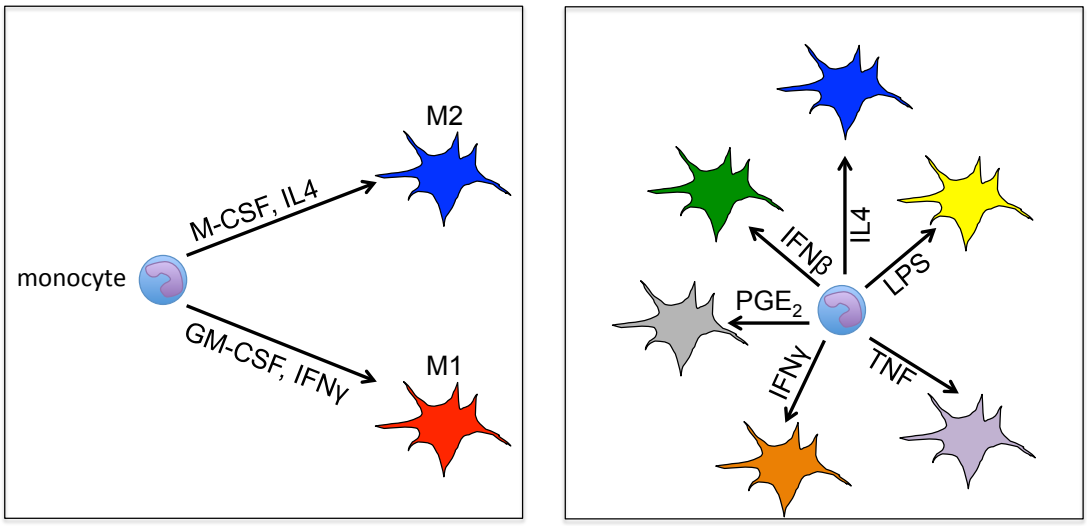

M1/M2 model of macrophage activation *(Mantovani, 2004)*

Spectrum model of macrophage activation *(Xu and Schultze, 2014)*

Figure 1.2 Models of macrophage activation
Left panel simplifies the M1/ M2 model of macrophage activation. M1= classically activated macrophage, M2= alternatively activated macrophage (Mantovani et al., 2004). Right panel simplifies the spectrum model of macrophage activation, based on transcriptome profiling of *in vitro* monocyte-derived macrophages (Xue et al., 2014). PGE_2 = prostaglandin E2; LPS=lipopolysaccharide; TNF= tumour necrosis factor; IFN=interferon.

1.2.6 Monocytes subsets and functions

Monocytes are a circulating population of MPs that can be rapidly recruited to tissues in inflammation. Monocyte contribution to the immune response is tissue and context-specific. This is largely attributable to the plasticity of monocytes in response to environmental cues.

There are at least two functionally distinct subsets of monocytes in mice and humans. In mice, monocyte subsets are separated by expression of a glycoprotein named lymphocyte antigen 6 complex, locus C1 (Ly6C). A major $Ly6C^{hi}$ population and a minor $Ly6C^{lo}$ population exist (Geissmann et al., 2003), (Shi and Pamer, 2011). In humans, monocytes subsets are identified by expression of CD14 and the low affinity Fcγ receptor CD16 (Ziegler-Heitbrock et al., 2010). CD14++CD16- cells, termed classical monocytes are transcriptionally similar to mouse $Ly6C^{hi}$ monocytes (Geissmann et al., 2003), (Ingersoll et al., 2010). CD14+CD16++ cells, termed non-

classical monocytes, overlap transcriptionally with mouse Ly6C^{lo} monocytes. An intermediate population of CD14++CD16+ monocytes can also be identified.

Ly6C^{hi} monocytes extravasate into tissue in steady state, with different fates depending on the tissue. In gut, Ly6C^{hi} cells differentiate into macrophages that maintain epithelial integrity, ingest free bacteria and sustain immune quiescence (Bain and Mowat, 2014). In skin, Ly6C^{hi} monocytes adopt DC or macrophage-specific transcriptional programmes and functions (Tamoutounour et al., 2013). In lung, monocytes with minimal differentiation can be identified (Jakubzick et al., 2013).

Ly6C^{hi} monocytes are rapidly recruited to tissue in acute inflammation. They are phagocytic, produce pro-inflammatory cytokines (TNFα, IL-1α/β, IL-6), nitric oxide and reactive oxygen species that may damage tissues, for example in inflammatory bowel disease, or aid resolution of infection (Bain and Mowat, 2014). Activated cells resembling Ly6C^{hi} monocytes are found in chronic inflammation, autoimmune disorders and cancer (Condamine et al., 2015). Termed mononuclear myeloid derived suppressor cells (M-MDSC), they inhibit T cell function via soluble factors such as nitric oxide and arginase-1 (Condamine et al., 2015).

Ly6C^{lo} and non-classical monocytes patrol the vascular endothelium (Auffray et al., 2007) and phagocytose damaged endothelial cells (Carlin et al., 2013). In steady state, they do not readily cross endothelium (Collison et al., 2015). Whether they enter tissues after adoptive transfer is disputed (Geissmann et al., 2003), (Bain and Mowat, 2014). In inflammation they may be recruited into tissues and produce TNFα (Auffray et al., 2007), (Cros et al., 2010). There is heterogeneity within the non-classical monocyte population: a proportion of cells have a carbohydrate-modification of P-selectin, termed 6-Sulfo LacNac (SLAN) (Schakel et al., 2002). The term ‘SLAN-DC’ arises in the literature as these cells exhibit some DC features, such as high levels of MHC class II, co-stimulatory ligand expression and the ability to drive Th1 responses (Hansel et al., 2011). By gene expression analysis, all monocyte subsets are distinct from DCs so the term does not have solid foundation (Robbins et al., 2008), (Haniffa et al., 2012).

1.2.7 Monocyte origins and mobilization

Ly6C^{lo} populations have been shown to depend on Ly6C^{hi} monocyte populations through fate mapping studies (Yona et al., 2013). Restoration of non-classical monocyte populations lags behind appearance of classical monocytes following bone marrow transplantation (McGovern et al., 2014). A similar trend is seen with uptake of deuterium-labelled glucose (Yona S, unpublished communication), supporting a parallel dependence of monocyte subsets in humans.

Proximal to Ly6C^{hi} monocytes is a common monocyte precursor (cMOP) arising from an oligopotent DC/ monocyte/ macrophage precursor (MDP) (Hettinger et al., 2013), (Fogg et al., 2006). In humans, monocyte potential has been identified in the granulocyte monocyte precursor (GMP) (Doulatov et al., 2010), but the more proximal precursors of monocytes remain undefined.

Monocytes are capable of rapid mobilization in response to stress. There is evidence from murine studies that marginal pools of monocytes exist in low velocity vascular beds such as those found in spleen and lung (Swirski et al., 2009). These pools may be rapidly released by neural stimulation (Steppich et al., 2000). Release of monocytes from the bone marrow can be triggered by low levels of circulating toll-like receptor (TLR) ligands. These levels are sufficient to promote monocyte chemoattractant protein-1 (MCP-1/ CCL2) secretion by marrow stromal cells and cause adjacent monocytes to up-regulate CCR2 and exit (Shi and Pamer, 2011). Myelopoiesis may also be altered during conditions of stress, skewing GMP outputs in favour of monocytes (Courties et al., 2015).

1.2.8 Monocyte-derived cells in vitro

Monocytes, though divergent from DCs during haematopoiesis, may adopt DC characteristics *in vitro*. In the Journal of Experimental Medicine's most cited article, Sallusto and Lanzavecchia described monocyte-derived DC (moDC) generation from blood monocytes using granulocyte macrophage colony stimulating factor (GM-CSF/ CSF2) and IL-4 (Sallusto and Lanzavecchia, 1994). These cells had dendritic morphology, the ability to stimulate naïve T cells, high expression of MHC class II, co-stimulatory molecules CD40 and CD80/86, cDC2 antigen CD1 and absence of

monocyte antigen CD14. Similar culture systems were used to generate DCs from mouse bone marrow (Inaba et al., 1992). More recent gene expression studies have shown that moDCs are distinct from primary lymphoid tissue DC, but do share expression of DC-specific genes (Robbins et al., 2008). It is recognized that monocytes may contribute to steady-state DC populations in mucosal tissues but not lymphoid tissue (Varol et al., 2007).

Monocytes cultured with GM-CSF or macrophage colony stimulating factor (M-CSF/ CSF1) adopt the morphology and functional characteristics of macrophages. GM-CSF, lipopolysaccharide (LPS), interferon-gamma (IFNγ) and TNFα skew macrophages towards a classically-activated (M1) state and M-CSF, IL-4, IL-10, IL-13, glucocorticoids and vitamin D towards an alternatively-activated state (Martinez and Gordon, 2014). *In vitro* M1 polarization of human monocytes incurs profound changes gene expression (5.2% of transcripts) while the effect of M2 polarization is less marked (0.3% of transcripts) (Martinez et al., 2006). Hallmark M1 and M2 genes in this setting are *CXCL11*, *CCL19*, *IDO* and *CCR7* (M1) and *MRC1, CCL13, CD36* and *CD209* (M2). In the murine setting only, *Ym1* and *Arg* are key discriminators of an M2 state (Raes et al., 2005).

While the plasticity of the monocyte allows differentiation and polarization into these distinct states, using them to understand inflammatory processes *in vivo* is challenging. In certain contexts, comparison to *in vitro*-derived monocytes or macrophages has clarified our understanding of inflammatory myeloid cells (Segura et al., 2013), (Sica and Mantovani, 2012). Yet, many oppose such comparisons as an oversimplification of the biology of inflammation and heterogeneity of myeloid populations (Hume, 2015), (Martinez and Gordon, 2014).

1.2.9 Inflammatory mononuclear phagocytes in vivo

Murine inflammatory MPs have been described in numerous infection and sterile inflammation models, for example *Leishmania major* infection (Leon et al., 2007), allergic airway inflammation mediated by house dust mites (Plantinga et al., 2013) and contact hypersensitivity mediated by topical haptens (Tamoutounour et al., 2013). Reliable discrimination of inflammatory macrophages from inflammatory DCs has been challenging as both share high expression of MHC class II, and both may

express CD11c, CD11b, Ly6C and F4/80 (Merad et al., 2013), (Segura and Amigorena, 2013). The combined expression of FcER1 and CD64 expression has been proposed the most reliable means of phenotypying inflammatory DCs (Plantinga et al., 2013). Expression of DC-specific transcription factor ZBTB46 has clarified identity in some cases. For example, the TNFα and inducible nitric oxide synthase (iNOS)- expressing DC (Tip-DC) does not express ZBTB46 and is most likely a macrophage (Satpathy et al., 2012a). Supplementing phenotype and gene expression with confirmation of lymph node migratory potential (e.g. using CCR7-deficient mice) and the ability to stimulate naïve T cells provides the most robust definition of a DC (Segura and Amigorena, 2013).

In general, inflammatory macrophages do not migrate to lymphoid tissue (Segura and Amigorena, 2013). Inflammatory macrophages can efficiently capture antigen and re-stimulate T cells but appear to be dispensable for T cell priming (Iijima et al., 2011). Inflammatory macrophages are efficient at phagocytosis but may also release lytic factors, reactive oxygen species and proteinases into the extracellular space (Narni-Mancinelli et al., 2011). The precise activities of inflammatory macrophages are tissue and context-specific (Jung and Schwartz, 2012). For example, monocyte-derived macrophages generated in the central nervous system during experimentally induced autoimmune encephalomyelitis are pro-inflammatory (Mildner et al., 2009), but those generated in injured spinal cord promote tissue repair (Shechter et al., 2009). Macrophages adopt various phenotypes during the resolution phase of inflammation, in part, instructed by the immune stimuli they have encountered (Ariel and Serhan, 2012). TGFβ production by persistent inflammatory macrophages has been implicated in tissue fibrosis, for example sclerodermatous chronic GvHD (Alexander et al., 2014).

Inflammatory DCs can stimulate both CD4 T cells by indirect antigen presentation (Leon et al., 2007) and CD8 T cells by cross-presentation (Segura et al., 2009). The polarization of CD4 T cells is context-dependent: both Th1 (Leon et al., 2007) and Th2 responses (Plantinga et al., 2013) have been reported. Inflammatory DCs can produce a range of inflammatory and T cell modulatory cytokines (type I interferon, IL-1, IL-12 and IL-23) (Plantinga et al., 2013). The interaction between inflammatory DCs and T cells can occur in both lymphoid and non-lymphoid tissue (Wakim et al., 2008). In an experimental model of asthma, the site of interaction depended on

antigen load, with low-dose exposure leading to tissue interactions and high-dose to lymph node interactions (Plantinga et al., 2013). Inflammatory DCs may also assist in the transport of antigen to lymphoid tissue (Hohl et al., 2009).

Both inflammatory macrophages and inflammatory DCs are depleted in CCR2-deficient animals (Iijima et al., 2011), (Nakano et al., 2009), (Bain et al., 2013) but they are unaffected in Flt3-deficient animals (Plantinga et al., 2013). This sets them apart from classical DCs and supports their development from CCR2-dependent monocytes, but does not strictly exclude origin from non-monocytic CCR2-dependent precursors. Ly6C^{hi} monocytes adoptively transferred into inflammatory models can be seen differentiating into DCs and macrophages (Leon et al., 2007), (Bain et al., 2013). This is highly suggestive that Ly6C^{hi} monocytes are the precursor of both inflammatory MPs.

Human inflammatory MPs found in skin and lung will be discussed in sections 1.4 and 1.5, but the work of Segura et al. on chronic inflammatory effusions also requires consideration (Segura et al., 2013). This study juxtaposed CD16+CD1c- inflammatory macrophages with CD16-CD1c+ inflammatory DCs detected in chronic rheumatoid joint effusions and malignant ascites. Definitions of their MPs were supported by gene expression and *in vitro* functional assays. Inflammatory DCs induced T cell proliferation, IFNγ and IL-17 production, while inflammatory macrophages only induced IFNγ production. Comparison of the inflammatory DC gene expression signature to a moDC signature through gene-set enrichment analysis demonstrated similarity. Inflammatory macrophages were enriched with a broadly-defined macrophage signature but had greater similarity to the moDC signature than to steady-state monocytes. This study provides an important reference for inflammatory MP identification in humans. However, their phenotypic definitions cannot be directly applied to tissues with resident macrophage and DC populations. For example, a CD11c+HLA-DR+CD1c+CD16- gate in human skin would capture the steady state cDC2. Furthermore, it may not reliably exclude the dermal macrophage, which is CD16- and can encroach upon a CD1c+ gate due to autofluorescence (personal observation).

1.3 Skin mononuclear phagocytes

1.3.1 Resident cell architecture

The skin is the largest barrier organ in the body and has unique physical and immunological adaptations to resisting infection. Resident cells of the innate and adaptive immune system are an important part of this adaptation.

The outer epidermis of the skin contains a network of interconnected LCs. There are few other resident leukocytes in human epidermis, besides a modest number of effector memory T cells which are principally CD8+ (Spetz et al., 1996), (Nomura et al., 2014). In contrast, the murine epidermis has an abundant network of γδ cells or dendritic epidermal T cells (DETCs), which sense barrier breach and orchestrate early immune responses (Sharp et al., 2005).

Beneath the epidermis, the dermis has an organized network of resident leukocytes that varies with depth (Wang et al., 2014). DCs are distributed uniformly beneath the dermo-epidermal junction but form perivascular sheaths in the deeper reticular dermis. FXIIIa+ macrophages and CD3+ T cells are found throughout the dermis, contributing to perivascular leukocyte architecture in the deeper layers. Both DCs and T cells are enriched in the skin relative to the blood (Clark, 2010), (Haniffa et al., 2012). Skin resident T cells comprise both CD4+ and CD8+ effector memory cells (Clark, 2010).

1.3.2 Skin mononuclear phagocytes in steady state

LCs are characterized by expression of non-polymorphic HLA CD1a and the C-type lectin receptor CD207 (Langerin). By electron microscopy they contain characteristic organelles named Birbeck granules (Romani et al., 1989). LCs are thought to maintain peripheral tolerance by transporting self peptides to the paracortex of skin-draining lymph nodes in the absence of a co-stimulatory signal (Steinman and Nussenzweig, 2002). Their necessity for induction of an adaptive immune response has been questioned as LC-depleted mice can generate effective antigen-specific responses (Bennett et al., 2005).

Steady state dermal DCs comprise at least two myeloid subsets (cDC1 and cDC2) but pDCs are not seen (Haniffa et al., 2012). The cDC1 subset is characterized by high expression of CD141 in humans and expression of CD103 in mice (Haniffa et al., 2012), (Merad et al., 2013). In both species, this subset expresses TLR3 for sensing viral antigen, and Clec9A for apoptotic cell uptake as well as Necl2 and XCR1 (Bachem et al., 2010), (Crozat et al., 2010), (Jongbloed et al., 2010), (Poulin et al., 2010), (Haniffa et al., 2012). Functionally, it can migrate to lymph nodes via CCR7, induce naïve T cell stimulation and cross-present exogenous antigen to CD8 T cells (Haniffa et al., 2012). The cDC2 subset is characteristically CD1c/ CD1a+ in humans and CD11b+ in mice (Merad et al., 2013). It is the major DC population in skin, present in approximately similar numbers to dermal macrophages (Zaba et al., 2007), (Haniffa et al., 2009), (Wang et al., 2014). The cDC2 subset expresses pattern recognition receptors TLR1-8 in addition to Dectins (CLEC6A/ 7A), the endocytic receptor CD205 and the macrophage mannose receptor CD206 (Collin et al., 2013). Like cDC1, it expresses CCR7 and can stimulate naïve T cell proliferation (Haniffa et al., 2009). It is less effective at cross-presenting antigen and produces a different profile of cytokines on stimulation: cDC1 produce TNFα and CXCL10 while cDC2 produce IL-10 and IL-12p70 (Haniffa et al., 2012), (Collin et al., 2013).

CD14 MDMs in humans skin were categorized as DCs for many years as they are morphologically distinct from FXIIIa+ macrophages and able to migrate out of skin explants (Nestle et al., 1993), (Klechevsky et al., 2008), (Haniffa et al., 2009). Recent reanalysis has shown transcriptional similarity with the monocyte/ macrophage lineage, dependence on circulating monocytes and the absence of spontaneous migration to lymphoid tissue (McGovern et al., 2014). This subset is analogous to the CD11b+CD64+$^{/lo}$Ly6C^{lo}CCR2- (P4, P5) populations in mouse dermis (McGovern et al., 2014), (Tamoutounour et al., 2013). Monocytes and monocyte-derived DCs in mouse dermis (P1-3) do not yet have a recognized counterpart in human dermis (Tamoutounour et al., 2013). CD14 MDMs are poor stimulators of naïve T cells (Haniffa et al., 2009), (Klechevsky et al., 2008) but can induce differentiation into T follicular helper cells (Klechevsky et al., 2008). The physiological relevance of this finding is unclear as CD14 MDMs do not migrate to lymph nodes (McGovern et al., 2014). CD14 MDMs produce TNFα, IL-1B, IL-6, IL-8, and IL-10 on stimulation (Haniffa et al., 2012).

Dermal macrophages can be distinguished from DCs and CD14 MDMs morphologically by their larger size and pigmented cytoplasmic granules (Haniffa et al., 2009). By immunostaining they are clearly identifiable as FXIIIa+CD11c- spindle-shaped cells, while the other resident myeloid populations are FXIIIa-CD11c+ (Zaba et al., 2007). As FXIIIa is predominantly cytoplasmic, it is not a useful antigen for discriminating macrophages by flow cytometry (Zaba et al., 2007), (Haniffa et al., 2009). Dermal macrophages can be distinguished by their autofluorescence (Haniffa et al., 2009). Autofluoresence occurs when cytoplasmic components, including melanin granules in dermal macrophages, are excited by low wavelength light and emit a fluorescence signal, primarily detectable in the fluorescein isothiocyanate (FITC) channel (Baumgarth and Roederer, 2000). There are few surface antigens differentially expressed by CD14 MDMs and macrophages (McGovern et al., 2014). Dermal macrophages are poor stimulators of naïve T cell proliferation but induce memory T cells to secrete IL-17 and interferon gamma (IFNγ) (Haniffa et al., 2009). Dermal macrophages produce IL-1 and IL-6 when stimulated (Haniffa et al., 2009).

1.3.3 Skin mononuclear phagocytes in inflammation

Superimposed on steady state MP subsets, monocytes enter inflamed skin and adopt macrophage or DC characteristics depending on the context. In murine cutaneous *Leishmania* infection, monocytes primarily adopt a DC phenotype, migrate to lymph node and promote Th1-mediated parasite clearance (Leon et al., 2007). In human cutaneous leprosy infection, monocytes may adopt either DC-SIGN+CD1b- macrophage or DC-SIGN-CD1b+ DC phenotypes in the localized tuberculoid form of the disease where effective Th1-mediated bacillus clearance occurs (Krutzik et al., 2005). In the lepromatous form, where bacillus is disseminated and an effective T helper response is lacking, monocyte-derived DCs do not occur. This suggests that the fate of recruited monocytes impacts upon the tenor of the adaptive immune response.

Considering non-infective inflammation, most studies of skin MP content have focused on psoriasis or atopic dermatitis (eczema). DCs are abundant in psoriatic lesions, outnumbering lymphocytes (Lowes et al., 2005). pDCs are recruited to early lesions (Albanesi et al., 2009). The CD11c+ “DCs” lack CD14, CD1c/ CD1a and Langerin, setting them apart from resident DCs (Lowes et al., 2005). They express

co-stimulatory ligands CD40 and CD86, SLAN, TNF and iNOS (Lowes et al., 2005), (Hansel et al., 2011). The terms SLAN-DC and Tip-DC have been applied to these cells (Lowes et al., 2005), (Hansel et al., 2011). Notably, the TipDCs originally described in murine *Listeria monocytogenes* infection (Serbina et al., 2003) were subsequently found to lack ZBTB46 expression (Satpathy et al., 2012a). On balance, they are likely to be monocyte-derived macrophages. The transcriptional profile of the psoriatic inflammatory "DC" is most similar to that of a moDC, but some macrophage-related transcripts are present e.g. CD163 (Zaba et al., 2010). In eczema lesions, both pDCs and myeloid DCs are found (Wollenberg et al., 1996), (Wollenberg et al., 2002a), (Wollenberg et al., 2002b), (Stary et al., 2005). The myeloid DCs isolated from epidermal suspensions have been termed inflammatory dendritic epidermal cells (IDECs), but phenotypically, they resemble resident dermal cDC2 (CD11c+, CD1a/c+). Studies that simultaneously identify steady state and inflammatory MPs, test expression of multiple surface antigens, assess function and use unbiased techniques to assess similarity to monocytes, DCs or macrophages are scarce.

1.4 Lung mononuclear phagocytes

1.4.1 Structure of the lung immune system

The lung has more anatomical variation than the skin. When considering the lung immune system, a distinction is made between the conducting airways and parenchymal lung (Holt et al., 2008).

The conducting airways present a mucosal barrier to the environment. The barrier has layers of defence against inhaled particulates and pathogens including surface mucus and IgA. Within the epithelium, macrophages, memory T cells and layers of interdigitating DCs can be found that appear similar to the LC network in skin (Heier et al., 2011). DCs extend projections through epithelial tight junctions into the airway lumen in order to constitutively sample antigen (Jahnsen et al., 2006). Follicles of lymphoid cells are found within the mucosa in children, but decline with age (Heier et al., 2011). The blood supply to the conducting airways is via the bronchial arteries

(systemic circulation) and the dogma of leukocyte migration through post-capillary venules applies (Holt et al., 2008).

The parenchymal lung includes the airspaces distal to the respiratory bronchioles (alveoli) and the interstitial space. The alveoli present a single layer of respiratory epithelium to the environment. Adherent to this epithelium are AM. DCs and T cells are also found within the alveoli (Holt et al., 2008). Beneath the respiratory epithelium, the interstitium contains scattered macrophages, DCs and T cells. Immune cells sequestered within the low flow pulmonary capillary bed have been identified. Marginated leukocytes represent 87% of total lung leukocytes (Barletta et al., 2012). Partly due to biophysical properties, monocytes and DCs are preferentially sequestered, comprising 57% of the marginal pool (Doherty et al., 1994), (Barletta et al., 2012). In contrast to the conducting airways, parenchymal lung receives blood supply from the low-pressure pulmonary arteries. Leukocyte recruitment through pulmonary capillaries is thought to be less stringent and rely on different combinations of integrins than post-capillary venule migration (Holt et al., 2008).

1.4.2 Lung mononuclear phagocytes in steady state

Insights into the MP content of human lung have come from studying digested lung tissue or bronchoalveolar lavage (BAL) fluid. Lung tissue surplus to diagnostic requirements can be accessed from cancer lobectomy/ pneumonectomy surgery or from un-transplantable donor lungs. Neither can be considered immunologically normal and both need enzymatic digestion to release leukocytes. Without micro-dissection, pulverizing parenchyma merges distinct anatomical compartments in the lung (alveoli, parenchyma, bronchioles). The pulmonary vasculature can be flushed with intact lobes but not with lobectomy surplus. This can minimize sampling of intravascular leukocytes, but if the sequestered leukocyte fraction is considered part of the lung immune system, this may not be desirable.

Early studies on digested lung tissue identified two subsets of myeloid DCs and plasmacytoid DCs, equivalent to the DC subsets found in blood (Demedts et al., 2005), (Masten et al., 2006). Demedts et al. described BDCA1+ (CD1c+) and BDCA3+ (CD141+) myeloid DC, characterized their TLR expression and cytokine

response to TLR stimulation (Demedts et al., 2005), (Demedts et al., 2006). Interpreting their results with a current understanding of DC subsets, they do not appear to have identified true cDC1 and cDC2 fractions. Both fractions express CD14, suggesting monocyte-derived cells have not been excluded. High production of TNFα, IL1B and IL-6 when stimulating cDC1 with LPS and limited TNFα when stimulating cDC1 with poly-IC does not occur in studies with stringent cDC1 isolation (Haniffa et al., 2012). A contemporary study, which identified cDC2 more stringently as CD14-CD1c+ cells, found steady state expression of co-stimulatory ligand CD86 and allostimulatory capacity, contrasting this with pDC which produced IFNα on TLR7 ligation but did not stimulate T cells (Masten et al., 2006). Both studies were limited by use of 4-parameter flow cytometry, which does not allow sufficient antigens to identify and discriminate DC subsets.

More recent studies have leveraged multi-parameter flow cytometry to simultaneously identify lung MPs. Desch et al. used intrabronchial versus intravascular antibody staining to demonstrate that CD1a and CD206 are expressed on airway but not blood MP (Desch et al., 2016). Whole lobes were lavaged, principally yielding AM, then digested. Tissue monocytes (CD206+CD14+CD1c-CD1a-), monocyte-derived cells (CD206+CD14+CD1c+CD1a+/-) and pulmonary DC (CD206-CD14^{lo}CD1c+CD1a+) were identified. Cells expressing CD1c were most capable of stimulating allogeneic T cells, but the authors did not separate pulmonary DCs and monocyte-derived cells in these experiments. The study addressed the confounding influence of blood DC subsets on our understanding of lung tissue DCs in an innovative way. However, their approach left many questions about human lung DCs unanswered. Their definition of blood versus lung DCs was too stringent. Applying topical antibody to an intact bronchial tree may label a proportion of bronchial leukocytes but will not reach the interstitium. CD206-CD1a- DCs within the interstitium may therefore have been disregarded as blood DCs. By defining their own DC subsets, without reference to literature on DCs in human blood and other tissues, we are left struggling to align subsets across compartments. The absence of pDCs and cDC1 in lung tissue has not been explored. The assumption that CD206+CD14+CD1c/a+ cells are monocyte-derived is unfounded as CD14 is a labile antigen and cannot be used to presume monocyte derivation. Overall, it is not a solid foundation for discussing recruitment and fate of DCs in inflammation.

By defining lung DCs in line with blood DCs, Schlizter et al. and Yu et al. identified two subsets of myeloid DCs: CD141-expressing cDC1s and CD1c-expressing cDC2s in a 1:3 ratio (Schlitzer et al., 2013), (Yu et al., 2013). Their immune functions were explored by parallel studies in mice. The cDC1 subset was primarily interstitial, perhaps explaining why they were not identified by the approach of Desch et al (Yu et al., 2013). The cDC2s were closely associated with epithelial cells, and were instrumental in generating epithelial-adherent effector CD8 T cells (Yu et al., 2013). A role for cDC2s in producing a maximal Th17 response to *Aspergillus fumigatus* was identified (Schlitzer et al., 2013).

BAL is a commonly used clinical procedure to sample the lumen of the lower airways, most commonly for the identification of pathogens. BAL retrieves large numbers of AM and additional leukocytes in both steady state and inflammation. It provides a more relevant and compartmentalized view of the airway immune system than digesting lung tissue as only the cells exposed to the lumen are sampled. Early studies of DCs in human BAL have been constrained by the technical limitations of magnetic bead isolation or 4-parameter flow cytometry/ sorting, but have successfully identified allostimulatory cells (Havenith et al., 1994), (van Haarst et al., 1994). Both cDCs and pDCs have been noted, but further exploration has not been attempted (Bratke et al., 2007), (Lommatzsch et al., 2007), (Tsoumakidou et al., 2006), (Ten Berge et al., 2009).

In contrast to DC populations, AM are abundant in lung and readily distinguished. They express CD206 and CD169, whereas interstitial macrophages express CD206 but not CD169 (Bharat et al., 2016), (Yu et al., 2016). AM adhere to alveolar epithelial cells and are maintained in a quiescent state through local TGFβ production (Munger et al., 1999). They produce few inflammatory cytokines, suppress the activation of DCs and T cells (Thepen et al., 1989), (Strickland et al., 1996), and do not migrate or participate in antigen presentation (Lambrecht, 2006).

Monocytes have not been well characterized in human lung due to the confounding influence of large numbers of marginated blood monocytes in un-perfused tissue. When perfusion has been achieved, CD206+ monocytes expressing CD14 and variable CD16 have been identified (Desch et al., 2016). In the absence of perfusion, reported CD206- monocytes are probably intravascular (Bharat et al., 2016). In

steady state BAL, monocytes are predominantly CD14+CD16+, in contrast to blood, where classical monocytes dominate (Brittan et al., 2012). Classical monocytes most effectively migrate across non-pulmonary vascular endothelium (Collison et al., 2015), and the equivalent Ly6C^{hi} monocyte in mouse is the subset constitutively entering tissue (Jakubzick et al., 2013). CD16 acquisition by classical monocytes entering lung is therefore more likely than preferential recruitment of intermediate monocytes. CD16 is not readily up-regulated in co-culture of monocytes and human umbilical vein endothelial cells (HUVECs) (McGovern et al., 2014), but a specific effect of pulmonary vascular endothelium or lung tissue microenvironment may contribute. In murine lung, Ly6C^{hi} monocytes enter lung tissue during steady state without differentiating into macrophages or DCs (Jakubzick et al., 2013). This appears to be a unique feature of the lung, as monocytes entering skin or gut differentiate rapidly into macrophages (Jakubzick et al., 2013).

1.4.3 Lung mononuclear phagocytes in inflammation

In a bacterial model of rat tracheitis, DCs are recruited to the mucosa very rapidly (between 4-8 hours) (McWilliam et al., 1994). Bacteria applied to the skin or peritoneum do not induce rapid DC recruitment, suggesting this may be a unique feature of pulmonary mucosa. In humans with allergic asthma, allergen challenge induces a similarly rapid accumulation of DCs in the bronchial mucosa. These DCs have a cDC2 phenotype. The time-course of accumulation is in keeping with direct recruitment from blood rather than differentiation from a precursor (Jahnsen et al., 2001). In mice challenged with intratracheal house dust mite (HDM), both CD11b+ DCs (cDC2) and moDCs accumulate within 16 hours (Plantinga et al., 2013). While CD11b+ counts remain stable over the following days, moDC accumulation peaks at 3 days. CD11b+ DCs are capable of transporting antigen to draining lymph nodes at any antigen dose, but moDCs and CD103+ DCs (cDC1) transport antigen only at higher doses. Both CD11b+ DCs and moDCs favour Th1 polarization *in vitro*, and are capable of HDM-sensitization *in vitro*. MoDCs are more capable of monocyte and eosinophil recruitment to the airway (Plantinga et al., 2013). In the context of human allergic rhinitis, TLSP and Th2 cytokines inhibit CCR7 up-regulation and keep DCs in the tissue, where they interact with effector memory T cells (Melum et al., 2014).

LPS inhalation in humans recruits monocytes to the airspace (Brittan et al., 2012). In contrast to steady state monocyte-derived cells, inflammatory monocyte-derived cells are CD14+CD16-. Recruited monocyte-derived cells produce pro-inflammatory cytokines IL-6, IL-8 and TNFα (Brittan et al., 2014). They express lower levels macrophage markers than resident monocyte-derived cells (CD206, CD163), in keeping with more a recent derivation from monocytes.

1.5 Bone marrow transplantation

1.5.1 Autologous versus allogeneic transplant

Bone marrow transplantation (BMT) is a curative treatment for haematological malignancies, congenital haematological disorders and immunodeficiency syndromes. Two types of bone marrow transplant exist: autologous and allogeneic. In autologous BMT, stem cells are harvested prior to high dose chemotherapy and then reintroduced to salvage haematopoiesis. In allogeneic BMT, stem cells are harvested from an HLA-matched related or unrelated donor and introduced to a conditioned recipient. The indications for and complications of these two types of BMT differ substantially. This work concerns allogeneic BMT only.

1.5.2 Indications

The commonest indication for an allogeneic BMT in adults is acute myeloid leukemia (AML), constituting approximately 40% of transplants (Pasquini and Zhu, 2014). Acute lymphoblastic leukaemia (ALL), myelodysplastic syndromes (MDS) and lymphomas each account for approximately 10% of transplants. Less common indications include myeloma (MM), chronic myeloid or chronic lymphocytic leukaemias (CML/ CLL) and aplastic anaemia. The majority of patients approaching BMT will have been extensively pre-treated with variable combinations of chemotherapy, biological agents and radiotherapy- depending on disease type and risk stratification- in order to induce remission or reduce disease burden. Patients with bone marrow failure syndromes e.g. aplastic anaemia or MDS, typically approach BMT without prior chemotherapy but may have a history of chronic or

recurrent infections. The immunologic health of a patient prior to transplant reflects a combination of these factors: primary disease, pre-treatment and infection history.

1.5.3 *Donor selection*

HLA-compatible stem cells are sourced from a sibling or from an unrelated registry-listed donor. Use of unrelated donors now exceeds that of siblings (Pasquini and Zhu, 2014). Donors are screened at 6 HLA loci: HLA-A, B, C, DRB1, DQB1 and DPB1. Matching all alleles is preferable, but DP mismatches can be tolerated (Petersdorf et al., 1993). Choice of stem cell source (G-CSF mobilized peripheral blood stem cells or bone marrow harvest) currently rests with the donor, though the majority choose peripheral blood donation (Pasquini and Zhu, 2014). Alternative sources include umbilical cord and haplo-identical donors.

1.5.4 Conditioning

Conditioning for BMT has a dual purpose: to deplete residual disease and to immunocompromise the host sufficiently for donor stem cells to engraft (Gratwohl and Carreras, 2008). Historically, all BMT conditioning was myeloablative or 'full-intensity', relying on intensive chemotherapy and radiotherapy to fully immunocompromise the host. Approximately 6000 myeloblative transplants occur internationally each year and this figure has changed little in the past decade (Pasquini and Zhu, 2014). The number of reduced intensity (RIC) transplants has almost doubled in the past decade, with the biggest expansion in patients over 50 years old (Pasquini and Zhu, 2014). RIC transplants typically prepare the host with myelosuppresive chemotherapy in combination with immunomodulatory drugs such as Alemtuzumab (Campath) or Methotrexate (Gratwohl and Carreras, 2008). Early transplant-related toxicity is lower following RIC BMT (Deeg et al., 2006). As a result, RIC BMT has become an option for an increasing number of patients with comorbidities, older age and intermediate risk conditions.

1.5.5 Immune reconstitution

After stem cell infusion, recipients remain pancytopenic for approximately 14 days (Mackall C, et al., 2009). The first leukocytes detectable are monocytes. Neutrophil recovery follows. NK lymphocytes recover early but T and B lymphocytes remain

suppressed throughout the first year post-transplant (Mackall C, et al., 2009). In the RIC setting, some recipient haematopoiesis initially recovers. This results in mixed chimerism of bone marrow and peripheral blood leukocytes. Mixed chimerism more commonly affects the lymphocyte compartment than the granulocyte compartment (Mackall C, et al., 2009).

1.5.6 Graft-verus-leukaemia effect and Graft-versus-Host Disease

The successful outcome of BMT involves a balance of competing risks. Recurrence of primary disease is the greatest risk post-transplant: 37-48% of allogeneic BMT recipients die from relapsed disease (Pasquini and Zhu, 2014). Relapse is minimized when the donor immune system is competent to recognize disease-associated epitopes and generate graft-verus-leukaemia (GVL) immunosurveillance (Anasetti et al., 1990). However, a GVL-competent immune system is generally capable of recognizing host tissue epitopes. The resulting inflammation and tissue damage is known as graft-versus-host disease (GvHD) and is the major cause of non-relapse mortality (Pasquini and Zhu, 2014). While 18-20% BMT recipients die from GvHD directly, deaths from infection (13-17% recipients) and organ failure (4-6% recipients) are intrinsically linked to GvHD and its treatments (Pasquini and Zhu, 2014). Manipulation of the graft and the immune system post-BMT can alter the balance between GvHD and GvL in clinical practice. A key intervention that reduces GvHD is *in vivo* T cell depletion with Alemtuzumab or anti-thymocyte globulin (ATG) (Ho and Soiffer, 2001), (Alousi et al., 2013). Interventions that reduce relapse include immunosuppression withdrawal (Kekre et al., 2015), and donor lymphocyte infusion (DLI) (Roddie and Peggs, 2011).

1.5.7 Donor lymphocyte infusion

The strategy of T-cell depletion at the time of stem cell infusion combined with donor lymphocyte infusion six months later is common in UK transplant. It provides effective GvHD prophylaxis with the option to manipulate chimerism and GvL at a later date (Roddie and Peggs, 2011).

1.6 Graft-versus-Host Disease

1.6.1 Historical descriptions

In 1959, van Bekkum and colleagues noted that irradiated mice died if infused with bone marrow or splenocytes from another mouse (Van Bekkum et al., 1959). Death was not a result of the primary intervention (irradiation or cell infusion), but occurred 10-14 days later from a combination of weight loss, diarrhoea, skin changes and liver disturbance. They named this syndrome secondary disease. Parallels with GvHD following BMT in humans were noted. Billingham condensed the required elements for secondary disease/ GvHD into three criteria (Billingham, 1966). In the first, he stated that the infusion/ graft must contain immunologically active cells. In the second, he noted that the host must express tissue antigens not present in the donor. In the third, he emphasized the importance of the host having a compromised immune system, or else the infusion/ graft would be rejected. Half a century of immunology later, these criteria are still considered a true and comprehensive summary of GvHD requirements. Adding to the detail, the immunologically active cells within the graft were identified as mature donor T cells (Korngold and Sprent, 1978) and the tissue antigens were found to be MHC encoded in the most part (Krensky et al., 1990) with contributions from minor histocompatibility antigens (Korngold and Sprent, 1980), (Middleton et al., 1998).

1.6.2 Clinical descriptions

GvHD has acute and chronic presentations. Acute GvHD involves any combination of erythematous rash, watery diarrhoea and deranged liver function. Chronic GvHD has a broader constellation of symptoms, which may involve dry or sclerotic skin, dry mucous membranes (eyes, mouth, genitals), diarrhoea and respiratory compromise (Ferrara et al., 2009). Early descriptions stated that acute GvHD occurs within 100 days of BMT and chronic GvHD occurs after 100 days. A more recent description recognizes that the conditions may overlap and that acute GvHD can occur with later onset, for example following DLI (Filipovich et al., 2005) (Figure 1.3).

Figure 1.3 Overview of acute and chronic GvHD

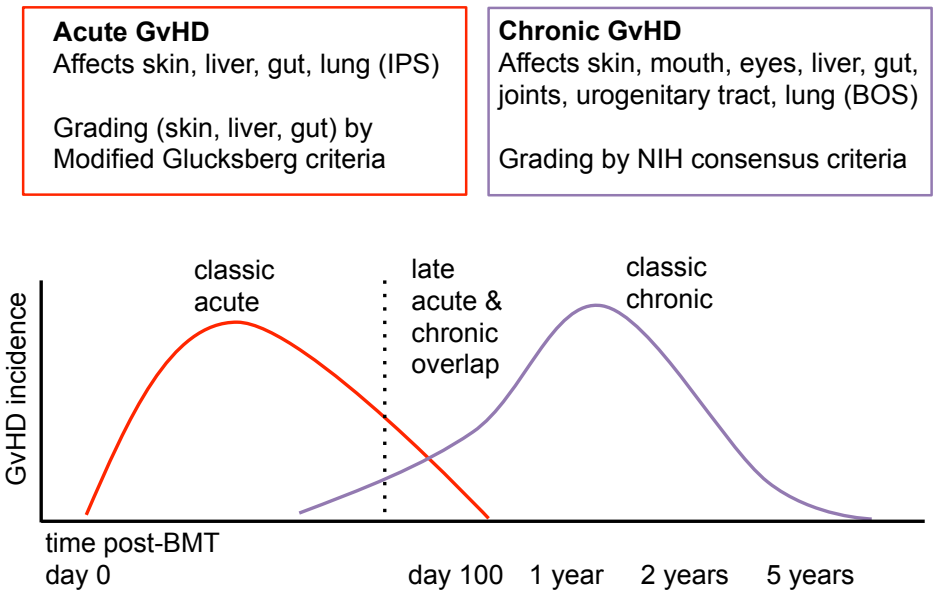

Figure 1.3 Overview of acute and chronic GvHD
Key tissue targets of acute and chronic GvHD and systems for grading the severity of tissue involvement. Schema of GvHD onset following BMT reproduced and modified from Pavletic and Fowler, 2012. IPS= idiopathic pneumonia syndrome; BOS= bronchiolitis obliterans syndrome.

The clinical severity of GvHD is graded according to modified Glucksberg criteria (Przepiorka et al., 1995), shown in Table 1.2. Importantly, clinical severity correlates with mortality (MacMillan et al., 2002), (Gratwohl et al., 1995)). Transplant-related mortality (TRM) of 28%, 27%, 68 and 92% has been reported for GvHD grades I-IV respectively (Gratwohl et al., 1995).

The incidence of acute GvHD in a 5000+ patient worldwide cohort is 39% in matched related donors and 59% in unrelated donors (severity grade I-IV) (Jagasia et al., 2012). In our centre, the incidence of acute GvHD ranges from 4% in matched related donors to 65% in unrelated donors (Jardine et al., 2015), (Green, K, personal communication). The incidence of severe acute GVHD (grades III/IV) is around 2% (Green, K, personal communication).

Table 1.2 Modified Glucksberg criteria for staging acute GvHD

Organ Stage			
	Skin (extent of rash)	**Liver** (serum bilirubin)	**Gut** (diarrhoea volume)
1	<25% body surface	34-50 µmol/L	500-100 mL
2	25-50% body surface	51-102 µmol/L	1000-1500mL
3	Generalized erythroderma	103-255 µmol/L	>1500mL
4	Erythroderma + blistering and desquamation	>255 µmol/L	Severe abdominal pain
Overall grade			
I	Skin stage 1-2		
II	Skin stage 1-3 Liver and or gut stage 1 Mild reduction in performance status		
III	Skin stage 2-3 Liver and or gut stage 2-3 Marked reduction in performance status		
IV	Skin stage 3-4 Liver and or gut stage 2-4 Extreme reduction in performance status		

Table 1.2 Modified Glucksberg criteria for staging acute GvHD
According to Glucksberg criteria, an organ stage (1-4) is applied to each of the key target organs of GvHD. An overall grade (I-IV) is then assigned according to the stage of involvement of each organ. Reproduced from (Apperley and Masszi, 2012).

The principal risk factor for developing acute GvHD is HLA disparity (Anasetti et al., 1990). HLA-being equal, unrelated donors typically incur a higher risk of GvHD than sibling donors (Flowers et al., 2011). Other risk factors less consistently reported include older recipient age, peripheral blood rather than bone marrow source of stem cells, female donors for male recipients, and prior alloimmunisation of donors (Anasetti et al., 1990), (Flowers et al., 2011). Transplant protocol has been shown to influence GvHD risk: higher intensity conditioning regimen and the use of total body irradiation increase risk, whereas *in vivo* T cell depletion reduces risk (Anasetti et al., 1990), (Flowers et al., 2011), (Remberger et al., 2008), (Soiffer et al., 2011). Post-BMT management is also risk-modifying, with dual agent prophylaxis (Remberger et al., 2008), protective isolation and gut decontamination conferring protection against GvHD (Storb et al., 1983) (Beelen et al., 1999).

A reliable method of predicting GvHD in a given patient, particularly predicting treatment-resistant GvHD, is being actively sought. Genetic polymorphisms in key components of the immune response, including IL-10 TNFα, IFNγ and IL-1, may

influence GvHD risk, though correlations have been inconsistent (Middleton et al., 1998), (Harris et al., 2013). Identifying incipient severe GvHD at an early stage through a combination of plasma biomarkers shows more promise and may allow clinicians to focus early interventions on high-risk patients (Levine et al., 2012).

1.6.3 Histological descriptions

Histologically, GvHD involves damage to the epithelia of target organs: the rete ridges of the epidermis, the crypts of intestinal mucosa and the ductal epithelium of the biliary tree (Sale et al., 1992), (Heymer, 2013).

Acute skin GvHD typically falls within a histopathological category termed acute lichenoid tissue reaction (LTR) or interface dermatitis (Sontheimer, 2009). Diseases in this category have epidermal basal cell injury and variable inflammatory infiltrate in the papillary and upper dermis. LTR infiltrates may include macrophages, DCs and T cells. LTRs with florid dermal infiltrate include lichen planus, lichenoid drug reactions and discoid lupus. Pauci-cellular LTRs include acute cutaneous lupus, erythema multiforme and acute GvHD (Sontheimer, 2009). Less commonly, acute GvHD has an eczematoid pattern of injury. In these cases, the mononuclear infiltrate is predominantly dermal and perivascular with less focus on the dermo-epidermal junction. In contrast to LTRs, there is less basal cell damage and more marked upper dermal oedema (Sloane et al., 1984). Sequential analysis suggests that eczematoid histology is a stable phenomenon within an individual rather than a transitional state towards an LTR (Thomas et al., 1984). By Lerner's criteria (see below), eczematoid changes can be difficult to diagnose as GvHD, but there is evidence of donor T cell dominance within lesions (Thomas et al., 1984) and fulminant progression (Creamer et al., 2007).

The relevance of detecting an inflammatory infiltrate in acute skin GvHD has been debated (Heymer, 2013). As donor T lymphocytes are considered the principal effector cell, some argue that a T cell infiltrate should be necessary for diagnosis. Other evidence suggests cytokines may be the principal effectors in some settings (Cohen, 1988), so detecting inflammatory cells may not be necessary. The inflammatory infiltrate is often sparser when biopsied early after the onset of rash. Additional variability in the degree of cytopenia and the extent of immunosuppression

can alter the degree of inflammatory infiltrate between patients (Heymer, 2013). The histological system for grading GvHD severity does not consider the inflammatory infiltrate. Lerner's classification, reproduced in Table 1.3 considers only the severity of damage to keratinocytes and the basal cell layer (Lerner et al., 1974), (Heymer, 2013). The changes in grades I and II are subtle and not pathognomonic, which risks inter-observer variability and misdiagnosis (Massi et al., 1999). Histological grading of GvHD does not correlate well with clinical severity and does not predict outcome (Ferrara and Deeg, 1991).

Table 1.3. Lerner's criteria for histopathological grading of acute skin GVHD

Grade	Histopathological description/ *plain language description*
I	Mild changes characterized by focal or diffuse vacuolar degeneration of epidermal basal cells and acanthocytes *Cells in the basal layer appear swollen and disconnected from each other*
II	Moderate changes, characterized by focal or diffuse spongiosis and eosinophilic degeneration (apopotosis) of scattered individual epidermal cells *Fluid accumulates around the epidermal cells. Some can be seen undergoing programmed cell death.*
III	Severe changes, characterized by separation of the dermo-epidermal junction and formation of clefts. *Fluid accumulation is more severe, causing separation of dermis from epidermis.*
IV	Maximal changes, characterized by extensive destruction and frank loss of epidermis. *Epidermis becomes separated from dermis and dies.*

Table 1.3. Lerner's criteria for histopathological grading of acute skin GVHD
Lerner's criteria classify the severity of skin damage in acute GvHD on a 4 point-scale based on histological features of skin biopsies. Reproduced and modified from Heymer, 2013.

Biopsy specimens of GvHD are routinely examined by haematoxylin and eosin staining without specific immunostains. However, the identity of infiltrating cells may add prognostic information and provide information about participating cell types in lesions. The presence of MHC class II-expressing cells in the infiltrate has been recognized for decades (Sloane et al., 1984). Use of a monoclonal antibody to the scavenger receptor CD163 has demonstrated macrophage-rich infiltration in more than a third of patients (Nishiwaki et al., 2009). While dermal DC content (by CD1a staining) and CD8 T cell content was not prognostic, having many macrophages predicted steroid resistance. Quantified as >200 macrophages per 4 fields at 200x magnification, macrophage-rich GvHD was significantly associated with worse survival (Nishiwaki et al., 2009). This association has been confirmed in a separate

cohort, although the sensitivity, specificity and positive predictive value were not sufficient to suggest clinical utility (Terakura et al., 2015).

1.6.4 Lung GvHD

The lung is not considered a principal target organ in acute GvHD because epithelial apoptosis does not occur (Sloane et al., 1983). However, alloreactive lung inflammation can be induced experimentally (Cooke et al., 1996), (Srinivasan et al., 2012) and clinical lung injury coincident with GvHD or DLI occurs in patients (Soubani and Pandya, 2010), (Nishie et al., 2016).

Clinically, alloreactive lung disease has been difficult to characterize. While the manifestations of skin or gut GvHD are usually clinically evident, alloreactive lung injury can be insidious and occur with distinct anatomical and clinical patterns (Soubani and Pandya, 2010). Three histopathological entities are seen: diffuse alveolar damage, organizing pneumonia and bronchiolitis (Xu et al., 2013). The bronchiolitis can be lymphocytic (with intraepithelial lymphocytes, eosinophils and perivasculitis) or may be constrictive (with fibrous thickening and obliteration of bronchioles) (Holbro et al., 2013). The constrictive appearance may represent a terminal stage of lymphocytic bronchiolitis, but no longitudinal studies have been performed to test this hypothesis. Such varying patterns of lung involvement lead to distinct clinical presentations. Diffuse alveolar damage presents as idiopathic pneumonia syndrome (IPS); organizing pneumonia presents as bronchiolitis obliterans organizing pneumonia/ cryptogenic organizing pneumonia (BOOP/ COP); and bronchiolitis presents as bronchiolitis obliterans syndrome (BOS). The clinical features of the three conditions are compared in Table 1.4. Accurate diagnosis of these conditions poses a major challenge.

The principal challenge is distinguishing between infection and GvHD. Diagnostic criteria for IPS and BOS require that bacterial, fungal and viral pathogens are reliably excluded (Panoskaltsis-Mortari et al., 2011). In practice, immunosuppressed BMT recipients are given prompt broad-spectrum antimicrobial treatment when infection is suspected. This reduces diagnostic yield from subsequent procedures such as BAL and makes accurate exclusion of infection difficult. Even when pathogens are detected, it does not exclude concurrent alloreactivity as superimposed infection is

seen in up to 50% of patients with BOS (Holbro et al., 2013). A clinical test for lung GvHD does not exist. Transbronchial biopsies are rarely performed in BMT recipients due to unacceptable risks. BAL is the safest window to the pulmonary immune system, but bronchoscopy/ BAL is not without risks in acutely unwell patients and cannot be performed if significant hypoxia is present. Interpreting the cytokine and cellular profiles of BAL is hampered by a lack of understanding about the effects of conditioning and BMT and an incomplete understanding of steady state lung immunology.

Table 1.4: Clinical features of pulmonary GVHD

	BOS	BOOP/COP	IPS
Incidence	1.7-26% [1]	1% [4]	2.2-15% [5]
Average onset post-BMT	1 year (median) [1]	108 days (median) [4]	19 days (median) [5]
Risk factors	Chronic GVHD [1, 2] Prior acute GVHD [1, 2] Immunosuppression without in vivo T cell depletion [1, 2] Busulfan based conditioning [1] Respiratory infection within 100 days post BMT [1, 2]	Acute GVHD Chronic GVHD Unrelated donor [1]	Full -intensity conditioning (with TBI) Acute GVHD Acute myeloid leukemia or myelodysplastic syndrome pre-BMT [5]
Clinical features	Non-productive cough, wheeze, dyspnea [1]	Non-productive cough, dyspnoea, fever (no wheeze) [1]	Cough, dyspnea, tachypnoea, hypoxaemia, crackles [5]
PFT	Obstructive (FEV1 <80% baseline) [1]	Restrictive, reduced lung volumes and DLCO possible [1]	Restrictive, reduced DLCO [5]
CT findings	Mosaic pattern of expiratory air trapping Bronchial wall thickening Bronchial dilation [1]	Migratory consolidation Subpleural and peribronchovascular distribution Nodules and ground glass opacity [1]	Multilobar infiltrates [5]
BAL	Neutrophilia or lymphocytosis [1]	Lymphocytosis with relative increase in CD8 T cells [1]	Nil consistent
Histology	2 groups: lymphocytic or constrictive bronchiolitis [3]	Organizing pneumonia [1]	Biopsy rarely performed Diffuse alveolar damage [5]
Treatment	Immunosuppression- often prednisolone + calcineurin inhibitor + mycophenylate mofetil [1]	Systemic steroid [4]	Antimicrobials (broad spectrum) Steroids Etanercept
Response/progression	Reversibility in lymphocytic histological subtype [3]	57% respond to steroid [4]	18% patients treated with steroid alone improve to allow ventilator wean; 53% in steroid+ etanercept [6]
Survival	3 year mortality 65% [1]	5 year mortality 69% [4]	60-80% mortality [5]

Table 1.4 Clinical features of pulmonary GvHD
The three diagnoses encompassed by the term 'pulmonary GvHD' have distinct clinical features. References: [1] Yoshihara et al., 2007, [2] Duque-Afonso et al., 2013, [3] Holbro et al., 2013, [4] Freudenberger et al., 2003, [5] Panoskaltsis-Mortari et al., 2011, [6] Tizon et al., 2012.

Current understanding of alloreactive lung disease comes primarily from animal models, with very few quality studies in humans. The most extensively reported IPS model is a complete MHC-mismatched murine BMT (Panoskaltsis-Mortari et al., 1997). Lung injury is T cell-dependent and associated with perivascular and peribronchiolar infiltrates of T cells (Th1 CD4 and CD8), and monocytes/

macrophages (Panoskaltsis-Mortari et al., 1997). A BOS-like pattern of injury can be achieved by delivering fewer T cells (Panoskaltsis-Mortari et al., 2007). While the chemokine and cytokine profiles of the IPS and BOS models do not differ, infiltrating MPs are recipient in IPS and donor in BOS (Panoskaltsis-Mortari et al., 1997), (Panoskaltsis-Mortari et al., 2007). In an MHC-matched, minor antigen-mismatched model with fractionated radiation to spare pulmonary toxicity, the pattern of injury and infiltration is similar (Cooke et al., 1996). LPS and TNFα are detectable in the BAL fluid.

Mice with GvHD outside the lung are more susceptible to developing lung-involvement following LPS inhalation (Cooke et al., 1996). This suggests that systemic GvHD confers vulnerability to a 'second hit'. Several studies have focused on LPS produced by translocated gut bacteria as the second hit (Nestel et al., 1992), (Cooke et al., 1996), (Cooke et al., 2000). The association between respiratory viral infection early after BMT and subsequent alloimmune lung injury suggests that other inflammatory stimuli may be capable of inducing damage (Versluys et al., 2010). Macrophage recognition of fungal polysaccharide α-mannan has recently been implicated in Th17 accumulation in lung and severe GvHD pathology (Uryu et al., 2015).

Human studies attempting to characterize lung GvHD have mainly reported BAL cytokines. Yanik et al. found elevated TNFα, soluble TNF receptors (TNFRI/ sTNFRII), IL-6, soluble CD14, lipopolysaccharide binding protein (LBP), IL-1 receptor antagonist, IL-8, MCP-1, and total protein at the onset of IPS (Yanik et al., 2008). Clark et al found elevated IL-1, IL-6, TNFα and LBP in a cohort of biopsy-confirmed IPS patients (Clark et al., 1999). Hauber et al compared BAL cytokines in lung infection and lung GvHD patients. TNFα and IL-18 did not discriminate between groups. Higher lymphocyte: neutrophil ratio and lower IL-10 correlated with IPS/ BOS (Hauber et al., 2002). The abundance of pro-inflammatory cytokines produced by MPs and MP-recruiting chemokine MCP-1 in BAL hints at the presence of MPs. Further high quality studies are required to deconvolute events and cellular players in post-BMT lung damage.

1.6.5 GvHD animal models

Many insights into the pathogenesis of GvHD have arisen from studying animal models. The advantages and limitations of these models deserve consideration before discussing GvHD pathogenesis in detail.

Mouse models of GvHD are widely used. They employ young, inbred mice housed in pathogen-free conditions. Using manipulation of specific genes, conditional depletion, labelling or tracing techniques, adoptive transfer and parabiosis experiments, rigorous hypothesis testing can be performed. Many mice can be transplanted in parallel, with *in vivo* tracing and sacrifice at various time-points giving insight into the dynamics of GvHD inflammation. Target organs in murine GvHD models show similar damage to affected human tissues (Markey et al., 2014b). HLA disparity in murine models affects the leukocytes involved in GvHD inflammation (Korngold and Sprent, 1985), (Korngold and Sprent, 1982). Minor antigen mismatched mouse models are more likely to reflect the type of inflammation seen in HLA-matched clinical BMT (Markey et al., 2014b).

Canine models of BMT have been valuable for studying therapeutics but are less readily scaled and manipulated than murine models.

Humans undergoing BMT tend to be older, sicker and exposed to a wide range of pathogens but, more importantly, undergo a procedure that is very different from a murine BMT. Murine BMTs use irradiation for conditioning. T cells or splenocytes are infused with the graft and post-BMT immunosuppression is not employed. Clinical BMT regimens are often radiation-free and T cell-depleted. The use of immunosuppressive medications targeting IL-2 (ciclosporin, tacrolimus) or purine biosynthesis (mycophenolate mofetil, methotrexate) is universal. While there is no dispute that murine models continue to provide unique mechanistic insight into GvHD, analysis of human tissues may reveal distinct pathways and cellular mediators operating in patients.

1.6.6 GvHD pathogenesis

Integrating insights from animal models with clinical data, Ferrara and Deeg have summarized the immune mechanisms underlying GvHD (Ferrara and Deeg, 1991) (Ferrara et al., 2009). Their model of GvHD induction recognizes three phases (Figure 1.4). In phase I, APCs are activated. In phase II, T cells are activated and in phase III, target organ damage occurs. Evidence in support of this model and areas of uncertainty pertaining to MPs will be discussed below.

Figure 1.4: Pathophysiology of acute GvHD

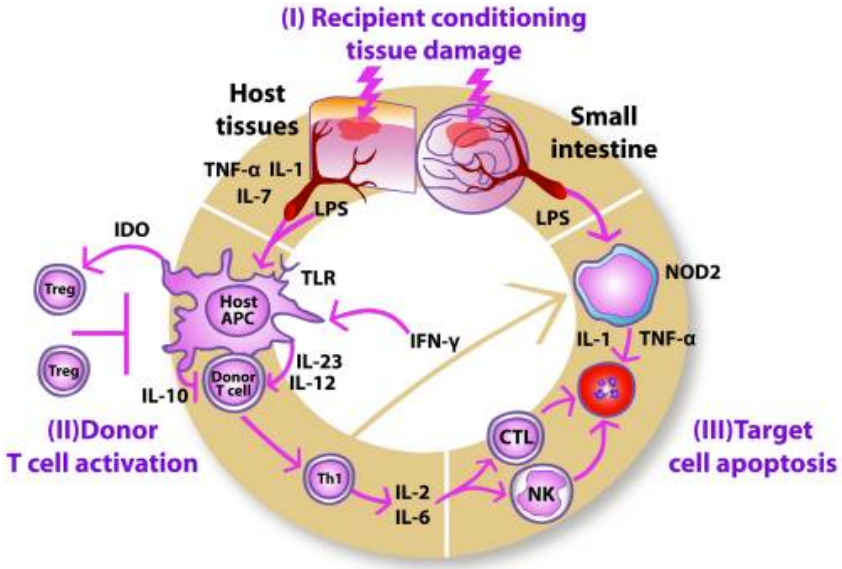

Figure 1.4 Pathophysiology of acute GvHD
Diagram of Ferrara's three stage model GvHD pathogenesis: I) damage to recipient tissues caused by BMT conditioning, II) activation of donor T cells by host APC and III) apoptosis of target cells by cytotoxic lymphocyte and cytokine activity. Image from Harris et al., 2013. IDO= indoleamine 2,3-dioxygenase; NOD2= nucleotide binding oligomerization domain containing 2 (a PRR); CTL= cytotoxic T lymphocyte; NK=natural killer lymphocyte.

APCs within tissues may be activated by PAMPs, endogenous danger signals and cytokines. Integrity of epithelial tissues, especially the gut, is damaged by intensive conditioning regimens (Hill et al., 1997), (Keefe et al., 2000). Damaged epithelial cells release alarmins and loss of barrier integrity can allow translocation of LPS and commensals across the mucosa (Zeiser et al., 2011), (Hill et al., 1997). Alteration to

gut commensal populations may also create a pro-inflammatory environment (Jenq et al., 2012). Activation of donor T cells has been demonstrated in gut draining lymph nodes (Murai et al., 2003). LPS entering the systemic circulation has the ability to activate APCs at distant sites, for example the lung (Nestel et al., 1992), (Cooke et al., 1996). TNFα, IL-1 and IL-6 in serum and colon are proportional to conditioning (Hill et al., 1997), (Xun et al., 1994). Cytokine production by innate lymphocytes may also tip the balance from mucosal protection to mucosal inflammation (Hanash et al., 2012). In summary, there is good evidence that BMT conditioning can provide an environment capable of stimulating APCs. The "cytokine storm" induced by irradiation and cyclophosphamide is likely to be less marked in RIC transplants. These transplants still incur a risk of GvHD. The "cytokine storm" cannot be an absolute requirement for GvHD induction as DLI, given more than six months after conditioning, is capable of inducing GvHD. In murine models where APC signal 1 is inhibited (MyD88-/-) and APC signal 2 cannot be conveyed (in CD40L-/-), GvHD may still be induced (Shlomchik, 2003).

During the second phase of GvHD induction, donor T cells reactive against host epitopes are activated and proliferate. In murine BMT models, splenocytes or purified T cells are infused alongside bone marrow and their distribution can be tracked. Donor T cells initially track to secondary lymphoid tissue (Beilhack et al., 2005), (Panoskaltsis-Mortari et al., 2004). Naïve donor T cells proliferate (Beilhack et al., 2005). Interaction with host APCs expressing co-stimulatory molecules and presenting host antigen are important triggers to this proliferation (Shlomchik et al., 1999). The type of T cells proliferating depends on the genetic backgrounds of the mice involved; with MHC I mismatches CD8 T cells are involved, with MHC II mismatches CD4 T cells are involved and with HLA-matched/ minor antigen-mismatched combinations both subsets are (Korngold and Sprent, 1985) (Korngold and Sprent, 1982). Importantly, effector memory T cells do not proliferate within secondary lymphoid tissue or migrate to GvHD target organs (Beilhack et al., 2005). Naïve CD4 T cell polarization is skewed towards Th1 generation in GvHD (Yi et al., 2009). The Th1 subset and its cytokines (IFNγ, IL-2 and TNFα) are most strongly implicated in gut GvHD (Yi et al., 2009), (Hill et al., 1997)) but Th17 and Th2 subsets may contribute to GvHD pathology in skin and lung (Yi et al., 2009). Donor Tregs are capable of suppressing GvHD, in part through production of IL-10 (Hoffmann et al., 2002). The insights from murine models in this second phase of GvHD induction are

particularly difficult to translate to human BMT. Rather than T cell infusion, many clinical BMTs involve T cell depletion with Alemtuzumab or ATG. The contribution of mature donor T cells to GvHD induction is likely to be less prominent. T cells emerge from new donor haematopoiesis at a very low level during the first year of transplant. In most transplanted adults, they encounter an involuted thymus and are constrained by IL-2 targeted immunosuppressive drugs. The conditions for T cell activation and proliferation are consequently rather different in patients. Cross-species interpretation aside, the details of T cell activation have been explored more fully than the details of the APCs they interact with. The role of APCs will be discussed in more detail below, but in the context of Ferrara's model of GvHD pathogenesis the following questions are raised. What cell types present antigen? Does all antigen presentation occur in secondary lymphoid tissue? Is there a role for non-migratory APCs, namely macrophages? Why does GvHD predominantly affect the skin if T cell priming occurs in gut draining lymph nodes? What is the relative contribution of host and donor APC? What is the relative contribution of resident APC and those recruited to tissue during inflammation?

In the final phase of GvHD pathogenesis, effector cells and soluble factors induce target organ damage. Trafficking of T cells out of secondary lymphoid tissue is an important step (Kim et al., 2003). Expression of chemokine receptors such as CCR2, CCR5 and CXCR3 allows T cells to respond to cytokine gradients and enter target tissues (Wysocki et al., 2005). Inflammation within target tissues may be required for optimal T cell recruitment (Chakraverty et al., 2006). CD8 T cells and their cytotoxic products (perforin, granzyme and Fas ligand) mediate tissue damage (Braun et al., 1996), (Baker et al., 1996). Soluble factors TNFα, nitric oxide and IFNγ can damage tissues directly (Piguet et al., 1987), (Garside et al., 1992), (Mowat, 1989). Neutralizing them can abolish GvHD (Teshima and Ferrara, 2002). Soluble factors are also important in modifying the effector functions of resident and recruited leukocytes. For example, IFNγ primes macrophages to produce TNFα in response to low levels of LPS (Nestel et al., 1992). The relative importance of cytotoxic T cells, soluble factors and accessory leukocytes depicted in Ferrara's scheme remains to be established in the human setting. Clinical trials suggest that interrupting a single aspect of the effector machinery, such as TNFα, CCR5 or IL-1, has limited capacity to reduce GvHD (Couriel et al., 2009), (Reshef et al., 2012), (Antin et al., 2002). Targeting accessory cells such as macrophages has only been attempted in murine

models to date (Alexander et al., 2014) but has the potential to inhibit multiple effector mechanisms simultaneously.

1.6.7 Mononuclear phagocyte turnover following BMT

Before considering the role of MPs in GvHD, the turnover of these cell types after BMT requires consideration.

Monocytes and DCs in blood and tissue are depleted by conditioning and are virtually absent for the first week after transplant (McGovern et al., 2014). Macrophages are reduced in number, but not entirely depleted. Recovery of classical monocytes is seen by about day 10, with pre-transplant levels rapidly achieved. Blood DCs and non-classical monocytes remain at lower numbers on day 14, either due to slower recovery or immunosuppression. CD14 MDM and DC populations in skin recover later than their blood counterparts. Like blood DCs, dermal DCs do not rapidly achieve pre-transplant levels (McGovern et al., 2014).

Following BMT, leukocytes transition from recipient to donor chimerism. MP turnover is not uniform across cell types or across tissues. GvHD inflammation is superimposed on this backdrop of transition.

Blood monocytes have the fastest transition to donor chimerism, reaching 100% by day 28 in myeloablative BMT (Auffermann-Gretzinger et al., 2002). Transition is slower after RIC, with only 10% donor chimerism at day 14 and 100% donor chimerism achieved by day 42 (Auffermann-Gretzinger et al., 2002). Blood DCs also turn over rapidly, with 100% donor chimerism achieved by day 28 in myeloablative and day 42 in RIC transplants (Auffermann-Gretzinger et al., 2002). Data from murine models suggests that recipient LCs can dominate for at least 2 months after BMT (Durakovic et al., 2006), (Merad et al., 2004). In a human transplant setting, turnover is more rapid, with >90% donor chimerism by 3 months post-BMT (Collin et al., 2006). Recipient LCs are present between 0 and 3 months. Their persistence is greater with RIC BMT and the absence of GvHD (Collin et al., 2006). Replacement of dermal DCs and CD14 MDMs is more rapid, with close to 100% donor chimerism at day 40 (Haniffa et al., 2009). Dermal macrophages are slowly replaced, with >10% recipient macrophages still present after 1 year (Haniffa et al., 2009).

While the fate of the human dermal APC compartment following BMT has been carefully mapped, data on turnover of lung APC subsets is scarce. Early work looking at AM chimerism in myeloablative BMT showed that donor-derived AM appear following transplant (Thomas et al., 1976). The dependence of this effect on conditioning (principally total body irradiation in this cohort) and the time course of reconstitution could not be determined. Murine studies suggest that AM have capacity to self-renew if conditioning radiation is administered in fractionated doses (Tarling et al., 1987). A small study in myeloablative BMT recipients demonstrated the proliferative capacity of AM, but a single sex-mismatched case showed that the proliferating population was donor-derived (Nakata et al., 1999). In this study, blood monocytes were 100% donor 40 days after BMT, whereas AM showed mixed chimerism beyond 80 days. The population dynamics of lung DCs have only been studied in rodents (Holt et al., 1994). Tracheal DC populations decline by 85% in the first 72 hours after dexamethasone treatment or x-irradiation. Donor cells repopulate the epithelium within 10 days. The turnover of parenchymal DCs (though not convincingly distinguished from AM) and LCs took longer than 15 days. Syngeneic mouse BMT models suggest that AM undergo functional changes as a result of BMT conditioning, with reduced capacity for phagocytosis and bacterial killing (Domingo-Gonzalez and Moore, 2013).

1.6.8 The role of mononuclear phagocytes in GvHD

The role of MPs as APCs in GvHD is well established. Antigen can be presented to donor T cells directly by host DCs (Shlomchik et al., 1999), (Duffner et al., 2004), LCs (Merad et al., 2004) or non-haematopoietic cells (Koyama et al., 2012). Donor APCs augment GvHD inflammation but are not required for its induction (Matte et al., 2004). Donor APCs can present exogenous host antigen on donor MHC class II to CD4 T cells or cross-present antigen via donor MHC class I to CD8 T cells. Alternatively, donor DC can “cross-dress” by acquiring intact membrane fragments from host cells including host MHC class I/ peptide complexes (Wakim and Bevan, 2011). In model settings, the contributions of cross-presentation and cross-dressing to antigen-specific T cell activation are variable (Wang et al., 2011), (Markey et al., 2014a). The role of these mechanisms in GvHD induction is predicted to be important at later time points post-BMT, when host APCs are abolished.

A role for inflammatory monocytes and macrophages in the effector phase of GvHD inflammation has been described. Macrophage production of IFNγ and TNFα can exacerbate tissue injury (Hill and Ferrara, 2000). Limiting macrophage accumulation with dexamethasone palmitate limited GvHD severity in a murine acute GvHD model (Nishiwaki et al., 2014). Targeting macrophages with CSF-1 antibody in an acute sclerodermatous GvHD model also reduced pathology (Alexander et al., 2014). The selective S1P1 receptor agonist CYM-5442 limited monocyte extravasation into skin and reduced GvHD severity in a murine model (Cheng et al., 2015).

Host macrophages may confer protection against GvHD by engulfing alloreactive donor T cells (Hashimoto et al., 2011), producing TGFβ and expanding Tregs (D'Aveni et al., 2015). Pre-transplant CSF-1 therapy to expand host macrophages reduced subsequent GvHD (Hashimoto et al., 2011). Immunoregulatory properties have also been ascribed to myeloid derived suppressor cells (MDSC) in GvHD (Wang et al., 2013). For example, a donor CD34+ population with mature monocyte properties killed IFNγ-producing T cells using nitric oxide (D'Aveni et al., 2015).

1.7 Experimental inflammation using lipopolysaccharide

1.7.1 Toll like receptors

Toll like receptors (TLRs) are a group of pattern recognition receptors that are evolutionarily conserved and recognize pathogen-specific epitopes. TLRs1-9 are relevant in humans (Beutler, 2009). TLRs1-2 and 4-6 are present in the plasma membrane and recognize bacterial, fungal and parasitic epitopes. TLRs3 and 7-9 are found within the endocytic compartment and recognize viral epitopes (Beutler, 2009). TLRs share common cell signaling pathways for activation of transcription factors such as NFkB and Interferon Regulatory Factors (IRFs). Pro-inflammatory cytokines and type I interferon are produced as a result.

1.7.2 Lipopolysaccharide

LPS is one of the most extensively characterized PAMPS. It requires detailed introduction because it is important to this thesis as a factor in the pathogenesis of GvHD and as a trigger for experimental inflammation.

LPS is a structural element in the outer membrane of Gram-negative bacteria. The molecule comprises a lipid membrane anchor (lipid A), an oligosaccharide core and a polysaccharide tail exposed on the bacterial surface (O antigen). Lipid A is the most immunogenic component (Lu et al., 2008). The LPS signal is transduced across target cell membranes by TLR4 (Poltorak et al., 1998) in complex with CD14 and two soluble factors: lipopolysaccharide binding protein (LBP) and MD-2/LY-96 (Lu et al., 2008). When occupied by LPS, TLR4 oligomerizes and binds an adaptor protein: either MyD88 or TRIF. The MyD88-dependent pathway culminates in activation of transcription factors IRF5, NF-κB and AP-1, resulting in pro-inflammatory cytokine gene transcription. The MyD88-independent pathway (TRIF pathway) activates IRF3, NF-κB and AP-1 and most characteristically induces type I interferons (Lu et al., 2008).

There is a sequential response to LPS in susceptible cells (Huang et al., 2012), (Raza et al., 2014). Primary response genes are activated between 0.5 and 2 hours after exposure. Genes include *Tnf* and *Ifnb1* encoding TNFα and IFNβ (Medzhitov and Horng, 2009). The transcription factors for these genes (NF-κB and IRFs) are poised for action in steady state and only require post-translation modifications such as phosphorylation and translocation to the nucleus (Medzhitov and Horng, 2009). Secondary response genes are activated between 2 and 8 hours after LPS exposure. The necessary transcription factors (ATF3, C/EBPδ) are induced as part of the primary response (Medzhitov and Horng, 2009). Responses to LPS are dose dependent, but additional signals, most notably interferon-γ (IFN-γ) can increase LPS sensitivity (Schroder et al., 2006).

Studies in animals with mutated TLR4, CD14 and signaling components have demonstrated the necessity of each for an inflammatory response to LPS (Poltorak et al., 1998), (Haziot et al., 1996), (Guha and Mackman, 2001). The susceptibility of a given cell population to LPS might then be predicted to depend on TLR4 and CD14

expression. While mRNA for TLR4 is present in most tissues, protein expression is restricted to haematopoietic tissues (Ponten et al., 2008). Amongst leukocytes, TLR4 expression is limited to MPs but may be up-regulated on neutrophils by inflammatory stimuli (Muzio et al., 2000). CD14 is primarily expressed on macrophages, monocytes and neutrophils but gradations of CD14 expression are seen on DCs, lymphocytes, basophils and non-leukocytes such as respiratory epithelial and endothelial cells (Jersmann, 2005). Low-level expression of CD14 in LPS-exposed sites such as the airway may function to minimize exaggerated inflammatory responses (Jersmann, 2005). CD14 lacks a transmembrane domain and can be cleaved from the surface of cells, yielding soluble CD14. The soluble form participates in LPS signaling in CD14 negative cells (Guha and Mackman, 2001), (Verhasselt et al., 1997). Thus, while CD14 and TLR4 expression are high in the well-studied LPS responsive cell types (monocytes and macrophages), the consequences of lower expression in other cell types are not fully understood.

At an organismal level, the response to *in vivo* LPS is highly species specific. Humans develop fever and cytokine release with 250ng intravenous LPS while laboratory mice can tolerate 500µg. Considering relative body weight, humans are approximately 10^5 fold more sensitive (Warren et al., 2010). Serum proteins are thought to underpin this difference, as *ex vivo* macrophages from both species are similarly responsive to LPS (Warren et al., 2010). LPS is capable of inducing a severe systemic inflammatory response even in the absence of pathogen (Taveira da Silva et al., 1993).

1.7.3 Experimental inflammation using LPS

LPS has been widely used in animal and human research to study mechanisms of acute inflammation. In human studies, intravenous LPS has been used to model sepsis and intrapulmonary LPS to model acute lung injury, occupational lung disease and asthma. Whether or not the models accurately reflect these diseases, they provide an opportunity to study early events in inflammation. LPS is generally considered a trigger for neutrophil influx but many of the additional events have been poorly characterized.

1.7.4 Human LPS inhalation studies

In human LPS inhalation models, doses of 20 to 100μg LPS have been delivered via nebulizer or inhalation chamber. These doses were selected to represent environmental LPS exposure during cotton manufacture (Sandstrom et al., 1992). Direct instillation of 4ng/kg LPS via bronchoscope (the dose used in intravenous studies) has also been reported (O'Grady et al., 2001). The administration method likely determines the tempo and character of the immune response. Direct instillation or nebulization provides bolus exposure whereas inhalation chambers deliver a dose over 30-60 minutes. All three methods may inoculate the bronchial mucosa rather than the alveolar space if improperly standardized and this is relevant as each compartment has a unique response (Moller et al., 2012).

Immune sequelae of pulmonary LPS exposure have been measured in the peripheral circulation and in the airway by BAL/ induced sputum. BAL is delivered to distal airways and samples the alveolar space while induced sputum samples the bronchial mucosa. Neither method involves penetrating the tight junctions of the airway mucosa, therefore mucosal surface rather than intraepithelial or interstitial immune cells are sampled. Induced sputum can be performed repeatedly without discomfort to the participant or precipitation of an inflammatory response. BAL is a more invasive technique. Transient leukocytosis and pyrexia are recognized consequences (Cohen and Batra, 1980). Repeated sampling would therefore be poorly tolerated and may alter the course of inflammation.

In the most comprehensive time-course of pulmonary LPS response, O'Grady et al. showed that neutrophil recruitment was maximal by 6 hours, while monocyte/ macrophage and lymphocyte recruitment occured between 6 and 12 hours (O'Grady et al., 2001). Pro-inflammatory cytokines and chemokines peaked between 6 and 12 hours. Most studies have performed bronchoscopy at 6-8 hours. As O'Grady et al. have demonstrated, this captures the neutrophilic phase of inflammation better than the mononuclear cell infiltrate.

Existing data consistently find neutrophils scarce in steady state BAL (650 cells/ml in Brittan et al., 2012) but 100-fold more abundant 6 hours after LPS inhalation (Sandstrom et al., 1992), (Maris et al., 2005), (Brittan et al., 2012). BAL lymphocytes

may be approximately doubled (Sandstrom et al., 1992), although some studies find no increment (Maris et al., 2005). With the exception of Brittan et al, all studies have determined BAL composition by microscopy and differential cell count. This makes for a crude assessment of MP repertoire. Brittan et al used 5-parameter flow cytometry to distinguish AM and two populations of pulmonary monocyte-like cells in BAL (Brittan et al., 2012). Compared with saline inhalation, LPS inhalation resulted in 8 times more CD14+CD16- monocytes in BAL (Brittan et al., 2012). CD14+CD16+ monocyte counts were consistent between LPS and saline and AM counts were not reported. This led the authors to consider CD14+CD16- monocytes an 'inducible' population, possibly recruited from blood classical monocytes. Airspace DCs have not been examined following LPS inhalation. Alexis et al. proposed that airway monocytes differentiated into DCs following LPS inhalation though presented no convincing evidence in support of this (Alexis et al., 2005).

1.8 Scope of the thesis

This work examines inflammation relevant to acute GvHD in the skin and lung. Only human tissue is used. MPs are central to this investigation. Tissue and blood MPs receive specific attention. Bone marrow and lymphoid tissue counterparts will be considered but not examined. The focus will therefore be on the diversity of MPs in inflamed skin and lung and their *in situ* functions, such as cytokine production and interactions with mature lymphocytes.

Two contrasting approaches are employed to manage the logistic and scientific difficulties of studying GvHD in skin and lung. In the skin, studying GvHD-affected tissues is tractable: tissue can be sampled shortly after presentation and before treatment, BMT recipients will volunteer control biopsies, and the incidence is high enough to yield necessary samples. Furthermore, we understand the MPS of the human skin in steady state sufficiently to interpret our findings.

In the lung, obtaining GvHD-affected material is difficult. Our clinical protocols indicate bronchoscopy and BAL in suspected lung GvHD, but delays in sampling are common. The clinical presentation may be insidious, multiple treatments may be attempted prior to sampling and patients may be too unwell for safe bronchoscopy.

Compounding these difficulties, the incidence of lung GvHD is relatively low. The greatest barrier to studying MPs in lung GvHD, however, is an inadequate understanding of the MPS in human lung. I have therefore focused attention on trying to bridge this knowledge gap by studying MPs in BAL during steady state, and following experimental acute inflammation produced by LPS inhalation. LPS inhalation is not intended as a model for lung GvHD, but does provide a starting point for MP characterization in acute inflammation with a clearly timed and controllable inflammatory insult. Insights from this model will inform more comprehensive studies of lung GvHD in the future.

1.9 Hypotheses and aims

1.9.1 Hypotheses

1) The MP repertoire in inflamed tissues will be altered
2) Inflammatory MPs derived from monocytes will be found in inflamed tissue
3) Tissue MPs will perpetuate the damage mediated by T lymphocytes in GvHD

1.9.2 General aims

In the skin strand of this work, I aim to define the MP composition of GvHD lesional skin. Through comparisons with steady state populations, I will characterize the inflammatory skin MP populations in terms of phenotype, gene expression and function. I will gather evidence to support/ refute the hypothesis that inflammatory MPs are monocyte-derived.

In the lung strand, I aim to define the MP composition of BAL in steady state and in response to LPS inhalation. Again, steady state populations will be used as a platform for characterizing inflammatory MPs in terms of phenotype, gene expression and function. BAL will be paired with serial blood samples to examine the temporal dynamics of blood MPs in response to tissue inflammation.

Each of the following chapters has a specific and detailed research aim, which is informed by the results of preceding investigation.

Chapter 2: Materials and methods

This chapter details general materials and methods used in multiple results chapters. Specific materials and methods tailored to each set of experimental aims are given in the results chapters. With this organization, details of the samples, ethics, processing and analysis techniques are proximal to the data presented.

2.1 General cell culture methods

2.1.1 Cell counting

Cells to be counted were re-suspended in a known volume of medium or phosphate buffered saline (PBS). Ten microlitres of cell suspension and 10µl 0.4% Trypan Blue were thoroughly mixed in a plastic cuvette and 10µl was transferred to a haemocytometer. Mean counts of live and dead cells were recorded from 5 squares (4 corners and centre). The number of cells per ml was calculated by the formula: Cells/ ml= mean cell count x dilution factor x 10^4

2.1.2 Freezing and thawing cells

Cells to be cryopreserved were pelleted by centrifugation at 500g for 5 minutes. All supernatant was completely aspirated. The pellet was re-suspended in 1ml 4°C freezing solution (Table 2.3) per 10^7 cells and rapidly transferred to labelled cryopreservation tubes. Tubes were wrapped in bubble plastic, stored at -80°C for 24-48 hours, then removed from plastic and transferred to -140°C for long-term storage.

In preparation for thawing, 15ml RF10 (Table 2.3) per sample were warmed to 37°C in polypropylene tubes. Cryopreservation vials were taken from the freezer and placed on ice. Samples were thawed by immersion in the water bath (37°C). In a class II Safety Cabinet, the thawed samples were rapidly transferred into the warmed medium and the sample tube rinsed with medium to collect all residual cells. Samples were pelleted by centrifugation (5 minutes at 500g) and the supernatant was discarded.

2.2 Cell isolation

2.2.1 Peripheral blood mononuclear cell (PBMC) isolation

Blood was collected into tubes containing Ethylenediaminetetraacetic acid (EDTA) and diluted 1:1 with room temperature PBS before layering over 15ml Lymphoprep™. All centrifugation steps were performed at room temperature. Centrifugation for 15 minutes at 800g with half-maximal acceleration/ braking yielded a mononuclear cell layer. The layer was gently aspirated with a Pasteur pipette and transferred to another tube for two washing steps. In the first, the tube was filled with 4°C PBS and centrifuged at 500g for 5 minutes to remove residual Lymphoprep™. In the second, the pellet was re-suspended, the tube filled with 4°C PBS and centrifuged at 300g for 7 minutes to remove platelets. Finally, the pellet was re-suspended in 1ml red blood cell (RBC) lysis buffer (Table 2.3) and incubated at room temperature for 10 minutes in the dark. The remaining mononuclear cells were washed with 4°C PBS and centrifuged at 500g for 5 minutes.

2.2.2 Magnetic bead isolation

A CD14 positive-selection kit was used to isolate monocytes (Miltenyi, 130-050-201). The PBMC pellet was re-suspended in 400µl 4°C sort buffer, mixed with 100µl positive selection beads per 50 $x10^6$ cells, and incubated at 4°C for 20 minutes. Unbound antibody was removed by addition of 10ml sort buffer, centrifugation (500g for 5 minutes), and removal of the supernatant. Cells were re-suspended in 500µl sort buffer and applied to an MS column within a magnet. The column was washed 3 times with 500µl sort buffer. CD14+ cells remained adhered to the column. Following removal from the magnet, 1ml PBS was flushed through to the column to release monocytes. Monocytes were cryopreserved, used in functional studies or differentiated in culture.

2.2.3 Immuno-density negative selection

Two immuno-density negative selection kits were used to isolate T lymphocytes (Human T cell enrichment cocktail, Stemcell 15021 and Human CD4+ T cell enrichment cocktail, Stemcell, 15022). This method uses tetrameric antibodies to

cross-link unwanted leukocyte populations to red cells. During density centrifugation, immune complexes are drawn into the red cell layer, leaving T cells at the interface. When performed on leukocyte cones, this was an economical method of isolating large numbers of un-stimulated T cells. Aliquots from the same preparation could be cryopreserved to allow consistency across T cell stimulation assays.

Leukocyte cones were obtained from the local NHS Blood and Transplant processing centre within 24 hours of collection. Cones were diluted with 45ml PBS and incubated with 50µl enrichment cocktail per ml cone for 20 minutes at room temperature. A further 1:4 dilution in PBS was used before density centrifugation. The T cell layer was removed and washed as described above. Aliquots of $5x10^5$ T cells were cryopreserved for functional studies.

2.2.4 Fluorescence activated cell sorting

Fluorescence activated cell sorting (FACS/ sorting) allowed the simultaneous isolation of up to 4 populations from preparations as small as $5x10^4$ cells. The use of up to 17 fluorescence parameters allowed fine control of the immunophenotype and purity of sorted populations. This method was invaluable for isolating MP subsets from blood and tissue.

Cells to be sorted were filtered through a sterile 100micron filter into a polypropylene FACS tube and washed in sort buffer (Table 2.3) (3ml 4°C sort buffer and centrifugation for 5 minutes and 500g). Cell pellets with fewer than $1x10^6$ cells were re-suspended in 100µl sort buffer. Larger samples were re-suspended at $1x10^7$ cells per 100µl sort buffer. Non-specific antibody binding was reduced by pre-incubation with 3µl 10% mouse IgG at 4°C for 10 minutes. Antibodies were added as per sort panels (detailed in results chapters), incubated at 4°C for 30 minutes and protected from light. Samples were washed with 3ml 4°C sort buffer and centrifuged for 5 minutes at 500g. Cell pellets were re-suspended at approximately $1x10^7$ cells per ml in sort buffer and kept on ice. Large samples from tissue isolates were passed through a 100micron filter immediately prior to sorting.

Sorting prior to June 2014 was performed on a 4-laser BD FACS Aria II. After June 2014, a 5-laser FACS Fusion running FACSDiva version 7 was used. Quality control

was verified daily by core facility staff. Sort panels were set up as detailed in section 2.3.3.

The 85micron nozzle was used for blood sorts and the 100micron nozzle used for all tissue sorts. As standard, the 1.5 neutral density filter was used in front of the forward scatter detector. With lung isolates the 2.0 filter was used in order to limit the intensity of scatter from alveolar macrophages. Stream alignment into the collection tubes was verified. Drop delay of the stream was set using Accudrop beads (BD, 345249). For 2-way sorts, a purity mask was selected for sort decisions and for 4-way sorts a 0-32-0 mask was used.

Cells were collected into 5ml polypropylene FACS tubes containing 3ml RF10. The collection tube holder was cooled to 4°C. The sort was paused and the drop delay reset if a deviation of more than 10 pixels occurred during sorting. This ensured that accurate sort decisions could be made.

2.3 Flow cytometry

2.3.1 Sample preparation

Cells for analysis were added to polystyrene FACS tubes, washed with 1-3ml flow buffer (Table 2.3) and centrifuged at 500g for 5 minutes. All remaining supernatant was aspirated and the pellet vortexed to re-suspend the cells. Non-specific antibody binding was blocked with mouse immunoglobulin for 10 minutes at 4°C. Antibodies were added for 30 minutes at 4°C. The sample was washed with flow buffer and re-suspended in 150-500µl flow buffer. DAPI was used for dead cell discrimination and was added at a 1in10 dilution shortly before data acquisition.

2.3.2 Intracellular staining

Intracellular staining was used to detect cytokines and the cytoplasmic molecule S100A8/9. Cell pellets were re-suspended in 150µl fixation/ permeabilization buffer (BD 554714) and incubated for 30 minutes at 4°C. Cells were washed with 1ml 4°C PermWash (BD 554714) and centrifuged at 500g for 5 min. Cell pellets were stained

with relevant antibodies as above and washed again with 1ml 4°C PermWash. Cells were re-suspended in 150-500µl PermWash for analysis.

2.3.3 CFSE labelling

T cell proliferation was quantified in mixed leukocyte reactions using the CFSE dilution method. This fluorescent ester readily crosses cell membranes but is subject to activity of intracellular esterases. Enzymatic activity cleaves the carboxyfluorescein molecule and prevents its egress from the cell. Each time cell division occurs, the fluorescent molecules are split between daughter cells and the fluorescence intensity is halved.

Cells were re-suspended in 50µl PBS and labelled with 1µM CFSE (Invitrogen) during a 10-minute incubation at 37°C. Enzymatic activity was terminated by adding cold RF10. CFSE-labelled cells were washed and recounted before use in functional studies.

2.3.4 Antibody panel design and setup

Where possible, antibodies were selected to maximize sensitivity. In general, the most weakly expressed or rarest antigens were assigned a bright fluorochrome e.g. phycoerythrin (PE) or PE tandems. Antibodies were selected to minimize spectral overlap into channels requiring high sensitivity (Maecker et al., 2004). For example, when using allophycocyanin (APC) to detect a subtle change in activation status such as HLA-DR expression on T-cell, it would not be optimal to use CD3 Alexa Fluor® A700 as its spillover into APC is considerable.

Voltages were decided using single-antibody stained cells. The aim was to achieve adequate separation of positive and negative populations and minimize spectral overlap. Next, positive and negative compensation beads labelled with each antibody were acquired. The automatic compensation function of FACSDIVA was used to calculate a compensation matrix.

Effort was made to keep panels consistent for similar samples throughout the thesis. Repeating setup and compensation was necessary at least once for each panel due

to upgrade and repair of instruments. Panels were revised when interim analyses or insights from literature strongly suggested that revision would provide new information.

2.3.5 Controls

Specific antigen expression was assessed by comparison with isotype or fluorescence-minus-one (FMO) controls. An FMO control contains every antibody in the panel except the one being controlled for. Both FMO and isotype controls are accepted methods of defining what is positive staining (Roederer, 2011). When isotype controls were used, the concentration of isotype was matched to the protein concentration of the test antibody.

2.3.6 Instruments, quality control and analysis

Data were acquired on 2 or 3-laser BD FACS Cantos, a 5-laser BD LSRII or 5-laser BD Fortessa X20, all running FACSDIVA version 7. Quality control was verified daily by core facility staff. Data analysis was performed with FlowJo version 9.5.2 (TreeStar).

2.4 Microscopy

2.4.1 Cytospin slide preparation

Cells in suspension were applied to slides by centrifugation (Cytospin) to view morphology or use in fluorescence microscopy experiments. Slides were prepared from single cell suspensions using a Thermo Cytospin^{TM} 4 cytocentrifuge and Shandon^{TM} coated slides (Thermo, 5991059). Up to $5x10^4$ cells were prepared in 100-200µl RF10, added to a funnel and centrifuged for 10 minutes at 500g. Slides were carefully removed, dried at room temperature, then fixed and stored as required for downstream application.

2.4.2 May-Grünwald Giemsa (Giemsa) staining

Samples for morphological inspection were stained with Giemsa. Cytospin slides were fixed with 100% methanol for 2 minutes. Automated staining was performed on an Advia S60 Autoslide System using Hematek Wright-Giemsa stain packs (Sigma). Coverslips were mounted with a mixture of distyrene, plasticizer and xylene (DPX) prior to microscopy.

2.4.3 Fluorescence in situ hybridization (FISH)

Cytospin slides were stored at -20°C and processed in batches. Slides were thawed at 4°C for 30 minutes, then fixed with 4°C 100% methanol for 2 minutes. Slides were fixed a second time in Carnoy's solution (3:1 methanol: acetic acid) for 5 minutes. A fluorescent probe mixture was applied to the slide and the coverslip was sealed with rubber glue. The sample and probe were denatured and hybridized on a ThermoBrite system (Abbott). After removing the coverslip, slides were washed in 0.4x saline sodium citrate for 2 minutes at 72°C, and rinsed in 2x saline sodium citrate with 0.1% NP-40 for 30 seconds at room temperature. Slides were mounted with DAPI anti-fade at least 30 minutes prior to microscopy.

Two FISH kits were used. Abbott's chromosome enumeration probes targeted X chromosome locus Xp11.1-q11.1 and Y chromosome locus Yq12. Probes were conjugated to SpectrumOrange (X) and SpectrumGreen (Y) fluorophores (Abbott, 07J22-050). Cytocell's dual labeled probe sets targeted the same regions and were conjugated to a green fluorophore (X) and a red fluorophore (Y) (Cytocell, LPE 0XYq).

2.4.4 Microscope

Slides were visualized on a Zeiss Axioimager II using AxioVision software.

2.5 Detection of secreted cytokines

Two methods for detecting cytokines in solution were used. Cytokine bead array (CBA) was used to detect a small set of inflammatory cytokines. Multiplexed enzyme-linked immunosorbant assay (ELISA) (Luminex®) provided a more streamlined workflow when a larger number of analytes were required. Both techniques employ specific cytokine-directed antibodies conjugated to beads and use small volumes of sample (50µl). In CBA, the capture beads are combined with detection beads to generate complexes with specific fluorescence properties. A flow cytometer such as a BD FACS Canto II is used for data acquisition. Position on a 2D flow cytometry plot determines the identity of the analyte and the fluorescence intensity is used to infer concentration. A Luminex assay is similar, except that beads are magnetic and reactions are performed in a 96-well plate. A set of biotinylated detection antibodies binds streptavidin PE. A Luminex dual laser analyser is required to assess bead position and fluorescence intensity. In both methods, analyte concentration is determined with reference to a standard curve.

2.5.1 Cytokine bead array

Concentrations of TNF, IL-1β, IL-6, IL-8, IL-10 and IL-12p70 were measured using the BD Human Inflammatory Cytokine CBA kit (BD, cat. 551811). Supernatants were thawed to room temperature and diluted 1in5 with assay buffer. Dilutions of standards were prepared as per the manufacturers instructions. FACS tubes containing well-mixed capture beads were prepared for each standard concentration and all unknowns. Supernatants/ standards and then PE-detection reagent were added to all tubes. The samples were incubated in the dark at room temperature for 3 hours, and washed before acquisition. Data were acquired on a BD FACS Canto, recording a minimum of 200 events per analyte. Data were imported into BD FCAPArray software version 2 for analysis. Standard curves and bead counts were inspected and concentrations derived from the standard curve were exported into Microscoft Excel.

2.5.2 Multiplexed ELISA (Luminex)

A multiplexed ELISA was used to simultaneously assess 34 cytokines and chemokines within a single sample (ProcartaPlex™ 34-plex, EBioscience) (Table 2.1). Capture antibody-conjugated beads were applied to a 96 well plate. A titration of standards was prepared according to the manufacturers instructions. For tissue culture supernatants, standards were diluted in RF10. For BAL fluid, standards were diluted in universal assay buffer. Standards and samples were added to the plate in duplicate or as neat and 1in10 dilutions. The plate was incubated at room temperature for 2 hours on a shaker (500rpm). Biotinylated detection antibodies, then streptavidin PE were applied for 30 minutes each, with wash steps following each incubation. Magnetic beads were re-suspended by shaking the plate for 5 minutes at 500rpm. Captured analytes were detected on a Qiagen Liquichip 200 running Luminex 100 integrated system software version 2.3. Procartaplex Analyst version 1.0 was used to define standard curves and interpolate analyte concentrations.

Table 2.1. Cytokines and chemokines detected with the EBioscience ProcartaPlex Immunoassay (34-plex)

Cytokines	Cytokines ctd.	Chemokines/ growth factors
IFNα	IL9	IL8
IFNγ	IL10	Eotaxin
TNFα	IL12p70	GROα (CXCL1)
TNFβ	IL13	IP-10 (CXCL10)
IL1α	IL15	MCP-1 (CCL2)
IL1β	IL17A	MIP-1α (CCL3)
IL1RA	IL18	MIP-1β (CCL4)
IL2	IL21	RANTES (CCL5)
IL4	IL22	SDF-1α (CXCL12)
IL5	IL23	GM-CSF
IL6	IL27	
IL7	IL31	

2.6 NanoString gene expression analysis

Gene expression analysis has become commonplace in the study of MPs. Numerous groups have demonstrated that MP subsets have distinct gene expression signatures and that signatures are conserved between species (Vu Manh et al., 2015). The combination of surface phenotyping, analysis of signature-gene expression and functional characterization is considered the most robust approach to studying MPs (Vu Manh et al., 2015). Gene expression data for this work were generated by NanoString.

2.6.1 Overview of the technology

NanoString nCounter® technology detects a set of messenger ribonucleic acids (mRNAs) within a sample. Analysis is multiplexed, allowing simultaneous detection of up to 800 mRNAs. For each mRNA, 50-base capture and detection probes are designed. Following hybridization, the capture probes allow the mRNAs to be immobilized on a cartridge. The detection probes contain individual barcodes to identify the mRNA. Barcodes are digitally imaged giving a direct count of mRNA molecules per sample.

The technology was chosen for this work as it can generate gene expression data from a small amount of starting material (<100ng total RNA). Measurements offer similar sensitivity to real-time polymerase chain reaction (PCR) and better sensitivity than microarray. Unlike real-time PCR, measurements are direct and free from amplification bias (Geiss et al., 2008). A sufficient number of genes are included to make clustering techniques developed for microarray plausible (Green K, unpublished communication). However the data sets are not so large that they require specialist programming knowledge to manipulate. One limitation of NanoString is that mRNAs are user-selected. Unlike RNA sequencing, which offers an unbiased snapshot of all gene transcripts, NanoString can only detect what the experimenter asks it to.

2.6.2 Panel composition

Two panels were used in this work: an off-the-shelf Human Immunology v 2 panel and a custom modification of this panel ("panel plus").

The Human Immunology v 2 panel contained 579 genes related to immunology. The panel plus contained the same 579 genes and an additional 30 genes relevant to differentiating MP subsets (Table 2.2). The 30 genes were selected based on microarray data published by our group (Haniffa et al., 2012). Kile Green, Muzlifah Haniffa and Venetia Bigley determined the panel plus composition.

Both panels incorporated controls: 8 negative controls, 6 positive controls spanning a range of concentrations and an additional 15 housekeeping genes.

2.6.3 Sample preparation

FACS sorted leukocytes were pelleted by centrifugation at 8000g for 4 minutes in 1.5ml eppendorf tubes. Buffer was completely aspirated and the pellet stored at -80°C for up to 2 years. RNA was released by thawing pellets, adding RNA lysis buffer, pipetting vigorously and vortexing for 30 seconds. The quantity of RNA lysis buffer for each sample was adjusted to yield up to $1x10^4$ cells in 5µl.

2.6.4 Hybridization and detection

Reactions were performed in 12-tube PCR strips. First, 5µl of each sample was added. Next, a master-mix containing detection probes and hybridization buffer was prepared and 20µl used for each reaction. Finally, 5µl capture probe per tube was added. Samples were mixed by inversion only and centrifuged at speeds lower than 1000g to avoid shearing the probes. PCR strips were added to a thermocycler set to 65°C for 12 to 30 hours.

After hybridization, 12 samples at a time were processed using the NanoString Prep Station. Cartridges were read on a NanoString Digital Analyzer to yield a Reporter Code Count (RCC) data set.

2.6.5 Quality control and data normalization

Raw data were imported into nSolver Analysis software version 2.0. Background correction subtracted the mean of 8 negative controls from each probe count. A positive control normalization factor was computed from the geometric mean of 6 positive controls. This controlled for differences in technical variables across the samples e.g. hybridization and binding efficiency, but not for differences in RNA input. A housekeeping gene content normalization factor was computed from the geometric mean of 15 housekeeping genes. This controlled for differences in RNA input between samples. Samples outside the normalization factor ranges (0.3-3 for positive control and 0.1-10 for housekeeping gene content) were flagged for further examination. Samples outside the positive control ranges were not encountered. Samples with high content normalization factors were seen when sample input was low. Typically, samples with factors >10 were outliers in further analysis. These were either excluded or re-normalized and analyzed with reference to other low-input samples only.

2.7 Statistical methods

2.7.1 Comparing means and distributions

Normality of data distribution was verified using the D'Agostino-Pearson test. For normal data, unless otherwise-stated, up to two means were compared with two-tailed unpaired t-tests. More than two means were compared with one-way ANOVA. Post-test comparison methods varied with the experimental design e.g. comparing 3 different controls to GvHD used the Dunnett test, comparing everything with everything used the Tukey test. Multiple comparison corrections are inbuilt with these methods.

For data with a non-Gaussian distribution, Mann-Whitney test was used to compare the means of up to two ranks. Non-parametric ANOVA used Dunn's multiple comparisons test.

For categorical outcomes, event counts were entered into contingency tables. The observed distribution was compared with the expected using Fisher's exact test and a two-tail p-value.

A p-value of less than 0.05 was deemed statistically significant, but significance was considered within the remit of each experiment. These analyses were performed using GraphPad Prism version 6.0.

2.7.2 Dimension-reduction and clustering

Dimension-reduction techniques are useful both to check for outliers and to identify patterns in gene expression. Two techniques were used in this work: Principal Components Analysis (PCA) and Hierarchical Clustering. Both were performed using MultiExperiment Viewer software version 4.8 (Saeed et al., 2003). Data sets were log2 transformed prior to analysis.

2.7.3 Gene-set enrichment analysis

Gene-set enrichment analysis is a means of testing whether a defined set of genes is better represented in one sample or another. For this work, gene sets were generated with the GeneSign function of BubbleGUM (Spinelli L, BM Genomics 2015). The BubbleMap function was used to test relative enrichment between pairs of samples.

2.7.4 Functional annotation

Standard descriptions of gene functions have been created by the Gene Ontology Consortium. A wide variety of tools are available for assigning these "GO terms" to a set of query genes. GeneMania was selected for this work as it has an accessible web-based interface and a capacity to expand query genes with predicted pathway partners (Mostafavi et al., 2008). This is a useful feature with a NanoString data set as not all potentially relevant genes are sampled.

2.7.5 Comparing average gene expression

Gene expression averages for populations/ conditions were performed in MultiExperiment Viewer using unpaired t-tests with alpha=0.05. Multiple comparison correction with the standard Bonferroni method was considered for all analyses. The correction was used where stated.

2.8 Buffers, reagents and consumables

Table 2.3 Custom buffers and media

Medium/ Buffer	Principal buffer/ medium	Additional reagents
RF10	RPMI 1640	100IU/ml Penicillin 10µg/ml Streptomycin L-glutamine, 2mM 10% heat inactivated fetal calf serum (FCS)
RH10	RPMI 1640	100IU/ml Penicillin 10µg/ml Streptomycin 2mM L-glutamine 10% heat inactivated human AB serum
Flow buffer	PBS	2% FCS 2mM EDTA
Sort buffer	PBS	0.1% FCS 2mM EDTA
RNA lysis buffer	Buffer RLT	1% beta-mercaptoethanol
Red cell lysis buffer (10x)	Sterile water	1.5M Ammonium chloride 100mM Potassium bicarbonate 1.2mM EDTA
Freezing solution	FCS (heat inactivated)	10% DMSO

Table 2.4 Cytokines, growth factors and enzymes

Product	Manufacturer	Stock concentration/ diluent	Working concentration
Dispase	Gibco	83mg/ml	0.83 mg/ml
Collagenase type IV	Worthington	160mg/ml	1.6 mg/ml
Recombinant human GM-CSF	R&D	10 µg/ml	50-100 µl/ml
Recombinant human M-CSF	R&D	5 µg/ml	100 ng/ml
Recombinant human IL-4	ImmunoTools	5 µg/ml	50 ng/µl
LPS from E.coli 026:B6	Sigma	1 mg/ml	100 ng/ml
Recombinant human IFNγ	R&D	1 µg/ml	5 ng/ml

Table 2.5 Consumables

Item	Source	Item	Source
Polypropylene tubes (15/50ml)	Cellstar, Greiner	Trypan blue	Invitrogen
FACS tubes	BD	Lymphoprep™	Stemcell technologies
Cryovials	Nunclon	DAPI	Partec
Tissue culture flasks	Bio-one, Greiner	DPX	Sigma
Tissue culture plates	Cellstar, Greiner	DAPI mounting medium	Vector
Cell strainers	BD	RPMI 1640	Lonza
Cell filters	Partec	PBS	Sigma
EDTA blood collection tubes	BD	Sterile water	Sigma
MS columns	Miltenyi	FCS	Sera Lab
Eppendorf tubes	Bio-one, Greiner	Buffer RLT	Qiagen
		Human AB serum	Sigma
		EDTA	Invitrogen
		DMSO (dimethyl sulphoxide)	Kocklight Ltd
		Penicillin and streptomycin	Invitrogen
		L-glutamine	Invitrogen

Chapter 3. Mononuclear phagocytes in skin Graft-versus Host Disease

3.1 Introduction

Skin is the most frequently affected organ in acute GvHD (Ferrara et al., 2009). In some situations, the extent of skin involvement is limited and the inflammation resolves with topical steroids and a therapeutic dose of calcineurin inhibitor. In other cases, skin involvement can be extensive, resistant to high-dose systemic steroids and fatal. Alternatively, disease may responds to steroids but recur when they are withdrawn, leading to substantial immunosuppression related morbidity and mortality. The biological processes underpinning these divergent clinical situations are poorly understood. The diagnostic methods for stratifying disease are insensitive and the treatments available are limited and globally immunosuppresive.

As outlined in Chapter 1, the importance of alloreactive T lymphocytes in GvHD pathogenesis is incontrovertible and T cell depletion offers significant protection against GvHD (Kottaridis et al., 2000). GvHD still occurs in around 20% of patients profoundly lympho-depleted with Alemtuzumab (Kottaridis et al., 2000), (Perez-Simon et al., 2002). It is possible that accessory cells and additional effector mechanisms contribute to GvHD inflammation in the lymphopenic patient; mechanisms that may not be apparent in lymphocyte-rich murine models of GvHD. Combining lymphocyte-directed with accessory cell-directed approaches may permit progress in GvHD prevention and treatment.

MPs are prime candidates as accessory cells in GvHD. Their role in initiating GvHD through alloreactive T cell priming is recognized, and host DCs are specifically implicated (Shlomchik et al., 1999), (Duffner et al., 2004). However, there is little consensus as to the specific cells responsible in humans, how they can be depleted, and whether there is therapeutic utility in doing so (Yuksel et al., 2006), (Kreutz et al., 2012). GvHD following BMT for GATA-2 deficiency, where recipients have profound DC immunodeficiency, suggests this may not be a tractable approach (Grossman et al., 2014). Greater consideration of MPs in maintaining GvHD is warranted.

The skin contains a rich complement of MPs (see section 1.3.2). There is growing appreciation that they function in peripheral regulation of inflammation as well as migrating to lymphoid tissue and interacting with naïve T cells (Bennett and Chakraverty, 2012). Both DCs and macrophages can re-stimulate effector T cells and secrete pro-inflammatory cytokines (Haniffa et al., 2009). Macrophages can also release directly damaging factors, including reactive oxygen species, proteases and TNFα (Takemura and Werb, 1984).

The macrophage content of GvHD lesions has been shown to correlate with disease severity in several patient cohorts (Nishiwaki et al., 2009), (Terakura et al., 2015). In murine models, macrophages are tractable to manipulation with a consequent reduction in GvHD (Alexander et al., 2014), (Nishiwaki et al., 2014). However, to propose macrophages as therapeutic target in GvHD requires a greater depth of knowledge. At present, we do not know whether macrophages in GvHD lesions are resident or recruited, how they relate to other inflammatory and steady state MPs and what their functions are.

In the existing literature, interpretative difficulties arise when inflammatory MPs are studied in isolation, studied without consideration for steady-state MPs specific to that tissue, and defined in way that prevent a cross-compartment or system-wide appreciation. At present, we define the heterogeneity of the MPS based on an accepted set of surface antigens. There is growing concern that this biases our understanding of cell populations and disguises functionally distinct subsets (Reynolds and Haniffa, 2015). Lability of surface antigens during inflammation and the need to resolve resident from recruited subsets adds additional stress to this fragile framework. The skin strand of this work aims to create a global picture of the MPS in GvHD and test the utility of *a priori* definitions in acute inflammation. Specific attention will be focused on macrophages within the dermal infiltrate.

3.2 Skin strand hypotheses

1) The MP repertoire in GvHD lesional skin will be altered
2) Inflammatory MPs derived from monocytes will be found in GvHD skin
3) Inflammatory MPs will promote T cell-mediated skin damage

3.3 Chapter Aims

3.3.1 Skin strand Aim 1: To characterize the mononuclear phagocyte composition of GvH lesional skin.

Acute skin rashes in BMT recipients at our centre are biopsied for histological confirmation of GvHD and exclusion of other pathologies such as drug reaction, viral exanthem or cutaneous relapse of malignancy. Care is taken to biopsy as soon as possible after presentation and before initiation of treatment. As typical biopsies are a 10-15mm^2 skin shaves, we have sufficient material to divide for diagnostic histology and MP analysis. Recognizing that not all acute rashes may be GvHD, diagnostic histology will be referenced. Taking all presentations of rash will permit analysis across a large cohort: up to 90 cases in 3 years can be predicted from our transplant activity and GvHD incidence (Jardine et al., 2015). Heterogeneity within the cohort is likely and concurrent clinical information will be essential to identifying subgroups. To separate the effects of GvHD from the effects of BMT on skin MPs, a BMT control cohort will be recruited. Further comparison with steady state is possible using normal skin (mammoplasty or abdominoplasty surplus). Within Aim 1 I will:

- Identify the MPs present in GvHD lesions using multi-parameter flow cytometry.
- Quantitate MPs and look for global patterns in MP composition.
- Correlate MP composition with clinical features, including concurrent and outcome measures of disease severity (clinical grade, chronic GvHD incidence and severity).

3.4 Materials and Methods for Chapter 3

3.4.1 Patient samples

Consent for blood and up to 3 skin shave biopsies was sought prior to BMT under ethical approval from Newcastle and North Tyneside 1 Research Ethics Committee. From August 2012-December 2015 77 samples were collected from 73 individuals presenting with acute rash post-BMT. Shave biopsies 5-15mm^2 were obtained via

Dermablade™ and transported in serum-free medium (X-VIVO™). A central 1-2mm strip was fixed in formalin for histological diagnosis.

Control biopsies were collected from 19 BMT recipients at day 28 or day 100 post-BMT, coinciding with the predicted onsets of acute and immunosuppression-withdrawal (ISW) GVHD.

Additional controls were sourced from normal skin obtained from 26 patients undergoing breast reduction or abdominoplasty. Skin shave biopsies from 3 patients with acute eczema and 1 patient with cutaneous sarcoidosis were used as non-BMT inflammatory dermatosis controls.

3.4.2 BMT regimens

Patients received a regimen of chemotherapy with or without total body irradiation and immunosuppressive treatment. Regimen was tailored to the disease, performance status and donor stem cell source in each case. Conditioning regimens were grouped into categories as shown in Table 3.1

Table 3.1 Conditioning regimens for BMT

Group	Regimen
Reduced intensity conditioning, T-cell depleted (RIC-TCD)	Flu/Mel (Fludarabine 150mg/m^2, Melphalan 140mg/m^2, Campath 30mg or 60mg, Ciclosporin)
	Flu/Bu (Fludarabine 150mg/m^2, Busulfan 8-10mg/kg, Campath 30mg or 60mg, Ciclosporin)
	Flu/Bu/ATG/MMF (Fludarabine 150mg/m^2, Busulfan 9.6mg/kg, ATG Fresenius 30mg/kg, MMF, Ciclosporin)
Reduced intensity conditioning, T-cell replete (RIC-TR)	Flu/Mel/Mtx (Fludarabine 150mg/m^2, Melphalan 140mg/m^2, Methotrexate 15mg/m^2, Ciclosporin)
	Flu/TBI (Fludarabine 90mg/m^2, 200cGy TBI, Methotrexate, MMF, Ciclosporin)
Pre-conditioned	FLAMSA-Flu/Bu/ATG/MMF (Fludarabine 120mg/m^2, Cytarabine 8g/m^2, Amsacrine 400mg m^2, Fludarabine 60mg/m^2, Busulfan 9.6mg/kg, ATG rabbit 5mg/kg, MMF, Ciclosporin)
	FLAMSA-TBI/ATG/MMF (Fludarabine 120mg/m^2, Cytarabine 8g/m^2, Amsacrine 400mg m^2, 4Gy TBI, ATG rabbit 5mg/kg, MMF, Ciclosporin)
	FLAMSA-TBI/Cy (Fludarabine 120mg/m^2, Cytarabine 8g/m^2, Amsacrine 400mg m^2, 4Gy TBI, Cyclophosphamide 80mg/kg, Campath 30-60mg)
Myeloablative	Cy/TBI (12Gy TBI, Cyclophosphamide 120mg/kg, Campath 30-60mg, Ciclosporin)
	MAC Haplo (12Gy TBI, donor lymphocyte infusion, Cyclophosphamide 120mg/kg, Ciclosporin, MMF)
Other	RIC haplo (Fludarabine 150mg/m^2, Cyclophosphamide 29mg/kg, 200cGy TBI, post-transplant Cyclophosphamide 100mg/kg, Tacrolimus, MMF)
	RIC cord (Cyclophosphamide 50mg/kg, Fludarabine 200mg/m^2, TBI 200cGy, MMF, Ciclosporin)

3.4.3 Clinical data

Patient, donor and transplant characteristics relevant to GvHD risk were collected from registry data (patient age, transplant indication, donor type, HLA match, gender match, conditioning regimen). On receipt of biopsy, data were recorded on time post-transplant, current immunosuppression use and blood parameters (white cell count and differential, c-reactive protein (CRP), ciclosporin level). GvHD skin stage and treatment were taken from medical records. Skin stage, according to modified Glucksberg criteria (Table 1.2), was usually stated. In some cases, stage had to be inferred from written descriptions using the rule of nines (e.g. rash on face and upper arms equates to 13.5% surface involvement and is skin stage 1).

Outcome data were completed for 66 participants and 19 controls that reached 1 year or died within the first year post-transplant. Outcome data for 5 participants was recorded at 6 months, but 1 participant was transplanted too late in the study period for sufficient follow-up. Outcome data included maximum severity of acute GvHD (modified Glucksberg grade), organs involved in acute GvHD, presence or absence of chronic GvHD, National Institutes of Health (NIH) cGvHD working group score (mild /moderate/ severe), date of death or follow-up and cause of death.

Formalin fixed samples were examined by an independent consultant Histopathologist and graded according to Lerner's criteria (Table 1.3). Formal diagnostic reports were used to obtain categorical data on diagnosis and severity grading.

3.4.4 Cohort characteristics

The GvHD and BMT control cohorts were well matched in terms of patient, donor and transplant characteristics (Table 3.2). White cell counts and differentials at the time of biopsy were not significantly different, though relatively increased lymphocyte, eosinophil and monocyte counts were seen in a small number of GVH participants (data not shown). CRP was significantly higher in patients presenting with GVH than BMT controls (means 35mg/L and 10mg/L respectively).

Table 3.2 Cohort characteristics

	GVH	BMT control	p value
Age; mean (SD)	54 (12)	52 (12)	0.53 unpaired t test
Disease; n (%) Acute leukemia Myelodysplasia Lymphoma Myeloma CLL Myeloproliferative neoplasms	 34 (44) 13 (17) 19 (25) 5 (7) 3 (4) 3 (4)	 11 (58) 1 (5) 4 (21) 1 (5) 0 (0) 2 (11)	 0.55 Chi-square
Donor type; n (%) MRD MUD Other	 19 (25) 55 (71) 3 (4)	 3 (16) 16 (84) 0 (0)	 0.41 Chi-square
Conditioning; n (%) RIC-TCD RIC-TR Pre-conditioned MAC Other	 61 (79) 6 (8) 6 (8) 2 (3) 2 (3)	 14 (74) 1 (5) 3 (16) 1 (5) 0 (0)	 0.39 Chi-square
Blood parameters *10^9/L; mean (SD) WCC Neutrophils Monocytes Lymphocytes Eosinophils CRP mg/L; mean (SD) Ciclosporin level; µg/L mean (SD)	 4.89 (3.86) 2.91 (2.02) 0.65 (0.43) 0.10 (2.12) 0.36 (0.71) 35 (48) 120 (146)	 3.61 (2.23) 2.38 (1.52) 0.54 (0.45) 0.47 (0.49) 0.20 (0.25) 9.7 (8.9) 159 (123)	 0.17 0.30 0.35 0.29 0.32 0.03 0.37 Unpaired t test

Table 3.1 Cohort characteristics

Categories highlighted in the same colour were grouped together for chi-squared analysis in order to meet assumptions of the test.

In the GvHD cohort, acute and ISW presentations were equally sampled, each representing 40% of cases (Figure 3.1). Seventeen percent of cases occurred after DLI, and 3% were acute flares on a background of chronic GVHD. The majority of specimens were taken from patients on no immunosuppression or ciclosporin monotherapy (92%). The remaining samples were taken from patients presenting with rash through topical steroids or low dose oral prednisolone (<10mg). There were no patients on combined immunosuppression at the time of biopsy. Almost half of all patients presented with widespread rash equating to skin stage 3. Histologically, most rashes were graded at low severity (72% grade I and II). There was little correlation between the clinical and histological severity of skin involvement.

Figure 3.1 GvHD cohort characteristics

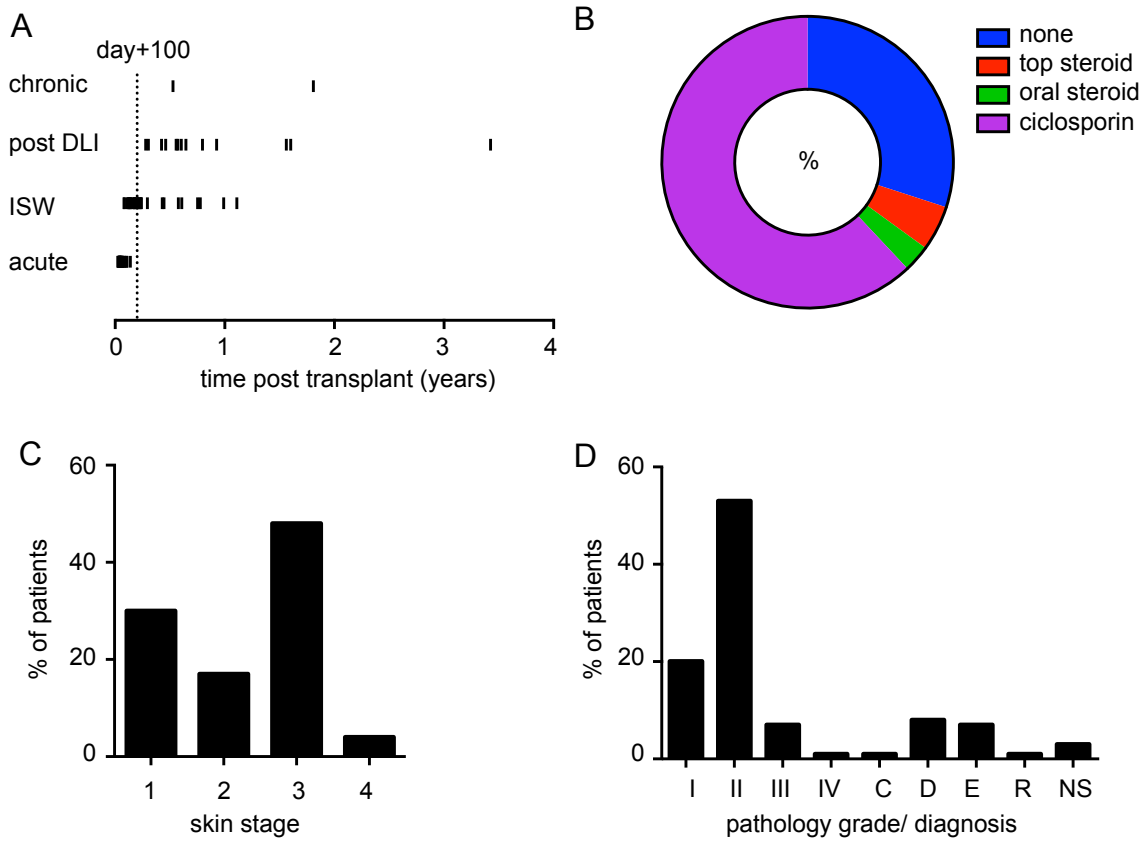

Figure 3.1 GvHD cohort characteristics

A) Time of onset of GvHD post-BMT. Each participant is indicated by a dash. Presentations are separated into acute, immunosuppression withdrawal (ISW), post- donor lymphocyte infusion (post DLI) and acute-on chronic presentations (chronic).
B) Proportion of patients receiving immunosuppression at the time of biopsy. Top steroid= topical steroid (typically 0.1% betamethasone).
C) Frequency of Glucksberg skin stage 1-4.
D) Frequency of Lerner grades I-IV on diagnostic histology of skin biopsies. Other diagnoses: C=chronic GvHD, D=drug reaction, E=eczema, R=relapsed disease, NS=no significant pathology.

3.4.5 Diagnostic histology

Samples were obtained and processed as soon as possible after presentation. Pathological confirmation of diagnosis took 2-3 days. Fourteen biopsies (18%) were given non-GvHD diagnoses (1 relapsed lymphoma, 5 eczema, 6 drug reaction and 2

no significant pathology). There was diagnostic uncertainty in several cases (Figure 3.2).

The diagnostic decision leaned towards “drug reaction” if eosinophils were present, even though this is an unreliable method for separating the conditions (Sharon et al., 2012). Four of the patients with a ‘drug reaction’ biopsy had clinical significant and persistent GvHD either at the time of biopsy or on subsequent immunosuppression withdrawal.

The diagnostic decision leaned towards “eczema” if epidermal thickening (acanthosis) was present and intercellular oedema (spongiosis) was marked. Most of the patients with eczema diagnoses had a single flare of inflammation responsive to topical steroid, but onset of the flare tended to correlate with immunosuppression withdrawal.

Figure 3.2 Examples of non-GvHD diagnoses and diagnostic uncertainty in histology

Drug reaction

“Sections show skin with mild perivascular infiltrates in the upper dermis, containing lymphocytes, a lesser proportion of eosinophils and occasional mast cells. The epidermis is generally of normal thickness, with foci of spongiosis, including a spongiotic vesicle, acanthosis and exocytosis of lymphocytes. Occasional dyskeratotic cells are seen within this region, some above the basal layer. The inflammatory process also affects hair follicle epithelium, where dyskeratotic cells are also seen.

The appearances are those of a combination of spongiotic and lichenoid changes associated with eosinophil-rich inflammation. While this could represent graft versus host disease, the presence of eosinophils is unusual, and more in keeping with a lichenoid drug eruption. Clinico-pathological correlation is suggested.”

Eczema

“Sections show a superficial biopsy of skin in which the epidermis exhibits parakeratosis, acanthosis and moderate to severe spongiosis. Occasional dyskeratotic cells are also present, but there is no clear evidence of hydropic degeneration of the basal layer. Spongiotic vesicle formation is present. The dermis appears oedematous, with a light lymphohistiocytic inflammatory infiltrate and scattered pigment incontinence. Eosinophils are not apparent, although there is little included dermis.

The changes are primarily those of a moderately severe subacute spongiotic dermatitis, in keeping with an eczematous reaction. The presence of dyskeratosis may indicate a drug aetiology; in the absence of hydropic change, it is less likely to represent coexisting graft versus host disease.”

GvHD

“Sections show skin with epidermis and dermis. The epidermis appears acanthotic and spongiotic. There is exocytosis of lymphocytes with occasional dyskeratotic keratinocytes. Within the papillary dermis some oedema is noted, with mild perivascular chronic inflammation with moderate numbers of dermal eosinophils.

The differential diagnosis includes eczematoid graft versus host disease and eczema, presence of eosinophils also raise possibility of allergic /drug aetiology. Clinical correlation is recommended.”

Figure 3.2 Examples of non-GvHD diagnoses and diagnostic uncertainty in histology

Full histology reports for 3 individuals where diagnosis was uncertain. Headings in bold are the diagnoses assigned for the purpose of this work. Key terms are highlighted.

As samples could not be reliably excluded based on pathological diagnosis, all were considered in primary analysis. Non-GvHD diagnoses were classified GvHD grade 0.

3.4.6 Tissue processing

Plastic surgery skin included reticular dermis to the depth of the fat layer. The first step in processing was to prepare skin shaves comparable to the clinical biopsies. Skin was immobilized on a cork block covered with sterile silicon and approximately 15mm^2 skin shaves were performed using a DermaBlade®. When a larger sample was required, the upper 200 microns of skin were harvested using a split skin graft knife.

Skin shave biopsies were used whole or split into dermis and epidermis. To release the epidermis, skin was cultured in X-VIVO^{TM} (Lonza) with 830µg dispase for 60-90 minutes at 37°C and 5%CO_2 and then peeled under a dissection microscope. At the beginning of the study period, fewer parameters were available on the flow cytometer/ sorter. Dermis was therefore preferred as it removed LCs from analysis. Whole skin was used later in the study period, when parameters to identify LCs became available.

Dermis or whole skin was digested in RF10 with 1.6mg/ml type IV collagenase for 12-16 hours at 37°C and 5%CO_2. Shave biopsies were digested in 500µl RF10 in one well of a 24 well plate. Larger plastic surgery preparations were digested in 1-2 90mm^2 petri dishes containing 30ml RF10 each. Digest was passed repeatedly through a 1ml pipette (10ml for large plastic surgery skin preparations) until no visible material remained. To yield a single cell suspension, digest was passed through a 100-micron filter into a polypropylene sorting tube. The well/ plate was washed twice using cold sort buffer without calcium or magnesium to collect residual and adherent cells.

For some experiments, an enzyme-free preparation of leukocytes was required. Skin was cultured as above but without collagenase. After 48 hours, migratory leukocytes were harvested from the supernatant.

3.4.7 Sample preparation

Dermal suspensions were processed immediately as yield was insufficient to recover after cryopreservation. Single cell suspensions were prepared for flow cytometry/ flow sorting as outlined in section 2.3.1. Antibody panels for sorting are detailed in Table 3.3. Four different panels were used during the study period as experiments transitioned from flow analysis to flow sorting and instruments were updated. While the core of the panel was conserved, fluorochrome choice was adapted to the specifications of each instrument.

Table 3.3 Flow cytometry panels used for sorting/ analysing biopsy digests

Analysis panel 1- LSR II, 12.2012-04.2014		**Sort panel 1- Aria, 05.2013-07.2013**	
Antigen	Fluorochrome	Antigen	Fluorochrome
CD3, 19, 20 56	FITC	AF	in FITC channel
Test	PE	CD14	PE
CD123	PERCPCY5.5	HLA-DR	PERCPCY5.5
CD1c	PECy7	CD1c	PECy7
HLA-DR	V450		
CD45	V500	CD45	V500
CD14	BV650		
CD141	APC	CD11c	APC
CD11c	AF700	CD1a	AF700
CD16	APCH7	CD16	APCH7
DAPI		DAPI	
Sort panel 2- Aria 07.2013-12.2013		**Analysis/ Sort panel 3- Fusion and X20 12.2014-12.2015**	
Antigen	Fluorochrome	Antigen	Fluorochrome
AF	in FITC channel	AF ± CD3	FITC
Test	PE	CD8 or 141	PE
CD123	PERCPCY5.5	CD123	PERCPCY5.5
CD1c	PECy7	CD1c	PECy7
	V450	HLA-DR	V450
CD45	V500	CD45	V500
CD14	BV650	CD14	BV650
CD141	APC	CD11b or 141	APC
HLA-DR	AF700		
CD11c	APCH7	CD11c	APCH7
DAPI		DAPI	

Table 3.3 Flow cytometry panels used for sorting/ analyzing biopsy digests

Combinations of antibodies used to define populations in skin digests. Antibody supplier details are listed in Appendix B. PERCP= peridinin chlorophyll protein, Cy= Cyanine, BV= Brilliant violet™, AF= Alexa Fluor™.

3.5 Results for Chapter 3

3.5.1. Analysis strategy for identifying skin mononuclear phagocytes by flow cytometry

An analysis strategy was required that identified the 2 macrophage and 2 DC populations in normal dermis and could also be applied to inflamed skin without arbitrarily dividing inflammatory populations (Figure 3.3, panel A-B).

First, live cells were gated as DAPI- events with forward scatter (FSC) >50,000. Events with lower FSC were debris such as erythrocytes and cell fragments. They were numerous in analysis files as FSC thresholds were not used for FACS sorting. This was necessary to ensure that debris was not sorted into tubes.

Doublets were excluded from the live cell gate by comparing side-scatter (SSC) height and SSC area. Cells passing through the laser singly had equivalent height and area but cells passing through in pairs had a greater area. While the height to area ratio for single lymphocytes was 1:1, the relationship for macrophages was <1. Stringency of the single cell discrimination gate was adjusted so that macrophages were not being removed from further analysis.

Next, leukocytes were separated from other dermal populations such as fibroblasts, keratinocytes and endothelial cells by CD45 expression. This was necessary as some CD45-negative cells expressed HLA-DR and would otherwise enter macrophage/ DC analysis.

Leukocytes were split by HLA-DR and SSC into macrophages/ DCs and lymphocytes. While a proportion of lymphocytes expressed HLA-DR in both normal and inflamed skin, consistent with an activated phenotype, expression was never so high as in macrophages/ DCs. Lower SSC in lymphocytes helped refine this distinction.

Figure 3.3 Analysis strategy for identifying skin mononuclear phagocytes by flow cytometry

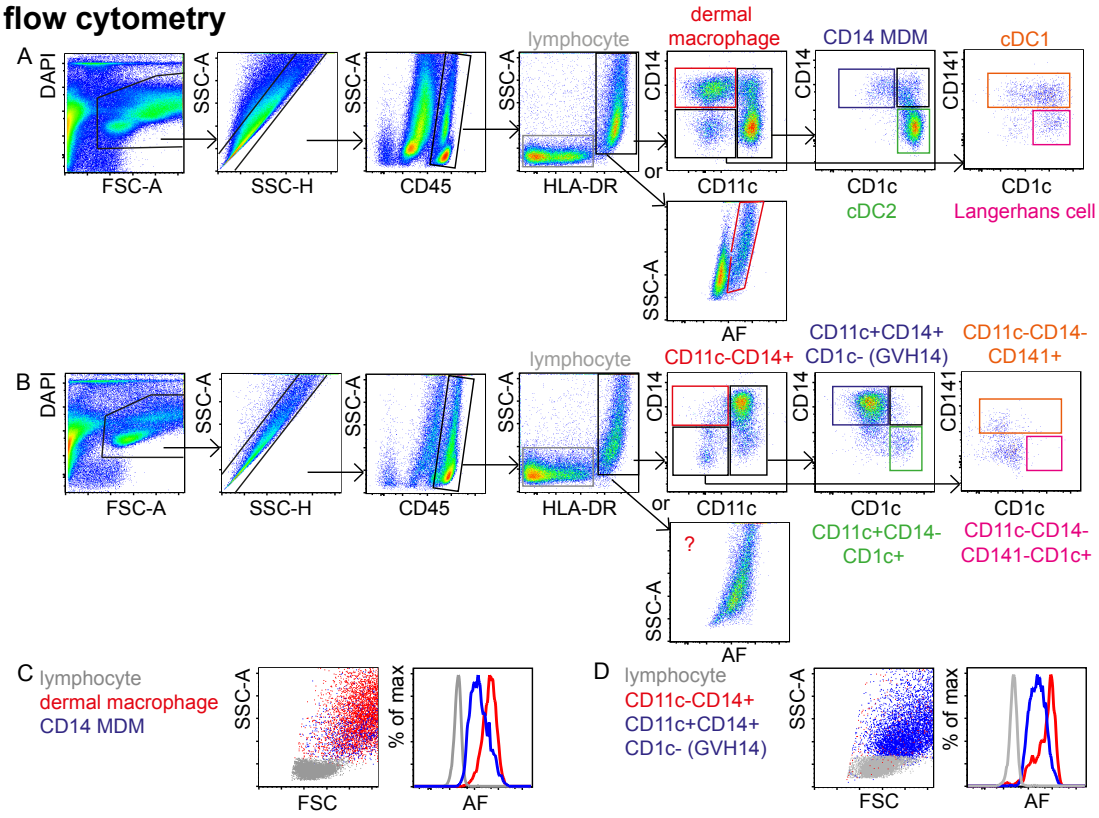

Figure 3.3 Analysis strategy for identifying skin mononuclear phagocytes by flow cytometry

Representative plots of digested dermis from normal skin (A) and GvHD lesion (B) are gated with the analysis strategy described in section 3.5.1. Alternative gating of macrophages using autofluorescence is shown for comparison. Black polygons are intermediate gates in the hierarchy. The gating process is depicted by arrows. Coloured polygons are terminal gates that define populations.
Macrophage populations identified in normal skin (C) and GvHD lesion (D) are compared in terms of scatter properties and autofluorescence. Lymphocytes are included for reference.
FSC/ FSC-A= forward scatter (area), SSC-A= side scatter area, SSC-H= side scatter height, AF=autofluorescence

Previous gating strategies have relied upon autofluorescence (AF) and SSC to separate HLA-DR+ cells into dermal macrophages and DCs/ CD14 MDM (Haniffa et al., 2009), (Haniffa et al., 2012), (McGovern et al., 2014). This strategy did not work well in inflamed skin as cells with intermediate AF and SSC dominated the HLA-DR+ gate. An alternative strategy was devised using CD14 and CD11c. In normal skin, dermal macrophages could be identified as CD11c- CD14+ cells. High AF and SSC were confirmed (Figure 3.3, panel C-D). In inflammation, the CD11c- CD14+

parameter space was sparsely populated because HLA-DR+ cells were predominantly CD11c+. The few cells within the CD11c- CD14+ gate had equivalent AF and SSC to dermal macrophages. In contrast, the CD11c+ CD14+ cells had lower AF and SSC than dermal macrophages. The identity of the CD11c+ CD14+ cells in inflammation will be fully explored in later sections. Regarding the scarcity of dermal macrophages in inflammation, it is possible that they enter the CD11c+ CD14+ parameter space by up-regulating CD11c. Proliferation and cell division could also reduce SSC and AF. Whole-mount microscopy of GvHD dermis does not identify CD11c on FXIIIa+ cells (Wang et al., 2014).

In normal skin, the CD11c+ gate can be split by CD14 and CD1c expression into CD14 MDMs and CD1c+ myeloid DCs (cDC2). Cells co-expressing CD14 and CD1c are frequently seen, but as they have not been adequately identified as DCs or macrophages to date, they are assigned a separate analysis gate.

Within the CD14-CD11c- gate in normal skin, cDC1 are defined as CD141+ cells. They are known to have variable CD1c expression (Haniffa et al., 2012). The CD141-CD1c+ population are consistent with the phenotype of Langerhans cells (Bigley et al., 2015). In keeping with this, increased CD141-CD1c+ cells were present in specimens where the epidermis was difficult to remove or when whole skin was analyzed.

3.5.2 Myeloid DC gates capture differences in steady state and inflammation

Comparison between CD14 MDM in normal dermis and CD11c+CD14+ cells in GvHD is described in subsequent sections. Comparison between myeloid DC populations in steady state and inflammation is not explored in such detail. However, limited antigen analysis by FACS provides some insight (Figure 3.4).

In inflamed skin, cells falling in the CD141+ parameter space were not consistent with cDC1. They had lower expression of CD1c and CD141 and had scatter properties typical of lymphocytes (Figure 3.4, panel B). CD141+ cells were back-gated onto the HLA-DR versus SSC-A plot to see if analysis had unwittingly included lymphocytes. CD141+ cells were distinct from the majority of lymphocytes due to higher HLA-DR expression. Furthermore, the mean fluorescence intensity of CD141

in this population was >1000 fold higher than in lymphocytes (data not shown). The possibility that these cells were pDC was considered. While absent from steady-state dermis, pDC are found in psoriasis-inflamed skin (Haniffa et al., 2015b). There are no comprehensive descriptions of pDC surface phenotype in inflamed skin. In blood, pDC have equivalent HLA-DR expression to myeloid DCs and higher CD123 expression (Jardine et al., 2013). CD141+ cells in GvHD skin did not fit this description. Their lower expression of HLA-DR and lower SSC compared with total HLA-DR+ cells is reminiscent of blood monocytes simultaneously analyzed with dermal digest (McGovern et al., 2014). CD141 expression on monocyte-derived cells is acknowledged (Haniffa et al., 2012). However, these cells were definitely CD14 negative, arguing against them being blood monocytes. My impression is that CD141+ cells in inflammation may be cDC1 either recently recruited from blood or blocked from adopting a normal phenotype on recruitment due to the inflammatory milieu. This hypothesis was not tested to due to the constraints of what is achievable with limited samples and the small numbers of these cells present. To reflect this uncertainty, they will be referred to as CD11c-CD141+ cells, not cDC1, in subsequent sections.

Figure 3.4 Myeloid DC gates capture differences in steady-state and inflammation

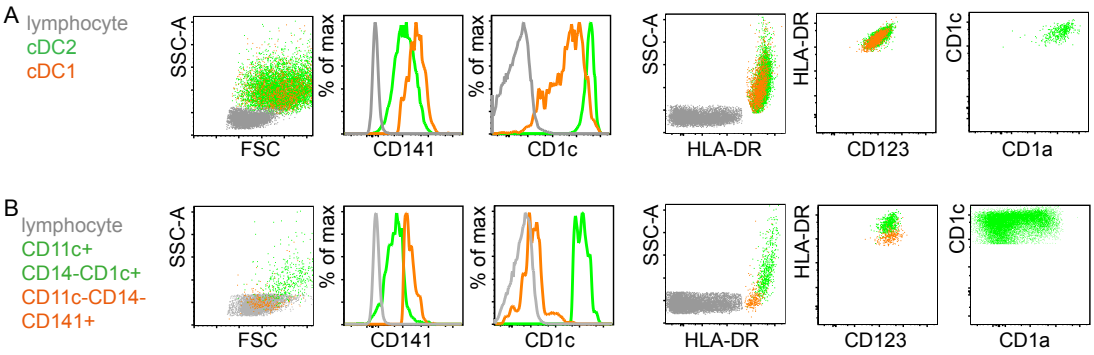

Figure 3.4 Myeloid DC gates capture differences in steady state and inflammation

(A) Scatter properties and selected antigen expression of myeloid DC populations from normal dermis. Populations are gated as in Figure 3.3 and compared with dermal lymphocytes. B) Populations from myeloid DC gates in GvHD dermis are compared with GvHD lymphocytes.

In inflamed skin, cells falling within the cDC2 parameter space were less obviously different from their steady state counterparts. The sort panel including CD1a antibody, used on only 3 GvHD specimens, identified reduced frequency of CD1a+ cells. The mean percentage of CD1a+ cells in the GvHD cDC2 gate was 45% (± standard deviation (SD) 7.2). Only one normal skin sample was sorted with this panel, but in keeping with previous reports, cDC2 were >99% CD1a+ (Haniffa et al., 2009). As blood cDC2 are CD1a negative (Segura et al., 2013), this would also be consistent with recent recruitment/ impaired tissue differentiation of blood cDC2. A full characterization of differences between steady state and inflamed skin cDC2 is warranted but has not been performed in this thesis. Cells within the cDC2 gate in inflamed skin will be termed CD14-CD1c+ cells to reflect their incomplete characterization.

3.5.3 Mononuclear phagocyte profile comparison between GvH lesion, BMT control, and inflammatory dermatoses

Using the analysis strategy outlined in 3.5.1, the MP profile of a typical acute GvHD lesion was qualitatively compared with controls (Figure 3.5). The GvHD biopsy was taken from a 43-year old female presenting with acute rash 22 days following a RIC-TCD transplant for ALL from an unrelated donor. The BMT control was from a 59-year old female, 40 days following an equivalent transplant (same conditioning, indication and donor-type). Cutaneous sarcoidosis and eczema were acute presentations at a tertiary referral dermatology clinic.

Comparing GvHD to BMT control, the GvHD lesion was more leukocyte-rich (Figure 3.5 A-B). HLA-DR+ MPs outnumbered lymphocytes in both. The lymphocyte: HLA-DR+ ratios were similar (30:60 in GVHD and 23:67 in BMT control) but GvHD lymphocytes had higher HLA-DR expression. Amongst HLA-DR+ cells, CD11c+CD14+ were most prominent in GvHD and CD1c+ cells were relatively depleted. The (CD11c+) CD14:CD1c ratio in GvHD was essentially reversed compared with BMT control (76:11 in GVHD and 20:60 in BMT).

Figure 3.5 FACS analysis of GvHD lesion, BMT control and inflammatory dermatoses

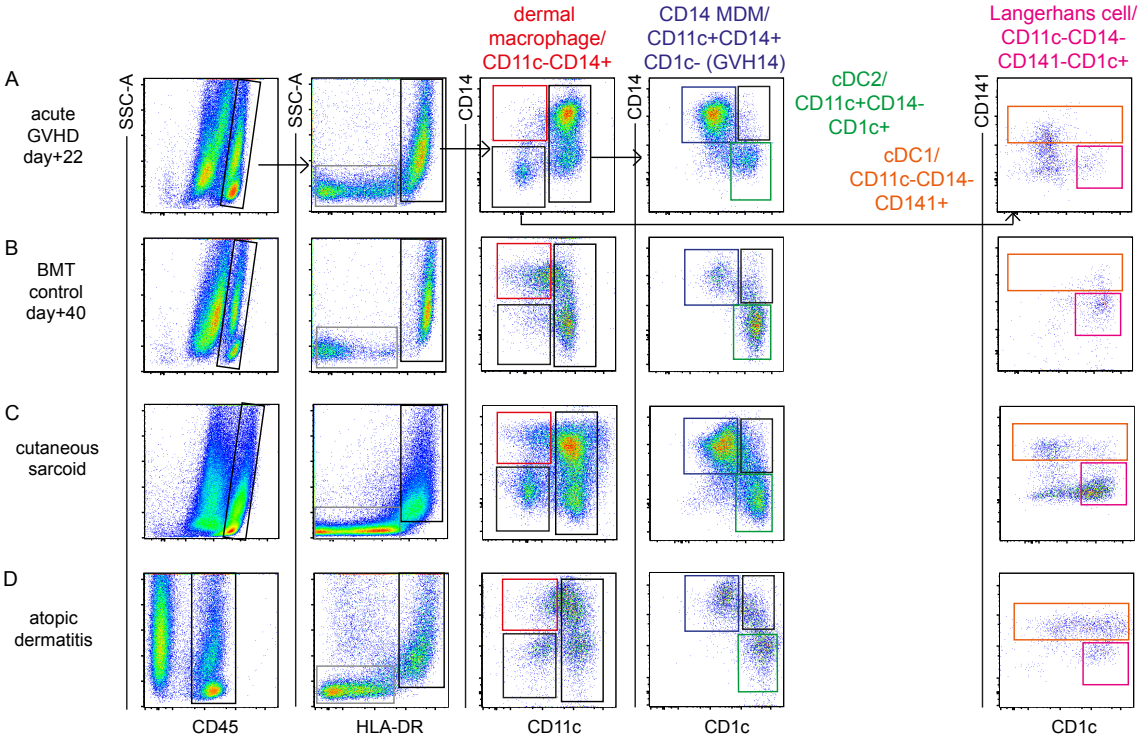

Figure 3.5 FACS analysis of GvHD lesion, BMT control and inflammatory dermatoses

FACS profile of digested material from A) acute GvHD lesion, B) BMT control, C) cutaneous sarcoid lesion and D) atopic dermatitis/ eczema lesion. A and D are dermal digests; C and D are whole-skin digests. The analysis strategy from Figure 3.3/ section 3.5.1 is used.

Inflammatory dermatosis controls were used to examine whether the profile associated with GvHD was specific. Eczema and sarcoidosis were selected as conditions associated with DC-rich and macrophage-rich inflammation respectively. The characteristic feature of cutaneous sarcoid lesions is the presence of non-caseating granulomas. Within sarcoid lesions, monocyte recruitment and IFNγ priming of macrophages by Th1 lymphocytes is recognized (Valeyre et al., 2014). Within eczematous lesions, myeloid DCs and pDCs have been described (Stary et al., 2005) (Bieber et al., 2000), (Wollenberg et al., 2002a), (Wollenberg et al., 2002b). The sarcoid lesion had a prominent CD11c+CD14+ population (Figure 3.5, panel C). The CD14:CD1c ratio was higher than normal (54:28), but not as extreme as in GvHD. The proportion of CD11c-CD14+ cells in eczema was greater than normal, but not so marked as in GvHD or sarcoidosis (Figure 3.5, panel D). In the eczema example shown, the CD141+ gate appeared normal, with numerous cells and well-

distributed CD1c expression. The sarcoid CD141+ gate had relatively few cells in proportion to the number of events, and as seen in GvHD, most cells were CD1c-.

While heavily focused on representative examples, this analysis has highlighted that GvHD incurs a pattern of changes in MPs. Some of these changes are shared with cutaneous sarcoidosis.

3.5.4 Quantification of mononuclear phagocytes in GvHD lesions and controls

The flow cytometry gating strategy detailed in 3.5.1 was used as a basis for quantitating MP subsets in GvHD lesions relative to BMT control and normal skin. Flow cytometry counted absolute events in the specimen (each event is a single cell) and percentage of cells as a proportion of the parent gate in the hierarchy. The appropriate denominator for quantitation was considered at length. The ideal quantitation would be MP subset number per area of affected skin. Biopsy area was measured on graph paper prior to processing. Mean area was 10 mm^2 for both GvHD and BMT specimens. This measure did not take into account thickness of the specimen, which varied substantially between patients and clinicians performing the biopsy. Histologically, GvHD damage to the dermo-epidermal junction was not uniform (Appendix C), so biopsy area would not necessarily correlate with affected area. It was decided that the measure least biased to sampling variability would be % of CD45+ cells.

As detailed in section 3.4.5, diagnostic histology was ambiguous in a number of cases. In this analysis, all samples that had been processed by digestion were included under the clinical descriptor “GvHD”. By histology, this included 36 GvHD, 5 drug reactions, 1 chronic GvHD, 3 eczema and 2 non-specific changes. Controls included 20 BMT recipients with rash and 21 healthy skin donors.

As shown in Figure 3.6, panel A, CD45+ leukocytes were a greater proportion of the dermal suspension in GvHD than in BMT or controls (mean ± SEM respectively 53.0 ± 3.5, 39.0 ± 4.3, 30.2 ± 2.8). Lymphocytes were a similar percentage of CD45+ cells in GvHD and controls (data not shown). Taking this information together, MP subsets occupying a higher proportion of CD45+ cells in GvHD are likely to be even

more enriched in absolute numbers. MP subsets occupying a lower percentage of CD45+ cells may still be present at greater numbers than in controls.

The only population significantly enriched in GvHD was CD11c+CD14+ (Figure 3.6, panel B). Both CD11c-CD14+ and CD11c+CD1c+ populations were reduced in GvHD (Figure 3.6, panels C and E). There was heterogeneity in the degree of enrichment/ depletion.

Figure 3.6 MP quantification in GvHD lesions and controls

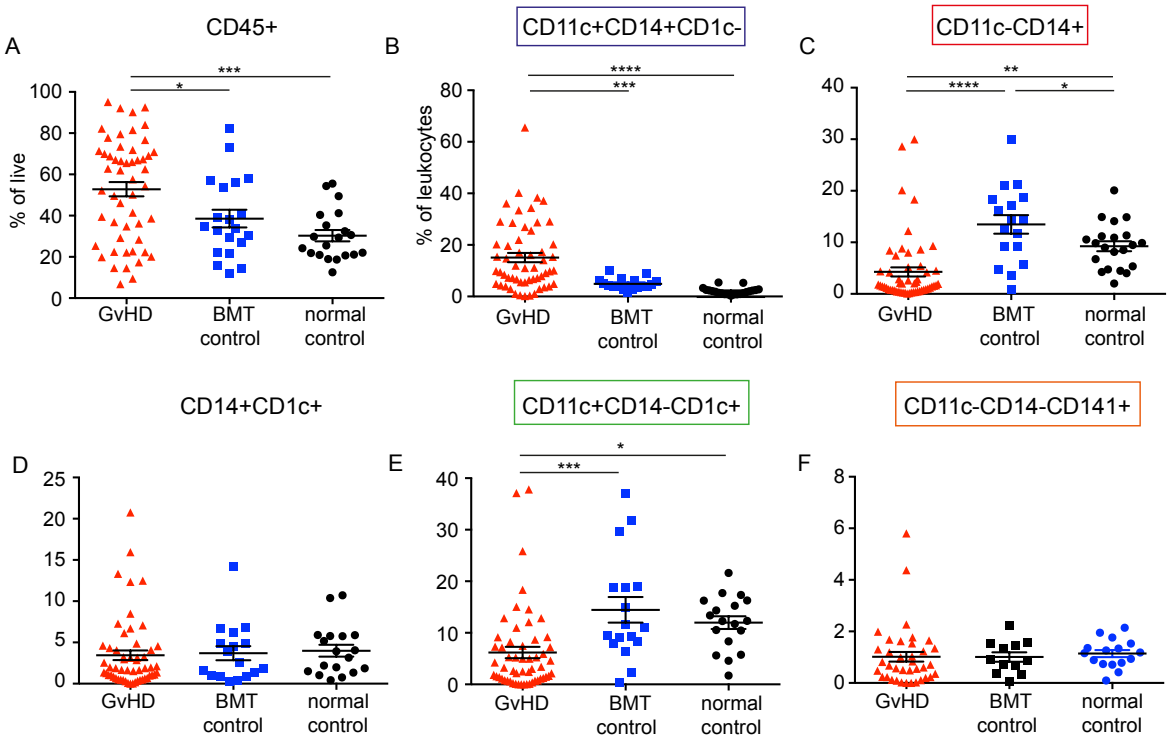

Figure 3.6 MP quantification in GvHD lesions and controls

Quantification of dermal leukocyte populations in digested GvHD dermis, BMT control skin and normal skin by flow cytometry. A) Total leukocytes as a percentage of live cells. B-F) MP populations as a percentage of total leukocytes. Bars show mean ± SEM. Comparison of means by 1-way ANOVA and post-tests * $p<0.05$, ** $p<0.01$, *** $p<0.005$, **** $p<0.001$. Where no * is shown, comparison was not significant.

3.5.5 Elevated CD14:CD1c ratio marks GvHD of greater severity

Knowledge of the MP profile in GvHD was used to split the cohort in order to explore factors underlying the heterogeneity in population numbers.

As demonstrated in Figure 3.3 and 3.5, GvHD inflammation is typified by a reversal in the CD14:CD1c ratio compared with normal skin. Mean ratios were 0.35 and 0.19 in BMT control and normal skin respectively. In inflammatory dermatoses, the mean ratio was higher (2.1), but not so high as in GvHD (13.7). The GvHD cohort (clinical descriptor) was divided into samples with a CD14:CD1c ratio greater than or less than 1 (Figure 3.7, panel B). This cutoff was chosen because the sum of sensitivity and specificity at this point was maximal (sensitivity 80%, specificity 88%, area under the curve 0.88) when discriminating histologically confirmed GvHD from BMT control (Figure 3.7, panel A).

Figure 3.7 Elevated CD14:CD1c ratio marks GvHD of greater severity

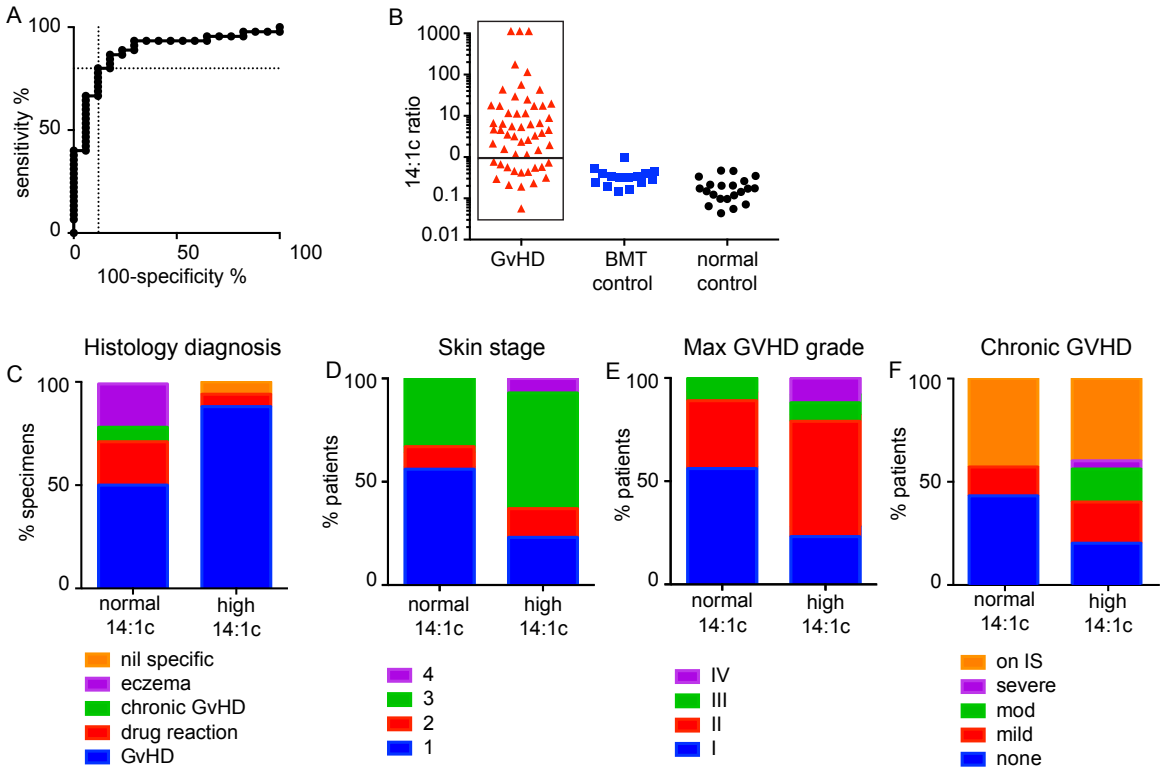

Figure 3.7 Elevated CD14:CD1c ratio marks GvHD of greater severity

A) ROC curve of CD14:CD1c ratio in histologically confirmed GvHD cases versus BMT controls. Dashed line shows sensitivity and 100-specificity at ratio=1. B) CD14:CD1c ratio in GvHD lesions and controls determined by FACS analysis. Boxes indicate GvHD cohort division into ratio>1 (n=37 and ratio <1 n=15). C,D) GvHD presentation characteristics and E,F) GvHD outcome characteristics compared between cohort groups. Colour-coded categories, as stated in legends, include histology diagnosis, skin stage at presentation (Glucksberg criteria), maximum GvHD grade post BMT (Glucksberg criteria), and chronic GVHD severity (NIH score). 'IS' denotes not scored as systemic immune suppression ongoing.

Fifteen out of 62 samples in the GvHD cohort (clinical descriptor) had a ratio <1 (mean 0.45) and 47 out of 52 had a ratio >1 (mean 19.0 excluding the 3 samples where ratio could not be calculated as no CD1c+ cells were present). Groups were termed “normal CD14:CD1c” and “high CD14:CD1c”. More samples with a non-GvHD diagnosis fell within the normal CD14:CD1c group (Figure 3.7, panel C). Considering only patients with a GvHD diagnosis, the normal CD14:CD1c group had less extensive rash at presentation (Figure 3.7, panel D). During the entire follow-up period, patients in the normal CD14:CD1c group experienced a lower severity of GvHD (Figure 3.7, panel E) and a reduced burden of chronic GVHD (Figure 3.7, panel F). Statistical analysis of these trends is shown in Table 3.4. The sample size becomes too small for statistical comparison when considering chronic GvHD. Few patients could be analyzed because a proportion died before the 1-year/ 6-month chronic GvHD assessment. Mortality was 40% in the high CD14:CD1c ratio group and 20% in the normal CD14:CD1c ratio group (Fisher’s exact test p=0.11). In both groups, 40% of patients could not be accurately assigned a chronic GvHD grade as systemic immune suppression was ongoing. In keeping with the trend for a lower severity of GvHD in the normal CD14:CD1c ratio group, no patients in this group experienced moderate or severe chronic GvHD, while 20% of patients in the high CD14:CD1c ratio group did.

Table 3.4 Contingency tests on GvHD severity measures split by CD14:CD1c ratio

		Outcome A (n)	**Outcome B (n)**	**Significance (Fisher’s exact test)**
Pathology diagnosis (all with clinical GvHD, n=62)		Histology did not confirm GvHD	Histology confirmed GvHD	
	Normal 14:1c	6	9	p=0.018 *
	High 14:1c	5	42	
Skin stage (all with clinical GvHD, n=62)		Stage 1	Stages 2-4	
	Normal 14:1c	9	6	p=0.007 **
	High 14:1c	13	34	
Skin stage (histologically confirmed GvHD, n=52)		Stage 1	Stages 2-4	
	Normal 14:1c	5	4	p=0.099 ns
	High 14:1c	10	33	
Max. GvH grade (all with clinical GvHD, n=62)		Grade I	Grades II-IV	
	Normal 14:1c	9	6	p=0.026 *
	High 14:1c	12	35	
Max. GvH grade (histologically confirmed GvHD, n=52)		Grade I	Grades II-IV	
	Normal 14:1c	5	4	p=0.099 ns
	High 14:1c	10	33	
Chronic GvH (all with clinical GvHD alive at 12 months, n=24)		None/ mild	Mod/ severe	
	Normal 14:1c	7	0	p=0.146 ns
	High 14:1c	12	5	
Chronic GvH (all with histologically confirmed GvHD alive at 12 months, n=19)		None/ mild	Mod/ severe	
	Normal 14:1c	4	0	p=0.530 ns
	High 14:1c	10	5	

3.5.6 Clinical features do not cluster by CD14:CD1c ratio groups

Further consideration was given as to whether the 9 patients with a histological diagnosis of GvHD and a normal CD14:CD1c ratio had common features. Clinical and transplant variables were compared between these patients and the 35 patients with histological GvHD and an elevated CD14:CD1c ratio. Formal multivariate analysis such as binary logistic regression was not possible with the sample size. To examine patterns in variables and associations with CD14:CD1c ratio a clinical variables matrix was constructed. Variables were condensed into categories coded between 0 and 4. The matrix was organized with each column representing a patient and each row representing a variable. Hierarchical clustering was used to organize the matrix into groups with shared features (Figure 3.8). Patients with a normal CD14:CD1c ratio were seen in all of the three broad clusters. Six of the 9 patients with normal CD14:CD1c ratio presented before day+50, 5 had a monocyte count < 0.5 $x10^9$/L and 5 had AML as their transplant indication. Patients within the first two months post-transplant, particularly those who have received prior myelosuppressive treatment, still have recovering haematopoiesis. It may be the case that macrophage infiltration into GvHD-affected tissue is limited when the capacity of the bone marrow produce monocyte is impaired. Firm conclusions cannot be made from this analysis.

Figure 3.8 Clinical details do not cluster by CD14:CD1c ratio groups

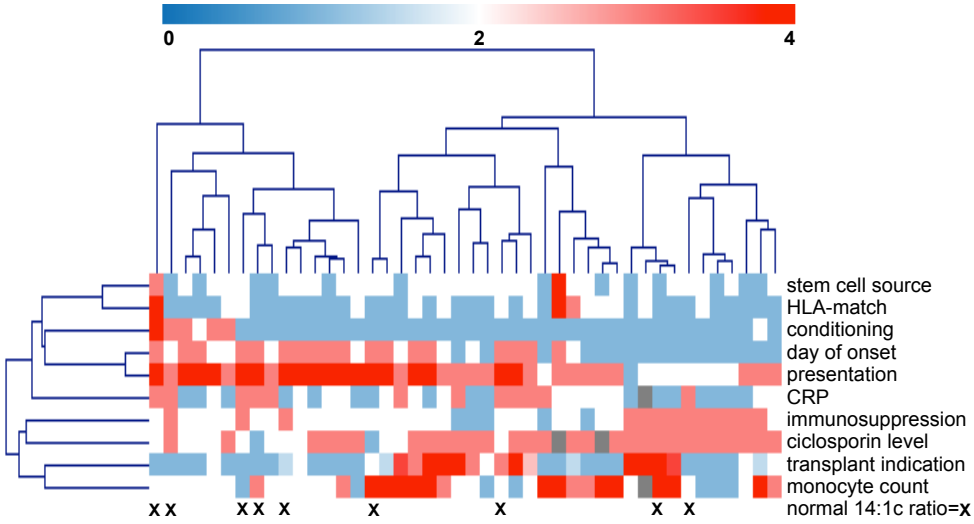

Figure 3.8 Clinical details do not cluster by CD14:CD1c ratio groups

Cluster dendrogram of a clinical details matrix. The matrix includes 10 clinical measures divided into categorical variables on a scale from 0-4. Coding of variables is as follows:
Stem cell source: 0= cord, 1= matched unrelated donor, 2= matched unrelated donor, 3= haploidentical
HLA-match: 0= 12/12, 1= 11/12, 2= 10/12, 3= 9/12, 4= 6/12
Conditioning: 0= other, 1= RIC-TCD, 2= RIC-TR, 3= preconditioned, 4= myeloablative
Day of onset: 0= >day 200, 1= day 150-200, 2= day 50-150, 3= <day 50
Presentation: 1= acute on chronic, 2= post-DLI, 3= ISW, 4= acute
CRP: 1= >30, 2= 10-30, 3= <10 (mg/L)
Immunosuppresion: 0= oral steroid, 1= topical steroid, 2= ciclosporin, 3= none
Ciclosporin level: 1= >200, 2= 50-200, 3= <50 (µg/L)
Transplant indication: 1= AML, 1.5= ALL, 2= MDS, 2.5= myeloproliferative neoplasm, 3= MM, 3.5= CLL, 4= lymphoma
Monocyte count: 0= <0.2, 1= 0.2-0.5, 2= 0.5-0.8, 3= >0.8 ($x10^9$/L)
X= the 9 patients with normal CD14:CD1c ratios.

3.5.7 Dermal leukocytes migrated out of GvHD explants also had elevated CD14:CD1c ratio

Many previous studies of human skin MPs have capitalized on their ability to migrate out of skin in culture. This property allows isolation of a dermal leukocyte suspension without the need for enzymatic digestion. Dermal macrophages do not migrate out of culture but CD14 MDM and dermal DCs do migrate (Klechevsky et al., 2008; Haniffa et al., 2009; Wang et al., 2014). While enzyme-sensitive antigens are preserved with this method, cells are susceptible to changes in gene and surface antigen expression

(McGovern N, Immunity 2014). Despite such changes, CD14+CD11c+ cells migrated from skin share more similarities in gene expression with CD14+CD11c+ digested from skin than they share with CD11c+CD1c+ cells migrated from skin (McGovern N, Immunity 2014).

Figure 3.9 Flow cytometry analysis of dermal leukocyte suspensions prepared by migration

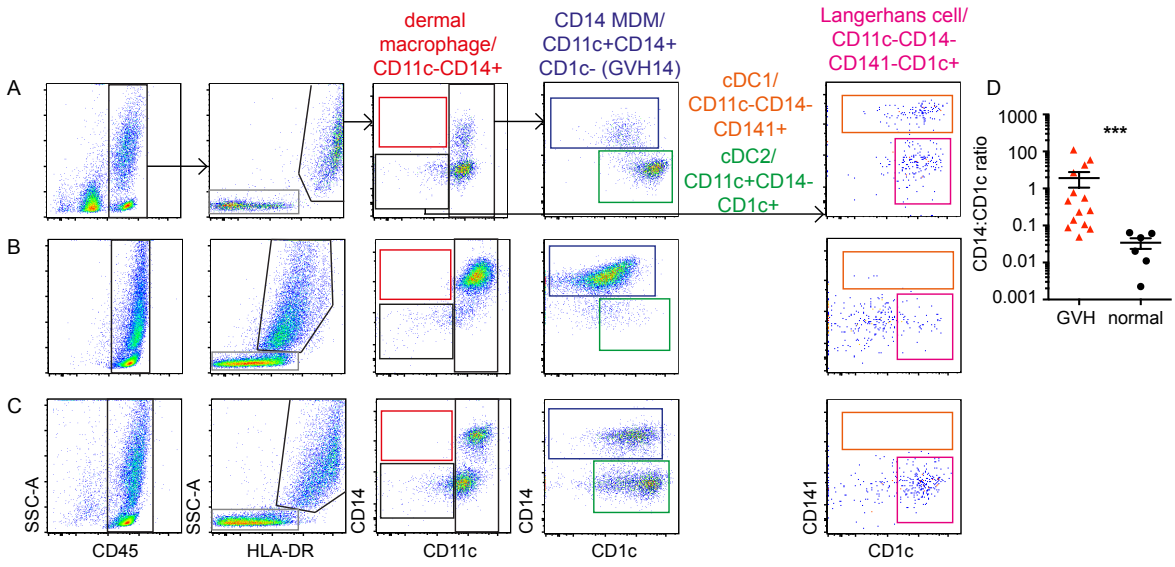

Figure 3.9. Flow cytometry analysis of dermal leukocyte suspensions prepared by migration
Flow cytometry analysis of leukocytes from normal skin (A) and from 2 patients with acute GvHD (B and C). Leukocytes were prepared by migration out of skin explants for 48 hours. D) Comparison of CD14:CD1c ratio in GvHD and normal skin, gating on CD11c+ cells. Normal skin samples n=6, GvHD specimens n=14. Bars show mean ± SEM. *** p=0.0002 by Mann-Whitney test.

The FACS analysis strategy used for digested skin was applied to migrated skin preparations (Figure 3.9). In normal skin, the CD11c-CD14+ gate was empty, in keeping with retention of dermal macrophages in the explant (Figure 3.9, panel A). CD141+ cells co-expressing CD1c were found in the CD11c-CD14- gate. CD141-CD1c+ cells, consistent with LCs, were also CD11c-CD14-. CD11c+ cells could be divided into CD14+ and CD14-CD1c+ fractions in similar proportions to those seen in digested skin. The flow cytometry profile of preparations migrated from GvHD skin mirrored that of GvHD digests (Figure 3.9, panels B, C). CD141+ cells were few, and those that were present had minimal CD1c expression. CD11c+CD14+ cells were

expanded compared with normal skin and CD14-CD1c+ cells tended to be fewer. The mean CD14:CD1c ratio was 0.34 in normal skin and 19.1 in GvHD (Figure 3.9, panel D).

3.5.8 The CD14+CD1c- infiltrate precedes lymphocyte accumulation in GvHD

Repeat biopsies were obtained from 3 individuals approximately 100 days following their presentation with GvHD. Clinical symptoms had resolved in all three at follow-up. The most dynamic population shifts occurred in HLA-DR-SSC^{lo} lymphocytes and CD14+CD1c- cells: mean 3.5 fold increase and 5.2 fold decrease respectively (Figure 3.10). This analysis suggests that biopsies are taken prior to peak lymphocyte accumulation in GvHD. The CD11c+CD14+ infiltrate seen in GvHD specimens is therefore likely to be an early event. On resolution of symptoms, the CD14:CD1c ratio is restored to normal.

Figure 3.10 Resolution of inflammation

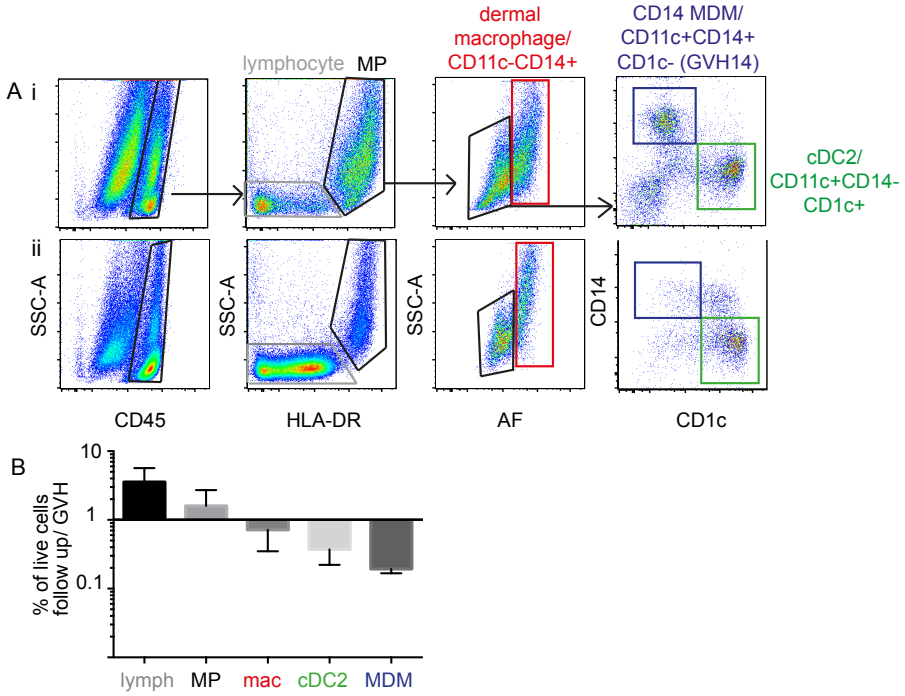

Figure 3.10 Resolution of inflammation

A) Flow cytometry analysis of skin biopsies from a patient at presentation with acute GvHD (i) and at follow-up 86 days later (ii). Gates and quantified populations are shown. Dermal macrophages were excluded by autofluorescence (AF) and side scatter in this analysis and CD11c staining was not performed.
B) Changes in gated populations between GvHD presentation and follow-up. Positive axis shows fold change in populations increased over this time period, negative axis shows fold change in populations reduced. Bars indicate mean ± SEM from n=3 patients.

3.6 Summary of results for Chapter 3

Using flow cytometry to dissect the MPs of GvHD dermis has demonstrated an expansion of cells in the CD14 MDM parameter space: HLA-DR+, AF^{mid}, CD14+, CD1c- cells. When combined with a contracted population in the cDC2 parameter space, this is a characteristic profile of acute GvHD. The CD14-rich, CD1c-poor profile is seen in three quarters of patients in the cohort. Patients with this profile are more likely to receive a histological diagnosis of GvHD and to experience clinically significant disease.

Chapter 4. Characterizing macrophages from cutaneous GvHD lesions

4.1 Introduction

Global analysis of MPs in clinical biopsies revealed that macrophage expansion is a common feature of GvHD lesions. These macrophages (GVH14) have a similar immunophenotype to steady-state monocyte-derived macrophages (CD14 MDM) by initial analysis. Clearly defining whether GVH14 are monocyte-derived or dermal macrophages will help understand their origins. Whether these cells are donor and recently recruited or recipient and sessile will provide insight into their immune function and their susceptibility to modifying treatments.

Valuable insights into the steady state MP diversity of human skin have been afforded by simple functional assays and comparative gene expression (Haniffa et al., 2009) (Haniffa et al., 2012). CD14 MDMs and myeloid DCs migrate out of cultured skin explants, but dermal macrophages remain in situ. Myeloid DCs stimulate allogeneic T cell proliferation, but CD14 MDMs and dermal macrophages do not. CD14 MDMs and macrophages share a monocyte-macrophage gene expression signature, but key genes are differentially expressed. A similar approach will be applied to explore the relationship of GVH14 to other skin MPs. Techniques will need to be scaled to accommodate the small number of cells available at biopsy.

4.2 Chapter Aims

4.2.1 Skin strand Aim 2: To compare GVH14 with candidate steady state counterparts

Comparison between GVH14 and CD14 MDM will include:

- Detailing immunophenotype by flow cytometry
- Testing ability to stimulate allogeneic T cells
- Quantifiying chemokine and cytokine production in response to LPS stimulation
- Assessing the chimerism of GVH14 and dependence on circulating monocytes

- Quantitating immune-relevant gene expression in GVH14 and steady-state subsets by NanoString.

4.3 Materials and Methods for Chapter 4

4.3.1 Patient samples

Experiments for Chapter 4 were performed on sorted cells from GvHD skin shave biopsies and from normal skin surplus to mammoplasty/ abdominoplasty. Ethics and cohort characteristics are described in section 3.3.

In 10 GvHD patients undergoing skin biopsy, a simultaneous blood sample (4-8ml) was collected into EDTA.

4.3.2 Sample processing and preparation

Single cell suspensions of dermis or whole skin were prepared (see 3.4.6). Sorted cells were used for cytospin, FISH or NanoString, as described in Chapter 2. Additional functional assays are detailed below.

Blood samples were subjected to density centrifugation to yield a mononuclear cell preparation (see Chapter 2). PBMC were cryopreserved and sorted/ analysed in batches.

4.3.3 MP isolation by Fluoresence activated cell sorting (FACS)

Individual MP populations were isolated from GvHD lesions and control skin by FACS. The sorting strategy is outlined in Figure 4.1. Further primary sorting data from normal skin is presented in Appendix B. Four-way sorting was employed. CD11c-CD14+ macrophages, CD11c+CD14+CD1c- cells and CD11c+CD14-CD1c+ cells were always sorted from GvHD lesions. The fourth population was CD11c+CD14+CD1c+ cells or lymphocytes depending on the downstream experiment. 7 MP populations were isolated from plastic surgery skin (section 4.3.) MP yield was between 200 and 20,000 cells depending on sample and subset.

Typically 4000 CD11c+CD14+CD1c- cells could be isolated. These yields were insufficient for routine purity testing.

Figure 4.1 MP isolation from GvHD lesions by FACS

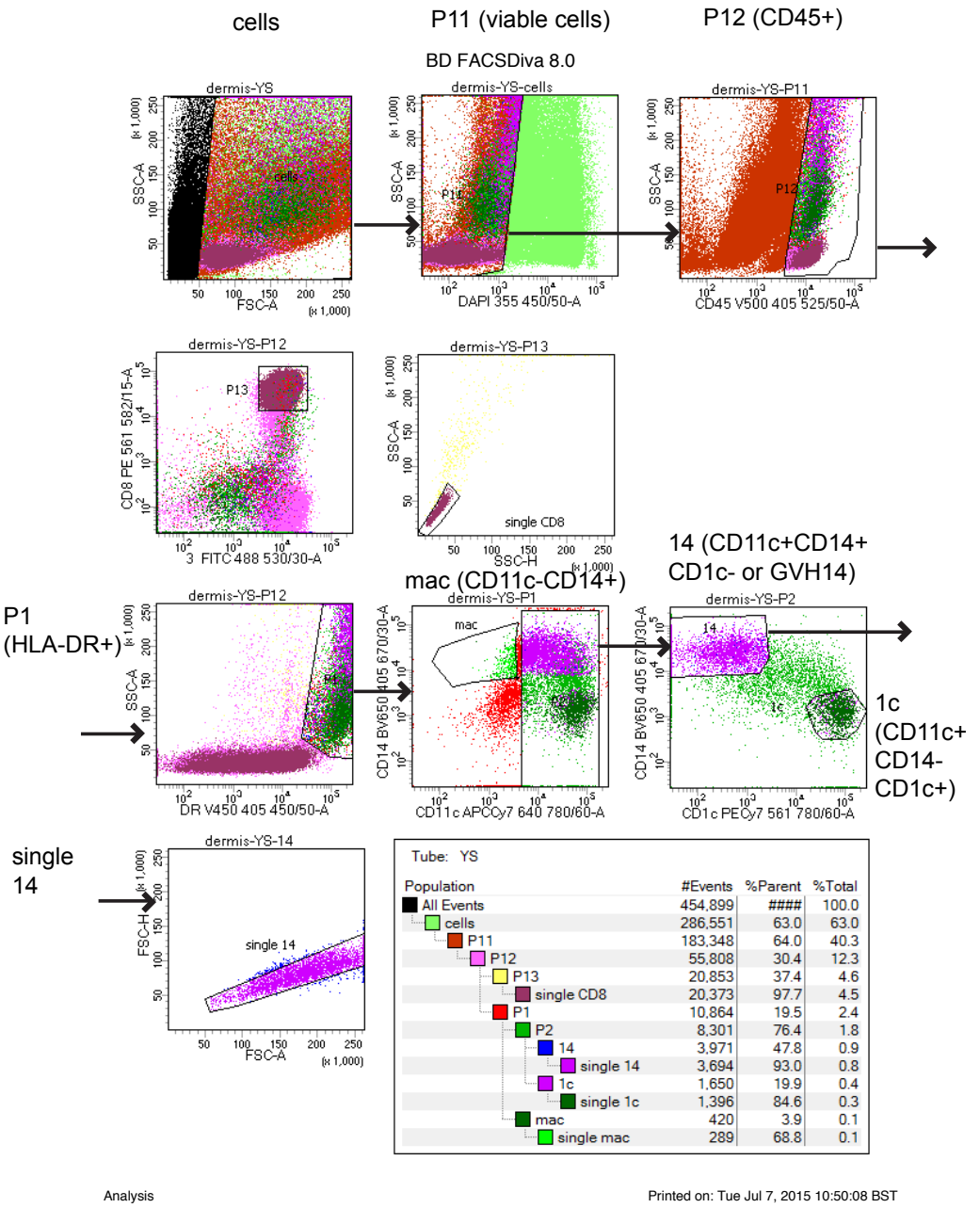

Figure 4.1 MP isolation from GvHD lesions by FACS

Strategy employed for flow cytometric sorting of MP populations from GvHD lesions. Top row: debris and dead cells were excluded and CD45+ leukocytes selected. Second row: single CD8+ T cells were isolated for experiments not included in this thesis. Third row: HLA-DR+ MPs were divided into CD11c-CD14+ macrophages, CD11c+CD14+CD1c- cells and CD11c+CD14-CD1c+ cells. Fourth row: each MP population was refined to single cells (only single 14 shown in this example).

4.3.4 Surface antigen profiling

Surface antigens were tested on GVH14 cells and CD14 MDMs migrating out of culture (each n=5). Cell preparations were divided between 5 tubes and stained as per Table 4.1. Separate preparations were subjected to fixation/ permeabilization and stained with S100A8/9 antibody or isotype (n=3). The staining protocol used 4µl of antibody in 50µl of flow buffer except where specified. Within total migrated cells, GVH14/ CD14 MDMs were identified as DAPI-CD14+ cells.

Table 4.1- Antibody panels for profiling surface antigens by flow cytometry

Tube	PE	APC	FITC	APCCy7	PECy7	
1	CD52	CD1c	CD14	CD14	CD1c	DAPI
2	SIRPa (2ul)	CD11c	CD16	CD14	CD1c	DAPI
3	CD86	CD206	HLA-DR	CD14	CD1c	DAPI
4	CD64	CD163	CD209	CD14	CD1c	DAPI
5	IgG1	IgG1	IgG1	CD14	CD1c	DAPI

Table 4.1 Antibody panels for profiling surface antigens by flow cytometry
Using DAPI and CD14 to identify live GVH14/ CD14 MDMs, expression of 12 surface antigens was tested in 4 combinations (tubes 1-4). The fifth tube included isotype controls.

4.3.5 Fluorescence in situ hybridization (FISH)

GVH14 and CD3+ T cells were sorted out of GvHD biopsies from participants with a gender-disparate BMT donor (n=5). FISH was performed as described in section 2.4.3. All cells with identifiable probes were counted (min 3; max 130).

The peripheral blood chimerism result most proximal to GvHD biopsy was taken from clinical records. All clinical chimerism measurements were performed on CD15+ and CD3+ fractions of peripheral blood using short-tandem-repeat PCR method.

4.3.6 T cell proliferation and activation assay

Bulk allogeneic T cells were prepared from whole blood by immunodensity negative selection. Preparations from 3 donors were made, cryopreserved and stored at -80°C. Aliquots were thawed and labelled with CSFE (section 2.2.3).

Three thousand sorted MPs and 750,000 T cells were re-suspended in 100µl RF10 in a 96-well v-bottomed plate. cDC2s served as a positive control and T cells incubated alone served as a negative control. Plates were incubated at 37°C and 5% CO_2 for 6-7 days.

Cells were re-suspended in flow buffer, prepared for flow cytometry (section 2.3.1) and stained with the following cocktail of antibodies: CD3 V500, CD4 PE, CD8 APCCY7, HLA-DR PERCPCY5.5 and CD69 PECY7. A minimum of 20,000 events was acquired on a FACS Canto II running Diva version 7.

Gates for proliferating T cells (CSFE-) and activated T cells (CD69+/HLA-DR+) were set using the negative control before applying to other samples as staining intensity for CSFE varied slightly between experiments.

4.3.7 Stimulation and cytokine production

GVH14 and CD14 MDM sorted from normal dermis were cultured for 10 hours with or without LPS: $5x10^4$ cells in 50µl RF10 were added to a 96-well U-bottom plate ± 100ng/ml LPS. Supernatants were stored at -80°C and cytokine profiles analysed by Luminex assay (section 2.5.2). Summary characteristics of the GVH14 donors are given in Table 4.2. For multivariate analysis, cytokine concentrations were normalized as follows:

$$\text{Normalized sample\_x cytokine\_n} = \frac{\text{measured sample\_x cytokine\_n}}{\text{Mean cytokine n(all samples)}} + 1$$

Table 4.2 Summary characteristics of GVH14 donors for cytokine and chemokine production experiments

Donor	Experiment	BMT type/ indication	Current immunosuppresion	GvHD onset	CD14: CD1c ratio by flow cytometry	Histology Grade (Lerner)	Max. clinical grade (Glucksberg)
1	Stim and unstim	RIC-TR for Myeloma	Topical steroid	ISW (day+58)	3	2	III
2	Stim only	RIC-TCD for Follicular lymphoma	Ciclosporin (41ng/ml)	ISW (day+71)	5	2	II
3	Stim only	RIC-TCD for Hodgkin lymphoma	None	post-DLI (day+ 302)	57	2	II

4.3.8 Normal skin NanoString

Control skin preparations (breast/ abdominoplasty surplus) were sorted to isolate 7 skin MP populations (n=4). The cDC2 subset was fractionated by CD5 expression for work not included in this thesis. For the purposes of this chapter both CD5- and CD5+ cDC2 were considered replicates of cDC2. Cell pellets were stored at -80°C and prepared in batches. Samples were lysed in a volume buffer RLT + 1% beta-mercaptoethanol to yield 20,000 cells per 5µl. The Immunology v2 panel plus custom code set (see section 2.6.2) was used.

4.3.9 GvHD skin NanoString

GvHD samples were sort-analysed and if sufficient numbers of GVH14 were present, cell pellets were stored. Four samples were selected based on having >3000 cells of CD14+CD1c- phenotype (Table 4.3). All were sorted from dermal digests. Lysates were prepared as above.

Table 4.3 Characteristics of GVH14 donors used for NanoString

Donor	Cell count	BMT type/ indication	Current immunosuppresion	GvHD onset	CD14: CD1c ratio by flow cytometry	Histology Grade (Lerner)	Max. clinical grade (Glucksberg)
1	4000	RIC-TCD for Follicular lymphoma	Oral prednisolone	ISW (day+495)	30	2	II
2	3000	RIC-TCD for AML	Topical steroid	Post-DLI (day+278)	6	2	II
3	3000	RIC-TCD for MDS	Oral prednisolone	ISW (day+215)	177	2 (eczematoid)	II
4	12000	Preconditioned RIC for AML	Ciclosporin (85mg/L)	Acute (day+13)	5	low 2	I

4.3.10 NanoString Quality Control and normalization

Thirty-one samples were run. All passed technical quality controls but 3 failed content normalization, indicating that there was insufficient RNA in these specimens. These samples were excluded and data were re-normalized. PCA was performed to verify quality control. Four subsets from one control skin sort were clear outliers and had low cell inputs/ high positive content normalization scores, so were excluded. The remaining 3 subsets from that sort had higher cell inputs and were retained. Data entering analysis included n=4 LCs, n=2 cDC1, n=6 cDC2, n=3 CD14+CD1c+, n=3 CD14 MDM, n=3 GVH14 and n=4 macrophages.

4.3.11 NanoString analysis

PCA was used to cluster samples, centering on the mean. The data set was filtered using monocyte/ macrophage and DC gene signatures from McGovern et al., 2014. Nineteen of the 111 monocyte/ macrophage genes and 10 of the 99 DC genes were included on the NanoString panel. With this 29-gene expression set hierarchical clustering was performed, with Pearson correlation as the distance metric.

Differential gene expression was tested by t-test between GVH14 and CD14 MDMs, assuming equal variance between groups and setting alpha=0.05. This 44-gene expression set was subjected to hierarchical clustering. Functional annotation of the 38 genes preferentially expressed in GVH14 (i.e. differentially expressed with highest expression in GVH14) was performed in GeneMania.

4.4 Results for Chapter 4

4.4.1 GVH14 have similar morphology and surface immunophenotype to steady state CD14+ MDM

Comparisons between GVH14 and its putative steady state counterpart were made. GVH14 and CD11c-CD14+ cells (dermal macrophage equivalents) were sorted from GvHD lesional skin according to the gating strategy shown in Figure 4.1. Morphology of these cells on cytospin preparations was compared with morphology of CD14

MDM and dermal macrophages from identically sorted normal skin. GVH14, like CD14 MDM had a smaller cytoplasmic volume and fewer basophilic granules than dermal macrophages (Figure 4.2, panel A).

To compare phenotype, GVH14 and CD14 MDM were migrated from explants. This removed macrophages from the analysis and excluded the effect of collagenase on surface antigens. Thirteen antigens were selected based on what is expressed by CD14 MDM and what might separate CD14 MDM from monocytes, as published in McGovern et al., 2014. GVH14 and CD14 MDM had equivalent expression of CD14, CD1c, CD11c and CD209 (Figure 4.2, panel B). HLA-DR and CD86, which are antigens associated with activation and tissue residence, were marginally lower on GVH14. Monocyte associated antigens S100A8/9, CD52, SIRPα and CD64 were more abundantly expressed on GVH14 than CD14 MDM. Macrophage-associated antigens CD163, CD16 and CD206 were also expressed at higher levels in GVH14. The overall immunophenotype of GVH14 was comparable to CD14 MDM but suggested differences in monocyte differentiation conditions. Neither an M1 nor an M2 macrophage phenotype could be inferred from this data: GVH14 shared features of both classically activated M1 (HLA-DR, CD86, CD64) and alternatively activated M2 macrophages (CD163, CD206).

Figure 4.2 Comparison of GVH14 with steady state CD14 MDM

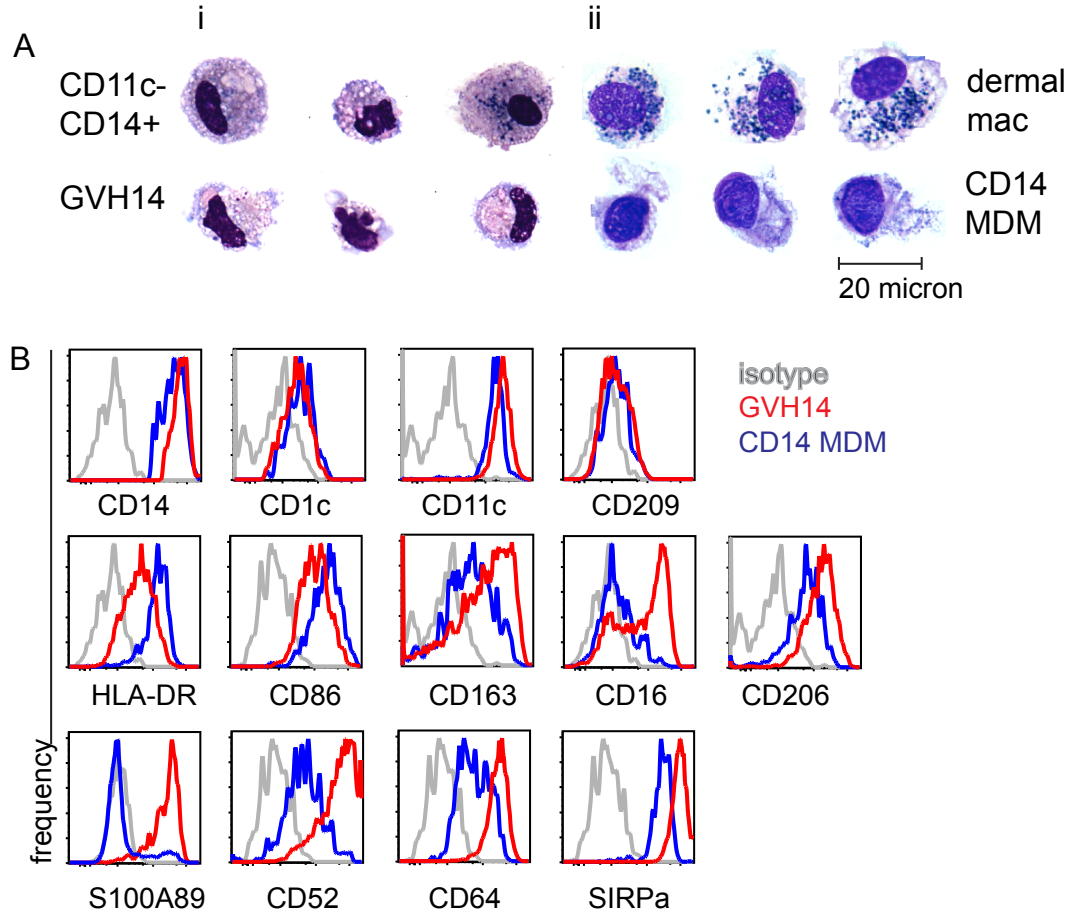

Figure 4.2 Comparison of GVH14 with steady state CD14 MDM

A) Giemsa-stained cytopsin images of cells sorted from GvHD skin (i) and normal skin (ii). B) Surface antigen expression by GVH14 (red line) and CD14 MDM (blue line) compared with isotype control (grey line). This is a representative example of n=6.

4.4.2 GVH14 are donor-derived and frequency correlates with monocyte availability

To examine the hypothesis that GVH14, like CD14 MDM, depend on circulating classical monocytes, correlations between blood and skin were tested. GVH14 were quantified as a proportion of CD45+ leukocytes in dermis by flow cytometry using the definition outlined in Figure 3.3 (HLA-DR+, CD11c+, CD14+, CD1c- cells). Classical monocytes in paired blood samples were quantified as a proportion of CD45+ leukocytes by flow cytometry. Monocytes were defined as lineage (CD3, CD19, CD20, CD56) negative, HLA-DR+, CD14+ CD16- cells (gated as per Figure 5.1).

There was a significant positive correlation between frequencies of these cell types (r^2=0.58, p=0.011) (Figure 4.3, panel A).

In 5 patients who had received transplants from a sex-disparate donor, GVH14 were sorted and subjected to XY FISH. GVH14 were 99.6% donor (mean 99.6%; SEM=0.44). This was similar to the chimerism of blood monocytes (mean 99.4%; SEM=0.6) (Figure 4.3, panels B-C).

Figure 4.3 GVH14 chimerism and relationship to blood monocytes

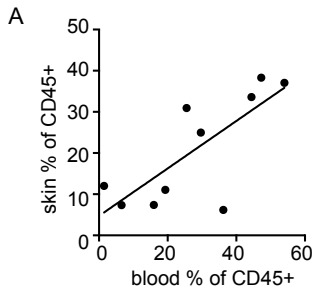

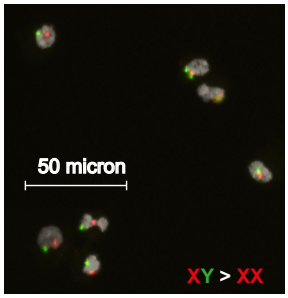

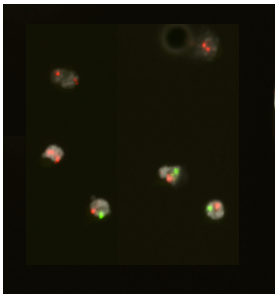

C

		Chimerism (% donor)		
Gender donor>recipient	Day post BMT	GVH 14	Skin T	Blood 15+/3+
M>F	26	97.5	nd	100/100
M>F	32	100	61	100/100
F>M	81	100	48	97/89
M>F	117	100	72	100/82
F>M	215	100	100	100/93

Figure 4.3 GVH14 chimerism and relationship to blood monocytes

A) Correlation between blood classical monocytes and skin GVH14 measured in paired samples by flow cytometry. Bi) Example GVH14 and ii) skin T cells sorted from a GvHD biopsy and subjected to XY FISH. Example shows a female recipient of male donor stem cells. C) Chimerism from M/F mismatched donor /recipient pairs. nd=not done.

4.4.3 GVH14 activate and recruit T cells and produce pro-inflammatory cytokines

When considering the role of GVH14 within a developing GvHD lesion, three properties warranted close inspection. Interactions of GVH14 with T lymphocytes were explored as donor T cells are critical to the pathogenesis of GvHD. Ability to influence local inflammation through cytokine production was tested. Additionally,

the contribution to inflammatory cell recruitment through chemokine production was measured.

Figure 4.4 GVH14 induce proliferation and activation of T lymphocytes

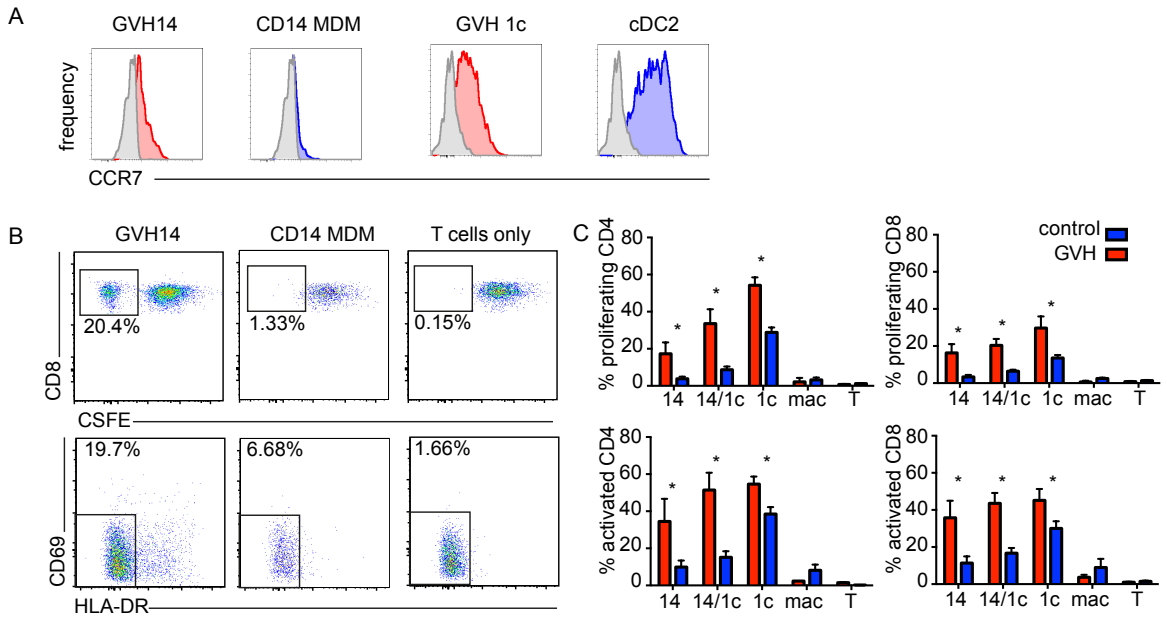

Figure 4.4 GVH14 induce proliferation and activation of T lymphocytes

A) CCR7 expression on CD11c+CD14+CD1c- and CD11c+CD14-CD1c+ cells from control (blue) and GvHD dermis (red) compared with isotype control. Representative staining from n=4. B) Flow cytometry analysis of a T cell stimulation/ activation assay output. Plots are gated on CD8 T cells in representative outputs from GVH 14 and CD14 MDM co-cultures with bulk T cells compared with T cells cultured alone (each co-culture minimum n=3). C) Summary data of T cell stimulation/ activation assays for all conditions. Bars present mean ± SEM; * $p<0.05$ by unpaired t-test.

GVH14s expressed low levels of CCR7, suggesting that they were not capable of migrating to lymphoid tissue via a CCL19/21 gradient (Figure 4.4, panel A). They may still interact with effector or memory T cells in situ. Bulk CD3 cells from three allogeneic donors were used in co-cultures with MP subsets. Both autologous and allogeneic interactions are possible *in vivo*: GVH14 are uniformly donor but skin T cells have mixed chimerism (Figure 4.4, panel B-C). Autologous interactions (donor macrophage to donor T cell) might be considered more important for GvHD pathogenesis. However, quiescent auto-reactive recipient memory T cells could

contribute to pathogenesis with appropriate stimulation or release from suppression. Autologous co-cultures were not performed as signal was predicted to be low and variable due to factors such as calcineurin inhibition. MP subsets were isolated from GvHD lesions by flow sorting. All subsets from GvHD lesions had enhanced ability to induce T cell proliferation and activation, with the exception of macrophages (Figure 4.4, panel C). The comparison to steady state populations was more marked for CD14+ cells than for CD1c+ cells. For example, mean CD4 T cell proliferation was 4.5-fold higher in GVH14 than CD14 MDM but only 1.9-fold higher in GVH CD1c+ cells than normal CD1c+ cells.

Figure 4.5 GVH14 cytokine and chemokine quantification by Luminex

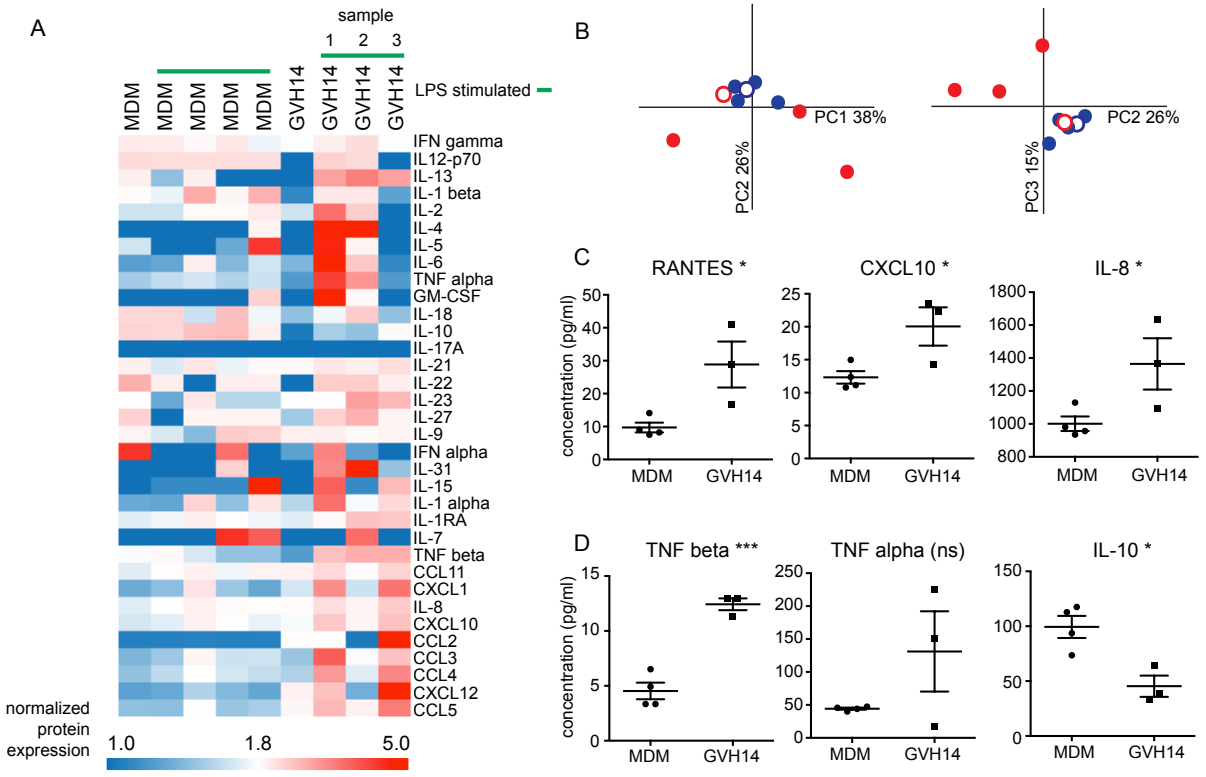

Figure 4.5 GVH14 cytokine and chemokine quantification by Luminex

A) Heat-map of cytokine and chemokine production by 5000 FACS-sorted macrophages during 10-hour stimulation with or without LPS. Samples are normalized to the mean concentration of each protein. Each column represents a specimen. B) PCA plots of normalized protein concentrations showing CD14 MDM in blue, GVH14 in red and un-stimulated samples with open circles. C) Selected chemokine concentrations in stimulated CD14 MDM and GVH14. D) Selected cytokine concentrations in stimulated CD14 MDM and GVH14. * $p<0.05$, ***$p<0.0001$ by unpaired t-test.

In response to a consistent stimulus (100ng/ml LPS), GVH14 samples produced a divergent chemokine and cytokine response from steady state CD14 MDM (Figure 4.5, panels A-B). The GVH14 response was heterogeneous. As demonstrated in the heat-map (Figure 4.5, panel A), GVH14 sample 1 had elevated pro-inflammatory cytokines (e.g. IL-6, TNFα, IFNα and IL-8) and chemokines (e.g. CCL11 and CCL5); GVH14 sample 2 had elevated pro-inflammatory cytokines but a less marked chemokine response and GVH14 sample 3 had minimal pro-inflammatory cytokines but a marked chemokine response. Solid conclusions about basal cytokine and chemokine production cannot be made as only 1 sample yielded sufficient cells for an un-stimulated control. However, it appears that GVH14 and CD14 MDM produce a similar repertoire. It may be the case that GVH14 are primed for an LPS response.

4.4.4 GVH14 and CD14 MDM share a lineage-specific gene expression profile separated by an IFNγ signature

Gene expression profiles of GVH14 and CD14 MDM were compared with those of all other MPs in steady state skin using a NanoString 638-gene panel. PCA was used as a means of dimension reduction: distilling the greatest variation in gene expression into a few key components. The first two components accounted for 54% of the variation. Component 1 divided macrophages from DCs (Figure 4.6, panel A). Component 2 split cDC1s/ LCs from cDC2s and CD14+CD1c+ cells from macrophages. None of the components effectively split CD14 MDM from dermal macrophages. GVH14 clustered with macrophages, overlaying CD14 MDM and dermal macrophages in PC1, 2 and 3. Looking specifically at PRR genes, GVH14 expressed a repertoire similar to CD14 MDM and CD14+CD1c+ cells (Figure 4.6, panel B). The PRR gene profile included *MRC1* (encoding mannose receptor CD206), *TLR1-2, TLR-4* and *TLR-8,* intracellular receptors *NOD1-2, CLEC4A, CLEC4E* and *CLEC5A,* and *CD209* (DC-SIGN). Expression of receptors for response to growth factors CSF1 (M-CSF) and Flt-ligand divided the samples into 2 groups (Figure 4.6, panel C). GVH14, CD14 MDM, dermal macrophages and CD14+CD1c+ cells expressed *CSFR1* but low levels of *FLT-3.* The converse was true of myeloid DCs and LCs. The data set was filtered to include monocyte/macrophage and DC “signature genes”, published in McGovern et al., 2014. Using unsupervised clustering, GVH14 grouped with macrophages (Figure 4.6, panel D).

Figure 4.6 GVH14 have a macrophage-specific gene expression signature

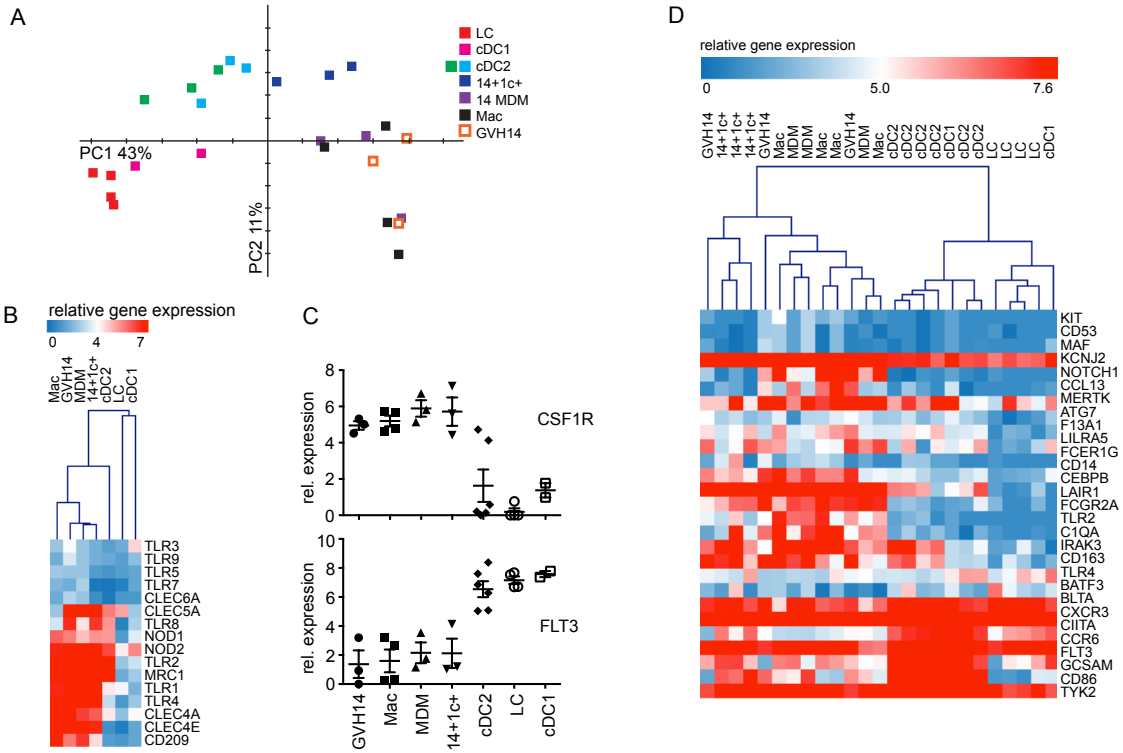

Figure 4.6 GVH14 have a macrophage-specific gene expression signature

A) PCA plot of GVH14 and steady state MP gene expression. B) Cluster dendrogram of PRR gene expression (mean expression values for each subset are shown). C) Relative expression of growth factor receptors CSF1R and FLT3 across the populations (bars show mean± SEM). D) Cluster dendrogram of monocyte/ macrophage and DC lineage gene expression.

Gene expression differences between GVH14 and CD14 MDM were quantified by t-tests. Using stringent criteria (alpha=0.05 and multiple comparison correction) there were no significant differences. Using less stringent criteria (alpha=0.05 only), 44 genes (7%) were differentially expressed between the populations (Figure 4.6). This analysis implied similar gene expression profiles.

Figure 4.7 Comparative gene expression between GVH14 and CD14 MDM

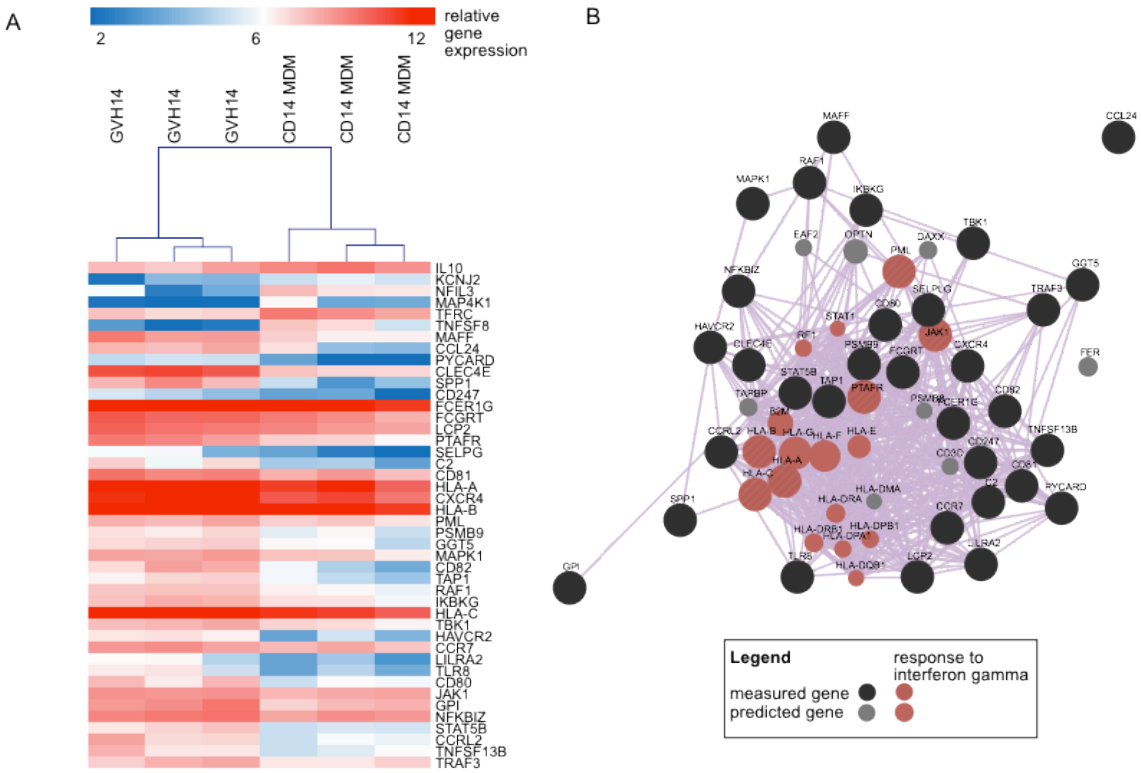

Figure 4.7 Comparative gene expression between GVH14 and CD14 MDM

A) Cluster dendrogram and heat-map of the 44 genes differentially expressed between GVH14 and CD14 MDM. B) Network plot of the 38 genes preferentially expressed by GVH14. Lines indicate co-expression. Nodes represent genes. Node size is maximal in measured genes and is inversely proportional to the rank prediction value in predicted genes (i.e. larger nodes are more significant). Measured genes are black and predicted genes are grey. Genes involved in response to IFNγ are red: solid red nodes are measured genes and striped red nodes are predicted genes.

Functional significance of the 38 genes preferentially expressed by GVH14 was explored using GeneMania. The top 30 functions retrieved are distilled in Table 4.4. IFNγ response and signaling was most significant. Antigen processing/ presentation and intracellular vesicle transport also featured prominently. Capacity to cross-present antigen was mentioned. Positive regulation of lymphocyte/ leukocyte activation was the third most-retrieved functional annotation.

Table 4.4 Functional annotations of genes preferentially expressed in GVH14 over steady state CD14 MDM

Function	Significance	Measured genes	Network genes
Interferon-gamma-mediated response or signaling	1,2,3	*PML, JAK2, PTFAR, HLA-A,B,C*	*STAT1, IRF1, TAPBP, B2M, HLA-E,F,G, HLA-DRA, DRB1, DPA, DPB1, DQB1*
Antigen processing and presentation	4,9,11,12,13, 15,22,24,27	*PSMB9, PYCARD, TAP1, HLA-A,B,C, FCGRT, CD81, LILRA2*	*TAPBP, B2M, HLA-E,F,G, HLA-DRA, DRB1, DPA, DPB1, DQB1, PSMB5*
Endocytosis & intracellular transport	5,6,7,8,10,14,16, 17,19 20,21, 29	*HLA-A,B,C, TAP1*	*TAPBP, HLA-E,F,G, HLA-DRA, DRB1, DPA, DPB1, DQB1, B2M*
Regulation of T cell activation	26,28	*CD80, CCR7, CD247, PYCARD, HLA-A*	*HLA-DRA, DRB1, DPA, DPB1, DQB1, HLA-G, IRF1, CD3D*

Table 4.4 Functional annotations of genes preferentially expressed in GVH14 over steady state CD14 MDM

Top 30 functional annotations retrieved by GeneMania for the genes preferentially expressed by GVH14 relative to steady state CD14 MDM. Network genes are introduced by predicted co-expression. Significance is ordered by false discovery rate (1= 2.9×10^{-24}; 30=3.4×10^{-12}).

4.5 Summary of results for Chapter 4

Functional, phenotypic and gene expression comparisons support the premise that CD14+ CD1c- cells expanded in GvHD lesions are the inflammatory counterpart of steady state CD14 MDMs. Differential gene expression suggests that IFNγ may feature in the derivation of GVH14 from monocytes. Functional assays have demonstrated that GVH14 can activate, expand and recruit T cells. Functional annotation of differential gene expression proposes that GVH14 are primed for antigen presentation and may also be capable of cross-presenting antigen.

Chapter 5. Modelling monocyte to macrophage differentiation in GvHD

5.1 Introduction

Evidence from Chapter 4 supports the premise that GvHD lesions are infiltrated with monocyte-derived macrophages. Monocytes recruited to tissue may have pro-inflammatory or immunomodulatory roles depending on the setting (Bain and Mowat, 2014), (Grainger et al., 2013). Gene expression and *in vitro* function assays suggest that GvHD skin monocyte-derived macrophages are pro-inflammatory and capable of stimulating T cells. Accordingly, they could be a novel target for disease-modifying therapy.

In this chapter, the activity of GVH14 in tissue is explored further. Using *in vitro* GVH14 equivalents, interactions with keratinocytes and functions within whole skin are tested. In order to generate GVH14 equivalents, the 'nature and nurture' of GvHD monocytes is considered. Recent work on a murine *Toxoplasma* model has demonstrated that distinct transcriptional programmes are initiated in monocyte precursors in bone marrow as a consequence of remote tissue inflammation (Askenase et al., 2015). This suggests that some attributes of monocyte-derived macrophages may be established before tissue recruitment and differentiation. Monocyte differentiation plasticity in response to cytokines, hormones and growth factors is well recognized. Varying stimuli *in vitro* can give rise to a spectrum of macrophage activation (Xue et al., 2014). Monocytes differentiating *in vivo* experience a more complicated milieu of stimuli and characterizing the tissue microenvironment may give additional insight into the activation and functional properties of inflammatory macrophages.

5.2 Chapter Aims

5.2.1 Skin strand Aim 3: To investigate the differentiation conditions and in situ functions of GvHD lesional macrophages.

The differentiation conditions of GVH14 are considered from two perspectives: firstly whether peripheral blood monocytes in GvHD are different from monocytes in steady state, and secondly what signals they receive on recruitment to inflamed skin. These results will be used to inform *in vitro* generation of GVH14 equivalents for use in a skin explant model of GvHD and a keratinocyte co-culture assay.

5.3 Materials and Methods for Chapter 5

5.3.1 Patient samples

Patient and healthy donor blood samples (see sections 3.4.1 and 4.3.1) were used to generate NanoString data.

Monocyte quantification from NHS full blood counts was recorded for GvHD patients, BMT controls and from healthy volunteers enrolled in the LPS inhalation study (see Chapter 7). Post-BMT patients with neutropenia (neutrophils $<1x10^9$/L) were excluded. GvHD counts taken >140 days post-transplant were excluded as there were no BMT controls to match later time points.

Cryopreserved pairs of PBMC from pre-treatment recipients and their donors were used to establish mixed leukocyte reactions (MLRs). Skin shave biopsies were obtained from 4 patients to set up skin explant experiments.

Skin shave biopsies from 12 BMT recipients with suspected GvHD were used for whole-skin NanoString. Rachel Dickinson collated this material as part of BloodWise grant 09031 “Conditioning the Host & Immune Activation.”

5.3.2 Blood monocyte NanoString

Monocytes were sorted from normal and GvHD blood PBMC preparations (Figure 5.1 and Appendix B). CD14 monocytes from n=6 GvHD donors with single-organ skin GvHD were selected (Table 5.1). Cell pellets were stored at -80°C. All three monocyte subsets from healthy donors were used for comparison. Classical monocyte data had previously been generated by Gary Reynolds. I added intermediate and non-classical monocyte data from an additional three donors. Samples were adjusted to concentration of 10,000 cells per 5µl in buffer RLT + 1 % beta-mercaptoethanol. NanoString Immunology v2 panel plus custom code set was used.

Table 5.1 Characteristics of patients for GVH blood NanoString experiment

	BMT type/ indication	Current immunosuppresion	GvHD onset	CD14: CD1c ratio by flow cytometry	Histology Grade (Lerner)	Max. clinical grade (Glucksberg)	Monocyte count $*10^9$/L	CRP mg/L
A	Preconditioned RIC for AML	Ciclosporin (85 ng/ml)	Acute (day+13)	5	2	I	0.3	283
B	RIC-TCD for AML	Ciclosporin (15 ng/ml)	ISW (day+388)	5	4	I	1.08	26
C	RIC-TCD for MDS	Ciclosporin (12 ng/ml)	ISW (day+102)	2	Eczematoid (no grade given)	III	0.74	12
D	RIC-TCD for Follicular lymphoma	Ciclosporin (41ng/ml)	ISW (day+71)	5	2	II	0.69	28
E	RIC-TR for ALL	None	ISW (day+ 376)	1	1-2	II	1.03	22
F	RIC-TCD for Hodgkin lymphoma	None	post-DLI (day+ 302)	57	2	II	1.25	6

Figure 5.1 Isolation of monocytes from PBMC by FACS

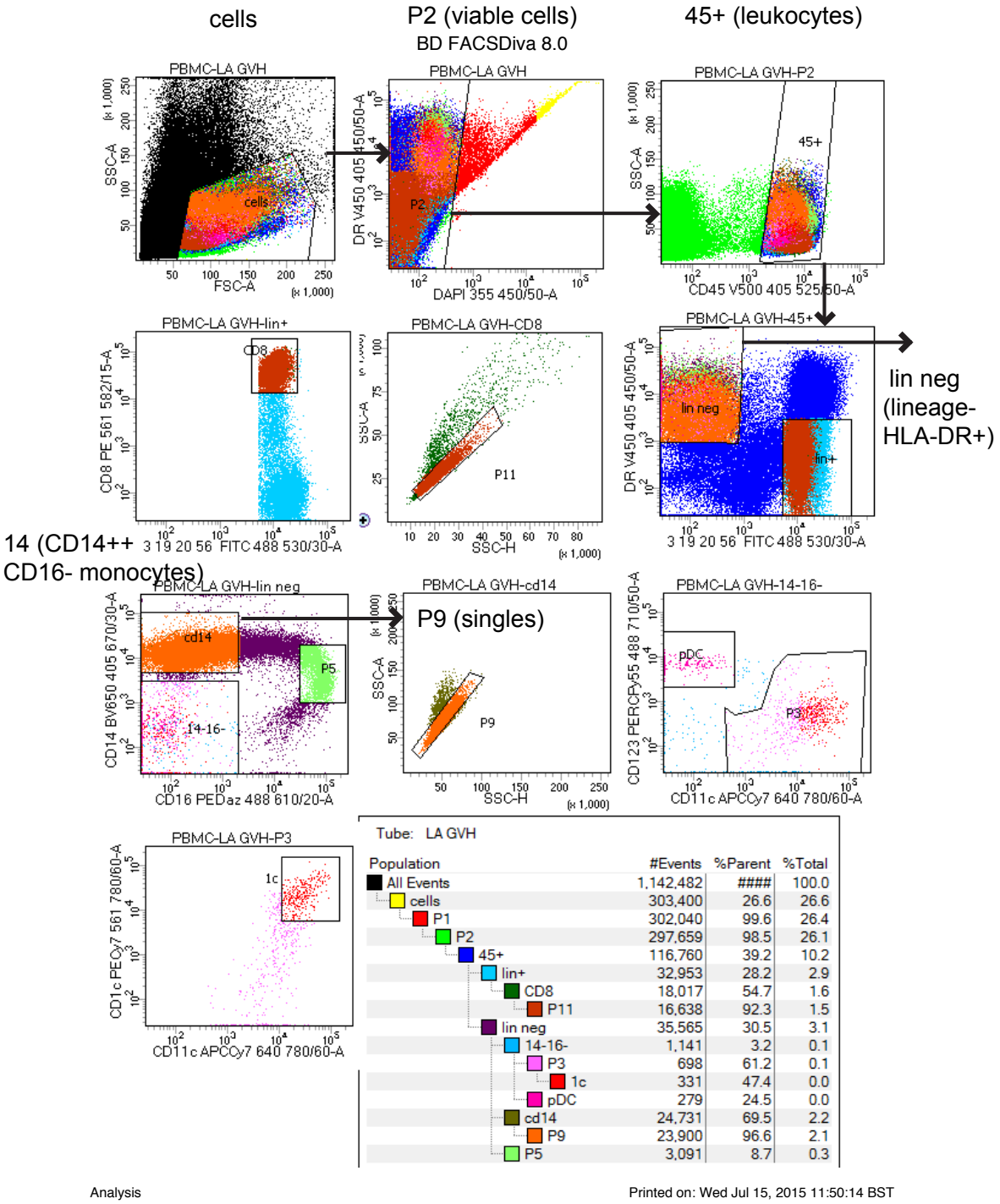

Figure 5.1 Isolation of monocytes from PBMC by FACS

Gating strategy for isolation of monocytes from PBMC illustrated by primary sorting data from a GvHD blood preparation. Top row: viable leukocytes are selected. Second row: lineage (CD3, 19, 20, 56) negative, HLA-DR positive cells are selected. Third row: single CD14++CD16- classical monocytes are sorted. Plots not discussed related to sorting not included in this thesis.

5.3.3 Whole skin NanoString

Rachel Dickinson processed skin for NanoString experiments. Skin shave biopsies were diced with a scalpel and transferred into 350µl buffer RLT + 1% beta-mercaptoethanol. Material was passed 15 times through a 21-gauge needle, vortexed and stored at -80°C. RNA was extracted from lysates so that a consistent amount could be used for NanoString. Samples were thawed at 37°C for 20 minutes, passed 15 times through an 18-gauge needle and centrifuged for 3 minutes at 17,000 x g. The supernatant was used for RNA extraction with Qiagen RNeasy Mini Kit (cat. 74104). RNA was eluted in 30µl water and quantified on a NanoDrop spectrophotometer. Experiments used 150ng RNA per sample with the NanoString Immunology v2 panel. All A260/280 ratios were >2.

Kile Green did the initial data processing. Quality control and normalization was performed in NSolver. Samples were separated by pathology grade into 2 categories: GvHD grade 0 and GvHD grade 2. The “grade 0” category included n=3 grade 0, n=2 grade 1 and n=1 borderline GvHD. The “grade 2” category included n=5 grade 2 and n=1 grade 3. Fold changes between gene expression in the 2 categories were calculated. I performed subsequent analyses.

5.3.4 Chemokine/ chemokine receptor analysis

Chemokine ligands on the Immunology v2 NanoString panel were filtered to include those with predicted impact on monocytes, T cells or both. Predictions were made using Entrez Gene Summary, GeneCards Summary and UniProtKB/Swiss-Prot information from the GeneGards website.

Chemokine receptor expression was inferred from GVH14 and GvHD monocyte NanoString data using the boxplot function of NSolver. Populations were considered to express the transcript if the median log2 expression was >2 and the lower tail of the boxplot (1.5 x lower limit of the interquartile range) was >0.

5.3.5 Quantifying cytokines from GvHD lesions

Skin conditioned media were prepared from n=12 GvHD biopsies and n=5 controls (1 normal skin surplus and 4 BMT recipients at day+100 without rash). A 3x1mm section of skin was cultured in 500µl RF10 for 48 hours. Supernatants were stored at -80°C and batch analysed by Luminex. The Procartaplex 45-plex panel was used (eBioscience). Concentrations were calculated from a standard curve in Procartaplex Analyst.

5.3.6 Monocyte-derived macrophage generation

CD14+ monocytes were isolated from healthy donor peripheral blood by magnetic bead positive selection or FACS sorting (see section 2.2.2). Five hundred thousand monocytes per well were cultured in 24-well plates in 500µl RF10 supplemented with 100ng/ml GM-CSF for M1 polarization or 100ng/ml M-CSF for M2 polarization. Medium and non-adherent cells were completely removed on day 3 and replaced with 500µl fresh medium plus G-MCSF/ M-CSF. Medium was removed again on day 7 and replaced with 500µl fresh medium with or without 25ng/ml IFNγ and 100ng/ml LPS for un-stimulated and stimulated conditions. To harvest cells, medium was removed, 500µl cold PBS without calcium or magnesium was added to each well and plates were kept on ice for 10 minutes to allow cells to detach. Cells could then be dislodged by pipetting. Surface antigen profile of cells was tested by flow cytometry, as detailed in 4.3.3. Aliquots of 20,000 cells were harvested for NanoString. The Immunology v2 panel plus was used.

5.3.7 Mixed leukocyte reaction macrophage generation

MLRs were established with cryopreserved PBMC from transplant donor recipient pairs. Recipient PBMCs (isolated prior to conditioning) were used as stimulator cells and were irradiated (20Gy) to prevent expansion. Donor PBMCs were added at a 1:1 ratio in 1ml RH10 per million donor cells. MLRs were incubated in vented T25 culture flasks for 7 days at 37°C and 5% CO_2. Cells were harvested and prepared for flow cytometry.

To sort macrophages the following antibodies were used: CD3+19+20+56 FITC (lineage), HLA-DR V500, CD14 Qdot 655, CD16 APCH7, CD64 PE and CD206 APC. Sort gating and antibody details are given in Appendix B. MLR macrophages were identified as DAPI-, HLA-DR+ cells co-expressing CD14 and CD16.

5.3.8 Skin explant assay

The skin explant assay, designed to test the effect of allogeneic cells in a donor-recipient MLR (Dickinson et al., 1998), was modified to test the function of MLR-macrophages.

A donor-recipient MLR was initiated, as described above, with 10-30 million stimulator/ responder PBMC. The yield and viability of harvested cells was assessed by counting with Trypan blue. One million cells were reserved as a positive control and the remaining cells were prepared for flow sorting. MLR macrophages were sorted as described above. MLR T cells were identified as DAPI-, lineage+, SSC^{lo} cells. Cells were re-suspended in 200µl RPMI containing penicillin, streptomycin, L-glutamine and 20% heat-inactivated patient serum and added to individual wells of a 96-well U-bottomed plate.

A recipient skin shave biopsy was taken prior to the initiation of BMT conditioning. Equal 1-2mm squares were added to each well. Test conditions were: medium only (negative control), $1x10^6$ PBMC (positive control), $3\text{-}4x10^5$ T cells (sorting control) and $6\text{-}8x10^4$ macrophages (test population). Skin was cultured for 72 hours, harvested in to 10% buffered formalin and stained with haematoxylin and eosin. Histological changes consistent with GvHD were graded using the Lerner classification. An experienced assessor without knowledge of the test conditions assigned grades (Xiao Nong Wang). Four independent experiments were performed.

5.3.9 Keratinocyte apoptosis assay

HaCaT, a transformed keratinocyte cell line, was acquired from PromoCell. HaCaT was cultured in T25 flasks in RF10. Cells were split twice weekly by detaching, counting, and reseeding in a flask with fresh medium. Cells were detached by

washing away culture medium with PBS, incubating with trypsin for 10 minutes at room temperature, re-suspending detached cells in fresh medium and spinning to pellet cells.

HaCaT were seeded into a 24-well plate at a density of 10,000 cells per well 24 hours prior to the assay, aiming to achieve approximately 80% confluence at time zero. MLR macrophages were generated and isolated as described above. Macrophages were added to the wells at effector to target ratios 50:1, 25:1 and 10:1 in RF10. Co-cultures were maintained at 37°C and 5% CO_2 for 5 hours.

To harvest, wells were treated twice with 1ml trypsin as described above. Adherent cells were detached by gentle pipetting. Care was taken to treat all wells identically, recognizing that the detachment process may damage membrane integrity. Cells were washed once in PBS and once in Annexin V binding buffer. CD45 FITC, Annexin V PE and 7-AAD were added for 15 minutes at room temperature. Data were acquired on a FACS Canto II. HaCaT were identified as CD45- cells with high SSC. Dead (annexin V+ 7AAD+) and early apoptotic (annexin V+ 7AAD-) cells were quantified in FlowJo.

5.4 Results for Chapter 5

5.4.1 Monocytes are expanded and DCs reduced in GvHD peripheral blood

Absolute monocyte counts were recorded from NHS full blood counts in GvHD patients, BMT controls and healthy volunteers (Figure 5.2, panel A). Mean counts (± SEM) were 0.66 ± 0.06, 0.61 ± 0.12 and 0.48 ± 0.02 respectively. The mean count in GvHD differed significantly from healthy blood (p=0.012) but not from BMT control (p=0.645). Twenty-eight percent of GvHD samples had a monocyte count higher than the normal range. Considering the two BMT samples with markedly elevated monocyte counts, one had quiescent GvHD and the other had developed GvHD shortly afterwards. This analysis demonstrates that while the expansion of monocytes in GvHD is subtle, it is absolute and not simply a proportional increase due to T cell depletion. Monocyte and DC subsets were quantified by flow cytometry in PBMC preparations from blood taken at the time of GvHD biopsy and compared

with healthy donor blood (Figure 5.2, panel B-C). As a proportion of leukocytes, classical monocytes were significantly expanded (mean ± SD 33% ± 17 in GvHD and 14% ± 6 in normal). Myeloid DCs were contracted in GvHD but pDCs were not significantly different. Taking a global view, the monocyte: DC ratio was 4-fold higher in GvHD than in normal blood (Figure 5.2, panel D).

Figure 5.2 Blood monocytes are expanded in GVHD

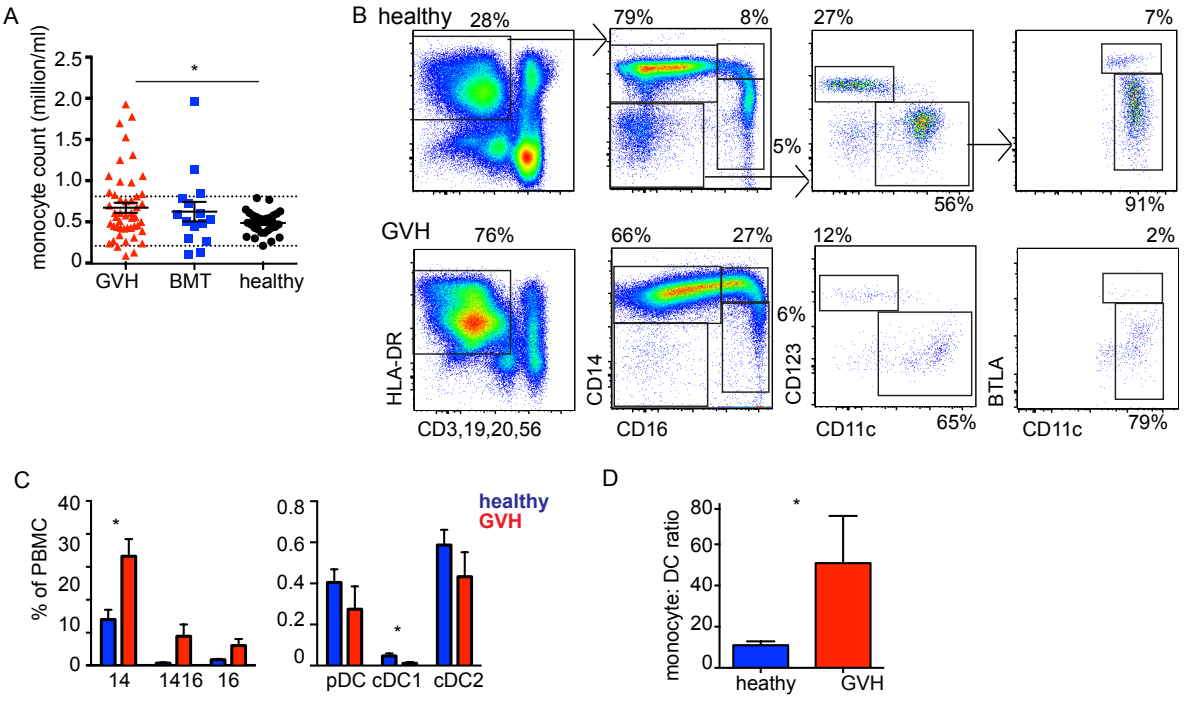

Figure 5.2 Blood monocytes are expanded in GvHD

A) Monocyte counts from NHS full blood counts in GvHD patients (n=47), BMT controls (n=15) and healthy volunteers in the LPS inhalation study (n=32). Bars show mean ± SEM. Dashed lines at y=0.2 and 0.8 demarcate the normal range.
B) Flow cytometry analysis of PBMC from healthy donor blood and GvHD blood. Classical, intermediate and non-classical monocytes are HLA-DR+, CD14++CD16-, CD14++CD16+ and CD14+CD16++ respectively. Plasmacytoid DCs are CD123+CD11c-, cDC1 are CD11c+BTLA++ and cDC2 are CD11c+BTLA$^{lo\text{-}mid}$. Percentages indicate the population frequency relative to the parent gate.
C) Frequency of each MP subset as a proportion of CD45+ cells in healthy blood (n=4) and GVH blood (n=10). Bars show mean ± SEM. D) Ratio of monocytes to DCs in healthy donors compared with GvHD. *p<0.05 by unpaired t-test (C) and Mann-Whitney test (D).

5.4.2 GvHD monocytes carry an IFNγ gene signature

In Chapter 4, differential gene expression was identified between monocyte-derived macrophages in GvHD relative to normal dermis. To address whether these differences arose from recruitment to inflamed skin or whether the monocytes themselves were altered in GvHD, NanoString was performed on classical monocytes. This monocyte subset was selected as it is the most likely precursor of a monocyte-derived macrophage. Six GvHD donors with single-organ skin GvHD were used (see Table 5.1). All 3 monocyte subsets were sorted from healthy donors for comparison.

Figure 5.3 Distinct gene expression in classical monocytes from GVHD versus healthy donor blood

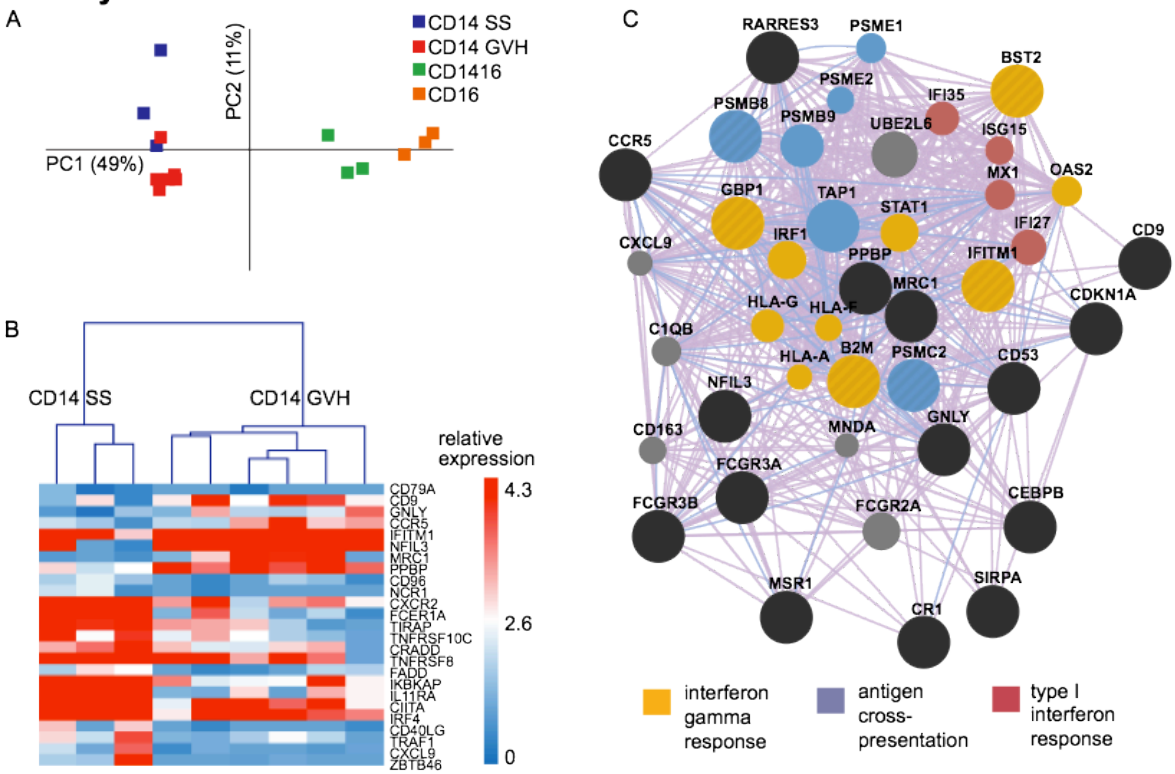

Figure 5.3 Distinct gene expression in classical monocytes from GvHD versus healthy donor blood

A) PCA plot of NanoString gene expression data from GvHD classical monocytes (CD14 GVH) and healthy donor classical (CD14 SS), intermediate (CD1416) and non-classical monocytes (CD16).
B) Cluster dendrogram and heat-map showing expression of the 25 genes differentially expressed between healthy donor classical monocytes and GvHD classical monocytes with $p<0.05$ and mean fold-difference>1.5.
C) Network plot of genes preferentially expressed by GvHD relative to healthy donor classical monocytes.

On PCA, component 1 divided intermediate and non-classical monocytes from classical monocytes (Figure 5.3, panel A). Component 2 separated normal blood from GvHD blood monocytes. One hundred and one (16%) of genes were differentially expressed between GvHD and steady state classical monocytes. Genes preferentially expressed in GvHD were fewer then those preferentially expressed in steady state (20 versus 81). Those with a fold difference >1.5 are displayed as a heat map (Figure 5.3, panel B).

Preferentially expressed by GvHD monocytes were IFNγ response genes *B2M, BST2, IFITM1* and *GBP1* (Figure 5.3, panel C). Genes involved in type I interferon response and antigen processing/ cross-presentation also featured. Phagocytic receptor genes *MRS1*, *MRC1* (CD206) and *FCGR3A/B* (CD16) were more highly expressed in GvHD monocytes. Elevated *CCR5* expression suggested heightened response to chemokine ligands CCL2-5. Preferential expression of *GNLY* (granulysin)- a cytotoxic granule component typically seen in CD8 T cells and NK cells, and *PPBP* (CXCL7)- a platelet-derived chemokine was noted, but not obviously explained.

GO annotations linked to genes preferentially expressed by steady state monocytes included “TLR-4 signalling pathway”, “positive regulation of innate immune response” and “positive regulation of cytokine production” (data not shown). Modest but significant elevations of *NOTCH1* and *NOTCH2* were seen and reinforced by elevations of signalling pathway members. As NOTCH proteins are critical in cell-fate determination, it is possible that GvHD blood monocytes have altered propensity for further differentiation.

5.4.3 GvHD skin microenvironment is poised to recruit and differentiate monocytes

Next, the ability of the GvHD lesion to recruit, instruct and differentiate monocytes was examined. Recruitment was predicted by chemokine receptor gene expression in the GvHD monocyte and skin GVH14 NanoString datasets. Both datasets were considered as interaction with inflamed endothelium may be expected to alter chemokine sensitivity. GvHD monocytes expressed genes for chemokine receptors CCR1, CCR2, CCR5, CX3CR1, CXCR2 and CXCR4. The expression pattern in skin

GVH14 cells was similar, except CCR2 and CX3CR1 transcripts were undetectable and CCR7 was expressed. Chemokine ligand transcripts were identified in the whole skin NanoString dataset (Rachel Dickinson & Kile Green). Ten of the 13 ligands capable of recruiting GvHD monocytes were up-regulated in GvHD skin relative to BMT control (Figure 5.4, panel A).

Figure 5.4 GvHD skin microenvironment is poised to recruit and differentiate monocytes

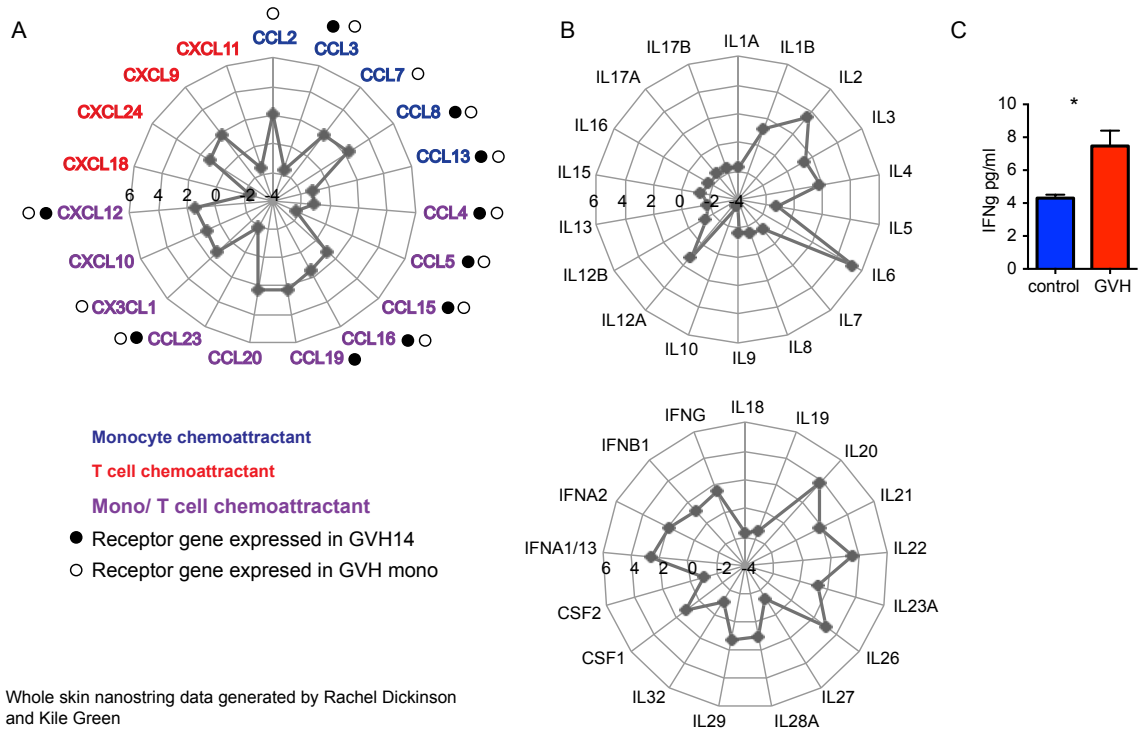

Whole skin nanostring data generated by Rachel Dickinson and Kile Green

Figure 5.4 GvHD skin microenvironment is poised to recruit and differentiate monocytes

Fold differences in selected gene expression by NanoString in GvHD relative to BMT control whole skin. A) Chemokine genes, organized by potential to attract monocytes (blue), T cells (red) or both monocytes and T cells (purple). Filled dot indicates the relevant chemokine receptor is expressed in skin GVH14 cells; open dot in GvHD blood monocytes. B) Growth factor, interferon and interleukin genes. C) IFNγ concentration in supernatant from GvHD biopsy culture. * $p<0.05$ by unpaired t-test.

Expression patterns concerning interleukin, interferon and colony stimulating factor genes in whole skin were surveyed to gauge the environmental influences facing recruited monocytes. Globally, GvHD skin was a Th1 environment, with elevated IL-2, IL-12 and IFNγ and reduced IL-10 transcripts (Figure 5.4, panel B). Genes for interleukins that maintain epithelial integrity (e.g. IL-20, IL-22) were over-expressed. IL-6 transcript was particularly elevated, but IL-8 suppressed, suggesting MP but not neutrophil innate immune activation.

According to simplified models of monocyte to macrophage transition, M-CSF, GM-CSF, IL-4 and IFN γ/β instruct distinct differentiation and activation programs. GM-CSF and IFNγ induce a classically activated (M1) phenotype, while M-CSF and IL-4 instruct an alternatively activated (M2) phenotype. Elevated expression of M-CSF, IL-4 and IFN γ/β genes were seen in GvHD lesions. Significantly higher levels of secreted IFNγ were detected in GvHD compared with control skin cultures (Figure 5.4, panel C). This suggests GVH14 macrophages are forged in an environment intermediate between the M1 and M2 paradigms.

5.4.4 Monocytes differentiated in an MLR resemble GVH14

A method of generating GVH14 equivalents *in vitro* was sought in order to perform more extensive tests on their function. Based on the data presented above, it was predicted that M1 or M2 protocols would be insufficient and that Th1 cytokines may be required. To provide a pathologically relevant context, MLRs were established from transplant donor and recipient PBMCs. Cells with macrophage morphology were clearly identified in the MLR output (Figure 5.5, panel A). Using flow cytometry to dissect the output, macrophages were identified as SSC^{hi} HLA-DR+ cells expressing CD14 and CD16 (Figure 5.5, panel B). In common with GVH14, MLR macrophages expressed CD64 and CD206. Macrophages varied from 3-24% of output cells. They were significantly more abundant in related donor than in unrelated donor MLRs (macrophage: lymphocyte ratio 0.4 ± 0.2 and 0.09 ± 0.05 respectively) (data not shown).

Testing similarity of MLR macrophages to GVH14s was challenging. MLR macrophages were significantly more autofluorescent, which made it difficult to compare surface antigen expression directly. With gene expression profiles, major differences between cultured blood cells and *ex vivo* tissue cells were anticipated. Comparing cultured macrophages and GVH14 by PCA, the first principal component split stimulated from un-stimulated cells, with GVH14 falling mid-way (Figure 5.5, panel C). The second principal component split cultured cells from GVH14. On the third principal component, M1 macrophages were separated from M2 macrophages, with GVH14 and MLR macrophages falling mid-way. GVH14 and macrophages shared similar expression of a number of GVH14-defining genes (Figure 5.4, panel

D). While MLR macrophages could be said to resemble GVH14 it was difficult to establish that they were the optimal *in vitro* model.

Figure 5.5 Monocytes differentiated in an HLA-matched MLR resemble GVH14

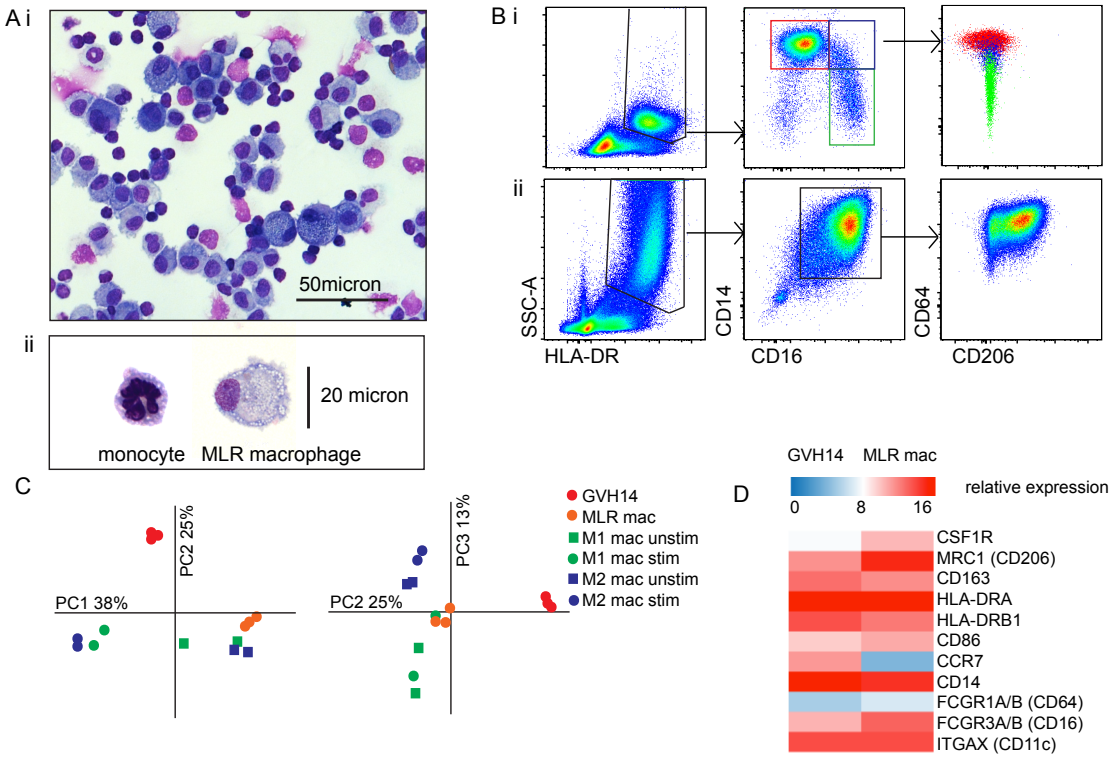

Figure 5.5 Monocytes differentiated in an HLA-matched MLR resemble GVH14.

Ai) Cytopsin of an MLR output at day 7, Giemsa stained, imaged at 20x magnification. Aii) Comparison of monocyte and MLR macrophage morphology at 40x magnification.
Bi) Flow cytometry analysis of PBMCs, gating HLA-DR+ MPs, and assessing CD64/ CD206 expression on classical (red), intermediate (blue) and non-classical (green) monocytes. Bii) Applying the same analysis to MLR output to identify CD14, CD16, CD64 and CD206 expression on MLR macrophages.
C) PCA plots of NanoString gene expression in GVH14 and cultured macrophages (stim= LPS and IFNγ stimulation for 24 hours)
D) Heat-map of selected gene expression in GVH14 and MLR macrophages.

5.4.5 MLR macrophages mediate skin damage in an explant model of GvHD

Functions of macrophages at the site of skin GvHD injury were tested using a skin explant model. Using the total output from a donor-recipient MLR generated recipient skin damage consistent with Lerner grade 3, as has previously been

reported (Figure 5.6, panel B). Introducing MLR macrophages in the absence of T cells could also induce recipient skin damage (median grade 2). Features of skin damage included swelling of basal keratinocytes (white arrow) and oedema at the dermo-epidermal junction (black arrow) in grade 2 (Figure 5.6, panel A). Keratinocyte apoptosis (yellow arrow) and extensive cleft formation at the dermo-epidermal junction (red arrow) occurred in grade 3.

Figure 5.6 MLR macrophages induce tissue damage in a skin explant model of GvHD

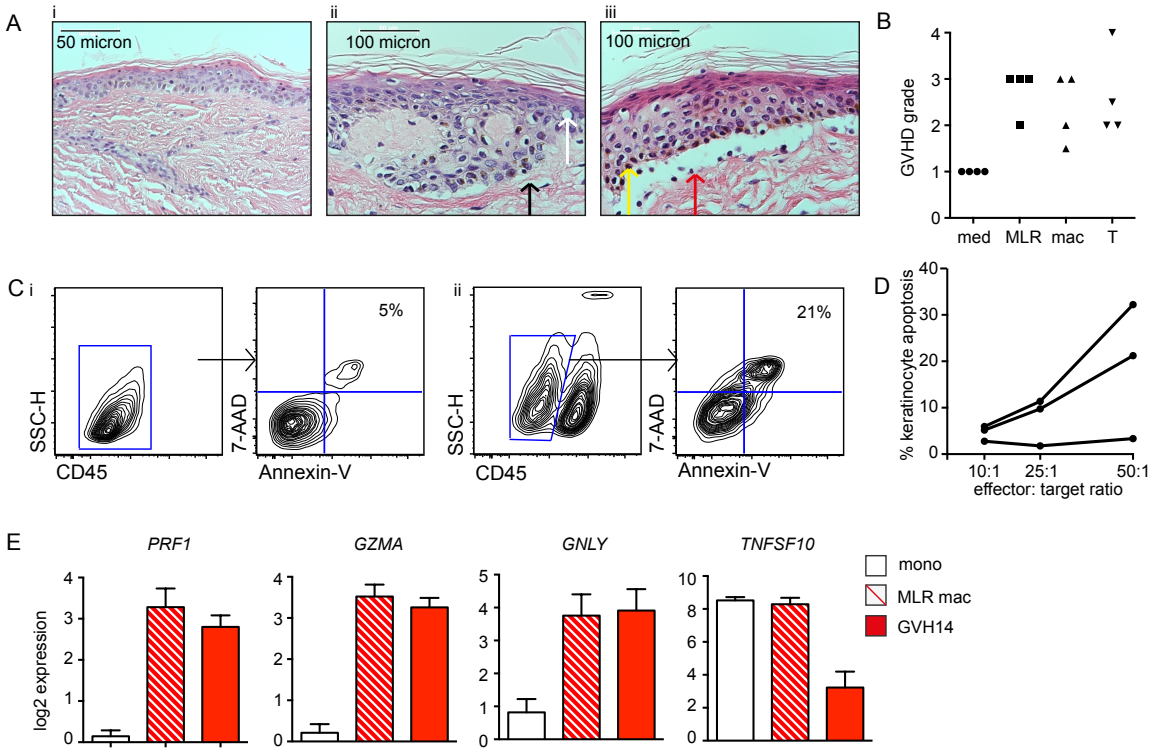

Figure 5.6 MLR macrophages induce tissue damage in a skin explant model of GvHD

A) H&E stained images of recipient skin co-cultured with medium alone (i) imaged at 20x magnification or with MLR macrophages (ii, iii) imaged at 40x magnification. Coloured arrows representing features of tissue damage are discussed in the text.
B) Median GvHD grade in explant skin co-cultured with the indicated cell type (summary of n=4).
C) Detection of apoptotic HaCaT when cultured alone (i) or in the presence of macrophages (ii).
D) Summary of keratinocyte apoptosis with 3 MLR macrophage lines.
E) Candidate cytotoxic effector gene expression by NanoString.

To examine direct effects of macrophages on keratinocytes, MLR macrophages were co-cultured with a keratinocyte cell line. Cells with established apoptosis were detected as Annexin V+ 7-AAD+ by flow cytometry (Figure 5.6, panel C). Co-culture with macrophages induced marked keratinocyte apoptosis using two of the three MLR macrophage lines tested (Figure 5.6, panel D).

Potential mediators of dermo-epidermal damage were considered. Activated macrophages have high secretory activity (Takemura and Werb, 1984). Potentially damaging products include proteinases such as collagenase, reactive oxygen species and cytolytic factors. As keratinocyte apoptosis, and not simply disruption of extracellular matrix was seen in explants, attention was focused on cytolytic or pro-apoptotic factors. Analysing candidate gene expression by NanoString, genes for cytotoxic effectors perforin (*PRF1*), granzyme A (*GZMA*) and granulysin (*GNLY*) were up-regulated in MLR macrophages and similarly expressed in GVH14 (Figure 5.6, panel E). Apoptosis-inducing ligand TRAIL (*TNFSF10*) was expressed in MLR macrophages but little was present in GVH14. Experiments are ongoing to confirm the cytotoxic potential and effector mechanisms of MLR macrophages.

5.5 Summary of results for Chapter 5

Analysis of gene expression by GvHD blood monocytes supports the concept that monocyte-derived macrophages have a subtly different precursor in inflammation. Whole skin NanoString indicates that GvHD inflamed skin is primed to recruit monocytes and that monocytes are differentiated under activation conditions that resemble neither M1 nor M2 paradigms. Differentiating monocytes under Th1 conditions in a MLR generated macrophages with similarity to GVH14 in terms of surface antigen and gene expression. In a skin explant model, these MLR macrophages induced GvHD-like skin damage in the absence of T cells. Potential cytolytic effectors were similarly expressed in MLR macrophages and GVH monocyte-derived macrophages.

Chapter 6. Skin strand discussion

6.1 Discussion point 1: Monocyte-derived macrophages accumulate in GvHD skin

Studies of human cutaneous GvHD lesions have demonstrated that monocyte-derived macrophages are the dominant MP. Previous studies on inflamed skin have detected inflammatory MP populations but reached different conclusions about their identity. The IDECs (inflammatory dendritic epidermal cells) described in the epidermis of eczema express CD1c and CD1a (Wollenberg et al., 1996), (Schuller et al., 2001), in contrast to the cells characterized here in GvHD. FACS analysis in this thesis suggests that eczema has a distinct MP profile to GvHD, typified by dominance of CD1c-expressing cells. It therefore seems likely that IDEC are different inflammatory population. How they relate to the steady-state CD1c-expressing DC population (cDC2) requires further clarification.

The inflammatory populations described in psoriasis may overlap with what I have identified in GvHD. The CD11c+HLA-DR+CD1c- inflammatory dermal DCs identified by Zaba et al had a similar immunophenotype and also expressed macrophage-typical genes (Zaba et al., 2009), (Zaba et al., 2010). A different conclusion was reached about their identity as they shared some gene-expression similarities with *in vitro* moDCs. An ostensibly separate inflammatory population in psoriasis with greater expression of macrophage surface antigens (CD163 and FXIIIa) was described (Fuentes-Duculan et al., 2010). In the absence of side-by-side comparison it is difficult to appreciate that this population is distinct from inflammatory dermal DCs.

The inflammatory infiltrate accompanying cutaneous sarcoidosis has received less attention. Lesions immuno-stain for CD11c and S100A8/9, but not CD68, consistent with what I describe in GvHD (von Bubnoff et al., 2011). Though only performed in one sample, FACS analysis of cutaneous sarcoidosis revealed a similar MP profile to GvHD, with dominance of cells in the monocyte-derived macrophage parameter space.

Accumulation of CD14+/CD163+/CD11c+ expressing-cells has been reported in other inflamed human tissues including the duodenum in Coeliac disease (Beitnes et al., 2011), the ileum in Crohn's disease (Ogino et al., 2013), (Tamoutounour et al., 2012) and the colon in Ulcerative colitis (Bain et al., 2013). Though not extensively characterized, these cells were compared with infiltrates detailed in parallel mouse studies (Tamoutounour et al., 2012), (Bain et al., 2013).

Murine Ly6C^{hi} monocytes are recruited to gut both in steady state and inflammation (Bain et al., 2013), (Tamoutounour et al., 2012), (Zigmond et al., 2012). In steady state, they enter tissue as Ly6C+, MHC class II- cells. They lose Ly6C and gain MHC class II, then sequentially acquire F4/80 and CX3CR1 (stages termed P1-4). Parabiosis experiments are in keeping with monocyte derivation of all these populations and adoptive transfer experiments support the sequential transition in phenotype. In inflammation, P1 and 2 expand, but differentiation appears to be blocked, leaving pro-inflammatory cells with monocytic features.

Similar analysis has been applied to mouse dermis in steady state and during contact hypersensitivity (Tamoutounour et al., 2013). Successors of Ly6C^{hi} monocytes at sequential stages of differentiation are seen in steady state, but in inflammation, the early derivatives of monocytes dominate. Type I interferon and IFNγ-mediated signalling is implicated in this differentiation block. In quiescent skin and gut, monocyte derivatives with DC features are described (Zigmond et al., 2012) (Tamoutounour et al., 2013), but in inflamed skin, these populations are diminished relative to cells with effector monocyte features (Tamoutounour et al., 2013). While the Ly6C^{hi}-MHC II waterfall plot used by Tamoutounour et al to identify monocyte-differentiation into DCs (P1-3) has superficial similarity to the human CD14 CD1c plot used in this thesis, human CD1c+ cells are not currently thought to arise from monocytes. Monocyte differentiation potential in both species needs further clarification, but the tendency of monocyte-derived effector cells to accumulate in inflamed tissue in both mouse and human can be agreed upon.

6.2 Discussion point 2: Parallels to a murine model of macrophage infiltration in chronic GvHD.

The closest murine parallel to my findings in human GvHD is the accumulation of macrophages in an IL-17 dependent sclerodermatous cGvHD model (Hill et al., 2010), (Alexander et al., 2014). The fact that this is a chronic GvHD model does not preclude comparison. As this thesis studies a T cell depleted BMT cohort, the boundaries between typical acute and chronic GvHD can be expected to overlap (Pavletic and Fowler, 2012).

In the cGvHD model, donor macrophages infiltrate the dermis from 7 days post transplant (Alexander et al., 2014). Infiltration is not lichenoid: macrophages are initially seen throughout the papillary (upper) dermis but become concentrated in the reticular (lower) dermis and subcutaneous fat by 3 weeks post-transplant and are implicated in the subsequent sclerosis of these tissues. Data on the distribution of human macrophage infiltration not presented in this thesis can be seen in Appendix C. Lichenoid infiltration was observed. Involvement of the lower dermis could not be excluded as biopsies were superficial. Sclerodermatous chronic GvHD did not develop in any patient, but all received some therapy to modify the course of their disease. In summary, the pattern of macrophage infiltration is not a definite parallel.

Infiltrating macrophages in the cGvHD model are said to have an M2 phenotype as they express CD206 but not iNOS by immunostaining (Alexander et al., 2014). Using a broader range of antigens, an M1 or M2 phenotype could not be ascribed to human GVH14. They do express CD206, but expression of MHC class II, CD86 and CD64 and production of TNFα are features of classical macrophage activation. The M1/M2 paradigm is increasingly recognized as an unhelpfully simplified view of macrophage activation (Martinez and Gordon, 2014), (Xue et al., 2014).

Macrophages in both the cGvHD model and human GvHD express the receptor for M-CSF (CSF1R) (Alexander et al., 2014). In the murine model, CSF1 dependence was demonstrated. CSF1 administration increases macrophage accumulation. Use of a CSF1 receptor knockout BMT donor or administration of a blocking CSF1 receptor antibody reduces both macrophage accumulation and cutaneous pathology.

The precursor of cGvHD infiltrating macrophages is considered to be the Ly6C^{lo} monocyte (Alexander et al., 2014). Using CSF1r-/- foetal liver chimeras (FLC) on a B6 background, the authors reduced the proportion of peripheral blood Ly6C^{lo} monocytes by approximately 50%. Mice receiving BMT from a CSF1r-/- FLC had reduced skin macrophage infiltration, but that does not necessarily implicate Ly6C^{lo} monocytes as the precursor. Ly6C^{hi} monocytes remain a likely candidate and may simply require CSF1 to differentiate into skin-infiltrating macrophages. When characterising human GVH14, an assumption was made that classical monocytes (Ly6C^{hi}-equivalent) were the most likely precursor. This assumption was based on the striking similarity between GVH14 and steady state CD14 MDMs. Connectivity map analysis (a gene set enrichment tool) aligns CD14 MDM with classical rather than intermediate or non-classical monocytes (McGovern et al., 2014). Murine models of inflammation demonstrate a precursor-product relationship between Ly6C^{hi} monocytes and inflammatory macrophages (Bain et al., 2013), (Tamoutounour et al., 2013). As Ly6C^{hi} monocytes are also the precursor of Ly6C^{lo} monocytes (Yona et al., 2013), it is not impossible that a Ly6C^{lo} state directly precedes an inflammatory macrophage state. However, a defined role for Ly6C^{lo} monocytes as an endothelial macrophage is emerging, and retention of Ly6C^{lo} monocytes in the intravascular space may be important for orchestration of the innate immune response (Carlin et al., 2013). Perhaps a more detailed analysis of monocyte dynamics in murine cGvHD would be warranted.

In summary, accumulation of macrophages in the murine cGvHD model has some parallels to findings described here in human acute GvHD. Detailing the exact similarities in inflammatory macrophages between species is challenging. This challenge should be addressed in future studies. A murine model that faithfully represents a pathological process seen in patients would be invaluable for developing a more detailing understanding of the process and its response to therapy. Cross species transcriptome profiling offers promise as a means of aligning findings in murine and human studies (Carpentier et al., 2016), (Haniffa et al., 2012), (Ingersoll et al., 2010), (McGovern et al., 2014).

6.3 Discussion point 3: GvHD monocyte-derived macrophages are pro-inflammatory

The monocyte-derived macrophages isolated from GvHD lesions secreted inflammatory cytokines (e.g. TNF, IL-8), produced little IL-10 and stimulated allogeneic T cells. *In vitro* equivalents caused GvHD-like cutaneous damage.

Experimental rigor must be considered for each of these observations. As the number of cells isolated from GvHD lesions was insufficient for routine purity testing, it cannot be disproven that contamination by other cell types influenced results. For example, DCs contaminating the GVH14/CD14 MDM gate would make the allostimulatory capacity of this population appear greater. The likelihood of contamination was reduced by good sorting technique, encompassing both experimental design and conduct. In sorting experiment design, single cell gates were used to avoid unwanted cells entering as doublets combined with cells of interest. Gates were applied tightly to populations with as little overlap as possible. When conducting a sort, filtered single cell suspensions were used and a sufficiently large nozzle size selected to promote stream stability. Sorts were monitored and the drop delay reset if deviation of more than 10 pixels occurred. This ensured that sort decisions were applied to the droplet of interest (i.e. the droplet containing the specified cell), not the one above or below (which may contain any cell and would contaminate the specified sort population). Even if a small number of DCs contaminated the GVH14 gate, this would be unlikely to occur without contaminating the CD14 MDM gate also. GvHD and control samples were sorted within the same period of time, using the same sort template and sometimes on the same day. The differences between GvHD and control are therefore more likely to arise from biological difference than inaccurate sorting.

Monocytes entering inflamed tissue have been ascribed both pro-inflammatory and immunoregulatory roles depending on the context. In a murine model of pathogen-driven inflammation, pro-inflammatory monocyte activity benefited the host by aiding pathogen clearance (Serbina et al., 2008). In models of inflammatory bowel disease, such activity is harmful and monocyte depletion can ameliorate pathology (Zigmond et al., 2012). In an elegant study of gut *Toxoplasma gondii* infection, infiltrating monocytes were credited with maintaining mucosal integrity via prostaglandin E

production and inhibitory effects on neutrophils (Grainger et al., 2013). Despite systemic infection in this model and monocyte recruitment to multiple tissues, regulatory monocytes were only present in gut.

Tissue-specific functions of recruitment monocytes require careful consideration in systemic diseases such as GvHD. It is possible that while monocytes recruited to GvHD skin are pro-inflammatory, monocytes recruited to gut could function to limit the extent of pathology. Without ruling out this possibility, attempts at therapeutic monocyte depletion may have undesirable consequences.

6.4 Discussion point 4: Monocytes are recruited to GvHD skin before peak lymphocyte accumulation

Follow-up biopsies after resolution of GvHD inflammation showed lymphocyte accumulation that was not apparent on presentation. It therefore seems likely that monocyte recruitment is an early event and lymphocyte accumulation peaks later in this cohort. It is worth reiterating that this is a cohort of older adults following T-cell depleted BMT. Lymphopenia is expected to be more pronounced and more prolonged than in T-replete regimens, younger patients or mouse models of GvHD. Therefore innate cells may take on greater importance in inflammation.

Is it possible that monocytes initiate the graft-versus-host reaction? The prevailing view in immunology is that T lymphocytes are the sensors of histocompatibility. Challenging this, all metazoan organisms can recognize histoincompatibility but only vertebrates possess adaptive immune systems (De Tomaso et al., 2005). In more primitive animals e.g. chordates, innate immune cells recognize and respond to the non-self products of polymorphic gene loci (De Tomaso et al., 2005). In vertebrates, innate immune recognition of histoincompatibility has precedent in NK cells. Rather than recognizing non-self MHC polymorphisms or peptides, NK cells respond to changes in the balance of activating and inhibitory signals received through interactions of MHC with various receptors (Kumar and McNerney, 2005). In lymphocyte-deficient murine models, monocytes can recognize histoincompatibility (Zecher et al., 2009), (Liu et al., 2012), (Oberbarnscheidt et al., 2014) and this recognition is independent of MHC (Zecher et al., 2009). For example, RAG(-/-) mice

given an intradermal injection of splenocytes have more florid inflammation (monocyte/ macrophage-rich) if the cells are allogeneic than if they are syngeneic (Zecher et al., 2009). This response requires prior allo-immunization. Monocytes retrieved from a sensitized animal can substitute a prior allo-immunization event. In lymphocyte-replete settings, rapid recruitment of monocytes to xenogenic or allogeneic organ grafts is followed by T cell recruitment (Oberbarnscheidt et al., 2014), (Fox et al., 2001). Reciprocal stimulation between monocyte-derived cells and T cells is noted, resulting in IFNγ, T cell proliferation and macrophage activation (Fox et al., 2001), (Oberbarnscheidt et al., 2014). Via phagocytosis, macrophages act as allogeneic effector cells (Liu et al., 2012).

Whether donor monocytes themselves recognize histoincompatibility in human skin, or whether they are recruited following a T cell initiating event, their ability to act as antigen presenting cells warrants consideration. GvHD monocyte-derived macrophages did not express CCR7 but were far superior to their steady state counterparts at stimulating allogeneic T cell proliferation and activation *in vitro*. Thus, while interactions with naïve T cells in lymphoid tissue are unlikely, interactions with T cells in tissue are possible. The ability of GvHD monocyte-derived macrophages to cross-present exogenous antigen was not tested, but was suggested from functional annotation of expressed genes. Cross-presentation or cross-dressing would be required for these donor cells to display host peptides to donor CD8 T cells. An additional possibility is that donor monocyte-derived macrophages interact with host T cells. Resident memory T cells are present in abundance in human skin (Clark et al., 2006). During Alemtuzumab treatment for cutaneous T cell lymphoma, skin T cells are protected from depletion because the necessary effectors of antibody-mediated cytotoxicity cannot enter skin (Clark et al., 2012). Data from this work and others has identified mixed T cell chimerism in skin following RIC BMT with Alemtuzumab-containing regimens (Collin M, unpublished communication). The effector constituent of resident memory T cells is held in check by Langerhans cells and skin resident regulatory T cells (Seneschal et al., 2012). It is plausible that BMT conditioning disturbs these regulatory mechanisms and allows effector function of residual host T cells upon stimulation by monocyte-derived macrophages. Both antigen specific mechanisms (assuming that normal skin may harbour some auto-reactive T cells), and antigen-independent mechanisms could be envisaged (Iijima et al., 2011). Finally, a more conventional view would be that donor monocyte-derived

macrophages presenting antigen contribute to the maintenance but not the initiation of GvHD (Matte et al., 2004).

6.5 Discussion point 5: The MP balance is distorted in GvHD inflammation with an increase in CD14:CD1c ratio

In the MP profile of GVHD, CD14+ cells were expanded and CD1c cells depleted relative to normal skin. While CD14+ accumulation was seen in other inflammatory dermatoses, drastic reversal of the CD14:CD1c ratio was unique to GvHD. This finding provokes three related questions. First, where are the myeloid DCs? Second, how will they be replaced? Third, is the absence of DCs and the abundance of monocytes-derived cells inter-linked?

Myeloid DCs express CCR7, allowing them to respond to a CCL19/21 gradient and migrate to draining lymph nodes (Dieu et al., 1998). It might be expected that skin DCs encountering danger signals mature and exit into lymphatics. However the homeostatic mechanisms governing their replacement are not well characterized. DCs arising from monocytes have been described murine models of infection (Leon et al., 2007), (Nakano et al., 2009), sterile inflammation (Hammad et al., 2010), (Campbell et al., 2011), (Rivollier et al., 2012) and in steady state (Tamoutounour et al., 2013), (Jakubzick et al., 2013). However the identifiers of DCs are not always watertight. Expression of few DC-characteristic antigens does not constitute DC identity, as many antigens are labile during inflammation. Transcriptional proximity to *in vitro* moDCs requires caution on two fronts. Firstly, attention must be given to the homogeneity of the *in vitro* preparation. Starting with an impure monocyte population or failing to remove undifferentiated cells will result in a mixed gene expression signature. Secondly, the outcomes of gene-set enrichment analysis common to this field are dependent on the populations juxtaposed: if important subsets are missing, a population may enrich with a signature that is not its closest match (Carpentier et al., 2016). Concerning functional identifiers, detecting an inflammatory population in draining lymph node does not necessarily mean the population has migrated from inflamed tissue. Monocyte-derived macrophages can be simultaneously recruited to regional lymph nodes but are not migratory (Tamoutounour et al., 2012). Further, the ability to stimulate T cells requires careful interpretation of the system used.

Macrophages can stimulate extensive T cell proliferation with peptide antigens (Tamoutounour et al., 2013). Despite the pitfalls in DC-identification, there is convincing evidence that monocyte-derived DCs exist in mouse, (Zigmond et al., 2012). In humans, it is difficult to reliably infer the origin of a cell, but single-cell technologies combined with trajectory algorithms could remedy this (Bendall et al., 2014).

Myeloid DCs were also relatively depleted from blood in GvHD. This depletion may arise from DC recruitment to lymph node or it may reflect reduced production in the bone marrow. Leukocyte production is known to fluctuate according to remote signals in tissue (Courties et al., 2015), (Dutta et al., 2015), (Weber et al., 2015). Such “demand-adapted haematopoiesis” results in a bias towards myeloid over lymphoid production (Takizawa et al., 2012). Whether inflammation biases the fate of common MP precursors is not known. However, signalling in bone marrow (via IFNγ and G-CSF) can alter the functional characteristics of circulating monocytic progeny (Askenase et al., 2015), (D'Aveni et al., 2015). Relevance to the development of subsequent GvHD has been demonstrated (D'Aveni et al., 2015).

The increased CD14:CD1c ratio seen in GvHD suggests that DC replacement is not immediate. The absence of DCs will have consequences for the balance of growth factor signals in tissue. Under experimental conditions of extreme myeloid DC deficiency, monocytes accumulate in tissue and develop inflammatory effector phenotypes (Birnberg et al., 2008), (Sivakumaran et al., 2016). Altered consumption of Flt-3 ligand and GM-CSF underpin these alterations. It is possible that more subtle changes in these growth factors affect monocyte accumulation in inflamed tissue when myeloid DCs are reduced.

6.6 Conclusions

This work provides the first detailed characterization of monocyte-derived macrophages in human skin during inflammation. Taking a broad view of the MPS has identified simultaneous changes in skin myeloid DCs and blood monocytes/ DCs. The inter-relationships of these populations and the tone of their haematopoietic precursors in inflammation are ripe for further investigation.

Chapter 7. Lung mononuclear phagocytes in steady state and inflammation

7.1 Introduction

Lung pathology accounts for approximately 50% of non-relapse deaths following BMT. Causative infections are found in only half of cases (Soubani and Pandya, 2010). Acute non-infective lung injuries are currently considered together as idiopathic pneumonia syndrome (IPS). Treatment responses to IPS are limited and survival is poor (Panoskaltsis-Mortari et al., 2011). Dissecting this syndrome and stratifying treatment accordingly may benefit patients with IPS.

Animal models and clinical correlations implicate alloreactive T cells in IPS (Cooke et al., 1996), (Soubani and Pandya, 2010), (Nishie et al., 2016). Dysregulated innate responses in the lung, for example in response to respiratory virus infection or LPS produced by translocated gut bacteria, have been identified as triggers for alloreactivity (Cooke et al., 1996), (Versluys et al., 2010). MPs are predicted to be important as sensors of PAMPs, innate immune effectors and stimulators of alloreactive T cells.

Patients with IPS are a difficult population to study. In fulminant form, IPS is rare, patients are ill and even if broncho-alveolar lavage (BAL) is performed, patients are heavily pre-treated with anti-microbials, making infective and non-infective presentations difficult to separate. As the normal immune composition of BAL fluid has been poorly detailed to date, interpreting inflammatory from resident cells would be challenging.

In the lung strand of this work, a human experimental model of sterile inflammation is exploited to characterize the steady state and inflammatory populations in BAL. This model offers a precise onset of inflammation, the ability to sample two compartments (blood and BAL), and the opportunity to test MP dynamics through serial samples. This work aims to provide a foundation for meaningful interpretation of IPS BAL fluid in future studies.

7.2 Lung strand hypotheses

1) Steady state BAL contains monocyte-derived MPs, myeloid DCs and pDCs
2) LPS inhalation will trigger inflammatory MP accumulation in BAL
3) Inflammatory MPs will be derived from monocytes

7.3 Chapter Aims

7.3.1 Lung Strand Aim 1: To define the MPs present in BAL in steady-state and in response to LPS inhalation

To test hypotheses 1 and 2, MPs of the lower airways will be sampled by BAL following standardized inhalation of LPS or saline. Samples will be analysed by flow cytometry using a gating strategy applicable to blood, so that populations are defined with reference to circulating MPs. Within Aim 1, the subsets of MPs present in BAL will be determined. The differences between steady state and induced inflammation will be quantified.

7.3.2 Lung Strand Aim 2: To understand how MPs transit from blood to lung following LPS inhalation

Two research aims will gather evidence to test hypothesis 3. Gene expression analysis will be used in next chapter. In this chapter, parallels between blood and BAL fluid will be used. Blood from experimental volunteers will be serially sampled to provide temporal information on MP dynamics. The chemokine profile of BAL fluid will be compared with the chemokine receptor distribution on circulating MPs to understand specificity of recruitment. Within Aim 2, blood MPs will be quantified using a flow cytometry TruCount method. The chemokine and cytokine profile of BAL fluid will be tested by Luminex. Repository data will be explored to examine differential chemokine receptor gene expression between MP subsets

7.4 Materials and Methods for Chapter 7

7.4.1 Overview of the LPS inhalation study

The LPS inhalation study was approved by Newcastle & North Tyneside 2 Research Ethics Committee (REC reference number 12/NE/0196) under the full title 'A lipopolysaccharide (LPS) inhalation model to characterise divergent cellular innate immune responses and presence of alveolar leak early in the course of acute lung inflammation.' The study was funded by the Joint Research Executive Scientific Committee of Newcastle upon Tyne Hospitals NHS Charity. Professor John Simpson was the Principal Investigator. Dr Sarah Wiscombe was the main co-investigator and led the trial for 3 years. I led the trial for the final year. This role included recruiting and screening approximately 30 participants, scheduling study visits, administering study interventions, monitoring the participants, processing samples and following up participants. An overview of the study groups and key assessments is shown in Figure 7.1. Details of volunteer recruitment, inclusion and exclusion criteria and informed consent are given in Appendix A.

Figure 7.1 Overview of the LPS inhalation study

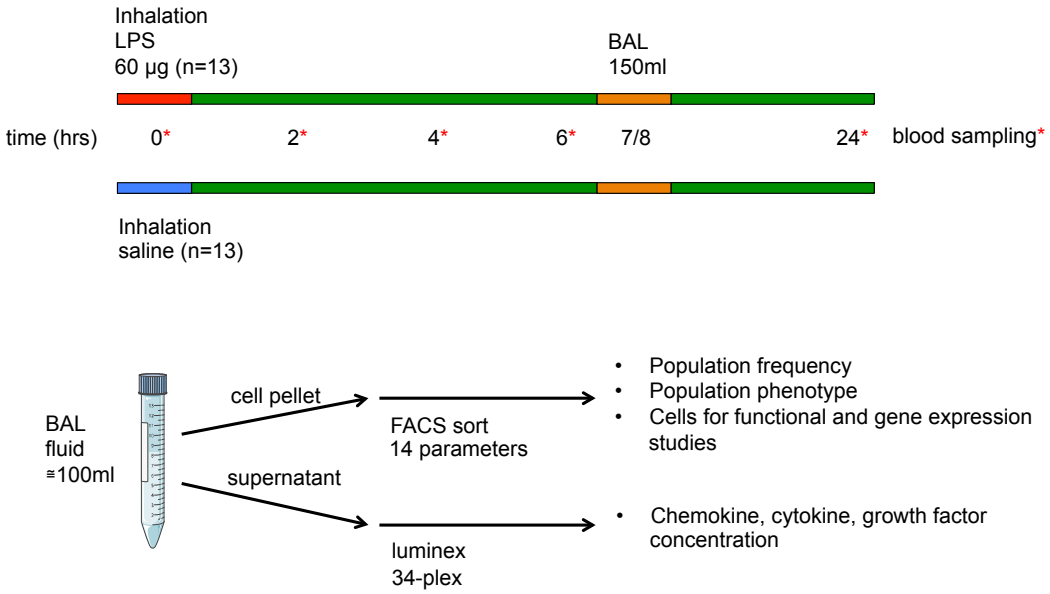

7.4.2 Group allocation

The first 16 participants were randomly allocated to receive saline or LPS. Allocation was made using sealed envelopes provided by a third party. This process was abandoned for the final 10 participants to allow greater control over experiments. Participants were not made aware which intervention they had received.

Samples from the first 7 participants were used to optimize protocols. Data reported in this chapter are from the subsequent 9 participants receiving saline and 10 participants receiving LPS. The characteristics of participants were well matched between saline and LPS groups (Table 7.1).

Table 7.1: Participant characteristics

	LPS	**Saline**	**p value**
Age (years) Mean (SD)	 21 (1.83)	 21 (1.39)	 0.92 (unpaired t-test)
Gender Male; n (%) Female; n (%)	 7 (70) 3 (30)	 4 (44) 5 (56)	 0.37 (Fisher's exact test)
Ethnicity Caucasian; n (%) Other; n (%)	 8 (80) 2 (20)	 8 (89) 1 (11)	 1.00 (Fisher's exact test)
Body surface area (m^2) Mean (SD)	 1.90 (0.19)	 1.74 (0.16)	 0.06 (unpaired t-test)
Forced vital capacity (L) Mean (SD)	 4.39 (0.73)	 3.93 (1.02)	 0.45 (unpaired t-test)
Forced expiratory volume in 1 second (L) Mean (SD)	 4.39 (0.72)	 3.93 (1.02)	 0.22 (unpaired t-test)

7.4.3 Study interventions

All volunteers provided written, informed consent. All were advised of the nature of bronchoscopy. Intravenous sedation with midazolam was available, but all participants elected for a non-sedated procedure. Participants received topical administration of 1% lignocaine spray to the mouth and pharynx. When nasal intubation was used, 1% lignocaine spray was applied topically to the nose.

An LPS solution for inhalation was prepared in sterile conditions immediately prior to use. Two milligrams of LPS from *E. coli* 026:B6 (Sigma) were reconstituted in 1.8ml 0.9% sodium chloride and mixed well. At time=0 participants inhaled 60µg (54µL) LPS solution or sterile 0.9% saline. Five controlled inhalations were performed using

an automatic inhalation-synchronized dosimeter nebulizer (Spira, Hameenlinna, Finland). The test solution was released once the participant had inhaled 50ml air, to ensure that laminar flow was established. Participants performed a 5 second breath hold at vital capacity to promote deposition of LPS in the lower respiratory tract (Darquenne et al., 2000).

Venous blood sampling was performed at 0, 2, 4, 6 and 24 hours after inhalation. At 7 hours after inhalation, participants underwent bronchoscopy. An experienced bronchoscopist (either Dr Sarah Wiscombe or Dr Ian Forrest) passed the flexible fibre-optic bronchoscope into a sub-segment of the medial segment of the right middle lobe and gently wedged the scope. An initial 20ml sterile 0.9% saline was instilled, gently aspirated and discarded as a 'bronchial sample'. A further 150ml warmed saline was instilled in 50ml aliquots and retrieved by gentle suction. Typically 80-120ml was retrieved (see Table 7.2).

Table 7.2 Sample characteristics

	LPS	Saline	p value (unpaired t test)
BAL volume (ml) Mean (SD)	98 (20)	93 (24)	0.68
Viable BAL leukocytes ($*10^6$) Mean (SD)	16.4 (8.32)	5.2 (2.49)	0.001
BAL red blood cells ($*10^6$) Mean (SD)	33 (31)	17 (28)	0.04
Blood neutrophil fold change (t=6/ t=0) Mean (SD)	3.31 (1.01)	1.17 (0.25)	<0.001

7.4.4 BAL collection, handling and storage

BAL fluid was passed through a 100micron filter and centrifuged at 500g for 7 minutes to pellet cells. Supernatant was stored in 1.5ml aliquots at -80°C. The cell pellet was re-suspended in 1ml of PBS without calcium and magnesium and mixed thoroughly. A 10µl sample was used for cell counting and viability assessment. Cells were either cryopreserved or prepared immediately for flow cytometry/sorting using antibody panels detailed in Table 7.3. Recovery following cryopreservation was poor and immediate use of samples was preferred.

Table 7.3 Antibodies used for LPS study BAL and blood flow cytometry/ sorting

Antigen	Fluorochrome conjugate	Clone	Manufacturer	Catalogue Number	Volume (µl)/ 10^{10} cells in 100µl buffer
CD45	V500	HI30	BD	560777	4
CD3, CD19, CD20, CD56	FITC	SK7 4G7 L27 NCAM 16	BD	345763 345776 345792 345811	4 each
HLA-DR	V450	G46-6	BD	561359	4
CD14	BV650	M5E2	Biolegend	301835	2.5
CD16	PE/ Dazzle™ 594	3G8	Biolegend	302053	3
CD11c	APCCy7	Bu15	Biolegend	337218	3
CD123	PERCPCy5.5	7G3	BD	558714	4
CD1c	PECy7	L161	Biolegend	331516	3
CD11b	APC	ICRF44	Biolegend	301310	4
BTLA	PE	J168-540	BD	558485	2
dead cells	DAPI		Partec	05-5005	1 in 10 dilution after final wash

7.4.5 Blood MP enumeration

Blood samples were obtained from all 10 participants receiving LPS and 8 of the 9 participants receiving saline. Venous access could not be obtained in one participant that would satisfy repeated sampling. At each time point, a full blood count (FBC) was performed on an automated haematology analyser (Sysmex XE-2100).

Detailed MP enumeration used a BD TruCount™ method. This employs flow cytometry to enumerate cells in whole blood by comparing event counts in a given volume to counts of polyfluorescent beads. According to the manufacturers instructions, 50-100µl whole blood should be used, lysed in 450 or 900µl and acquired at a low event rate, taking 10-20 minutes per sample. In previous experience, this method permitted enumeration of monocytes and DCs but event counts for DCs were low (Jardine et al., 2013). An adapted method was devised to allow enumeration of MPs in 1ml blood with the same volume of reagents and time-scale as the manufacturers protocol.

1-2 ml blood was collected into EDTA. 1ml was transferred into a 15ml falcon tube and lysed with 2ml red cell lysis buffer for 10 minutes. Leukocytes were washed and pelleted by centrifugation (5 minutes at 500g). Care was taken to fully remove all supernatant. Cells were re-suspended in their own volume (50µl) and transferred to

a TruCount tube (BD), containing a standard number of beads. Residual cells were re-suspended in 50µl flow buffer and added to the TruCount tube. Antibodies were added (detailed in Table 7.3) for 20 minutes at 4°C. The sample was re-suspended in 400µl red cell lysis buffer and acquired on a Fortessa X20. No forward or side-scatter thresholds were set so that all bead events were recorded. A low CD45 threshold was set so that red cell/ platelet debris could be excluded but $CD45^{lo}$ granulocytes included. Samples were acquired slowly to ensure stable background subtraction by the cytometer.

7.4.6 Chemokine/ cytokine analysis

Chemokines and cytokines in BAL supernatant were quantified using the Procartaplex 34-plex luminex assay (see section 2.5.2). Concentrations were inferred from standard curves in Procartaplex Analyst software.

7.4.7 MP chemokine receptor gene analysis

Normalized microarray repository data on blood monocyte and DC subsets were used (Haniffa et al., 2012). Mean expression of 7 chemokine receptors capable of responding to the ligands present in LPS BAL fluid was calculated for each subset. Mean log2 expression data were imported into MeV software for heat-map generation.

7.4.8 Alveolar macrophage NanoString

Alveolar macrophages were sorted from saline and LPS BAL (each n=4) using the gating strategy shown in Figure 7.2 on a FACS Fusion cytometer. Approximately $1x10^5$ cells were pelleted and stored at -80°C. Cells were prepared and run on a NanoString Immunology v2 panel as described in section 2.6.2. Lysis volumes were adjusted so that 20,000 cells from each population were used. Normalization and QC were performed as described in 2.6.5. One LPS sample failed positive content normalization (indicating that too little material was used) and was excluded.

7.4.9 Macrophage and CD14 stimulation assay

Alveolar macrophages and CD14+ cells were sorted from LPS BAL (n=4 each) as above. $1x10^5$ sorted cells were cultured in 96-well round bottom plates in 100µl RF10 containing 100ng/ml LPS. After 10 hours, supernatants were harvested and stored at -80°C. Supernatants were batch-analysed by cytometric bead array (see section 2.5.1). Briefly, samples or standards were combined with antibody-coated bead mixes. Antibodies to detect IL-10, IL1β, TNF, IL-6 and IL-8 were used in this experiment. Bead populations were resolved using 2 fluorescence parameters on a FACS Canto II running FACSDIVA Version 7 and bead events were quantified (count and mean fluorescence intensity). FCAP Array software version 3 was used to generate standard curves and calculate concentrations from flow cytometry data.

7.5 Results Aim 1

7.5.1 Flow cytometry identifies 7 MP populations in BAL

MP populations in BAL fluid and blood were identified in parallel in order to simplify discussion about cross-compartment flux. AM do not have a parallel in blood. They were identified first within CD45+SSC^{hi} cells (Figure 7.2, panel A). An additional $CD45^{hi}$CD14+ gate removed neutrophils and identified a homogenous population of AM. Further analysis demonstrated AM to be CD16+, CD11c+, autofluorescent and CD11b+.

In BAL fluid, CD45+SSC^{lo} mononuclear cells could be compared with blood mononuclear cells. It is well established that blood MPs are negative for T, B and NK lineage markers (CD3, 19, 20, 56) and positive for HLA-DR (Ziegler-Heitbrock et al., 2010). Use of a lineage cocktail is optimal to remove HLA-DR+ B cells and activated T cells from further analysis. Without stringent removal of NK cells, CD16-expressing $CD56^{dim}$ NK cells appear in the non-classical monocyte parameter space. Amongst lineage-HLA-DR+ cells, three subsets of monocytes are defined by expression of CD14 and CD16. In order of abundance these are classical (CD14++CD16-), non-classical (CD14+16++), and intermediate (CD14++CD16+) monocytes (Ziegler-Heitbrock et al., 2010). In BAL, CD14++CD16- and CD14+CD16++ cells were

scarce. CD14++CD16+ cells were relatively abundant (see Table 7.4). While they overlap AM in terms of HLA-DR, CD11c, CD14 and CD16 expression, BAL CD14++CD16+ cells are small, non-autofluorescent and have uniformly high CD11b expression (Figure 7.2, panel C). Subtle phenotypic distinctions can also be made from intermediate monocytes.

Figure 7.2 Parallel identification of MPs in BAL fluid and blood

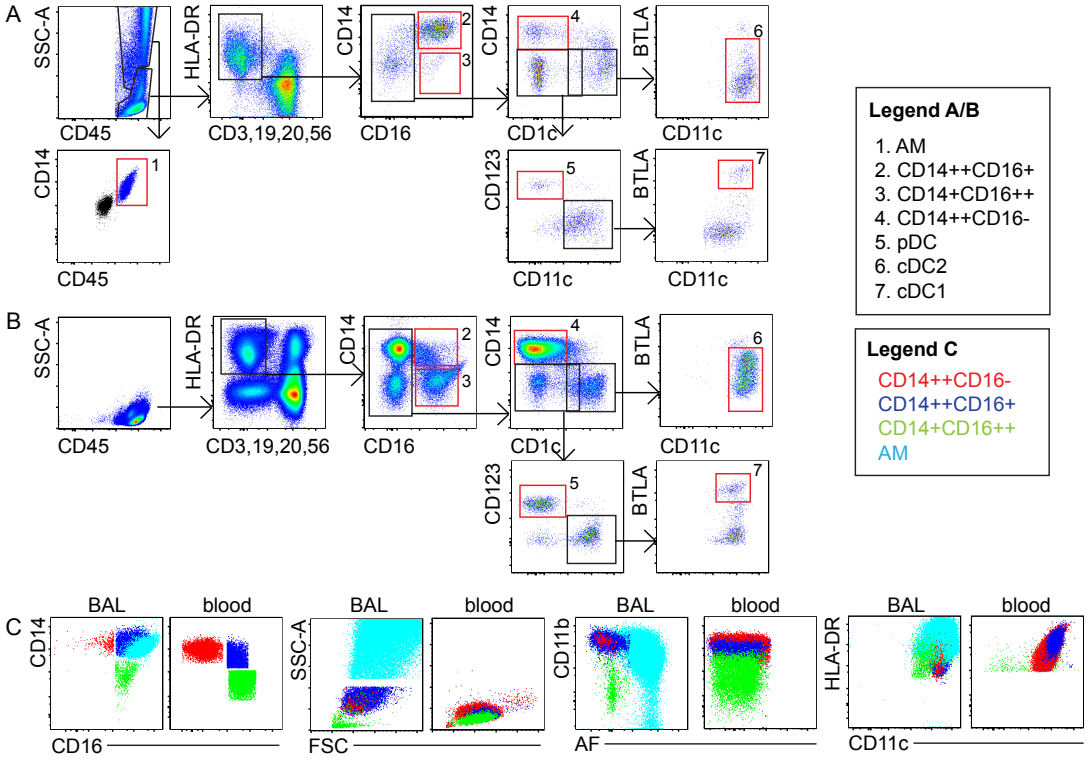

Figure 7.2 Parallel identification of MPs in BAL fluid and blood

Gating strategy used to identify MPs in steady state BAL (A) and blood (B) by flow cytometry. Prior exclusion of dead cells and debris is not shown. Black rectangles show intermediate gates. Red rectangles show MP populations 1-7. The same gating is applied in A as in B. C) Overlay plots of BAL monocyte/ macrophage populations compared with blood monocyte populations.

Blood DCs are typically identified within the CD14-CD16- fraction of lineage-HLA-DR+ cells (Ziegler-Heitbrock et al., 2010). There is negligible co-expression of CD14 and cDC2 antigen CD1c in blood (Figure 7.2, panel B). This was not the case in BAL fluid, where 10-15% of CD1c+ cells were CD14+ (Figure 7.2, panel A). A gating strategy was chosen which allowed this fraction to be analysed separately from

CD14+ cells. The CD14-CD1c+ gate could be refined to visualize CD11c+BTLA$^{lo\text{-}mid}$ cDC2. cDC2 are approximately 2-fold more abundant in BAL fluid than blood.

Table 7.4 MP frequency in BAL and blood

Proportion of leukocytes (%) Mean (SD)	AM	CD14++ CD16-	CD14++ CD16+	CD14+ CD16++	pDC	cDC1	cDC2
Whole blood	0	8.01 (2.04)	0.47 (0.22)	1.29 (0.85)	0.23 (0.05)	0.02 (0.01)	0.30 (0.1)
BAL fluid	75.0 (9.8)	0.17 (0.18)	2.01 (0.99)	0.14 (0.16)	0.09 (0.06)	0.05 (0.04)	0.74 (0.45)

A broad CD1c negative gate was set on CD14- cells in order that all cDC1 would be identified (Figure 7.2, panel A). Although blood cDC1 are CD1c-, skin cDC1 have variable CD1c expression and BAL fluid cDC1 characteristics were unknown. Within the CD14-CD1c- gate, CD11c- cells expressing the IL-3 receptor alpha chain (CD123) were identified as pDC. CD11c positive cells with high BTLA expression were identified as cDC1. In common with cDC2, cDC1 were twice as abundant in BAL than in blood. The converse was true of pDC.

In summary, 7 distinct MP populations were identified in BAL. AM were abundant and clearly distinguished. Three MPs had parallel surface antigen expression to blood monocytes (CD14++CD16-, CD14++CD16+ and CD14+CD16++) although their relationship to circulating monocytes needs further exploration. Two myeloid populations were enriched in BAL relative to their blood counterparts and pDCs were proportionally reduced.

7.5.2 CD14+ and cDC2 populations expand following LPS inhalation

The gating strategy described above was used to determine the MP composition of BAL fluid 8 hours after LPS inhalation. MP frequency was compared with BAL fluid 8 hours after saline inhalation (steady state) (Figure 7.3 panel A-B). Differences were clearly evident from the first analysis plot: CD45^{lo}SSC^{mid} neutrophils and CD45+SSC^{lo} mononuclear populations were expanded. On subsequent gates, expanded mononuclear cells were notable in the CD14++CD16- and the CD14-CD1c+ parameter spaces (Figure 7.3, panel A).

Figure 7.3 MP profile of BAL fluid following LPS inhalation

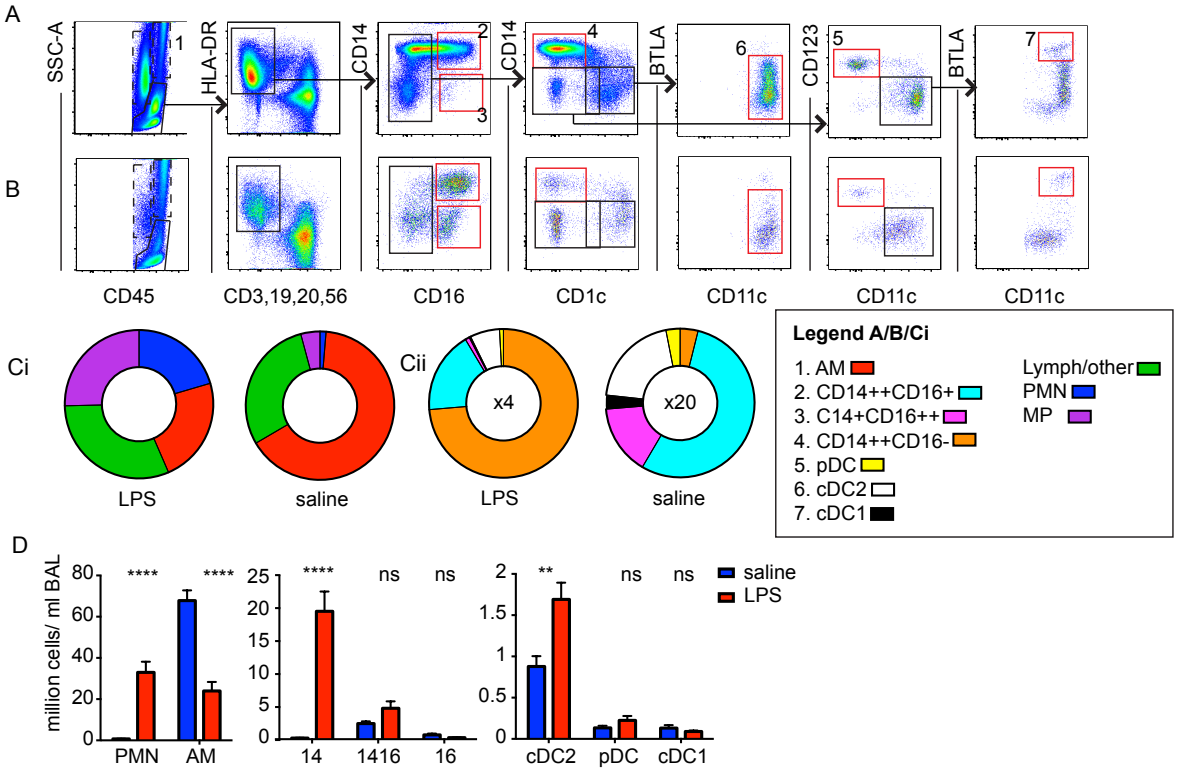

Figure 7.3 MP profile of BAL fluid following LPS inhalation

A) MP populations in BAL fluid following LPS inhalation are gated as in Figure 7.2. Black polygons are intermediate gates. Dashed polygons overlying neutrophil and AM populations indicate that these are not terminal gates: an additional CD45 versus CD14 plot (not shown) was used to resolve overlaps in these populations, as shown in Figure 7.2. Red rectangles denote MP populations.
B) MP populations following saline inhalation (steady state) were used for comparison to A).
Ci) The most abundant gated populations expressed as a mean proportion of CD45+ cells for LPS (n=10) and saline (n=9) samples. "MP" encompasses the non-AM MPs. Cii) The least abundant populations expressed as a mean proportion of "MP". The number within each pie illustrates the magnification that would be required if pies were scaled to MP % of 45.
D) Quantification of neutrophils and MPs following LPS inhalation compared with saline inhalation. The proportion of each MP relative to CD45+ cells on flow cytometry was combined with manual cell counts and measurements of BAL fluid volume to give absolute MP count/ml BAL fluid. LPS and saline were compared by unpaired t test. **** p<0.001, ** p<0.01, ns=not significant, PMN=neutrophil, AM=alveolar macrophage, 14=CD14++CD16-, 1416=CD14++CD16+, 16=CD14+CD16++.

The greatest MP expansion was in CD14++CD16- cells: mean concentration per ml BAL fluid was increased 115 fold after LPS relative to saline inhalation (Figure 7.3,

panel C). The significant increase in cDC2 concentration after LPS inhalation was smaller in magnitude (2-fold). Juxtaposed with static numbers of pDC and cDC1, the selective expansion of cDC2 is intriguing and will be fully explored in subsequent sections. A significant reduction in AM frequency was seen, and given that absolute counts were considered, this cannot be attributed to expansion of other leukocytes. Viability of CD45+SSC^{hi} cells was quantified by flow cytometry. There was a non-significant trend towards lower macrophage survival in LPS participants relative to saline controls (mean % viability ± SD was 60.6 ± 3.37 in LPS versus 68.0 ± 2.3 in controls; p=0.12). Macrophage survival *in vivo* may have been impaired by LPS inhalation. Alternatively, LPS inhalation may have induced changes in expression of molecules such as integrins, which mediate adherence to the alveolar epithelium. Either of these possibilities would result in lower AM retrieval in BAL fluid.

7.6 Results Aim 2

7.6.1 Dynamic changes in blood neutrophils, monocytes and myeloid DCs follow LPS inhalation

The expansion of CD14+ and CD1c+ MPs in LPS BAL fluid could arise by movement of leukocytes across compartments in the lung (interstitial to airspace) or by recruitment of leukocytes from blood. Blood leukocytes were serially quantified to look for evidence of direct recruitment. It was anticipated that heavily enriched populations might decline in the blood at approximately 4-6 hours post inhalation, prior to their detected expansion in BAL fluid, and later be restored by a homeostatic response in bone marrow.

Total white cell count began to rise in LPS relative to saline groups 2-4 hours post-inhalation (Figure 7.4, panel A). By 24 hours, the groups had converged as both were recovering from bronchoscopy. Transient leukocytosis following BAL is well recognized (Cohen and Batra, 1980). Examining the white cell differential counts, lymphocytes and eosinophils were static while neutrophils and monocytes accounted for the leukocyte expansion between 4 and 6 hours (Figure 7.4, panels B-E). There was no decline in blood neutrophil count at any point between LPS inhalation and BAL. Instead, neutrophil release/ production steadily increased. A fractional decline

in blood monocytes was noted in the first 2 hours after LPS inhalation but this was not statistically significant.

MP populations were quantified in more detail at 6 hours post-inhalation in participants receiving LPS. MP concentration in whole blood was measured by flow cytometry at 6 hours relative to MP concentration at baseline. This revealed further information on monocyte subsets and permitted quantification of DCs. Classical monocyte expansion was accompanied by stasis in intermediate and non-classical monocytes (Figure 7.4, panel F). Both myeloid DC populations significantly declined, while pDC counts remained constant. cDC2 recruitment to the lung may account for this decline. Alternatively, monocytes may be produced or released from the bone marrow at the expense of myeloid DCs. This hypothesis cannot be tested in the current model, but the fact that both cDC1s and cDC2s decline in blood while only cDC2s are recruited favours altered haematopoiesis over recruitment.

Figure 7.4 Peripheral blood leukocyte dynamics

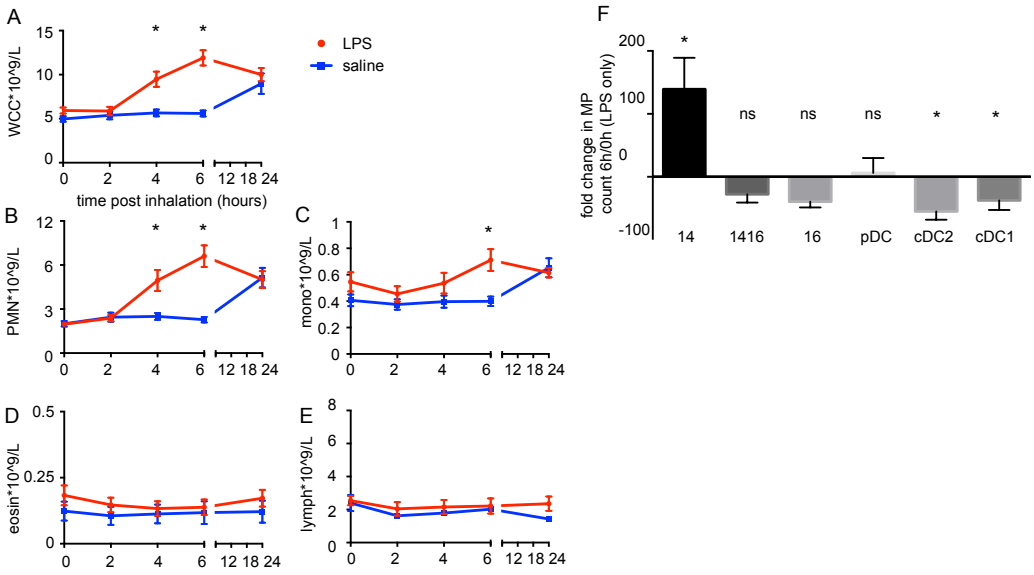

Figure 7.4 Peripheral blood leukocyte dynamics

A) Total white cell count following LPS (red circles) or saline inhalation (blue squares). Points indicate mean and error bars indicate SEM of LPS n=10 and saline n=8. B) Neutrophil count, C) monocyte count, D) eosinophil count, E) Lymphocyte count. F) Mean fold change in blood MP count by flow cytometry at 6 hours relative to baseline in LPS participants only. Bars show SEM.

* denotes p<0.05. Panels A-E used unpaired t -test with Holm Sidak multiple comparison correction. Panel F used two-sided paired t-test.

7.6.2 AM contribute pro-inflammatory cytokines and chemokines following LPS inhalation

The chemokine and cytokine profile of the LPS-exposed airspace was measured by Luminex assay to explore the selectivity of MP recruitment and understand the milieu in which recruited cells might mature, differentiate or function.

Cytokines significantly enriched in LPS relative to saline BAL in order of magnitude were IL-6, IL1RA, IL-1β, TNFα, IL-2 and IL-4 (Figure 7.5, panel A). CXC chemokines included CXCL8, which attracts neutrophils, CXCL10 (IFNγ-induced protein 10) and CXCL12 (stromal cell derived factor-1), which are best recognized for attracting lymphocytes via CXCR3 and CXCR4 respectively. CC chemokines included CCL2 (monocyte chemotactic factor 1, CCL3/4 (macrophage inflammatory protein 1a/b), CCL5 (regulated on activation normal T cell expressed and secreted; RANTES) and CCL11 (eotaxin). CCL2 potently recruits monocytes via CCR2. CCL3-5 and 11 act on CCR1, 3 and 5 on a number of cell types.

The differential sensitivity of MP subsets to inflammatory chemokines is not well described. Chemokine receptor gene expression was surveyed as a starting point, recognizing that gene expression and surface expression may differ and that surface expression may not necessarily confer a functional chemotactic response to ligand. A published Illumina microarray dataset was used, rather than the Nanostring data generated alongside this thesis as more of the genes in question were covered. Classical monocytes had higher expression of relevant chemokine receptors than intermediate and non-classical monocytes, specifically CCR2 and CCR5 (Figure 7.5, panel B). The preferential recruitment of cDC2 over cDC1 correlates with higher expression of CCR1 and CXCR4 genes in cDC2. Relevant chemokine genes are expressed at high levels in pDC, while they are not recruited. Clearly chemokine gene expression is only one aspect of the propensity of cells to enter the LPS-inflamed lung.

Figure 7.5 Recruitment of inflammatory cells following LPS inhalation

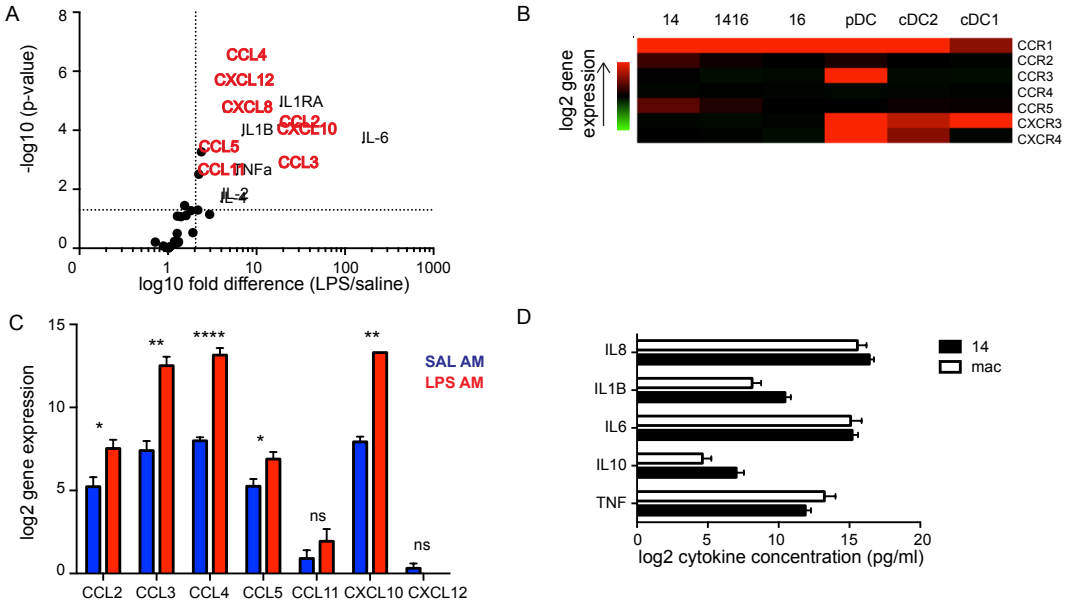

Figure 7.5 Recruitment of inflammatory cells following LPS inhalation

A) Volcano plot of chemokines and cytokines in LPS relative to saline BAL. Those significantly higher in LPS BAL are depicted in text (red text for chemokines; black text for cytokines). n=11 saline; n=12 LPS.
B) Relative expression of chemokine receptor genes in steady state blood monocyte and DC subsets. Microarray data from Haniffa et al 2012 is used. Each column in the heat-map represents the mean of n=5 replicates per subset.
C) Expression of chemokine genes by AM from saline and LPS participants by NanoString. Bars indicate mean ± SEM; * indicate p<0.01 by unpaired t-test; n=4 saline and n=3 LPS.
D) Inflammatory cytokine production by 14+ cells and AM isolated from LPS participants and stimulated with LPS ex vivo (each n=4)

Finally, the cells responsible for inflammatory cytokine and chemokine production were considered. LPS was delivered to the lower airways in this model. Type I and II pneumocytes and AM cover the majority of this surface area. LPS sensitivity has been reported in all three cell types (Wong and Johnson, 2013) but only AM could be isolated by BAL and tested further. AM isolated after LPS inhalation expressed genes for all the detectable chemokines with the exception of CXCL12 (Figure 7.5, panel C). *Ex vivo* AM stimulated with LPS produced high concentrations of TNF, IL-6 and IL-8, detectable IL-1β and low level IL-10 (Figure 7.5, panel D). However, a similar profile was seen in 14+ cells. It is likely that resident cells, such as AM, are

important in establishing an inflammatory milieu and chemotactic gradient, but that recruited cells subsequently contribute.

7.7 Summary of results for Chapter 7

Flow cytometry analysis of BAL fluid in steady state revealed 7 distinct MP populations. BAL fluid MPs expressing monocytic markers were proportionally less frequent than their counterparts in blood and BAL myeloid DCs were more frequent. Following LPS inhalation, the most dynamic changes occurred in neutrophils, CD14+ cells and CD1c+ cells. While blood monocyte abundance rose steadily following LPS inhalation, a skew towards classical monocytes was apparent. In contrast, blood myeloid DCs declined following LPS inhalation. Putative chemokines for MP recruitment were enriched in LPS BAL fluid. AM exposed to LPS *in vivo* were capable of elaborating many of these chemokines. Inflammatory cytokine production was demonstrated in both resident (AM) and recruited (CD14+) cells.

Chapter 8. Heterogeneity of lung myeloid dendritic cells

8.1 Introduction

Analysis in Chapter 7 revealed that the cDC2 subset of myeloid DCs is expanded in BAL fluid within 8 hours of induced inflammation. Enrichment of myeloid DCs in chronic inflammatory diseases of the skin and joints has been reported (Zaba et al., 2009), (Segura et al., 2013). In the most detailed characterizations, inflammatory DCs co-express monocyte/ macrophage antigens and have transcriptional similarity to *in vitro* monocyte-derived DCs (Segura et al., 2013). However, none of these studies have had the perspective of an early time-point in acute inflammation. It would be surprising if monocyte to DC differentiation, which takes 5 days *in vitro* (Sallusto and Lanzavecchia, 1994), occurred during the time-course of the LPS inhalation study. Examining the inflammatory expansion of myeloid DCs may reveal novel detail about the relationship between blood and tissue DCs during inflammation.

It has recently come to light that blood cDC2 comprises two distinct subsets (Reynolds, G., personal communication). The subsets are separable by surface expression of B- and T- cell lymphocyte attenuator (BTLA). BTLA negative cDC2 have transcriptional similarity to monocytes while BTLA positive cDC2 have a more "DC-like" gene signature (Reynolds, G., personal communication). The subsets have contrasting effects on T cell polarization and have distinct differentiation potentials. While BTLA+ cDC2 induce regulatory T cell generation and IL-4 production from T-helper cells, BTLA- cDC2 induce Th1 cytokine production. BTLA+ cDC2 more readily adopt characteristics of Langerhans cells *in vitro* while BTLA- cDC2 preferentially undergo osteoclast differentiation (Reynolds, G., personal communication). Separating the contributions of the two cDC2 subsets in humans and unpicking the heterogeneity of the analogous CD11b population in mouse has the potential to transform our understanding of myeloid DC immunology.

In chronic joint inflammation, BTLA- cDC2 are enriched (Reynolds, G., personal communication). However, the fate of BTLA positive cDC2 in acute inflammation is unknown and the stability of the functional differences outside blood have not been tested.

8.2 Chapter Aims

8.2.1 Lung Strand Aim 3: To examine heterogeneity within the cDC2 expansion in the inflamed airspace

The inflammatory expansion of cDC2 will be dissected further using flow cytometry. FACS-sorted populations will be subjected to *in vitro* functional assays or gene-expression analysis to address the questions:

- Are cDC2 most likely derived from monocytes or blood cDC2?
- Is there heterogeneity in the inflammatory-expansion of cDC2?
- Is there evidence for differential recruitment of BTLA+ or BTLA- cDC2?
- Are functional differences between BTLA+ and BTLA– cDC2 conserved on entry to inflamed tissue?
- How do cDC2 differ across compartments in steady state and inflammation?

8.4 Materials and Methods for Chapter 8

8.4.1 Testing surface antigens by flow cytometry

Candidate antigens that may separate blood from inflammatory or tissue cDC2 populations were selected from Segura et al., 2013, McGovern et al., 2014 and Desch et al., 2015. Antibodies used were CD1a AF700, FcER1 PE, CD11b APC, CD206 PE, Axl APC, CD86 PE and BTLA PE and CD1c PECy7 (details in Appendix B). Expression was assessed relative to FMO or isotype control.

8.4.2 T cell proliferation assay

The ability of MP populations isolated from BAL to stimulate allogeneic T cells was tested in a mixed leukocyte reaction. The T cell proliferation and activation assay described in Chapter 4 (section 4.3.5) was used. Briefly, this comprised a 6-7 day co-culture of 3000 sorted MPs with 75,000 CSFE-labelled bulk allogeneic peripheral blood T cells. The output was analysed by flow cytometry and T cell proliferation was quantified by CSFE dilution. Three experiments were performed on populations sorted from LPS BAL.

8.4.3 T cell cytokine production assay

CD4 T cells were isolated from peripheral blood of healthy donors by immunodensity negative selection (see section 2.2.3), and aliquots were cryopreserved at -80°C.

$3x10^4$ FACS-sorted DC populations were added to 96-well round-bottom plates in 200µl RF10. $1x10^5$ CD4 T cells were added to DCs or incubated alone. Following a 6-day incubation at 37°C and 5% CO_2, medium was replenished with RF10 with 10U/ml IL-2. At day 10, cells were stimulated with phorbol 12-myristate 13-acetate (PMA, 10ng/ml) and ionomycin (1µg/ml) for 4 hours to elicit cytokine production. Brefeldin A (10µg/ml) was added to cultures after 1 hour to concentrate cytokines within the endoplasmic reticulum. Dead cells were stained with a fixable viability dye (Zombie Aqua) prior to fixation and permeabilization (see section 2.3.2). Antibodies to IFNγ, IL-17, and IL-4 were used to identify T-cell cytokines. Antibody details are provided in Appendix B. Data were acquired on a Fortessa X20.

8.4.4 Monocyte-derived DC, LPS-stimulated cDC2 and blood DC/monocytes for NanoString

Gary Reynolds prepared moDC for NanoString. Classical monocytes were isolated from healthy donor PBMC by FACS sorting. $5x10^5$ monocytes were cultured in 500µl RF10 in 24-well plates for 5 days at 37°C and 5%CO_2. Medium contained 50ng/ml GM-CSF and 50ng/ml IL-4. Medium and cytokines were refreshed on day 3. Cells were harvested and FACS-sorted on day 5, to exclude undifferentiated CD14+ monocytes and include only CD1a+ moDC.

I isolated blood cDC2 from healthy donor PBMC by FACS-sorting. $3x10^4$ cDC2 were cultured in 96-well round-bottom plates containing 200µl RF10 and 100ng/ml LPS from *E. coli* 0.26:B6 (Sigma). Cells were harvested at 6 hours.

Gary Reynolds isolated monocytes, BTLA+ and BTLA- cDC2 from healthy donor PBMC by FACS-sorting.

Cell pellets for all preparations were stored at -80°C and lysed to a concentration of $1x10^4$ cells per 5µl RNA lysis buffer prior to NanoString.

8.4.5 BAL samples for NanoString

Cells from BAL fluid were FACS-sorted according to the gating analysis shown in Figure 7.2. In LPS BAL, cDC2 were either fractionated into BTLA+ and BTLA- subsets or resident cDC2 ($CD1c^{hi}$±Axl+) and recruited cDC2 ($CD1c^{lo}$±Axl-) subsets. Samples were selected for NanoString if more than 4000 cells were sorted. Cell pellets for all preparations were stored at -80°C and lysed to a concentration of 1-$2x10^4$ cells/ 5µl RNA lysis buffer prior to NanoString

8.4.6 NanoString data acquisition, normalization and QC

Immune relevant gene expression in samples isolated from BAL fluid was tested with the Immunology v2 panel. All other samples were tested on the Immunology v2 panel plus custom code-set (see section 2.6.2) to align with experiments not included in this thesis. Data from both panels could be combined for QC and normalization without producing a "batch" or "panel" effect. Only expression of the 579 genes common to both panels could be considered.

Normalization and QC was performed as described in section 2.6.5. Samples with a positive content normalization score>10 were excluded and data were re-normalized. Principal component analysis was used to screen for outliers. One normal blood donor, 1 saline BAL cDC2 sample and 1 resident/ recruited LPS BAL cDC2 pair were excluded. Samples entering analysis included triplicates of blood monocytes, blood BTLA- cDC2, blood BTLA+ cDC2, saline BAL cDC2, LPS BAL cDC2, resident LPS BAL cDC2 and recruited LPS BAL cDC2 and duplicates of moDC and LPS-stimulated cDC2.

8.4.7 BTLA+/- Gene expression analysis

Samples from n=3 BTLA+/- blood and n=3 BTLA+/- LPS BAL samples were pooled and normalized. One LPS BAL pair failed positive content normalization and was excluded. The BTLA+/- differentially expressed gene (DEG) set was created by

unpaired t-test of blood BTLA+ and BTLA- samples using alpha=0.05 and omitting multiple comparison correction. With standard Bonferroni correction only 1 gene (*ZEB1*) was significant. Using the DEG set, gene-expression similarity between samples was tested by hierarchial clustering using Pearson correlation as the distance metric and average linkage clustering.

8.4.8 Gene expression analysis

Clustering was tested by PCA in MeV software, centering on the mean. The first 3 components accounted for 66% of variation in gene expression. Gene-set enrichment was performed in Bubble GUM software. Gene signatures were generated in GeneSign using a one versus all comparison of mean(test)/mean(ref), a minimal linear fold-change of 2, and Benjamini-Hochberg false discovery correction limit of 0.05. Gene-set enrichment was tested using BubbleMap. Differential gene expression between blood, saline-BAL and LPS-BAL was assessed in MeV using an unpaired t-test with alpha=0.05.

8.5 Results Aim 3

8.5.1 cDC2 in BAL fluid are heterogeneous following LPS inhalation

BAL fluid from participants obtained 6 hours following LPS inhalation was re-visited using the gating strategy introduced in Figure 7.2. Mononuclear cells that were lineage-HLA-DR+CD16- were visualized on a two-dimensional plot of CD14 versus CD1c expression. From this plot, it was apparent that cDC2s present after LPS inhalation differed from the cDC2s seen in after saline inhalation (steady state) (Figure 8.1, panel Ai). In steady state, cDC2 were $CD1c^{hi}$ $CD14^{mid}$. After LPS inhalation, most cDC2s had lower expression of both CD14 and CD1c, but a small population of $CD1c^{hi}$ $CD14^{mid}$ cDC2 could also be seen. A similar image could be created by superimposing equivalent plots from saline BAL and blood (Figure 8.1, panel Aiii). This analysis was consistent with the hypothesis that $CD1c^{hi}$ $CD14^{mid}$ cells are airway resident and $CD1c^{mid}CD14^{-}$ cells are recruited from blood.

Figure 8.1 The inflammatory expansion of cDC2 following LPS inhalation is heterogenous

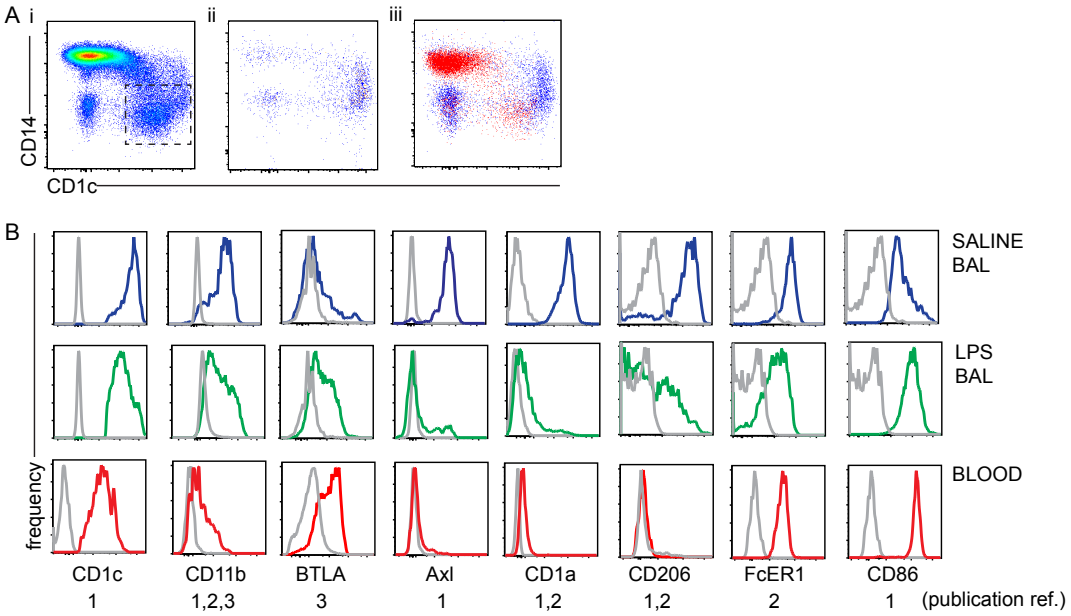

Figure 8.1 The inflammatory expansion of cDC2 following LPS inhalation is heterogeneous.

A) CD14 versus CD1c analysis plots displaying lineage-HLA-DR+CD16- mononuclear cells from i) BAL fluid following LPS inhalation and ii) BAL fluid following saline inhalation. Panel iii shows an overlay plot of panel ii (blue dots) plus steady state blood lineage-HLA-DR+CD16- cells (red dots).
B) Expression of selected surface antigens on cDC2. cDC2 were gated as lineage-HLA-DR+CD16-CD14$^{lo\text{-}mid}$CD1c$^{mid\text{-}high}$ cells. Representative histograms from saline BAL (n=2), LPS BAL (n=2) and blood (n=3) are shown. Antibody expression (coloured lines) is shown relative to isotype or FMO control (grey lines). Numbers indicate publication antigen was selected from: 1=Desch et al, 2=Segura et al, 3=McGovern et al.

Surface antigen expression was tested between saline BAL, LPS BAL and blood to explore this hypothesis further. Eight antigens were selected based on their ability to distinguish blood and tissue cDC2 in three publications: Desch et al (blood and digested lung tissue cDC2 analysed by microarray), Segura et al (blood and inflammatory fluid cDC2 analysed by flow cytometry) and McGovern et al (blood and steady state skin DC analysed by flow cyometry) (Desch et al., 2016), (Segura et al., 2013), (McGovern et al., 2014).

Saline BAL cDC2 expressed CD1a, CD14, CD206, CD11b and FcER1, in common with Segura's inflammatory fluid DC, perhaps suggesting that they are markers of

tissue-residence rather than inflammation per se (Figure 8.1, panel B). LPS BAL cDC2 expression was heterogeneous. However the majority of cells had lower CD1a, CD14, CD206 and FcER1 expression, in keeping with more recent derivation from blood cDC2.

Consistent with gene expression data from Desch et al, saline BAL cDC2 expressed receptor tyrosine kinase Axl. Axl is not expressed by blood cDC2. The 2-dimensional plot of CD1c versus Axl was best at distinguishing resident from recruited cDC2 in LPS BAL samples.

In summary, BAL cDC2 expressed a range of tissue-associated antigens in steady state. In inflammation BAL cDC2 antigen expression was more similar to blood.

8.5.2 Both subsets of blood cDC2 are recruited to the airspace in inflammation

In blood, BTLA expression splits the cDC2 population approximately 50:50 (Figure 8.2, panel A-B). In saline BAL cDC2, the ratio of BTLA+ to BTLA– is 20:80 but in LPS BAL the ratio is 50:50. This is consistent with recruitment of both BTLA+ and BTLA– cDC2 from blood.

Before analyzing specific properties of cDC2 subsets, functional verification of cDC2 identity was sought. cDC2 were isolated from LPS BAL and their T cell stimulation capacity was compared with two other MP subsets. Unlike AM and CD14++CD16- cells, cDC2 induced proliferation of allogeneic T cells (Figure 8.2, panel C). Experiments were not repeated in BAL following saline inhalation as fewer cells were isolated in this context.

The first specific property of cDC2 subsets tested was the ability to skew T cell cytokine production. BTLA+ and BTLA– cDC2 from saline and LPS BAL were co-cultured with T cells. Bulk T cells isolated from the peripheral blood of allogeneic donors were used. As adult peripheral blood contains only 50% naïve T cells (Hannet et al., 1992), this cannot precisely be called a polarization experiment. Bulk T cells were favoured because BAL fluid lymphocytes are predominantly memory cells (Jardine L, unpublished data) and this thesis is concerned with MP activity in tissues. Both cDC2 subsets isolated from BAL fluid favoured Th1 cytokine

production (Figure 8.2, panel D). This was true of steady state (saline inhalation) and inflammation (LPS

Figure 8.2 Both subsets of cDC2 are recruited in inflammation

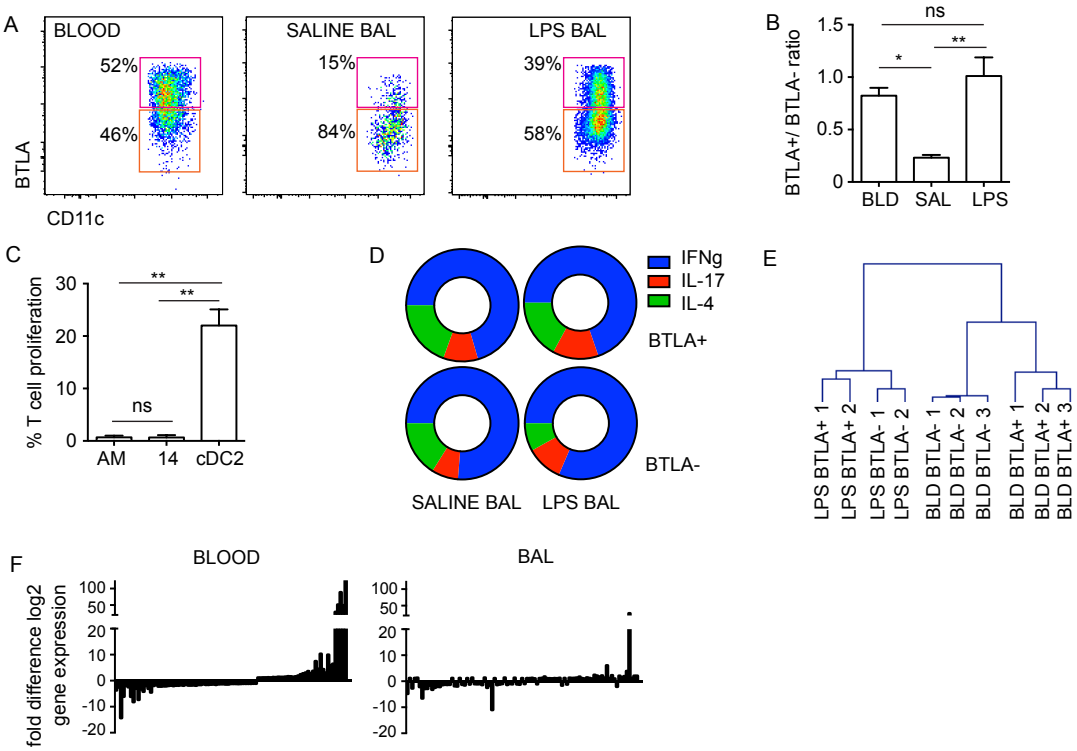

Figure 8.2 Both subsets of cDC2 are recruited in inflammation

A) Flow cytometry analysis of cDC2 in blood, saline BAL and LPS BAL. Plots show lineage-HLA-DR+CD16-CD14-CD1c+ cells. Frequency of BTLA+ and BTLA- subsets in representative examples are shown.
B) Ratio of BTLA+ to BTLA- cDC2 in blood (n=4), saline BAL (n=5) and LPS BAL (n=4). Bars indicated mean ± SEM, * $p<0.05$ and ** $p<0.01$ from 1-way ANOVA with Tukey's multiple-comparison adjusted post-test.
C) Proliferation of allogeneic T cells in MLRs established with alveolar macrophages (AM), CD14++CD16- cells (14) and cDC2 isolated from LPS BAL as stimulators. % T cell proliferation was quantified by CSFE dilution on flow cytometry. ** $p<0.01$ with 1-way ANOVA and post-test as above.
D) Mean T-cell cytokine production following co-culture with BTLA+ or BTLA- cDC2 from saline or LPS BAL (each n=2). Cytokine production was quantified by flow cytometry. Each cytokine is expressed as a proportion of total cytokine produced. There was no dual production of cytokines.
E) Hierarchical clustering of gene expression data in BTLA+ and BTLA- cDC2 from LPS BAL and blood. Clustering was performed on the 93 gene BTLA+/- DEG set.
E) Fold differences in gene expression between BTLA+ and BTLA- cDC2 from blood and BAL using the BTLA +/- DEG set. Each bar represents mean expression of a gene in BTLA+ divided by mean expression in BTLA-. Positive bars are therefore "BTLA+ genes" and negative bars are "BTLA- genes".

inhalation). In contrast to blood BTLA+ cDC2, BAL fluid BTLA+ cDC2 did not induce significant IL-4 production. This suggests functional convergence of cDC2 subsets on entering the lung.

Next, cDC2 subset gene expression signatures were probed. NanoString data were used to test whether distinct gene expression signatures seen in blood subsets were conserved in tissue subsets. Only cDC2 from LPS BAL fluid were used in this analysis and insufficient BTLA+ cDC2 were present in saline BAL fluid to use for NanoString. Ninety-three genes (16%) were differentially expressed between blood BTLA+ and BTLA– cDC2. This gene-set clustered BAL fluid BTLA+ cDC2 separately from BAL fluid BTLA- cDC2, indicating some conserved differential gene expression (Figure 8.2, panel E). As evidenced by the height of cluster-connecting lines in the dendrogram and the fold-difference plots from blood and BAL (Figure 8.3 panel E-F), BAL cDC2 subsets were more similar to each other than blood cDC2 subsets. This supports the concept of subset convergence upon entry to inflamed tissue.

8.5.3 Comparison of cDC2 across compartments in steady state and inflammation

Data presented above support the recruitment of blood cDC2 to BAL fluid in inflammation and identify convergence of blood cDC2 subsets on entering the lung. Gene expression data were explored further to detail differences between cDC2 in the intravascular and airspace compartments and to contrast the resident and recruited cDC2 populations seen inflammation.

For this analysis, cDC2 were isolated from BAL fluid following saline inhalation (steady state) and LPS inhalation (inflammation). LPS BAL cDC2 were isolated either as total cDC2, i.e. lineage-HLA-DR+CD16- cells that were $CD14^{lo\text{-}mid}$ and $CD1c^{mid\text{-}hi}$, or as resident and recruited populations. Resident populations were sorted as $CD1c^{hi}CD14^{mid}$ or as $CD1c^{hi}$Axl- cells. Recruited populations were sorted as $CD1c^{mid}$CD14- or as $CD1c^{mid}$Axl+ cells. Gene expression was consistent between samples despite the use of two sorting strategies (Figure 8.3, panel A). Blood cDC2, blood classical monocytes and two *in vitro* manipulated MPs were used for comparison: moDCs generated from classical monocytes and blood cDC2 stimulated *ex-vivo* with LPS.

Figure 8.3 Comparison of cDC2 across compartments in steady state and inflammation

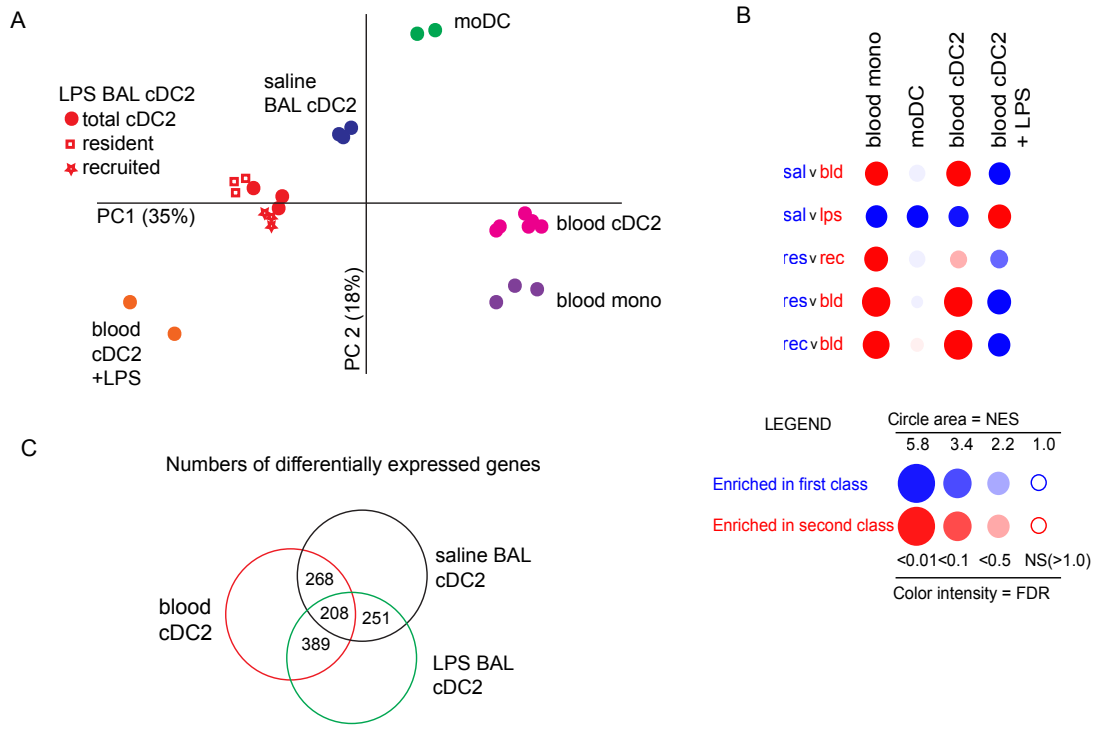

Figure 8.3 Comparison of cDC2 across compartments in steady state and inflammation

A) PCA plot of BAL and blood cDC2, blood monocytes, moDC and blood cDC2 simulated *ex-vivo* with LPS.
B) Bubblemap showing pairwise gene-set enrichment with monocyte, moDC, blood cDC2 and LPS-stimulated blood cDC2 gene signatures. Columns represent gene signatures. Red circles indicate that the signature is enriched in the test population written in red relative to the population written in blue. Larger, more intensely coloured circles indicate more significant enrichment. sal= saline BAL cDC2, bld= blood cDC2, lps=total LPS BAL cDC2, res= resident LPS BAL cDC2, rec= recruited LPS BAL cDC2, NES= normalized enrichment score, FDR= false discovery rate.
C) Venn diagram showing numbers of differentially expressed genes in blood, saline and total LPS BAL cDC2.

By PCA, the most defining point of cDC2 identity was whether it was blood-derived (positive axis of PC1) or BAL-derived (negative axis of PC1). Saline BAL cDC2 were readily distinguished from LPS BAL cDC2 on PC1 and PC2. Resident and recruited LPS BAL cDC2 formed distinct, but proximal clusters. If resident cDC2 were once equivalent to saline BAL cDC2, and recruited cDC2 were once equivalent to blood cDC2, they underwent significant gene expression convergence on LPS exposure/ inflammatory recruitment. The third principal component (13% of variation; not

shown) separated out *ex-vivo* manipulated cells (moDC and LPS-stimulated cDC2) and offered little additional information on BAL subsets.

Gene-set enrichment analysis was used to probe for specific gene signatures in inflamed BAL cDC2. Neither total, resident, nor recruited cDC2 in LPS BAL enriched with a moDC signature (Figure 8.3, panel B). The blood monocyte signature was more enriched in saline BAL cDC2 and blood cDC2 than LPS BAL. When the recruited and resident subsets of LPS BAL were compared, the blood monocyte signature enriched most with recruited cells. This type of analysis cannot prove or disprove whether a particular MP is monocyte-derived. However the results are in keeping with cDC2 in inflammation not arising from monocytes.

While LPS BAL cDC2 had surface antigen similarity to blood cDC2 (Figure 8.1), they did not have a blood cDC2 gene expression signature. An LPS-activated cDC2 signature was enriched in LPS BAL subsets (total, resident and recruited). Saline BAL had more of an LPS-activated cDC2 signature than blood, perhaps reflecting the heightened activation state of tissue DCs. When comparing resident to recruited LPS BAL cDC2, the resident subset has a stronger LPS-activation signature, supporting the concept that it was present in the airspace when LPS was administered.

Forty-six percent of genes (268) tested by NanoString were differentially expressed between blood and steady state BAL cDC2 (Figure 8.3, panel C). Genes preferentially expressed by saline BAL cDC2 were associated with mature DC function: T cell co-stimulation (*CD40, CD80)* migration to lymph node (*CCR7*); complement-mediated immunity (*CQ1A/B, C2, C8B*); anti-viral response (*TLR7*); and chemokine production (*CCL18, CCL19, CCL22, CXCL10, CXCL11*). Thirty-six percent (208) of these differentially expressed genes were also different between blood and LPS BAL cDC2. While forty-three percent of genes (251) were differentially expressed between saline and LPS BAL, the magnitude of these differences were smaller. Genes preferentially expressed in saline BAL cDC2 encoded complement components, scavenger receptors (*CD163, MSR1, MARCO*), and pathogen detection molecules (*CLEC6A, TLR5, TLR8, NOD1*) consistent with a role in airway immune defense. Fewer genes were preferentially expressed by LPS BAL cDC2 (18 with fold change>1.5 compared with 54 for saline BAL cDC2).

8.6 Summary or results for Chapter 8

Analyses in this chapter have demonstrated that the inflammatory expansion of cDC2 in BAL is heterogeneous. LPS BAL cDC2 comprise a major recruited and a minor resident fraction. The recruited cDC2 have surface antigen similarity to blood cDC2. Both BTLA+ and BTLA- blood cDC2 appear to be recruited to the airspace in inflammation, but their functions and gene expression signatures converge. There is no evidence for monocyte derivation of recruited cDC2. Compartment of residence is the most important defining feature in cDC2 identity. Differentially expressed genes between blood and BAL DC support a specialized role for airspace cDC2 in pathogen detection and clearance and support of complement-mediated immunity.

Chapter 9. Lung strand Discussion

9.1 Discussion point 1: BAL fluid contains 7 distinct MP populations

Using multi-parameter flow cytometry, 7 distinct MP populations were identified in steady state BAL fluid. These were identified with a parallel gating strategy in blood, in order to facilitate comparison across compartments.

Accurate characterization of human lung tissue MPs has been difficult as lung is a vascular organ. Without adequate perfusion of vessels prior to digestion- a procedure difficult to achieve without an intact lung- overlay of blood MP populations can confound analysis (Desch et al., 2016). Lung MPs with negligible blood contamination have been characterized in this thesis. Around 20 million erythrocytes were detected in BAL specimens. Given that the normal circulating red blood cell count is around $5x10^{12}$/L, this suggests a whole-blood leak into the airspace equivalent to 4µl. With a blood myeloid DC concentration of around 15 cells/µl (Jardine et al., 2013) and around 40,000 myeloid DCs detected in a saline BAL, blood contamination can be assumed to be minimal (<0.01%). Enrichment of certain DC populations in BAL, differences in surface phenotype and differential gene expression between blood and BAL populations all support the assertion that a distinct compartment has been sampled.

In the most comprehensive description of human lung tissue MPs to date, Desch et al carefully excluded blood contamination and concluded that 5 MPs subsets were resident in lung. Three of these were variations of myeloid DCs, one was described as a tissue monocyte, and the last was the AM (Desch et al., 2016). Plasmacytoid DCs and cDC1 were declared absent. In this thesis, pDCs and cDC1 were clearly identifiable in BAL fluid. As has been described previously, pDCs were CD11c-negative (Dzionek et al., 2000). It is probable that Desch et al excluded their pDCs prior to analysis as CD11c-enrichment was performed before flow cytometry. The BAL cDC1 identified in this thesis had modest expression of CD1c and CD206. They probably occupied the territory between gates in the definitions used by Desch et al (Figure 9.1). cDC1s are rare and difficult to identify in tissue preparations unless multiple parameters are used (Haniffa et al., 2012). The tissue monocyte described by Desch et al was CD14+CD16+, consistent with the “resident pulmonary-

monocyte-like" cell described previously (Brittan et al., 2012) and the CD14++CD16+ cell identified in this thesis. The rare CD14++CD16- cells identified in steady state in this thesis expressed a full spectrum of CD206. Some will have been captured in the tissue monocyte gate of Desch et al. and the others will have been excluded. The three myeloid DC variations described by Desch et al. were separated by CD206 and CD1a expression. Based on absence of dendritic morphology, the CD206 subsets were designated "monocyte-derived." Expression differences across a selected set of genes were presented, but overall, the evidence to support 3 distinct subsets of myeloid DCs is unconvincing.

Figure 9.1 Location of Jardine MP subsets in Desch et al analysis

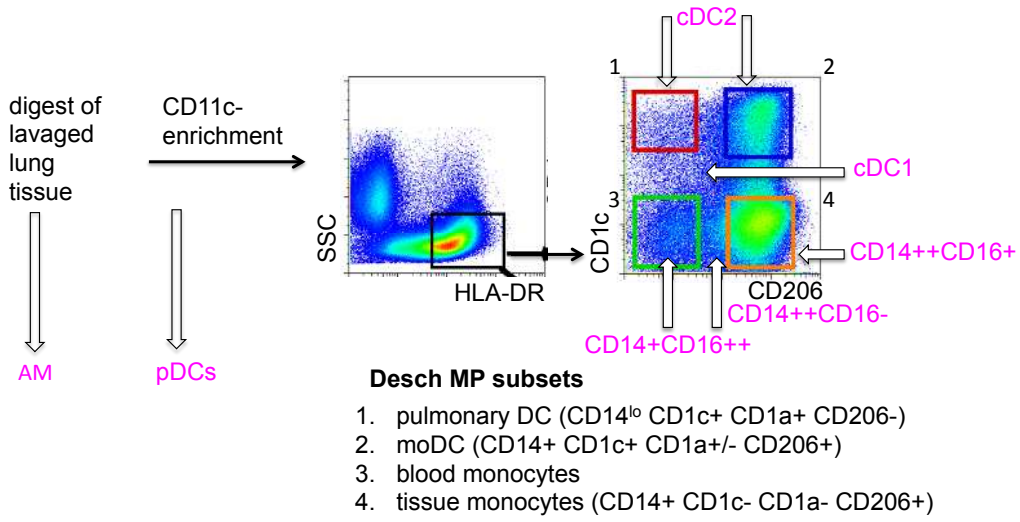

Figure 9.1 Location of Jardine MP subsets in Desch et al analysis

The strategy used by Desch et al. to analyse lung MPs is depicted (Desch et al., 2016). Gates 1, 2 and 4 in the second analysis plot encompass 4 of the 5 MPs described in that publication (moDC are divided into CD1a+ and CD1a- subsets, AM are the additional population). Pink labels display the MP populations described in this thesis. White arrows indicate their probable location in this analysis strategy.

In summary, this thesis reliably concludes that 7 subsets of MPs are present in BAL fluid and that no subset is present as a result of blood contamination. Insufficient understanding of how BAL samples pulmonary MPs and how the MP composition across lung compartments might vary prevents a complete understanding of the pulmonary MPS.

9.2 Discussion point 2: LPS inhalation is associated with accumulation of monocytes and cDC2 myeloid DCs in BAL

LPS inhalation recreated the influx of CD14+CD16- monocytes into 6-hour BAL fluid described previously (Brittan et al., 2012) and identified an accumulation of CD1c-expressing DCs.

CD1c accumulation in murine lung has been described following a range of inflammatory stimuli including viral infection (GeurtsvanKessel et al., 2008), TLR agonist application (Hammad et al., 2009) and asthma (Hammad et al., 2010). These cells were presumed to originate from monocytes (Lambrecht and Hammad, 2012). When time-course is considered, accumulation of DCs between 4 and 8 hours can be seen in both humans and animal models, (McWilliam et al., 1994). *In vitro*, the induction of CD1 molecules on human monocytes takes 5 days (Assier et al., 2007). It is therefore unlikely that monocytes could differentiate into the recruited DC population identified in this thesis. Uniformly low expression of monocyte markers CD14 and CD11b on recruited DCs supports this assertion. As concluded by the authors of the allergen challenge-recruited DCs, rapid accumulation of DCs in this thesis is consistent with cDC2 recruitment from blood (Jahnsen et al., 2001).

9.3 Discussion point 3: Convergence and the importance of tissue identity

Both of the recently identified blood cDC2 subsets were present in the LPS-recruited DC population. On entering lung, convergence was seen in both gene expression and functional interaction with T cells. Considering inflamed and steady state blood and BAL together, the most important defining feature of cDC2 was their tissue of residence.

The concept of convergence occurs repeatedly in MP biology and is most hotly debated with regard to macrophages (Epelman et al., 2014b). Macrophages with distinctly different ontogeny (fetal/ yolk sac precursor versus adult monocyte) coexist in certain tissues such as the heart (Epelman et al., 2014a). It remains unknown whether ontogeny is relevant to the function of these cells (Epelman et al., 2014b). Certainly tissue exerts a major influence on macrophage identity (Amit et al., 2015).

The publication of data regarding two distinct origins of human cDC2 will bring a similar debate to DCs. Though the differences in ontogeny are not so stark as with macrophages, it will be important to understand whether mature tissue DCs arising from BTLA+ and BTLA- blood DCs always converge or under what conditions subset-specific properties persist.

When considering gene expression data sets derived from analogous populations in multiple tissues, anatomical site is recognized as the major source of variation (Satpathy et al., 2012b), (Elpek et al., 2011), (Miller et al., 2012), (Gautier et al., 2012). This variation can be explored to provide meaningful insight into tissue-specific immunity. For example, Eplek et al. examined CD4 and CD8 DC subsets from murine lymphoid tissue and found greater similarity between subsets from the same tissue than they found between subsets from different tissues (Elpek et al., 2011). Both CD4 and CD8 DCs from mesenteric lymph nodes expressed *Aldh1a2* gene and its product aldehyde dehydrogenase 2, while neither subset from spleen expressed *Aldh1a2*. As the product of this enzyme (retinoic acid) is implicated in imprinting primed T cells with a gut-homing signature, a mesenteric lymph node-specific function was proposed.

Often, with the goal of overlaying analogous populations from different tissues or species on a PCA plot, tissue-specific gene signatures are removed (Robbins et al., 2008), (Ingersoll et al., 2010), (Haniffa et al., 2012). There is no doubt that this approach has rationalized our understanding of DC subsets and harmonized efforts between murine and human immunologists, but I would argue these signatures harbour useful information. The validity of removing tissue-specific signatures from datasets with a smaller number of user-selected genes, such as with NanoString, remains to be proven.

Both gene expression and surface antigen data generated from BAL cDC2 have identified characteristics not seen in blood cDC2. Surface expression of CD206 and Axl, expression of PRR, complement component and chemokine genes needs further interrogation to understand the functions and interactions of pulmonary cDC2.

9.4 Discussion point 4: Benefits and limitations of experimental inflammation for understanding lung GvHD

A significant focus in performing the LPS inhalation study was to understand the MP content of normal (saline) BAL. This important foundation for examining BAL in BMT patients with respiratory compromise was previously absent.

An additional focus was to use LPS as a well-tolerated, reproducible inflammatory stimulus to see how the MPS was perturbed. Heightened sensitivity to LPS derived from gut bacteria has been implicated in the pathogenesis of IPS and alloimmune lung injury (Cooke et al., 1996), (Cooke et al., 2000), (Garantziotis et al., 2007), (Martinu et al., 2014). Mice without GvHD following BMT can be induced to develop lymphocytic bronchiolar infiltrates and epithelial injury following LPS inhalation (Garantziotis et al., 2007).

Critics of LPS-exposure studies argue that inter-supplier and inter-batch variability in LPS preparations make it difficult to ascertain exactly what immune responses are being stimulated (Mathiak et al., 2003). This study used LPS from *Escherichia coli*. The relative TLR4 versus TLR2 ligation is not of great importance to this work, but with enteric bacterial LPS, TLR4 is the predominant ligand (Takeda and Akira, 2005).

The LPS inhalation study afforded the unique perspective of an early time point in inflammation. From these data, it is possible to generate new hypotheses about the role of LPS in the initiation of alloreactive lung disease and test these in animal models. For example, the influx of cDC2 may be important in stimulating alloreactive T cells. The limitation is that LPS inhalation gives rise to short-lived, self-resolving inflammation. It is not clear whether the BAL 6-hours following LPS inhalation represents what we would see in evolving sterile inflammation or how generic the features of early inflammation actually are. Furthermore, we will never be able to sample BMT recipients at such an early time point in the acquisition of lung injury. The cellular profile of LPS-exposed BAL is therefore of limited use as a comparison for BAL in BMT recipients.

9.5 Conclusions

This work provides a comprehensive analysis of MPs in the human airspace that challenges data recently published. It provides a benchmark for investigating BAL in disease. Study of BAL following LPS inhalation has focused on the novel finding that cDC2 are recruited. Data support the conclusion that cDC2 arise from blood DCs and not monocytes in this setting. The gene expression data set of steady state and inflammatory populations can be exploited further to learn more about the immune functions and tissue-specialization of airway MPs.

Chapter 10. General discussion and future work

Key insights from the data presented in this thesis have been discussed in Chapters 6 and 9. Here, findings will be reviewed against the hypotheses made in Chapter 1 (section 1.9). Unresolved issues will be detailed and future avenues of investigation discussed.

10.1 GvHD skin: review of hypotheses

In GvHD skin, the MP repertoire was altered. Myeloid DCs were reduced and macrophages were expanded. Monocyte-derived MPs were found in tissue. Several lines of evidence supported the derivation of inflammatory "GVH14" macrophages from classical monocytes. The possibility that monocyte-derived DCs were present in GvHD lesional skin was not addressed. In murine skin, "P3" monocyte-derived DCs can be identified in steady state and are modestly expanded in inflammation (Tamoutounour et al., 2013). Counterparts of P3 and of the murine tissue monocytes "P1/P2" have not been identified in human skin to date. Evidence indirectly presented in this thesis suggests that CD14+CD1c+ may be the human P3. CD14+CD1c+ cells from steady state dermis expressed a monocyte/ macrophage gene signature (Figure 4.5A,D) but were capable of stimulating proliferation and activation of T cells (Figure 4.3C). The mean proportion of CD14+CD1c+ cells in GvHD lesional skin was not significantly higher than in controls (Figure 3.6D), but some specimens did have CD14+CD1c+ enrichment. Flow cytometry data from atopic dermatitis lesions suggested that CD14+CD1c+ cells may be expanded under alternative inflammatory conditions (Figure 3.5D). Detailed characterisation and cross-species comparison of these cells is warranted.

The hypothesis that inflammatory MPs perpetuate T cell-mediated skin damage has not been rigorously tested. This was largely due to the constraints of working with small amounts of infrequently available human material. GVH14 elaborated pro-inflammatory cytokines and chemokines capable of recruiting activated T cells to lesions (RANTES and CXCL10). GVH14 were capable of stimulating T cell proliferation and activation in an allogeneic *in vitro* setting. This evidence is in keeping with a role for GVH14 in supporting T lymphocyte activity, but several important questions remain unanswered. It needs to be established whether GVH14-

T cell interactions are antigen specific. If so, what are the mechanisms of antigen presentation? For donor macrophages to present host antigens to donor T cells, cross-presentation to CD8 T cells, indirect presentation to CD4 T cells and cross-dressing need to be considered. Development of an assay testing *in vitro* cross-presentation of minor antigen HY has been unsuccessful during the course of this work. These mechanisms would be better dissected in murine models.

10.2 BAL: review of hypotheses

Studies on BAL fluid required an evaluation of steady state MPs before inflammatory MPs could be considered. All 6 of the MP subsets present in human blood could be detected in BAL. Alveolar macrophages (AM) constituted a 7th subset. These findings are discordant with a recent description of MPs in human lung tissue (Desch et al., 2016). A consensus definition of pulmonary MPs would facilitate human immunology and the investigation of clinical states. The definitions used in this thesis were purposefully based on accepted definitions in human blood (Haniffa et al., 2015a) and nomenclature agreed between human and murine MPS immunologists (Guilliams et al., 2014). The definitions used here in BAL fluid have also been tested in lung tissue surplus to lung cancer resections. Data were not presented in this thesis because confounding by blood MP subsets has not been adequately resolved. Whole lung donations unsuitable for transplant would be the optimal material for resolving MP subsets in specific compartments (blood, bronchoalveolar, interstitial).

As in GvHD-inflamed skin, the MP repertoire of LPS-inflamed BAL fluid was altered. The predominant inflammatory MP was a CD14++CD16- cell, which shared phenotypic similarity to a classical blood monocyte. This inflammatory MP has already been reported and partially characterized (Brittan et al., 2012), (Brittan et al., 2014). Efforts were therefore directed at the novel finding of cDC2 expansion in inflamed BAL fluid. Evidence presented in this thesis supported cDC2 derivation from blood DCs rather than monocytes. Using material I have collected from the LPS inhalation study, the trajectories of monocytes in inflamed BAL fluid are currently being scrutinized by single cell RNA sequencing and associated computational techniques.

The role for inflammatory MP in lung GvHD has not been investigated in this thesis. Now the MP composition of steady state BAL fluid has been characterized, it will be possible to identify inflammatory perturbations in BAL fluid from patients with lung GvHD. Careful consideration will be required as to how patients can be identified early in the evolution of lung inflammation and with minimal confounding from infection. Insights from human studies can be used to inform mechanistic studies in animal models. Understanding the pathogenesis of lung injury will be an important step in rationalizing the diagnosis and treatment of non-infective lung injury post-BMT.

10.3 Unresolved issues in MPS biology

The boundaries between MPs, their inter-relationships and differentiation potentials are continually being revised. The discovery of two cDC2 subsets will bring a substantial change to our understanding of the MPS. Data presented in this thesis demonstrated that steady state BAL had a BTLA- cDC2 bias, but acute inflammation recruited both BTLA+ and BTLA- cDC2 from blood. Unfortunately, BTLA is labile in culture and destroyed by enzymatic digestion of skin, so the subset composition of skin cDC2 could not be addressed. BTLA- cDC2s expressed monocyte-associated genes. It will be important to identify proximal precursors of both BTLA+ and BTLA- cDC2s and to clearly define the relationships between BTLA- cDC2 precursors and monocytes. It is possible that some previous descriptions of monocyte-derived DCs have actually characterized BTLA- cDCs. The DC repertoire in inflammation will need to be revisited.

Both GvHD skin and blood demonstrated an augmented dominance of monocytes/ monocyte-derived cells over classical DCs compared with steady state. The mechanisms and consequences of this dominance need to be addressed. Proximal precursors of human DCs have been reported (Breton et al., 2015), (Lee et al., 2015) but a comprehensive description of steady state monocyte and DC production has not yet been achieved. Once the steady state has been deconvoluted, the acute and chronic effects of inflammation on MP haematopoiesis can be explored. It may be the case that inflammation biases haematopoiesis towards monocyte production. If so, what would be the consequences for tissue DC turnover in chronic inflammation

and how would that impact upon the individual's response to subsequent immune challenge? If tissue DCs were replaced by monocyte-derived cells, would they be a faithful replicate? The concepts of monocyte plasticity and convergence have been discussed in this thesis, but would convergence be so absolute that tolerance to commensals and immunity to pathogens is conserved?

10.4 Unresolved issues in GvHD

In analysing the MP repertoire of GvHD lesional skin, the dermal macrophage was difficult to identify. As shown in Figure 3.6C, the dermal macrophage was a significantly lower proportion of leukocytes in GvHD skin than in control skin. Efforts are continuing to quantify absolute numbers of dermal macrophages in GvHD skin by microscopy. The activity of dermal macrophages in skin GvHD warrants consideration. As dermal macrophages are the longest surviving host MP in human skin following BMT (Haniffa et al., 2009), they may continue to present host antigen to donor T cells. Some murine models have demonstrated that host macrophages protect against GvHD in the early post-BMT period by engulfing alloreactive T cells (Hashimoto et al., 2011). Detailing whether dermal macrophages survive skin GvHD will help inform the relevance of these potential functions.

Classical monocytes in the blood of patients with skin GvHD showed transcriptional differences compared with healthy volunteers. Comparisons with well-matched BMT controls have not yet been made, but these will be important. It has been established in a murine model that remote tissue signals can prime monocytes developing in bone marrow (Askenase et al., 2015). Isolated skin GvHD cannot strictly be considered a remote tissue signal as sub-clinical systemic inflammation is likely. However, the extent of monocyte priming is of academic interest, and may be a predictor of disease severity.

10.5 Ongoing challenges to studying the human MPS in inflammation

This work was approached with the assumption that inflammatory populations should be studied with reference to steady state populations. This was considered important

for two reasons. The first was that inflammation represents a shift in a homeostatically maintained system. Inflammatory populations are therefore more likely to have a steady state counterpart than to be a completely foreign entity. Secondly, tissues have a resident leukocyte population. If this is not adequately identified, incorrect conclusions can be made about recruited inflammatory cells. Parsing resident from recruited cells was difficult, especially in the context of skin GvHD. Few surface antigens adequately distinguish dermal macrophages from CD14+ monocyte-derived macrophages. In steady state, physical parameters (side-scatter and autofluorescence) provided adequate separation, but this was not the case in inflammation. Absence of CD11c expression was the best method to identify dermal macrophages in the GvHD flow cyometry data, but this is clearly not an optimal strategy. Work is in progress to apply dimensionality reduction algorithms to the flow cytometry data to see if subtle differences in fluorescence across the 10-12 channels might afford better resolution of resident from inflammatory cells.

10.6 Opportunities arising from new technologies

Ultimately, the goal will be to analyse GvHD skin using high-dimensional single cell techniques, such as mass cytometry or RNA sequencing. Testing 50 or more surface antigens with CyTOF, for example, should identify better antigens for discriminating dermal macrophages from inflammatory monocyte-derived macrophages.

The expansion of single-cell techniques offers the potential to enter new territory in human immunology. It can reveal previously unseen heterogeneity. It can validate the antigens we currently use for *a priori* definition of populations or can highlight better alternatives. It can provide reams of information from small samples of human tissue. Computational techniques can be applied to RNA sequencing data to understand functions, interactions and developmental relationships between cells. Using the knowledge acquired from lower dimensional analysis, such as in this thesis, new techniques can be targeted to the biological questions unanswered in disease and weaknesses in our knowledge of the immune system. For example, it could be possible to distinguish whether there is a developmental trajectory from monocytes to DCs in inflamed human tissue.

In addition to single-cell techniques, methods for analysing small populations of human material are now tangible. It is possible to laser micro-dissect material from slides of FFPE-preserved tissue and generate gene-expression data by NanoString. This will allow retrospective analysis of GvHD biopsies, incorporating material from across centres and stratifying variables to give greater statistical power to analysis than was possible with the prospective cohort study performed in this thesis.

As methods are evolving in research, techniques are entering clinical practice which provide new diagnostic information. Next generation sequencing can assist pathogen detection (Naccache et al., 2015). This may be particularly revealing in BMT recipients with lung injury, and may help distinguish infective from alloreactive aetiology.

10.7 Future directions

Studying inflammatory perturbations of the human MPS has potential to yield important insights into the pathogenesis of transplantation-associated, autoimmune and pathogen-driven inflammation. Greater appreciation of the MPS is required to direct therapeutic manipulation with monoclonal antibodies and inform vaccine strategies. As a clinician scientist working with BMT recipients, I have found the timely diagnosis and effective management of post-BMT lung injury a pressing unmet need. Using research insights to bring clarity to the spectrum of lung injuries following BMT will be an important extension of this thesis.

References

ALBANESI, C. et al. (2009) Chemerin expression marks early psoriatic skin lesions and correlates with plasmacytoid dendritic cell recruitment. *J Exp Med*, **206**, 249-258.

ALEXANDER, K.A. et al. (2014) CSF-1-dependant donor-derived macrophages mediate chronic graft-versus-host disease. *J Clin Invest*, **124**, 4266-4280.

ALEXIS, N.E. et al. (2005) Acute LPS inhalation in healthy volunteers induces dendritic cell maturation in vivo. *J Allergy Clin Immunol*, **115**, 345-350.

ALOUSI, A.M., BOLANOS-MEADE, J. & LEE, S.J. (2013) Graft-versus-host disease: state of the science. *Biol Blood Marrow Transplant*, **19**, S102-8.

AMIT, I., WINTER, D.R. & JUNG, S. (2015) The role of the local environment and epigenetics in shaping macrophage identity and their effect on tissue homeostasis. *Nat Immunol*, **17**, 18-25.

ANASETTI, C. et al. (1990) Effect of HLA incompatibility on graft-versus-host disease, relapse, and survival after marrow transplantation for patients with leukemia or lymphoma. *Hum Immunol*, **29**, 79-91.

ANTIN, J.H. et al. (2002) A phase I/II double-blind, placebo-controlled study of recombinant human interleukin-11 for mucositis and acute GVHD prevention in allogeneic stem cell transplantation. *Bone Marrow Transplant*, **29**, 373-377.

APPERLEY, J. & MASSZI, T. (2012) Graft-versus-host disease. *Haematopoietic Stem Cell Transplantation. 6th edition. ESH-EBMT Handbook*, 233.

ARIEL, A. & SERHAN, C.N. (2012) New Lives Given by Cell Death: Macrophage Differentiation Following Their Encounter with Apoptotic Leukocytes during the Resolution of Inflammation. *Front Immunol*, **3**, 4.

ASKENASE, M.H. et al. (2015) Bone-Marrow-Resident NK Cells Prime Monocytes for Regulatory Function during Infection. *Immunity*, **42**, 1130-1142.

ASSIER, E. et al. (2007) TLR7/8 agonists impair monocyte-derived dendritic cell differentiation and maturation. *J Leukoc Biol*, **81**, 221-228.

AUFFERMANN-GRETZINGER, S. et al. (2002) Rapid establishment of dendritic cell chimerism in allogeneic hematopoietic cell transplant recipients. *Blood*, **99**, 1442-1448.

AUFFRAY, C. et al. (2007) Monitoring of blood vessels and tissues by a population of monocytes with patrolling behavior. *Science*, **317**, 666-670.

BACHEM, A. et al. (2010) Superior antigen cross-presentation and XCR1 expression define human CD11c+CD141+ cells as homologues of mouse CD8+ dendritic cells. *J Exp Med*, **207**, 1273-1281.

BAIN, C.C. et al. (2014) Constant replenishment from circulating monocytes maintains the macrophage pool in the intestine of adult mice. *Nat Immunol*, **15**, 929-937.

BAIN, C.C. & MOWAT, A.M. (2014) Macrophages in intestinal homeostasis and inflammation. *Immunol Rev*, **260**, 102-117.

BAIN, C.C. et al. (2013) Resident and pro-inflammatory macrophages in the colon represent alternative context-dependent fates of the same Ly6Chi monocyte precursors. *Mucosal Immunol*, **6**, 498-510.

BAKER, M.B., ALTMAN, N.H., PODACK, E.R. & LEVY, R.B. (1996) The role of cell-mediated cytotoxicity in acute GVHD after MHC-matched allogeneic bone marrow transplantation in mice. *J Exp Med*, **183**, 2645-2656.

BARLETTA, K.E. et al. (2012) Leukocyte compartments in the mouse lung: distinguishing between marginated, interstitial, and alveolar cells in response to injury. *J Immunol Methods*, **375**, 100-110.

BAUMGARTH, N. & ROEDERER, M. (2000) A practical approach to multicolor flow cytometry for immunophenotyping. *J Immunol Methods*, **243**, 77-97.

BEELEN, D.W., ELMAAGACLI, A., MULLER, K.D., HIRCHE, H. & SCHAEFER, U.W. (1999) Influence of intestinal bacterial decontamination using metronidazole and ciprofloxacin or ciprofloxacin alone on the development of acute graft-versus-host disease after marrow transplantation in patients with hematologic malignancies: final results and long-term follow-up of an open-label prospective randomized trial. *Blood*, **93**, 3267-3275.

BEILHACK, A. et al. (2005) In vivo analyses of early events in acute graft-versus-host disease reveal sequential infiltration of T-cell subsets. *Blood*, **106**, 1113-1122.

BEITNES, A.C. et al. (2011) Density of CD163+ CD11c+ dendritic cells increases and CD103+ dendritic cells decreases in the coeliac lesion. *Scand J Immunol*, **74**, 186-194.

BENDALL, S.C. et al. (2014) Single-cell trajectory detection uncovers progression and regulatory coordination in human B cell development. *Cell*, **157**, 714-725.

BENNETT, C.L. & CHAKRAVERTY, R. (2012) Dendritic cells in tissues: in situ stimulation of immunity and immunopathology. *Trends Immunol*, **33**, 8-13.

BENNETT, C.L. et al. (2005) Inducible ablation of mouse Langerhans cells diminishes but fails to abrogate contact hypersensitivity. *J Cell Biol*, **169**, 569-576.

BEUTLER, B.A. (2009) TLRs and innate immunity. *Blood*, **113**, 1399-1407.

BHARAT, A. et al. (2016) Flow Cytometry Reveals Similarities Between Lung Macrophages in Humans and Mice. *Am J Respir Cell Mol Biol*, **54**, 147-149.

BIEBER, T. et al. (2000) Fc [correction of Ec] epsilon RI expressing dendritic cells: the missing link in the pathophysiology of atopic dermatitis? *J Dermatol*, **27**, 698-699.

BIGLEY, V. et al. (2011) The human syndrome of dendritic cell, monocyte, B and NK lymphoid deficiency. *J Exp Med*, **208**, 227-234.

BIGLEY, V. et al. (2015) Langerin-expressing dendritic cells in human tissues are related to CD1c+ dendritic cells and distinct from Langerhans cells and CD141high XCR1+ dendritic cells. *J Leukoc Biol*, **97**, 627-634.

BILLINGHAM, R.E. (1966) The biology of graft-versus-host reactions. *Harvey Lect*, **62**, 21-78.

BIRNBERG, T. et al. (2008) Lack of conventional dendritic cells is compatible with normal development and T cell homeostasis, but causes myeloid proliferative syndrome. *Immunity*, **29**, 986-997.

BOGUNOVIC, M. et al. (2009) Origin of the lamina propria dendritic cell network. *Immunity*, **31**, 513-525.

BRATKE, K. et al. (2007) Dendritic cell subsets in human bronchoalveolar lavage fluid after segmental allergen challenge. *Thorax*, **62**, 168-175.

BRAUN, M.Y., LOWIN, B., FRENCH, L., ACHA-ORBEA, H. & TSCHOPP, J. (1996) Cytotoxic T cells deficient in both functional fas ligand and perforin show residual cytolytic activity yet lose their capacity to induce lethal acute graft-versus-host disease. *J Exp Med*, **183**, 657-661.

BRETON, G. et al. (2015) Circulating precursors of human CD1c+ and CD141+ dendritic cells. *J Exp Med*, **212**, 401-413.

BRITTAN, M. et al. (2012) A novel subpopulation of monocyte-like cells in the human lung after lipopolysaccharide inhalation. *Eur Respir J*, **40**, 206-214.

BRITTAN, M. et al. (2014) Functional characterisation of human pulmonary monocyte-like cells in lipopolysaccharide-mediated acute lung inflammation. *J Inflamm (Lond)*, **11**, 9.

CAMPBELL, I.K. et al. (2011) Differentiation of inflammatory dendritic cells is mediated by NF-kappaB1-dependent GM-CSF production in CD4 T cells. *J Immunol*, **186**, 5468-5477.

CARLIN, L.M. et al. (2013) Nr4a1-dependent Ly6C(low) monocytes monitor endothelial cells and orchestrate their disposal. *Cell*, **153**, 362-375.

CARPENTIER, S. et al. (2016) Comparative genomics analysis of mononuclear phagocyte subsets confirms homology between lymphoid tissue-resident and dermal XCR1 DCs in mouse and human and distinguishes them from Langerhans cells. *J Immunol Methods*,

CHAKRAVERTY, R. et al. (2006) An inflammatory checkpoint regulates recruitment of graft-versus-host reactive T cells to peripheral tissues. *J Exp Med*, **203**, 2021-2031.

CHENG, Q. et al. (2015) The S1P1 receptor-selective agonist CYM-5442 reduces the severity of acute GVHD by inhibiting macrophage recruitment. *Cell Mol Immunol*, **12**, 681-691.

CHENG, S.C. et al. (2014) mTOR- and HIF-1alpha-mediated aerobic glycolysis as metabolic basis for trained immunity. *Science*, **345**, 1250684.

CLARK, J.G. et al. (1999) Idiopathic pneumonia after bone marrow transplantation: cytokine activation and lipopolysaccharide amplification in the bronchoalveolar compartment. *Crit Care Med*, **27**, 1800-1806.

CLARK, R.A. (2010) Skin-resident T cells: the ups and downs of on site immunity. *J Invest Dermatol*, **130**, 362-370.

CLARK, R.A. et al. (2006) The vast majority of CLA+ T cells are resident in normal skin. *J Immunol*, **176**, 4431-4439.

CLARK, R.A. et al. (2012) Skin effector memory T cells do not recirculate and provide immune protection in alemtuzumab-treated CTCL patients. *Sci Transl Med*, **4**, 117ra7.

COHEN, A.B. & BATRA, G.K. (1980) Bronchoscopy and lung lavage induced bilateral pulmonary neutrophil influx and blood leukocytosis in dogs and monkeys. *Am Rev Respir Dis*, **122**, 239-247.

COHEN, J. (1988) Cytokines as mediators of graft-versus-host disease. *Bone Marrow Transplant*, **3**, 193-197.

COLLIN, M., MCGOVERN, N. & HANIFFA, M. (2013) Human dendritic cell subsets. *Immunology*, **140**, 22-30.

COLLIN, M.P. et al. (2006) The fate of human Langerhans cells in hematopoietic stem cell transplantation. *J Exp Med*, **203**, 27-33.

COLLISON, J.L., CARLIN, L.M., EICHMANN, M., GEISSMANN, F. & PEAKMAN, M. (2015) Heterogeneity in the Locomotory Behavior of Human Monocyte Subsets over Human Vascular Endothelium In Vitro. *J Immunol*, **195**, 1162-1170.

CONDAMINE, T., MASTIO, J. & GABRILOVICH, D.I. (2015) Transcriptional regulation of myeloid-derived suppressor cells. *J Leukoc Biol*, **98**, 913-922.

COOKE, K.R. et al. (2000) Hyporesponsiveness of donor cells to lipopolysaccharide stimulation reduces the severity of experimental idiopathic pneumonia syndrome: potential role for a gut-lung axis of inflammation. *J Immunol*, **165**, 6612-6619.

COOKE, K.R. et al. (1996) An experimental model of idiopathic pneumonia syndrome after bone marrow transplantation: I. The roles of minor H antigens and endotoxin. *Blood*, **88**, 3230-3239.

COURIEL, D.R. et al. (2009) A phase III study of infliximab and corticosteroids for the initial treatment of acute graft-versus-host disease. *Biol Blood Marrow Transplant*, **15**, 1555-1562.

COURTIES, G. et al. (2015) Ischemic stroke activates hematopoietic bone marrow stem cells. *Circ Res*, **116**, 407-417.

CREAMER, D. et al. (2007) Eczematoid graft-vs-host disease: a novel form of chronic cutaneous graft-vs-host disease and its response to psoralen UV-A therapy. *Arch Dermatol*, **143**, 1157-1162.

CROS, J. et al. (2010) Human CD14dim monocytes patrol and sense nucleic acids and viruses via TLR7 and TLR8 receptors. *Immunity*, **33**, 375-386.

CROZAT, K. et al. (2010) The XC chemokine receptor 1 is a conserved selective marker of mammalian cells homologous to mouse CD8alpha+ dendritic cells. *J Exp Med*, **207**, 1283-1292.

DARQUENNE, C., PAIVA M. & PRISK GK. (1985) Effect of gravity on aerosol dispersion and deposition in the human lung after periods of breath holding. *J Appl Physiol,* **89**, 1787-1792.

D'AVENI, M. et al. (2015) G-CSF mobilizes CD34+ regulatory monocytes that inhibit graft-versus-host disease. *Sci Transl Med*, **7**, 281ra42.

DAVIES, L.C., JENKINS, S.J., ALLEN, J.E. & TAYLOR, P.R. (2013) Tissue-resident macrophages. *Nat Immunol*, **14**, 986-995.

DE TOMASO, A.W. et al. (2005) Isolation and characterization of a protochordate histocompatibility locus. *Nature*, **438**, 454-459.

DEEG, H.J., MARIS, M.B., SCOTT, B.L. & WARREN, E.H. (2006) Optimization of allogeneic transplant conditioning: not the time for dogma. *Leukemia*, **20**, 1701-1705.

DEMEDTS, I.K., BRACKE, K.R., MAES, T., JOOS, G.F. & BRUSSELLE, G.G. (2006) Different roles for human lung dendritic cell subsets in pulmonary immune defense mechanisms. *Am J Respir Cell Mol Biol*, **35**, 387-393.

DEMEDTS, I.K., BRUSSELLE, G.G., VERMAELEN, K.Y. & PAUWELS, R.A. (2005) Identification and characterization of human pulmonary dendritic cells. *Am J Respir Cell Mol Biol*, **32**, 177-184.

DESCH, A.N. et al. (2016) Flow Cytometric Analysis of Mononuclear Phagocytes in Nondiseased Human Lung and Lung-Draining Lymph Nodes. *Am J Respir Crit Care Med*, **193**, 614-626.

DICKINSON, A.M. et al. (1998) Predicting graft-versus-host disease in HLA-identical bone marrow transplant: a comparison of T-cell frequency analysis and a human skin explant model. *Transplantation*, **66**, 857-863.

DIEU, M.C. et al. (1998) Selective recruitment of immature and mature dendritic cells by distinct chemokines expressed in different anatomic sites. *J Exp Med*, **188**, 373-386.

DOHERTY, D.E., DOWNEY, G.P., SCHWAB, B.R., ELSON, E. & WORTHEN, G.S. (1994) Lipolysaccharide-induced monocyte retention in the lung. Role of monocyte stiffness, actin assembly, and CD18-dependent adherence. *J Immunol*, **153**, 241-255.

DOMINGO-GONZALEZ, R. & MOORE, B.B. (2013) Defective pulmonary innate immune responses post-stem cell transplantation; review and results from one model system. *Front Immunol*, **4**, 126.

DOULATOV, S. et al. (2010) Revised map of the human progenitor hierarchy shows the origin of macrophages and dendritic cells in early lymphoid development. *Nat Immunol*, **11**, 585-593.

DUFFNER, U.A. et al. (2004) Host dendritic cells alone are sufficient to initiate acute graft-versus-host disease. *J Immunol*, **172**, 7393-7398.

DUQUE-AFONSO, J. et al. (2013) Identification of risk factors for bronchiolitis obliterans syndrome after reduced toxicity conditioning before hematopoietic cell transplantation. *Bone Marrow Transplant*, **48**, 1098-1103.

DURAKOVIC, N. et al. (2006) Host-derived Langerhans cells persist after MHC-matched allografting independent of donor T cells and critically influence the alloresponses mediated by donor lymphocyte infusions. *J Immunol*, **177**, 4414-4425.

DUTTA, P. et al. (2015) Myocardial Infarction Activates CCR2(+) Hematopoietic Stem and Progenitor Cells. *Cell Stem Cell*, **16**, 477-487.

DZIONEK, A. et al. (2000) BDCA-2, BDCA-3, and BDCA-4: three markers for distinct subsets of dendritic cells in human peripheral blood. *J Immunol*, **165**, 6037-6046.

ELPEK, K.G. et al. (2011) Lymphoid organ-resident dendritic cells exhibit unique transcriptional fingerprints based on subset and site. *PLoS One*, **6**, e23921.

EPELMAN, S. et al. (2014a) Embryonic and adult-derived resident cardiac macrophages are maintained through distinct mechanisms at steady state and during inflammation. *Immunity*, **40**, 91-104.

EPELMAN, S., LAVINE, K.J. & RANDOLPH, G.J. (2014b) Origin and functions of tissue macrophages. *Immunity*, **41**, 21-35.

FERRARA, J.L. & DEEG, H.J. (1991) Graft-versus-host disease. *N Engl J Med*, **324**, 667-674.

FERRARA, J.L., LEVINE, J.E., REDDY, P. & HOLLER, E. (2009) Graft-versus-host disease. *Lancet*, **373**, 1550-1561.

FILIPOVICH, A.H. et al. (2005) National Institutes of Health consensus development project on criteria for clinical trials in chronic graft-versus-host disease: I. Diagnosis and staging working group report. *Biol Blood Marrow Transplant*, **11**, 945-956.

FLOWERS, M.E. et al. (2011) Comparative analysis of risk factors for acute graft-versus-host disease and for chronic graft-versus-host disease according to National Institutes of Health consensus criteria. *Blood*, **117**, 3214-3219.

FOGG, D.K. et al. (2006) A clonogenic bone marrow progenitor specific for macrophages and dendritic cells. *Science*, **311**, 83-87.

FOX, A., MOUNTFORD, J., BRAAKHUIS, A. & HARRISON, L.C. (2001) Innate and adaptive immune responses to nonvascular xenografts: evidence that macrophages are direct effectors of xenograft rejection. *J Immunol*, **166**, 2133-2140.

FREUDENBERGER, T.D. et al. (2003) Association between acute and chronic graft-versus-host disease and bronchiolitis obliterans organizing pneumonia in recipients of hematopoietic stem cell transplants. *Blood*, **102**, 3822-3828.

FUENTES-DUCULAN, J. et al. (2010) A subpopulation of CD163-positive macrophages is classically activated in psoriasis. *J Invest Dermatol*, **130**, 2412-2422.

GARANTZIOTIS, S. et al. (2007) Alloimmune lung injury induced by local innate immune activation through inhaled lipopolysaccharide. *Transplantation*, **84**, 1012-1019.

GARSIDE, P., HUTTON, A.K., SEVERN, A., LIEW, F.Y. & MOWAT, A.M. (1992) Nitric oxide mediates intestinal pathology in graft-vs.-host disease. *Eur J Immunol*, **22**, 2141-2145.

GAUTIER, E.L. et al. (2012) Gene-expression profiles and transcriptional regulatory pathways that underlie the identity and diversity of mouse tissue macrophages. *Nat Immunol*, **13**, 1118-1128.

GEISS, G.K. et al. (2008) Direct multiplexed measurement of gene expression with color-coded probe pairs. *Nat Biotechnol*, **26**, 317-325.

GEISSMANN, F., GORDON, S., HUME, D.A., MOWAT, A.M. & RANDOLPH, G.J. (2010) Unravelling mononuclear phagocyte heterogeneity. *Nat Rev Immunol*, **10**, 453-460.

GEISSMANN, F., JUNG, S. & LITTMAN, D.R. (2003) Blood monocytes consist of two principal subsets with distinct migratory properties. *Immunity*, **19**, 71-82.

GEURTSVANKESSEL, C.H. et al. (2008) Clearance of influenza virus from the lung depends on migratory langerin+CD11b- but not plasmacytoid dendritic cells. *J Exp Med*, **205**, 1621-1634.

GINHOUX, F. et al. (2010) Fate mapping analysis reveals that adult microglia derive from primitive macrophages. *Science*, **330**, 841-845.

GINHOUX, F. & GUILLIAMS, M. (2016) Tissue-Resident Macrophage Ontogeny and Homeostasis. *Immunity*, **44**, 439-449.

GRAINGER, J.R. et al. (2013) Inflammatory monocytes regulate pathologic responses to commensals during acute gastrointestinal infection. *Nat Med*, **19**, 713-721.

GRATWOHL, A. et al. (1995) Acute graft-versus-host disease: grade and outcome in patients with chronic myelogenous leukemia. Working Party Chronic Leukemia

of the European Group for Blood and Marrow Transplantation. *Blood*, **86**, 813-818.

GRATWOHL, A. & CARRERAS, E. (2008) Principles of conditioning. Haematopoietic Stem Cell Transplantation. The EBMT Handbook, 5th edn. Forum Service Editore: Genoa, Italy, 129-142.

GROSSMAN, J. et al. (2014) Nonmyeloablative allogeneic hematopoietic stem cell transplantation for GATA2 deficiency. *Biol Blood Marrow Transplant*, **20**, 1940-1948.

GUHA, M. & MACKMAN, N. (2001) LPS induction of gene expression in human monocytes. *Cell Signal*, **13**, 85-94.

GUILLIAMS, M. et al. (2013) Alveolar macrophages develop from fetal monocytes that differentiate into long-lived cells in the first week of life via GM-CSF. *J Exp Med*, **210**, 1977-1992.

GUILLIAMS, M. et al. (2014) Dendritic cells, monocytes and macrophages: a unified nomenclature based on ontogeny. *Nat Rev Immunol*, **14**, 571-578.

HAMMAD, H. et al. (2009) House dust mite allergen induces asthma via Toll-like receptor 4 triggering of airway structural cells. *Nat Med*, **15**, 410-416.

HAMMAD, H. et al. (2010) Inflammatory dendritic cells--not basophils--are necessary and sufficient for induction of Th2 immunity to inhaled house dust mite allergen. *J Exp Med*, **207**, 2097-2111.

HANASH, A.M. et al. (2012) Interleukin-22 protects intestinal stem cells from immune-mediated tissue damage and regulates sensitivity to graft versus host disease. *Immunity*, **37**, 339-350.

HANIFFA, M., BIGLEY, V. & COLLIN, M. (2015a) Human mononuclear phagocyte system reunited. *Semin Cell Dev Biol*, **41**, 59-69.

HANIFFA, M. et al. (2009) Differential rates of replacement of human dermal dendritic cells and macrophages during hematopoietic stem cell transplantation. *J Exp Med*, **206**, 371-385.

HANIFFA, M., GUNAWAN, M. & JARDINE, L. (2015b) Human skin dendritic cells in health and disease. *J Dermatol Sci*, **77**, 85-92.

HANIFFA, M. et al. (2012) Human tissues contain CD141hi cross-presenting dendritic cells with functional homology to mouse CD103+ nonlymphoid dendritic cells. *Immunity*, **37**, 60-73.

HANNET, I., ERKELLER-YUKSEL, F., LYDYARD, P., DENEYS, V. & DEBRUYERE, M. (1992) Developmental and maturational changes in human blood lymphocyte subpopulations. *Immunol Today*, **13**, 215, 218.

HANSEL, A. et al. (2011) Human slan (6-sulfo LacNAc) dendritic cells are inflammatory dermal dendritic cells in psoriasis and drive strong TH17/TH1 T-cell responses. *J Allergy Clin Immunol*, **127**, 787-94.e1-9.

HARRIS, A.C., FERRARA, J.L. & LEVINE, J.E. (2013) Advances in predicting acute GVHD. *Br J Haematol*, **160**, 288-302.

HASHIMOTO, D. et al. (2011) Pretransplant CSF-1 therapy expands recipient macrophages and ameliorates GVHD after allogeneic hematopoietic cell transplantation. *J Exp Med*, **208**, 1069-1082.

HASHIMOTO, D. et al. (2013) Tissue-resident macrophages self-maintain locally throughout adult life with minimal contribution from circulating monocytes. *Immunity*, **38**, 792-804.

HAUBER, H.P. et al. (2002) TNFalpha, interleukin-10 and interleukin-18 expression in cells of the bronchoalveolar lavage in patients with pulmonary complications following bone marrow or peripheral stem cell transplantation: a preliminary study. *Bone Marrow Transplant*, **30**, 485-490.

HAVENITH, C.E. et al. (1994) Enrichment and characterization of dendritic cells from human bronchoalveolar lavages. *Clin Exp Immunol*, **96**, 339-343.

HAZIOT, A. et al. (1996) Resistance to endotoxin shock and reduced dissemination of gram-negative bacteria in CD14-deficient mice. *Immunity*, **4**, 407-414.

HEIER, I. et al. (2011) Characterisation of bronchus-associated lymphoid tissue and antigen-presenting cells in central airway mucosa of children. *Thorax*, **66**, 151-156.

HETTINGER, J. et al. (2013) Origin of monocytes and macrophages in a committed progenitor. *Nat Immunol*, **14**, 821-830.

Heymer, B. (2013) *Clinical and diagnostic pathology of graft-versus-host disease*. Springer Science & Business Media,

HILL, G.R. et al. (1997) Total body irradiation and acute graft-versus-host disease: the role of gastrointestinal damage and inflammatory cytokines. *Blood*, **90**, 3204-3213.

HILL, G.R. & FERRARA, J.L. (2000) The primacy of the gastrointestinal tract as a target organ of acute graft-versus-host disease: rationale for the use of cytokine shields in allogeneic bone marrow transplantation. *Blood*, **95**, 2754-2759.

HILL, G.R. et al. (2010) Stem cell mobilization with G-CSF induces type 17 differentiation and promotes scleroderma. *Blood*, **116**, 819-828.

HO, V.T. & SOIFFER, R.J. (2001) The history and future of T-cell depletion as graft-versus-host disease prophylaxis for allogeneic hematopoietic stem cell transplantation. *Blood*, **98**, 3192-3204.

HOEFFEL, G. et al. (2012) Adult Langerhans cells derive predominantly from embryonic fetal liver monocytes with a minor contribution of yolk sac-derived macrophages. *J Exp Med*, **209**, 1167-1181.

HOFFMANN, P., ERMANN, J., EDINGER, M., FATHMAN, C.G. & STROBER, S. (2002) Donor-type CD4(+)CD25(+) regulatory T cells suppress lethal acute graft-versus-host disease after allogeneic bone marrow transplantation. *J Exp Med*, **196**, 389-399.

HOHL, T.M. et al. (2009) Inflammatory monocytes facilitate adaptive CD4 T cell responses during respiratory fungal infection. *Cell Host Microbe*, **6**, 470-481.

HOLBRO, A. et al. (2013) Lung histology predicts outcome of bronchiolitis obliterans syndrome after hematopoietic stem cell transplantation. *Biol Blood Marrow Transplant*, **19**, 973-980.

HOLT, P.G., HAINING, S., NELSON, D.J. & SEDGWICK, J.D. (1994) Origin and steady-state turnover of class II MHC-bearing dendritic cells in the epithelium of the conducting airways. *J Immunol*, **153**, 256-261.

HOLT, P.G., STRICKLAND, D.H., WIKSTROM, M.E. & JAHNSEN, F.L. (2008) Regulation of immunological homeostasis in the respiratory tract. *Nat Rev Immunol*, **8**, 142-152.

HUANG, H., FLETCHER, A., NIU, Y., WANG, T.T. & YU, L. (2012) Characterization of lipopolysaccharide-stimulated cytokine expression in macrophages and monocytes. *Inflamm Res*, **61**, 1329-1338.

HUME, D.A. (2015) The Many Alternative Faces of Macrophage Activation. *Front Immunol*, **6**, 370.

IIJIMA, N., MATTEI, L.M. & IWASAKI, A. (2011) Recruited inflammatory monocytes stimulate antiviral Th1 immunity in infected tissue. *Proc Natl Acad Sci U S A*, **108**, 284-289.

INABA, K. et al. (1992) Generation of large numbers of dendritic cells from mouse bone marrow cultures supplemented with granulocyte/macrophage colony-stimulating factor. *J Exp Med*, **176**, 1693-1702.

INABA, K., METLAY, J.P., CROWLEY, M.T., WITMER-PACK, M. & STEINMAN, R.M. (1990) Dendritic cells as antigen presenting cells in vivo. *Int Rev Immunol*, **6**, 197-206.

INGERSOLL, M.A. et al. (2010) Comparison of gene expression profiles between human and mouse monocyte subsets. *Blood*, **115**, e10-9.

JAGASIA, M. et al. (2012) Risk factors for acute GVHD and survival after hematopoietic cell transplantation. *Blood*, **119**, 296-307.

JAHNSEN, F.L. et al. (2001) Rapid dendritic cell recruitment to the bronchial mucosa of patients with atopic asthma in response to local allergen challenge. *Thorax*, **56**, 823-826.

JAHNSEN, F.L. et al. (2006) Accelerated antigen sampling and transport by airway mucosal dendritic cells following inhalation of a bacterial stimulus. *J Immunol*, **177**, 5861-5867.

JAKUBZICK, C. et al. (2013) Minimal differentiation of classical monocytes as they survey steady-state tissues and transport antigen to lymph nodes. *Immunity*, **39**, 599-610.

JARDINE, L. et al. (2013) Rapid detection of dendritic cell and monocyte disorders using CD4 as a lineage marker of the human peripheral blood antigen-presenting cell compartment. *Front Immunol*, **4**, 495.

JARDINE, L. et al. (2015) A comparative study of reduced dose alemtuzumab in matched unrelated donor and related donor reduced intensity transplants. *Br J Haematol*, **168**, 874-881.

JENQ, R.R. et al. (2012) Regulation of intestinal inflammation by microbiota following allogeneic bone marrow transplantation. *J Exp Med*, **209**, 903-911.

JERSMANN, H.P. (2005) Time to abandon dogma: CD14 is expressed by non-myeloid lineage cells. *Immunol Cell Biol*, **83**, 462-467.

JONGBLOED, S.L. et al. (2010) Human CD141+ (BDCA-3)+ dendritic cells (DCs) represent a unique myeloid DC subset that cross-presents necrotic cell antigens. *J Exp Med*, **207**, 1247-1260.

JUNG, S. & SCHWARTZ, M. (2012) Non-identical twins - microglia and monocyte-derived macrophages in acute injury and autoimmune inflammation. *Front Immunol*, **3**, 89.

KEEFE, D.M., BREALEY, J., GOLAND, G.J. & CUMMINS, A.G. (2000) Chemotherapy for cancer causes apoptosis that precedes hypoplasia in crypts of the small intestine in humans. *Gut*, **47**, 632-637.

KEKRE, N. et al. (2015) Efficacy of immune suppression tapering in treating relapse after reduced intensity allogeneic stem cell transplantation. *Haematologica*, **100**, 1222-1227.

KIM, Y.M., SACHS, T., ASAVAROENGCHAI, W., BRONSON, R. & SYKES, M. (2003) Graft-versus-host disease can be separated from graft-versus-lymphoma effects by control of lymphocyte trafficking with FTY720. *J Clin Invest*, **111**, 659-669.

KLECHEVSKY, E. et al. (2008) Functional specializations of human epidermal Langerhans cells and CD14+ dermal dendritic cells. *Immunity*, **29**, 497-510.

KORNGOLD, R. & SPRENT, J. (1978) Lethal graft-versus-host disease after bone marrow transplantation across minor histocompatibility barriers in mice. Prevention by removing mature T cells from marrow. *J Exp Med*, **148**, 1687-1698.

KORNGOLD, R. & SPRENT, J. (1980) Selection of cytotoxic T-cell precursors specific for minor histocompatibility determinants. I. Negative selection across H-2 barriers induced with disrupted cells but not with glutaraldehyde-treated cells: evidence for antigen processing. *J Exp Med*, **151**, 314-327.

KORNGOLD, R. & SPRENT, J. (1982) Features of T cells causing H-2-restricted lethal graft-vs.-host disease across minor histocompatibility barriers. *J Exp Med*, **155**, 872-883.

KORNGOLD, R. & SPRENT, J. (1985) Surface markers of T cells causing lethal graft-vs-host disease to class I vs class II H-2 differences. *J Immunol*, **135**, 3004-3010.

KOTTARIDIS, P.D. et al. (2000) In vivo CAMPATH-1H prevents graft-versus-host disease following nonmyeloablative stem cell transplantation. *Blood*, **96**, 2419-2425.

KOYAMA, M. et al. (2012) Recipient nonhematopoietic antigen-presenting cells are sufficient to induce lethal acute graft-versus-host disease. *Nat Med*, **18**, 135-142.

KRENSKY, A.M., WEISS, A., CRABTREE, G., DAVIS, M.M. & PARHAM, P. (1990) T-lymphocyte-antigen interactions in transplant rejection. *N Engl J Med*, **322**, 510-517.

KREUTZ, M. et al. (2012) Whole-body UVB irradiation during allogeneic hematopoietic cell transplantation is safe and decreases acute graft-versus-host disease. *J Invest Dermatol*, **132**, 179-187.

KRUTZIK, S.R. et al. (2005) TLR activation triggers the rapid differentiation of monocytes into macrophages and dendritic cells. *Nat Med*, **11**, 653-660.

KUMAR, V. & MCNERNEY, M.E. (2005) A new self: MHC-class-I-independent natural-killer-cell self-tolerance. *Nat Rev Immunol*, **5**, 363-374.

LAMBRECHT, B.N. (2006) Alveolar macrophage in the driver's seat. *Immunity*, **24**, 366-368.

LAMBRECHT, B.N. & HAMMAD, H. (2012) Lung dendritic cells in respiratory viral infection and asthma: from protection to immunopathology. *Annu Rev Immunol*, **30**, 243-270.

LAVIN, Y., MORTHA, A., RAHMAN, A. & MERAD, M. (2015) Regulation of macrophage development and function in peripheral tissues. *Nat Rev Immunol*, **15**, 731-744.

LAVIN, Y. et al. (2014) Tissue-resident macrophage enhancer landscapes are shaped by the local microenvironment. *Cell*, **159**, 1312-1326.

LEE, J. et al. (2015) Restricted dendritic cell and monocyte progenitors in human cord blood and bone marrow. *J Exp Med*, **212**, 385-399.

LEON, B., LOPEZ-BRAVO, M. & ARDAVIN, C. (2007) Monocyte-derived dendritic cells formed at the infection site control the induction of protective T helper 1 responses against Leishmania. *Immunity*, **26**, 519-531.

LERNER, K.G. et al. (1974) Histopathology of graft-vs.-host reaction (GvHR) in human recipients of marrow from HL-A-matched sibling donors. *Transplant Proc*, **6**, 367-371.

LEVINE, J.E. et al. (2012) Acute graft-versus-host disease biomarkers measured during therapy can predict treatment outcomes: a Blood and Marrow Transplant Clinical Trials Network study. *Blood*, **119**, 3854-3860.

LIU, W., XIAO, X., DEMIRCI, G., MADSEN, J. & LI, X.C. (2012) Innate NK cells and macrophages recognize and reject allogeneic nonself in vivo via different mechanisms. *J Immunol*, **188**, 2703-2711.

LOMMATZSCH, M. et al. (2007) Airway dendritic cell phenotypes in inflammatory diseases of the human lung. *Eur Respir J*, **30**, 878-886.

LOWES, M.A. et al. (2005) Increase in TNF-alpha and inducible nitric oxide synthase-expressing dendritic cells in psoriasis and reduction with efalizumab (anti-CD11a). *Proc Natl Acad Sci U S A*, **102**, 19057-19062.

LU, Y.C., YEH, W.C. & OHASHI, P.S. (2008) LPS/TLR4 signal transduction pathway. *Cytokine*, **42**, 145-151.

MACKALL, C. et al. (2009) Background to hematopoietic cell transplantation, including post transplant immune recovery. *Bone Marrow Transplant*, **44**, 457-462.

MACKANESS, G.B. (1962) Cellular resistance to infection. *J Exp Med*, **116**, 381-406.

MACMILLAN, M.L. et al. (2002) Response of 443 patients to steroids as primary therapy for acute graft-versus-host disease: comparison of grading systems. *Biol Blood Marrow Transplant*, **8**, 387-394.

MAECKER, H.T., FREY, T., NOMURA, L.E. & TROTTER, J. (2004) Selecting fluorochrome conjugates for maximum sensitivity. *Cytometry A*, **62**, 169-173.

MALISSEN, B., TAMOUTOUNOUR, S. & HENRI, S. (2014) The origins and functions of dendritic cells and macrophages in the skin. *Nat Rev Immunol*, **14**, 417-428.

MANTOVANI, A. et al. (2004) The chemokine system in diverse forms of macrophage activation and polarization. *Trends Immunol*, **25**, 677-686.

MARIS, N.A. et al. (2005) Antiinflammatory effects of salmeterol after inhalation of lipopolysaccharide by healthy volunteers. *Am J Respir Crit Care Med*, **172**, 878-884.

MARKEY, K.A. et al. (2014a) Cross-dressing by donor dendritic cells after allogeneic bone marrow transplantation contributes to formation of the immunological synapse and maximizes responses to indirectly presented antigen. *J Immunol*, **192**, 5426-5433.

MARKEY, K.A., MACDONALD, K.P. & HILL, G.R. (2014b) The biology of graft-versus-host disease: experimental systems instructing clinical practice. *Blood*, **124**, 354-362.

MARTINEZ, F.O. & GORDON, S. (2014) The M1 and M2 paradigm of macrophage activation: time for reassessment. *F1000Prime Rep*, **6**, 13.

MARTINEZ, F.O., GORDON, S., LOCATI, M. & MANTOVANI, A. (2006) Transcriptional profiling of the human monocyte-to-macrophage differentiation and polarization: new molecules and patterns of gene expression. *J Immunol*, **177**, 7303-7311.

MARTINU, T. et al. (2014) Allogeneic splenocyte transfer and lipopolysaccharide inhalations induce differential T cell expansion and lung injury: a novel model of pulmonary graft-versus-host disease. *PLoS One*, **9**, e97951.

MASSI, D. et al. (1999) A reappraisal of the histopathologic criteria for the diagnosis of cutaneous allogeneic acute graft-vs-host disease. *Am J Clin Pathol*, **112**, 791-800.

MASTEN, B.J. et al. (2006) Characterization of myeloid and plasmacytoid dendritic cells in human lung. *J Immunol*, **177**, 7784-7793.

MATHIAK, G. et al. (2003) Lipopolysaccharides from different bacterial sources elicit disparate cytokine responses in whole blood assays. *Int J Mol Med*, **11**, 41-44.

MATTE, C.C. et al. (2004) Donor APCs are required for maximal GVHD but not for GVL. *Nat Med*, **10**, 987-992.

MATZINGER, P. (1994) Tolerance, danger, and the extended family. *Annu Rev Immunol*, **12**, 991-1045.

MATZINGER, P. (2002) The danger model: a renewed sense of self. *Science*, **296**, 301-305.

MCGOVERN, N. et al. (2014) Human dermal CD14(+) cells are a transient population of monocyte-derived macrophages. *Immunity*, **41**, 465-477.

MCWILLIAM, A.S., NELSON, D., THOMAS, J.A. & HOLT, P.G. (1994) Rapid dendritic cell recruitment is a hallmark of the acute inflammatory response at mucosal surfaces. *J Exp Med*, **179**, 1331-1336.

MEDZHITOV, R. & HORNG, T. (2009) Transcriptional control of the inflammatory response. *Nat Rev Immunol*, **9**, 692-703.

MELUM, G.R. et al. (2014) A thymic stromal lymphopoietin-responsive dendritic cell subset mediates allergic responses in the upper airway mucosa. *J Allergy Clin Immunol*, **134**, 613-621.e7.

MERAD, M. et al. (2004) Depletion of host Langerhans cells before transplantation of donor alloreactive T cells prevents skin graft-versus-host disease. *Nat Med*, **10**, 510-517.

MERAD, M., SATHE, P., HELFT, J., MILLER, J. & MORTHA, A. (2013) The dendritic cell lineage: ontogeny and function of dendritic cells and their subsets in the steady state and the inflamed setting. *Annu Rev Immunol*, **31**, 563-604.

MIDDLETON, P.G., TAYLOR, P.R., JACKSON, G., PROCTOR, S.J. & DICKINSON, A.M. (1998) Cytokine gene polymorphisms associating with severe acute graft-versus-host disease in HLA-identical sibling transplants. *Blood*, **92**, 3943-3948.

MILDNER, A. et al. (2009) CCR2+Ly-6Chi monocytes are crucial for the effector phase of autoimmunity in the central nervous system. *Brain*, **132**, 2487-2500.

MILLER, J.C. et al. (2012) Deciphering the transcriptional network of the dendritic cell lineage. *Nat Immunol*, **13**, 888-899.

MOLLER, W. et al. (2012) Differential inflammatory response to inhaled lipopolysaccharide targeted either to the airways or the alveoli in man. *PLoS One*, **7**, e33505.

MOSTAFAVI, S., RAY, D., WARDE-FARLEY, D., GROUIOS, C. & MORRIS, Q. (2008) GeneMANIA: a real-time multiple association network integration algorithm for predicting gene function. *Genome Biol*, **9 Suppl 1**, S4.

MOWAT, A.M. (1989) Antibodies to IFN-gamma prevent immunologically mediated intestinal damage in murine graft-versus-host reaction. *Immunology*, **68**, 18-23.

MUNGER, J.S. et al. (1999) The integrin alpha v beta 6 binds and activates latent TGF beta 1: a mechanism for regulating pulmonary inflammation and fibrosis. *Cell*, **96**, 319-328.

MURAI, M. et al. (2003) Peyer's patch is the essential site in initiating murine acute and lethal graft-versus-host reaction. *Nat Immunol*, **4**, 154-160.

Murphy, K.M. (2011) *Janeway's immunobiology*. New York, Garland Science.

MUZIO, M. et al. (2000) Differential expression and regulation of toll-like receptors (TLR) in human leukocytes: selective expression of TLR3 in dendritic cells. *J Immunol*, **164**, 5998-6004.

NACCACHE, S.N. et al. (2015) Diagnosis of neuroinvasive astrovirus infection in an immunocompromised adult with encephalitis by unbiased next-generation sequencing. *Clin Infect Dis*, **60**, 919-923.

NAIK, S.H. et al. (2007) Development of plasmacytoid and conventional dendritic cell subtypes from single precursor cells derived in vitro and in vivo. *Nat Immunol*, **8**, 1217-1226.

NAKANO, H. et al. (2009) Blood-derived inflammatory dendritic cells in lymph nodes stimulate acute T helper type 1 immune responses. *Nat Immunol*, **10**, 394-402.

NAKATA, K. et al. (1999) Augmented proliferation of human alveolar macrophages after allogeneic bone marrow transplantation. *Blood*, **93**, 667-673.

NARNI-MANCINELLI, E. et al. (2011) Inflammatory monocytes and neutrophils are licensed to kill during memory responses in vivo. *PLoS Pathog*, **7**, e1002457.

NATSUAKI, Y. et al. (2014) Perivascular leukocyte clusters are essential for efficient activation of effector T cells in the skin. *Nat Immunol*, **15**, 1064-1069.

NESTEL, F.P., PRICE, K.S., SEEMAYER, T.A. & LAPP, W.S. (1992) Macrophage priming and lipopolysaccharide-triggered release of tumor necrosis factor alpha during graft-versus-host disease. *J Exp Med*, **175**, 405-413.

NESTLE, F.O., ZHENG, X.G., THOMPSON, C.B., TURKA, L.A. & NICKOLOFF, B.J. (1993) Characterization of dermal dendritic cells obtained from normal human skin reveals phenotypic and functionally distinctive subsets. *J Immunol*, **151**, 6535-6545.

NISHIE, M. et al. (2016) Vigorous inflammatory responses in noninfectious pulmonary complication induced by donor lymphocyte infusion. *Transfusion*, **56**, 231-236.

NISHIWAKI, S. et al. (2014) Dexamethasone palmitate ameliorates macrophages-rich graft-versus-host disease by inhibiting macrophage functions. *PLoS One*, **9**, e96252.

NISHIWAKI, S. et al. (2009) Impact of macrophage infiltration of skin lesions on survival after allogeneic stem cell transplantation: a clue to refractory graft-versus-host disease. *Blood*, **114**, 3113-3116.

NOMURA, T., KABASHIMA, K. & MIYACHI, Y. (2014) The panoply of alphabetaT cells in the skin. *J Dermatol Sci*, **76**, 3-9.

O'GRADY, N.P. et al. (2001) Local inflammatory responses following bronchial endotoxin instillation in humans. *Am J Respir Crit Care Med*, **163**, 1591-1598.

OBERBARNSCHEIDT, M.H. et al. (2014) Non-self recognition by monocytes initiates allograft rejection. *J Clin Invest*, **124**, 3579-3589.

OGINO, T. et al. (2013) Increased Th17-inducing activity of CD14+ CD163 low myeloid cells in intestinal lamina propria of patients with Crohn's disease. *Gastroenterology*, **145**, 1380-91.e1.

ONAI, N. et al. (2007) Identification of clonogenic common Flt3+M-CSFR+ plasmacytoid and conventional dendritic cell progenitors in mouse bone marrow. *Nat Immunol*, **8**, 1207-1216.

OPPENHEIM, J.J. & YANG, D. (2005) Alarmins: chemotactic activators of immune responses. *Curr Opin Immunol*, **17**, 359-365.

PANOSKALTSIS-MORTARI, A. et al. (2011) An official American Thoracic Society research statement: noninfectious lung injury after hematopoietic stem cell transplantation: idiopathic pneumonia syndrome. *Am J Respir Crit Care Med*, **183**, 1262-1279.

PANOSKALTSIS-MORTARI, A. et al. (2004) In vivo imaging of graft-versus-host-disease in mice. *Blood*, **103**, 3590-3598.

PANOSKALTSIS-MORTARI, A. et al. (1997) The critical early proinflammatory events associated with idiopathic pneumonia syndrome in irradiated murine

allogeneic recipients are due to donor T cell infusion and potentiated by cyclophosphamide. *J Clin Invest*, **100**, 1015-1027.

PANOSKALTSIS-MORTARI, A., TRAM, K.V., PRICE, A.P., WENDT, C.H. & BLAZAR, B.R. (2007) A new murine model for bronchiolitis obliterans post-bone marrow transplant. *Am J Respir Crit Care Med*, **176**, 713-723.

PASQUINI, M.C. & ZHU, X. (2014) Current uses and outcomes of hematopoietic stem cell transplantation: 2014 CIBMTR Summary Slides.

PAVLETIC, S.Z. & FOWLER, D.H. (2012) Are we making progress in GVHD prophylaxis and treatment? *Hematology Am Soc Hematol Educ Program*, **2012**, 251-264.

PEREZ-SIMON, J.A. et al. (2002) Nonmyeloablative transplantation with or without alemtuzumab: comparison between 2 prospective studies in patients with lymphoproliferative disorders. *Blood*, **100**, 3121-3127.

PETERSDORF, E.W. et al. (1993) The role of HLA-DPB1 disparity in the development of acute graft-versus-host disease following unrelated donor marrow transplantation. *Blood*, **81**, 1923-1932.

PETTERSEN, J.S. et al. (2011) Tumor-associated macrophages in the cutaneous SCC microenvironment are heterogeneously activated. *J Invest Dermatol*, **131**, 1322-1330.

PIGUET, P.F., GRAU, G.E., ALLET, B. & VASSALLI, P. (1987) Tumor necrosis factor/cachectin is an effector of skin and gut lesions of the acute phase of graft-vs.-host disease. *J Exp Med*, **166**, 1280-1289.

PLANTINGA, M. et al. (2013) Conventional and monocyte-derived CD11b(+) dendritic cells initiate and maintain T helper 2 cell-mediated immunity to house dust mite allergen. *Immunity*, **38**, 322-335.

POLTORAK, A. et al. (1998) Defective LPS signaling in C3H/HeJ and C57BL/10ScCr mice: mutations in Tlr4 gene. *Science*, **282**, 2085-2088.

PONTEN, F., JIRSTROM, K. & UHLEN, M. (2008) The Human Protein Atlas--a tool for pathology. *J Pathol*, **216**, 387-393.

POULIN, L.F. et al. (2010) Characterization of human DNGR-1+ BDCA3+ leukocytes as putative equivalents of mouse CD8alpha+ dendritic cells. *J Exp Med*, **207**, 1261-1271.

PRZEPIORKA, D. et al. (1995) 1994 Consensus Conference on Acute GVHD Grading. *Bone Marrow Transplant*, **15**, 825-828.

QUILL, H. & SCHWARTZ, R.H. (1987) Stimulation of normal inducer T cell clones with antigen presented by purified Ia molecules in planar lipid membranes: specific induction of a long-lived state of proliferative nonresponsiveness. *J Immunol*, **138**, 3704-3712.

RAES, G. et al. (2005) Arginase-1 and Ym1 are markers for murine, but not human, alternatively activated myeloid cells. *J Immunol*, **174**, 6561; author reply 6561-6561; author reply 6562.

RAZA, S. et al. (2014) Analysis of the transcriptional networks underpinning the activation of murine macrophages by inflammatory mediators. *J Leukoc Biol*, **96**, 167-183.

REIZIS, B., BUNIN, A., GHOSH, H.S., LEWIS, K.L. & SISIRAK, V. (2011) Plasmacytoid dendritic cells: recent progress and open questions. *Annu Rev Immunol*, **29**, 163-183.

REMBERGER, M. et al. (2008) Risk factors for acute graft-versus-host disease grades II-IV after reduced intensity conditioning allogeneic stem cell transplantation with unrelated donors: a single centre study. *Bone Marrow Transplant*, **41**, 399-405.

RESHEF, R. et al. (2012) Blockade of lymphocyte chemotaxis in visceral graft-versus-host disease. *N Engl J Med*, **367**, 135-145.

REYNOLDS, G. & HANIFFA, M. (2015) Human and Mouse Mononuclear Phagocyte Networks: A Tale of Two Species? *Front Immunol*, **6**, 330.

RIVOLLIER, A., HE, J., KOLE, A., VALATAS, V. & KELSALL, B.L. (2012) Inflammation switches the differentiation program of Ly6Chi monocytes from antiinflammatory macrophages to inflammatory dendritic cells in the colon. *J Exp Med*, **209**, 139-155.

ROBBINS, S.H. et al. (2008) Novel insights into the relationships between dendritic cell subsets in human and mouse revealed by genome-wide expression profiling. *Genome Biol*, **9**, R17.

RODDIE, C. & PEGGS, K.S. (2011) Donor lymphocyte infusion following allogeneic hematopoietic stem cell transplantation. *Expert Opin Biol Ther*, **11**, 473-487.

ROEDERER, M.E.A. (2011) FMO vs. Isotype Controls. *The Daily Dongle*, "The Daily Dongle". *The Daily Dongle*. N.p., 2016. Web. 6 June 2016.

ROMANI, N. et al. (1989) Cultured human Langerhans cells resemble lymphoid dendritic cells in phenotype and function. *J Invest Dermatol*, **93**, 600-609.

SAEED, A.I. et al. (2003) TM4: a free, open-source system for microarray data management and analysis. *Biotechniques*, **34**, 374-378.

SAEED, S. et al. (2014) Epigenetic programming of monocyte-to-macrophage differentiation and trained innate immunity. *Science*, **345**, 1251086.

SALE, G.E., ANDERSON, P., BROWNE, M. & MYERSON, D. (1992) Evidence of cytotoxic T-cell destruction of epidermal cells in human graft-vs-host disease. Immunohistology with monoclonal antibody TIA-1. *Arch Pathol Lab Med*, **116**, 622-625.

SALLUSTO, F. & LANZAVECCHIA, A. (1994) Efficient presentation of soluble antigen by cultured human dendritic cells is maintained by granulocyte/macrophage colony-stimulating factor plus interleukin 4 and downregulated by tumor necrosis factor alpha. *J Exp Med*, **179**, 1109-1118.

SANDSTROM, T., BJERMER, L. & RYLANDER, R. (1992) Lipopolysaccharide (LPS) inhalation in healthy subjects increases neutrophils, lymphocytes and fibronectin levels in bronchoalveolar lavage fluid. *Eur Respir J*, **5**, 992-996.

SATPATHY, A.T. et al. (2013) Notch2-dependent classical dendritic cells orchestrate intestinal immunity to attaching-and-effacing bacterial pathogens. *Nat Immunol*, **14**, 937-948.

SATPATHY, A.T. et al. (2012a) Zbtb46 expression distinguishes classical dendritic cells and their committed progenitors from other immune lineages. *J Exp Med*, **209**, 1135-1152.

SATPATHY, A.T., WU, X., ALBRING, J.C. & MURPHY, K.M. (2012b) Re(de)fining the dendritic cell lineage. *Nat Immunol*, **13**, 1145-1154.

SCHAKEL, K. et al. (2002) 6-Sulfo LacNAc, a novel carbohydrate modification of PSGL-1, defines an inflammatory type of human dendritic cells. *Immunity*, **17**, 289-301.

SCHLITZER, A. et al. (2013) IRF4 transcription factor-dependent CD11b+ dendritic cells in human and mouse control mucosal IL-17 cytokine responses. *Immunity*, **38**, 970-983.

SCHRODER, K., SWEET, M.J. & HUME, D.A. (2006) Signal integration between IFNgamma and TLR signalling pathways in macrophages. *Immunobiology*, **211**, 511-524.

SCHULENBURG, H., HOEPPNER, M.P., WEINER, J.R. & BORNBERG-BAUER, E. (2008) Specificity of the innate immune system and diversity of C-type lectin

domain (CTLD) proteins in the nematode Caenorhabditis elegans. *Immunobiology*, **213**, 237-250.

SCHULLER, E. et al. (2001) In situ expression of the costimulatory molecules CD80 and CD86 on langerhans cells and inflammatory dendritic epidermal cells (IDEC) in atopic dermatitis. *Arch Dermatol Res*, **293**, 448-454.

SCOTT, C.L., HENRI, S. & GUILLIAMS, M. (2014) Mononuclear phagocytes of the intestine, the skin, and the lung. *Immunol Rev*, **262**, 9-24.

SEGURA, E., ALBISTON, A.L., WICKS, I.P., CHAI, S.Y. & VILLADANGOS, J.A. (2009) Different cross-presentation pathways in steady-state and inflammatory dendritic cells. *Proc Natl Acad Sci U S A*, **106**, 20377-20381.

SEGURA, E. & AMIGORENA, S. (2013) Inflammatory dendritic cells in mice and humans. *Trends Immunol*, **34**, 440-445.

SEGURA, E. et al. (2013) Human inflammatory dendritic cells induce Th17 cell differentiation. *Immunity*, **38**, 336-348.

SENESCHAL, J., CLARK, R.A., GEHAD, A., BAECHER-ALLAN, C.M. & KUPPER, T.S. (2012) Human epidermal Langerhans cells maintain immune homeostasis in skin by activating skin resident regulatory T cells. *Immunity*, **36**, 873-884.

SERBINA, N.V., JIA, T., HOHL, T.M. & PAMER, E.G. (2008) Monocyte-mediated defense against microbial pathogens. *Annu Rev Immunol*, **26**, 421-452.

SERBINA, N.V., SALAZAR-MATHER, T.P., BIRON, C.A., KUZIEL, W.A. & PAMER, E.G. (2003) TNF/iNOS-producing dendritic cells mediate innate immune defense against bacterial infection. *Immunity*, **19**, 59-70.

SHARON, V.R., KONIA, T.H., BARR K.L., & FUNG M.A. (2012) Assessment of the 'no eosinophils' rule: are eosinophils truly absent in pityriasis lichenoides, connective tissue disease, and graft-vs.-host disease? *J Cutan Pathol,* **4,** 413-418.

SHARP, L.L., JAMESON, J.M., CAUVI, G. & HAVRAN, W.L. (2005) Dendritic epidermal T cells regulate skin homeostasis through local production of insulin-like growth factor 1. *Nat Immunol*, **6**, 73-79.

SHECHTER, R. et al. (2009) Infiltrating blood-derived macrophages are vital cells playing an anti-inflammatory role in recovery from spinal cord injury in mice. *PLoS Med*, **6**, e1000113.

SHI, C. & PAMER, E.G. (2011) Monocyte recruitment during infection and inflammation. *Nat Rev Immunol*, **11**, 762-774.

SHLOMCHIK, W.D. (2003) Antigen presentation in graft-vs-host disease. *Exp Hematol*, **31**, 1187-1197.

SHLOMCHIK, W.D. et al. (1999) Prevention of graft versus host disease by inactivation of host antigen-presenting cells. *Science*, **285**, 412-415.

SICA, A. & MANTOVANI, A. (2012) Macrophage plasticity and polarization: in vivo veritas. *J Clin Invest*, **122**, 787-795.

SIVAKUMARAN, S. et al. (2016) Depletion of CD11c(+) cells in the CD11c.DTR model drives expansion of unique CD64(+) Ly6C(+) monocytes that are poised to release TNF-alpha. *Eur J Immunol*, **46**, 192-203.

SLOANE, J.P. et al. (1983) Histopathology of the lung after bone marrow transplantation. *J Clin Pathol*, **36**, 546-554.

SLOANE, J.P., THOMAS, J.A., IMRIE, S.F., EASTON, D.F. & POWLES, R.L. (1984) Morphological and immunohistological changes in the skin in allogeneic bone marrow recipients. *J Clin Pathol*, **37**, 919-930.

SOIFFER, R.J. et al. (2011) Impact of immune modulation with anti-T-cell antibodies on the outcome of reduced-intensity allogeneic hematopoietic stem cell transplantation for hematologic malignancies. *Blood*, **117**, 6963-6970.

SONTHEIMER, R.D. (2009) Lichenoid tissue reaction/interface dermatitis: clinical and histological perspectives. *J Invest Dermatol*, **129**, 1088-1099.

SOUBANI, A.O. & PANDYA, C.M. (2010) The spectrum of noninfectious pulmonary complications following hematopoietic stem cell transplantation. *Hematol Oncol Stem Cell Ther*, **3**, 143-157.

SPETZ, A.L., STROMINGER, J. & GROH-SPIES, V. (1996) T cell subsets in normal human epidermis. *Am J Pathol*, **149**, 665-674.

SPINELLI, L., CARPENTIER, S., MONTANANA SANCHIS, F., DALOD, M. & VU MANH, T.P. (2015) BubbleGUM: automatic extraction of phenotype molecular signatures and comprehensive visualization of multiple Gene Set Enrichment Analyses. *BMC Genomics*, **16**, 814.

SRINIVASAN, M. et al. (2012) Donor B-cell alloantibody deposition and germinal center formation are required for the development of murine chronic GVHD and bronchiolitis obliterans. *Blood*, **119**, 1570-1580.

STARY, G., BANGERT, C., STINGL, G. & KOPP, T. (2005) Dendritic cells in atopic dermatitis: expression of FcepsilonRI on two distinct inflammation-associated subsets. *Int Arch Allergy Immunol*, **138**, 278-290.

STEINMAN, R.M. & COHN, Z.A. (1973) Identification of a novel cell type in peripheral lymphoid organs of mice. I. Morphology, quantitation, tissue distribution. *J Exp Med*, **137**, 1142-1162.

STEINMAN, R.M. & COHN, Z.A. (1974) Identification of a novel cell type in peripheral lymphoid organs of mice. II. Functional properties in vitro. *J Exp Med*, **139**, 380-397.

STEINMAN, R.M. & HEMMI, H. (2006) Dendritic cells: translating innate to adaptive immunity. *Curr Top Microbiol Immunol*, **311**, 17-58.

STEINMAN, R.M., LUSTIG, D.S. & COHN, Z.A. (1974) Identification of a novel cell type in peripheral lymphoid organs of mice. 3. Functional properties in vivo. *J Exp Med*, **139**, 1431-1445.

STEINMAN, R.M. & NUSSENZWEIG, M.C. (2002) Avoiding horror autotoxicus: the importance of dendritic cells in peripheral T cell tolerance. *Proc Natl Acad Sci U S A*, **99**, 351-358.

STEINMAN, R.M. & WITMER, M.D. (1978) Lymphoid dendritic cells are potent stimulators of the primary mixed leukocyte reaction in mice. *Proc Natl Acad Sci U S A*, **75**, 5132-5136.

STEPPICH, B. et al. (2000) Selective mobilization of CD14(+)CD16(+) monocytes by exercise. *Am J Physiol Cell Physiol*, **279**, C578-86.

STORB, R. et al. (1983) Graft-versus-host disease and survival in patients with aplastic anemia treated by marrow grafts from HLA-identical siblings. Beneficial effect of a protective environment. *N Engl J Med*, **308**, 302-307.

STRICKLAND, D., KEES, U.R. & HOLT, P.G. (1996) Regulation of T-cell activation in the lung: alveolar macrophages induce reversible T-cell anergy in vitro associated with inhibition of interleukin-2 receptor signal transduction. *Immunology*, **87**, 250-258.

SWIRSKI, F.K. et al. (2009) Identification of splenic reservoir monocytes and their deployment to inflammatory sites. *Science*, **325**, 612-616.

TAKEDA, K. & AKIRA, S. (2005) Toll-like receptors in innate immunity. *Int Immunol*, **17**, 1-14.

TAKEMURA, R. & WERB, Z. (1984) Secretory products of macrophages and their physiological functions. *Am J Physiol*, **246**, C1-9.

TAKIZAWA, H., BOETTCHER, S. & MANZ, M.G. (2012) Demand-adapted regulation of early hematopoiesis in infection and inflammation. *Blood*, **119**, 2991-3002.

TAMOUTOUNOUR, S. et al. (2013) Origins and functional specialization of macrophages and of conventional and monocyte-derived dendritic cells in mouse skin. *Immunity*, **39**, 925-938.

TAMOUTOUNOUR, S. et al. (2012) CD64 distinguishes macrophages from dendritic cells in the gut and reveals the Th1-inducing role of mesenteric lymph node macrophages during colitis. *Eur J Immunol*, **42**, 3150-3166.

TARLING, J.D., LIN, H.S. & HSU, S. (1987) Self-renewal of pulmonary alveolar macrophages: evidence from radiation chimera studies. *J Leukoc Biol*, **42**, 443-446.

TAUBER, A.I. (2003) Metchnikoff and the phagocytosis theory. *Nat Rev Mol Cell Biol*, **4**, 897-901.

TAVEIRA DA SILVA, A.M. et al. (1993) Brief report: shock and multiple-organ dysfunction after self-administration of Salmonella endotoxin. *N Engl J Med*, **328**, 1457-1460.

TEN BERGE, B. et al. (2009) A novel method for isolating dendritic cells from human bronchoalveolar lavage fluid. *J Immunol Methods*, **351**, 13-23.

TERAKURA, S., MARTIN, P.J., SHULMAN, H.M. & STORER, B.E. (2015) Cutaneous macrophage infiltration in acute GvHD. *Bone Marrow Transplant*, **50(8)**, 1135-1137.

TESHIMA, T. & FERRARA, J.L. (2002) Understanding the alloresponse: new approaches to graft-versus-host disease prevention. *Semin Hematol*, **39**, 15-22.

THEPEN, T., VAN ROOIJEN, N. & KRAAL, G. (1989) Alveolar macrophage elimination in vivo is associated with an increase in pulmonary immune response in mice. *J Exp Med*, **170**, 499-509.

THOMAS, E.D., RAMBERG, R.E., SALE, G.E., SPARKES, R.S. & GOLDE, D.W. (1976) Direct evidence for a bone marrow origin of the alveolar macrophage in man. *Science*, **192**, 1016-1018.

THOMAS, J.A. et al. (1984) Chimerism in skin of bone marrow transplant recipients. *Transplantation*, **38**, 475-478.

TIZON, R. et al. (2012) High-dose corticosteroids with or without etanercept for the treatment of idiopathic pneumonia syndrome after allo-SCT. *Bone Marrow Transplant*, **47**, 1332-1337.

TRAPNELL, B.C. & WHITSETT, J.A. (2002) Gm-CSF regulates pulmonary surfactant homeostasis and alveolar macrophage-mediated innate host defense. *Annu Rev Physiol*, **64**, 775-802.

TSOUMAKIDOU, M., TZANAKIS, N., PAPADAKI, H.A., KOUTALA, H. & SIAFAKAS, N.M. (2006) Isolation of myeloid and plasmacytoid dendritic cells from human bronchoalveolar lavage fluid. *Immunol Cell Biol*, **84**, 267-273.

TUSSIWAND, R. et al. (2015) Klf4 expression in conventional dendritic cells is required for T helper 2 cell responses. *Immunity*, **42**, 916-928.

TUSSIWAND, R. et al. (2012) Compensatory dendritic cell development mediated by BATF-IRF interactions. *Nature*, **490**, 502-507.

URYU, H. et al. (2015) alpha-Mannan induces Th17-mediated pulmonary graft-versus-host disease in mice. *Blood*, **125**, 3014-3023.

VALEYRE, D. et al. (2014) Sarcoidosis. *Lancet*, **383**, 1155-1167.

VAN DE LAAR, L. et al. (2016) Yolk Sac Macrophages, Fetal Liver, and Adult Monocytes Can Colonize an Empty Niche and Develop into Functional Tissue-Resident Macrophages. *Immunity*, **44**, 755-768.

VAN FURTH, R. et al. (1972) The mononuclear phagocyte system: a new classification of macrophages, monocytes, and their precursor cells. *Bull World Health Organ*, **46**, 845-852.

VAN HAARST, J.M. et al. (1994) Dendritic cells and their precursors isolated from human bronchoalveolar lavage: immunocytologic and functional properties. *Am J Respir Cell Mol Biol*, **11**, 344-350.

VAN, BEKKUM, D.W., VOS, O. & WEYZEN, W.W. (1959) The pathogenesis of the secondary disease following foreign bone marrow transplantation in irradiated mice. *Bull Soc Int Chir*, **18**, 302-314.

VAROL, C. et al. (2007) Monocytes give rise to mucosal, but not splenic, conventional dendritic cells. *J Exp Med*, **204**, 171-180.

VERHASSELT, V. et al. (1997) Bacterial lipopolysaccharide stimulates the production of cytokines and the expression of costimulatory molecules by human peripheral blood dendritic cells: evidence for a soluble CD14-dependent pathway. *J Immunol*, **158**, 2919-2925.

VERSLUYS, A.B. et al. (2010) Strong association between respiratory viral infection early after hematopoietic stem cell transplantation and the development of life-threatening acute and chronic alloimmune lung syndromes. *Biol Blood Marrow Transplant*, **16**, 782-791.

VON BUBNOFF, D. et al. (2011) Indoleamine 2,3-dioxygenase-expressing myeloid dendritic cells and macrophages in infectious and noninfectious cutaneous granulomas. *J Am Acad Dermatol*, **65**, 819-832.

VU MANH, T.P., BERTHO, N., HOSMALIN, A., SCHWARTZ-CORNIL, I. & DALOD, M. (2015) Investigating Evolutionary Conservation of Dendritic Cell Subset Identity and Functions. *Front Immunol*, **6**, 260.

WAKIM, L.M. & BEVAN, M.J. (2011) Cross-dressed dendritic cells drive memory CD8+ T-cell activation after viral infection. *Nature*, **471**, 629-632.

WAKIM, L.M., WAITHMAN, J., VAN ROOIJEN, N., HEATH, W.R. & CARBONE, F.R. (2008) Dendritic cell-induced memory T cell activation in nonlymphoid tissues. *Science*, **319**, 198-202.

WANG, D. et al. (2013) Dynamic change and impact of myeloid-derived suppressor cells in allogeneic bone marrow transplantation in mice. *Biol Blood Marrow Transplant*, **19**, 692-702.

WANG, X. et al. (2011) Mechanisms of antigen presentation to T cells in murine graft-versus-host disease: cross-presentation and the appearance of cross-presentation. *Blood*, **118**, 6426-6437.

WANG, X.N. et al. (2014) A three-dimensional atlas of human dermal leukocytes, lymphatics, and blood vessels. *J Invest Dermatol*, **134**, 965-974.

WARREN, H.S. et al. (2010) Resilience to bacterial infection: difference between species could be due to proteins in serum. *J Infect Dis*, **201**, 223-232.

WATCHMAKER, P.B. et al. (2014) Comparative transcriptional and functional profiling defines conserved programs of intestinal DC differentiation in humans and mice. *Nat Immunol*, **15**, 98-108.

WEBER, G.F. et al. (2015) Interleukin-3 amplifies acute inflammation and is a potential therapeutic target in sepsis. *Science*, **347**, 1260-1265.

WOLLENBERG, A., KRAFT, S., HANAU, D. & BIEBER, T. (1996) Immunomorphological and ultrastructural characterization of Langerhans cells and a novel, inflammatory dendritic epidermal cell (IDEC) population in lesional skin of atopic eczema. *J Invest Dermatol*, **106**, 446-453.

WOLLENBERG, A. et al. (2002a) Expression and function of the mannose receptor CD206 on epidermal dendritic cells in inflammatory skin diseases. *J Invest Dermatol*, **118**, 327-334.

WOLLENBERG, A. et al. (2002b) Plasmacytoid dendritic cells: a new cutaneous dendritic cell subset with distinct role in inflammatory skin diseases. *J Invest Dermatol*, **119**, 1096-1102.

WONG, M.H. & JOHNSON, M.D. (2013) Differential response of primary alveolar type I and type II cells to LPS stimulation. *PLoS One*, **8**, e55545.

WYSOCKI, C.A., PANOSKALTSIS-MORTARI, A., BLAZAR, B.R. & SERODY, J.S. (2005) Leukocyte migration and graft-versus-host disease. *Blood*, **105**, 4191-4199.

XU, L., DRACHENBERG, C., TAVORA, F. & BURKE, A. (2013) Histologic findings in lung biopsies in patients with suspected graft-versus-host disease. *Hum Pathol*, **44**, 1233-1240.

XUE, J. et al. (2014) Transcriptome-based network analysis reveals a spectrum model of human macrophage activation. *Immunity*, **40**, 274-288.

XUN, C.Q., THOMPSON, J.S., JENNINGS, C.D., BROWN, S.A. & WIDMER, M.B. (1994) Effect of total body irradiation, busulfan-cyclophosphamide, or cyclophosphamide conditioning on inflammatory cytokine release and development of acute and chronic graft-versus-host disease in H-2-incompatible transplanted SCID mice. *Blood*, **83**, 2360-2367.

YANIK, G.A. et al. (2008) The impact of soluble tumor necrosis factor receptor etanercept on the treatment of idiopathic pneumonia syndrome after allogeneic hematopoietic stem cell transplantation. *Blood*, **112**, 3073-3081.

YI, T. et al. (2009) Reciprocal differentiation and tissue-specific pathogenesis of Th1, Th2, and Th17 cells in graft-versus-host disease. *Blood*, **114**, 3101-3112.

YONA, S. et al. (2013) Fate mapping reveals origins and dynamics of monocytes and tissue macrophages under homeostasis. *Immunity*, **38**, 79-91.

YOSHIHARA, S., YANIK, G., COOKE, K.R. & MINEISHI, S. (2007) Bronchiolitis obliterans syndrome (BOS), bronchiolitis obliterans organizing pneumonia (BOOP), and other late-onset noninfectious pulmonary complications following allogeneic hematopoietic stem cell transplantation. *Biol Blood Marrow Transplant*, **13**, 749-759.

YU, C.I. et al. (2013) Human CD1c+ dendritic cells drive the differentiation of CD103+ CD8+ mucosal effector T cells via the cytokine TGF-beta. *Immunity*, **38**, 818-830.

YU, Y.R. et al. (2016) Flow Cytometric Analysis of Myeloid Cells in Human Blood, Bronchoalveolar Lavage, and Lung Tissues. *Am J Respir Cell Mol Biol*, **54**, 13-24.

YUKSEL, M. et al. (2006) Peritransplant use of ultraviolet-B irradiation (UV-B) therapy is detrimental to allogeneic stem cell transplantation outcome. *Biol Blood Marrow Transplant*, **12**, 665-671.

ZABA, L.C. et al. (2009) Psoriasis is characterized by accumulation of immunostimulatory and Th1/Th17 cell-polarizing myeloid dendritic cells. *J Invest Dermatol*, **129**, 79-88.

ZABA, L.C. et al. (2010) Identification of TNF-related apoptosis-inducing ligand and other molecules that distinguish inflammatory from resident dendritic cells in patients with psoriasis. *J Allergy Clin Immunol*, **125**, 1261-1268.e9.

ZABA, L.C., FUENTES-DUCULAN, J., STEINMAN, R.M., KRUEGER, J.G. & LOWES, M.A. (2007) Normal human dermis contains distinct populations of CD11c+BDCA-1+ dendritic cells and CD163+FXIIIA+ macrophages. *J Clin Invest*, **117**, 2517-2525.

ZECHER, D., VAN ROOIJEN, N., ROTHSTEIN, D.M., SHLOMCHIK, W.D. & LAKKIS, F.G. (2009) An innate response to allogeneic nonself mediated by monocytes. *J Immunol*, **183**, 7810-7816.

ZEISER, R., PENACK, O., HOLLER, E. & IDZKO, M. (2011) Danger signals activating innate immunity in graft-versus-host disease. *J Mol Med (Berl)*, **89**, 833-845.

ZIEGLER-HEITBROCK, L. et al. (2010) Nomenclature of monocytes and dendritic cells in blood. *Blood*, **116**, e74-80.

ZIGMOND, E. et al. (2012) Ly6C hi monocytes in the inflamed colon give rise to proinflammatory effector cells and migratory antigen-presenting cells. *Immunity*, **37**, 1076-1090.

Appendix A

A.1 Conduct of the LPS inhalation study

A.1.1 Volunteer recruitment and screening

The study was advertised to medical, dental and biomedical science students at Newcastle University by email, in accordance with the study's ethical approval. Potential recruits were invited to a screening interview to assess their suitability for participation. Written consent to screen was documented. The interview comprised:

- short medical interview
- cardio-respiratory examination
- bedside observations (heart rate, blood pressure, oxygen saturation, temperature)
- blood tests (full blood count, urea, creatinine, electrolytes and liver function tests)
- pregnancy test (urinary b-HCG)
- spirometry (forced expiratory volume in 1 second (FEV1) and forced vital capacity (FVC)
- practice inhalation using the nebulizer dosimeter (to check ease of following instructions and co-ordinating breathing).

A.1.2 Inclusion and exclusion criteria

Inclusion criteria were:

- healthy adult volunteers aged 18 to 40
- able to give informed consent.

Exclusion criteria based were:

- age <18 or >40 years
- history of chronic respiratory disease, diabetes, heart disease, renal disease or recurrent infections
- current respiratory tract infection
- taking prescription medication (except oral contraceptives)

- current smoking or history of smoking 20 cigarettes per day for more than 2 years or any smoking in the past year
- alcohol intake of more than 21 units per week
- pregnancy or lactation
- abnormal examination findings: temperature >37.3 °C; oxygen saturation <95% breathing room air
- abnormal blood results: haemoglobin concentration, total white cell count or neutrophil count outside the gender-specific laboratory reference ranges; platelet count <100 $x10^9$/L; serum sodium, potassium, creatinine or alanine aminotransferase outside laboratory reference ranges; serum urea >10mg/dL; serum bilirubin >30µmol/L
- Abnormal spirometry: FEV1 or FVC <80% predicted or FEV1:FVC ratio <70%.

When volunteers were found to be ineligible, permission was sought to inform their general practitioner with the reason and results of screening tests.

A.1.3 Informed consent and confidential data storage

Eligible volunteers were given verbal and written information about the study and at least 24 hours to consider their participation before signing a consent form. All primary research documents were anonymised and participant details kept confidentially in accordance with Caldicott guidelines.

A.1.4 Participant safety

To ensure safety of participants, the study was conducted in a fully staffed clinical research facility and clinical bronchoscopy suite. History, bedside observations, cardio-respiratory examination and spirometry were performed immediately before LPS/ saline inhalation. Bedside observations were repeated hourly and spirometry repeated at 6 hours after inhalation. If FEV1 fell by 10% from baseline, bronchoscopy was cancelled. Prior to bronchoscopy, participants were fasted for 4 hours. There was constant monitoring of oxygen saturations and electrocardiogram during bronchoscopy. Patients were observed for 30-60 minutes after bronchoscopy and allowed to leave if beside observations and cardio-respiratory examinations were normal. Written and verbal advice was given to avoid eating and drinking within two

hours of local anaesthetic administered to the mouth and pharynx. Participants were informed that LPS inhalation and bronchoscopy may result in temperature, mild headache, shivering, dry cough, and upper airway discomfort. Advice was to try paracetamol in the first instance and to contact the clinical research fellow if symptoms were severe or persistent.

A.2 Ethical approval for the LPS inhalation study (most recent amendment)

NHS
Health Research Authority
North East - Newcastle & North Tyneside 2 Research Ethics Committee
Room 001
Jarrow Business Centre
Rolling Mill Road
Jarrow
NE32 3DT

Tel: 0191 428 3476

21 September 2015

Professor John Simpson
Professor of Respiratory Medicine
Newcastle University and Newcastle Hospitals NHS Foundation Trust
Institute of Cellular Medicine
Medical School
Newcastle University
Framlington Place
Newcastle upon Tyne
NE2 4HH

Dear Professor Simpson

Study title:	**A lipopolysaccharide (LPS) inhalation model to characterise divergent cellular innate immune responses and presence of alveolar leak early in the course of acute lung inflammation**
REC reference:	**12/NE/0196**
Amendment number:	**Substantial Amendment 2, 12/08/2015**
Amendment date:	**04 September 2015**
IRAS project ID:	**99089**

The above amendment was reviewed by the Sub-Committee in correspondence.

Summary of Amendment

This amendment was submitted to reflect changes to the protocol, participant information sheet and consent form.

Ethical opinion

The members of the Committee taking part in the review gave a favourable ethical opinion of the amendment on the basis described in the notice of amendment form and supporting documentation.

Approved documents

The documents reviewed and approved at the meeting were:

Document	*Version*	*Date*
Covering letter on headed paper [Covering letter for REC 07-09-2015 v1.2]	v1.2	07 September 2015
Notice of Substantial Amendment (non-CTIMP)	Substantial Amendment 2, 12/08/2015	04 September 2015

Other [Summary of changes to the LPS inhalation study Final]	v1.1	10 August 2015
Other [Timeline Group 4AB, v2.1 Final]	v2.1	03 August 2015
Other [Timeline Group 4CDE, v2.2 Final]	v2.2	03 August 2015
Participant consent form [Group 4 (6hr BAL +- d-glucose) Consent Form v2.1 03-08-15 Final]	v2.1	03 August 2015
Participant information sheet (PIS) [Group 4 (6hr BAL +-d-glucose) PIS v2.1 03-08-15 Final]	v2.1	03 August 2015
Research protocol or project proposal [LPS Study Protocol v1.7 03-08-15 Final]	v1.7	03 August 2015

Membership of the Committee

The members of the Committee who took part in the review are listed on the attached sheet.

R&D approval

All investigators and research collaborators in the NHS should notify the R&D office for the relevant NHS care organisation of this amendment and check whether it affects R&D approval of the research.

Statement of compliance

The Committee is constituted in accordance with the Governance Arrangements for Research Ethics Committees and complies fully with the Standard Operating Procedures for Research Ethics Committees in the UK.

We are pleased to welcome researchers and R & D staff at our NRES committee members' training days – see details at http://www.hra.nhs.uk/hra-training/

12/NE/0196:	**Please quote this number on all correspondence**

Yours sincerely
Pp

Dr Alasdair MacSween
Chair

E-mail: nrescommittee.northeast-newcastleandnorthtyneside2@nhs.net

Enclosures: *List of names and professions of members who took part in the review*

Copy to: *Miss Jillian Peacock, RVI, Newcastle*

A.3 Ethical approval for GvHD studies in BMT recipients (most recent amendment)

NHS
National Research Ethics Service
Newcastle & North Tyneside 1 Research Ethics Committee

TEDCO Business Centre
Room 002
Rolling Mill Road
Jarrow
NE32 3DT

Tel: 0191 428 3564
Fax: 0191 428 3432

09 March 2011

Professor Matthew Collin
Haematological Sciences
Newcastle University
Framlington Place
Newcastle upon Tyne
NE2 4HH

Dear Professor Collin

Study title: **Reconstitution of the cutaneous immune system after haematopoietic stem cell transplantation**
REC reference: **05/Q0905/200**
Amendment number: **Amendment 1 20.02.2011**
Amendment date: **25 February 2011**

The above amendment was reviewed at the meeting of the Sub-Committee held on 08 March 2011.

Ethical opinion

The members of the Committee taking part in the review gave a favourable ethical opinion of the amendment on the basis described in the notice of amendment form and supporting documentation.

Approved documents

The documents reviewed and approved at the meeting were:

Document	Version	Date
Notice of Substantial Amendment (non-CTIMPs)	Amendment 1 20.02.2011	25 February 2011
Investigator CV	Dr Stephen Todryk	22 February 2011
Investigator CV	Tracey Brown	22 February 2011
Investigator CV	Naomi McGovern	22 January 2011
Investigator CV	Rachel Emma Dickinson	22 February 2011

Membership of the Committee

The members of the Committee who took part in the review are listed on the attached sheet.

R&D approval

All investigators and research collaborators in the NHS should notify the R&D office for the relevant NHS care organisation of this amendment and check whether it affects R&D approval of the research.

Statement of compliance

The Committee is constituted in accordance with the Governance Arrangements for Research Ethics Committees (July 2001) and complies fully with the Standard Operating Procedures for Research Ethics Committees in the UK.

05/Q0905/200:	Please quote this number on all correspondence

Yours sincerely

L. Kirkbride

Miss Laura Kirkbride
Committee Co-ordinator

E-mail: laura.kirkbride@sotw.nhs.uk

Enclosures: *List of names and professions of members who took part in the review*

Copy to: *Newcastle upon Tyne Hospitals NHS Foundation Trust*

Subject: Notification of Newcastle upon Tyne Hospitals NHS Foundation Trust Acceptance of Amendment
Date: Wednesday, 23 March 2011 15:23
From: Walker, Jennifer <Jennifer.Walker@nuth.nhs.uk>
To: Matthew Collin <matthew.collin@newcastle.ac.uk>

Dear Professor Collin

Study Title: Reconstitution of the cutaneous immune system after haematopoietic stem cell transplantation
Trust ref: 3599
REC Reference: 05/Q0905/200

Date of submission to REC: 25th February 2011
REC favourable opinion letter: 9th March 2011

Sponsor's Unique Amendment Number: Amendment 1 20.02.2011

Following review of the above amendment, Newcastle upon Tyne Hospitals NHS Foundation Trust can confirm that we can accommodate this amendment.

The amendment may therefore be immediately implemented at this site under the existing NHS Permission. Please note that you may only implement changes that were described in the amendment notice or letter.

I am pleased to confirm that the extension to the study duration is approved. This does not affect Trust approval, which will remain in place until **31st December 2014.**

Kind regards,

Jenn Walker
Research and Development Facilitator
Newcastle Upon Tyne Hospitals NHS Foundation Trust

Joint Research Office
Level 6, Leazes Wing
Royal Victoria Infirmary
Queen Victoria Rd
Newcastle upon Tyne
NE1 4LP

(: 0191 28 24520 **Fax:** 0191 28 24524
For more information please visit: http://www.newcastle-hospitals.org.uk/about-us/staff-information_research-development.aspx <http://www.newcastle-hospitals.org.uk/about-us/staff-information_research-development.aspx>

Appendix B. Sort gates and antibody details

B.1 MLR macrophage sort gates

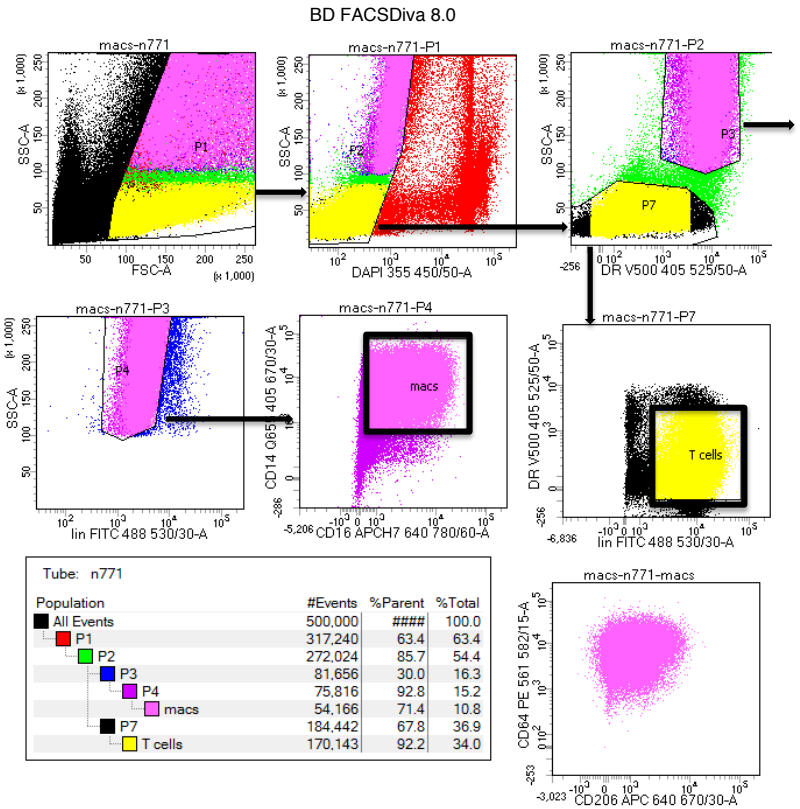

Legend
Viable cells were split into HLA-DR+SSC^{hi} MPs and HLA-DR$^{lo\text{-}mid}$SSC^{lo} lymphocytes. Lymphocytes expressing lineage markers CD3/19/20/56 were sorted. MPs expressing CD14 and CD16 were sorted. Black arrows show gating strategy. Bold black boxes show sorted populations.

B.2 Dermal digest sort gates

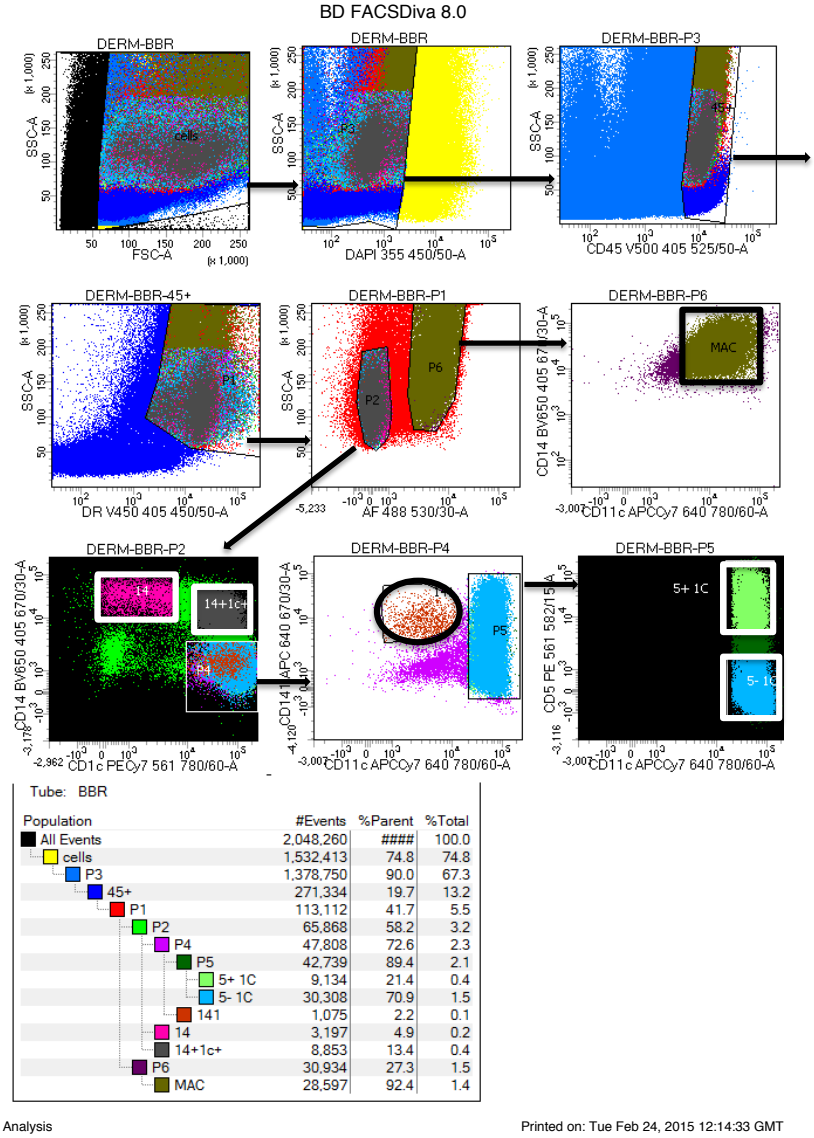

Dermal digest sort gates

Viable leukocytes were gated as DAPI-CD45+. HLA-DR+ MPs were separated into autofluorescent (AF+) and AF- populations. AF+ cells were CD14+ dermal macrophages. From AF- cells, CD14+CD1c- CD14 MDM and CD14+CD1c+ populations were sorted. CD14-CD1c+ cells were split into CD141+ cDC1 and 2 populations of CD11c+ cDC2. Black arrows show gating strategy. Bold black or white boxes show sorted populations.

B.3 Epidermal digest sort gates

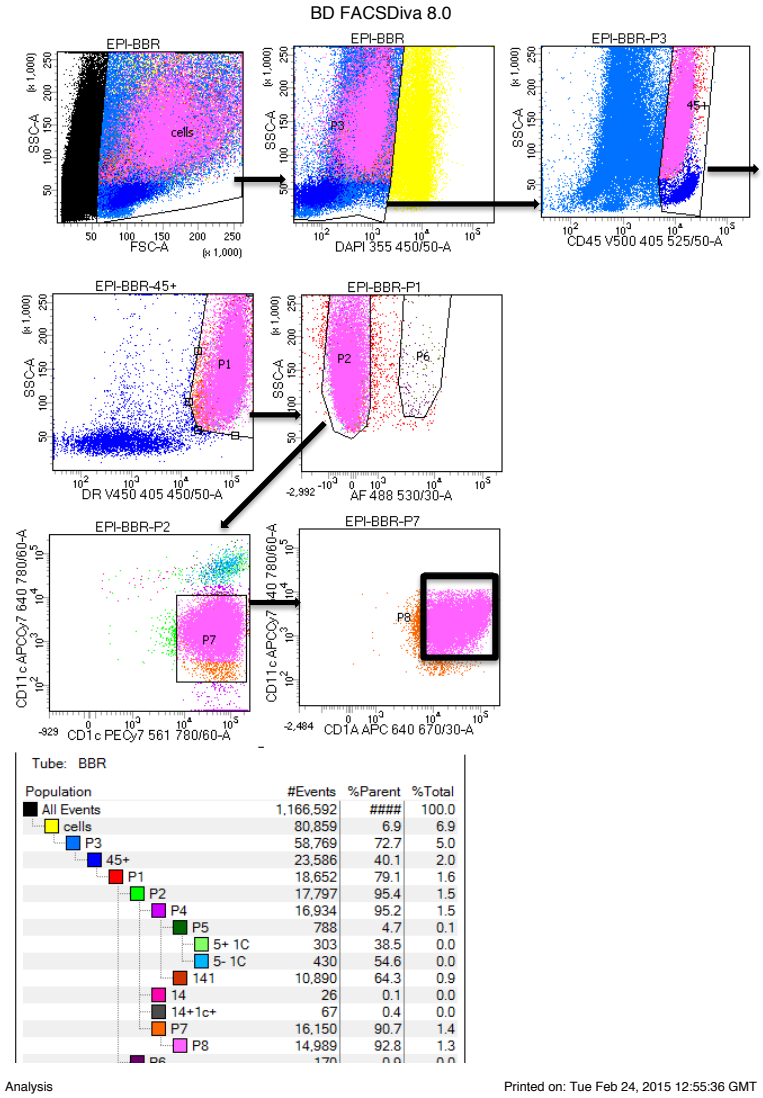

Epidermal digest sort gates
Viable leukocytes were gated as DAPI-CD45+. LCs were identified as AF-CD1c+CD11c^{lo}CD1a+ cells. Black arrows show gating strategy. Bold black box shows sorted populations.

B.4 Blood sort gates

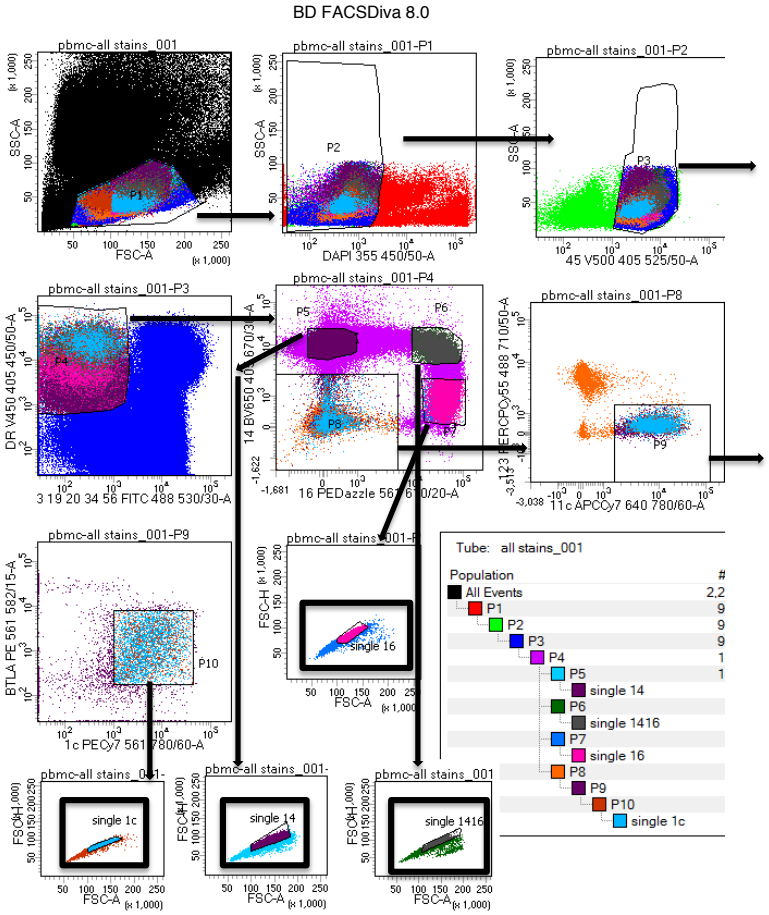

B4 Blood sort gates

Viable MPs were identified as DAPI-CD45+lineage-HLA-DR+ cells. Classical monocytes were sorted as CD14++CD16- cells. Intermediate monocytes were sorted as CD14++CD16+ cells. Non-classical monocytes were sorted as CD14+CD16++ cells. cDC2 were identified as CD11c+CD1c+ cells expressing low to intermediate levels of BTLA. SSC versus area plots were used to confirm sorting of single cells. Black arrows show gating strategy. Bold black boxes show sorted populations.

B.5 Details of antibodies used in flow cytometry experiments

Antigen	Fluorochrome conjugate	Supplier	Catalogue number
7-AAD	n/a	BD	51-66121E
Annexin V	PE	BD	51-65875X
Axl	APC	R&D	FAB154A
BTLA	PE	BD	558485
CD11b	APC	BioLegend	301309
CD11c	APC	BD	559877
CD11c	AF700	BD	561352
CD11c	APCCy7	BioLegend	337218
CD123	PERCPCy5.5	BD	558714
CD14	FITC	BD	555397
CD14	APCCy7	BD	557831
CD14	BV650	BD	301835
CD14	PE	BD	555398
CD14	Q.655	Invitrogen	Q10056
CD141	APC	Miltenyi	130-090-907
CD141	PE	BD	559781
CD16	APCH7	BD	560195
CD16	FITC	BD	335035
CD16	PE/Dazzle^{TM} 594	BioLegend	302054
CD163	APC	R&D	FAB1607A
CD1a	AF700	BioLegend	300120
CD1c	APC	BD	559775
CD1c	PECy7	BioLegend	331506
CD20	FITC	BD	345792
CD206	APC	BD	550889
CD206	PE	BD	555954
CD209	FITC	BD	551264
CD3	V500	BD	561416
CD3	FITC	BD	345763
CD4	PE	BD	555347
CD45	FITC	BD	345808
CD45	V500	BE	560777
CD52	PE	Serotec	SFL1642PE
CD56	FITC	BD	345811
CD64	PE	BioLegend	305007
CD69	PECy7	BD	557745
CD8	APCCy7	BD	557834
CD8	PE	BD	345773
CD86	PE	BD	555658
CD9	FITC	BD	345776
FcER1	PE	eBioscience	12-5899-42
HLA-DR	PERCPCy5.5	BD	339126

Antigen	Fluorochrome conjugate	Supplier	Catalogue number
HLA-DR	V500	BD	561224
HLA-DR	FITC	BD	556643
HLA-DR	V450	BD	642276
HLA-DR	PERCPCy5.5	BD	339216
HLA-DR	AF700	BD	560743
HLA-DR	BV786	BioLegend	307642
IFNγ	PE/Dazzle^{TM} 594	BioLegend	505845
IL-17	AF647	BioLegend	512309
IL-4	PECy7	Biolegend	500823
SIRPa	PE	BioLegend	323805
zombie aqua	n/a	BioLegend	423101

Appendix C. GvHD immunohistochemistry

C.1 Immunohistochemistry methods

Formalin-fixed and paraffin-embedded skin shave biopsies surplus to diagnostic requirements were used. Anna Long and Stacey Newton performed sectioning and staining (Immunocytochemistry Department, Newcastle upon Tyne Hospitals NHS Foundation Trust). Maharani Paramitha (MRes student under my supervision) imaged the specimens.

4μm sections were made. Antigen retrieval and staining were performed using the BenchMark autostainer (Ventana). CD163 and Ki67 primary antibodies and the 'ultraview' detection kit were used. CD163 was conjugated to a red chromagen and Ki67 to a brown chromagen.

C.2 Inflammatory macrophage distribution in GvHD skin

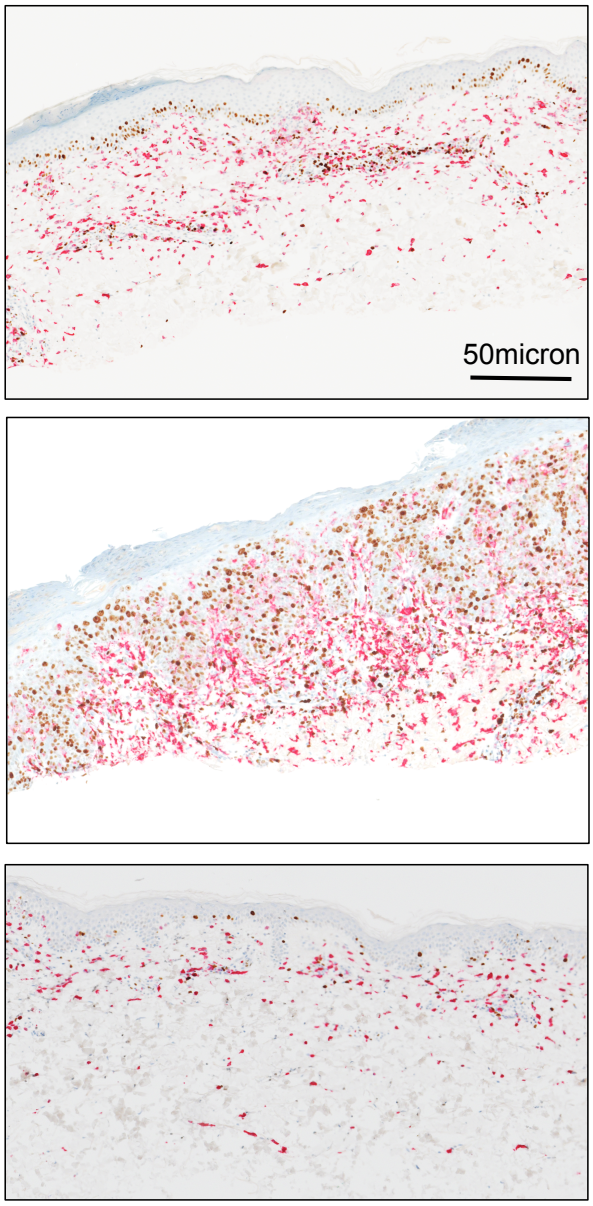

Inflammatory macrophage distribution in GvHD skin
Three GvHD specimens stained with CD163 (red) and Ki67 (brown) are shown. Imaged at 20x magnification, distribution of CD163+ macrophages along the dermo-epidermal junction can be appreciated. This is a lichenoid pattern. Reticular dermis was limited in these specimens due to the biopsy method.

Appendix D. Gene Lists

D.1 Genes differentially expressed between BTLA+ and BTLA- cDC2

Gene name	fold change in blood cDC2 (BTLA+/-)	fold change in BAL cDC2 (BTLA+/-)
BTLA	43.19	10.14
HLA-DQA1	24.00	12.37
HLA-DQB1	12.16	7.49
KIT	11.97	-1.3
IDO1	6.94	-1.26
IL18RAP	6.71	-1.67
ZEB1	6.70	1.38
DPP4	6.31	1.2
CD5	5.81	6.42
PIGR	5.23	-1.42
CD40LG	5.21	2.26
CD22	4.83	1.89
CXCR3	4.19	-1.69
CAMP	4.14	-1.36
CCL4	4.09	-2.67
CD45RA	4.05	2.59
SLAMF7	4.01	1.04
CD79A	3.85	-1.82
XCL1	3.85	-1.59
HLA-DOB	3.84	1.43
IL18R1	3.75	2.24
CCBP2	3.45	-1.03
LTA	3.45	-3.04
IL7	3.40	-1.3
ITLN1	3.32	-1.3
SLC2A1	3.24	2.19
TLR3	3.09	1.53
EBI3	3.06	-1.17
LAG3	3.04	2.01
LILRA5	-3.25	2.28
CMKLR1	-3.26	-5.08
LILRA3	-3.35	-5.75
CD9	-3.36	-2.91
CCL24	-3.39	-1.36
KLRC4	-3.41	-1.3
IKBKE	-3.53	1.22
ITGAM	-3.65	-1.47
FCGR2B	-3.74	-3.93

Gene name	fold change in blood cDC2 (BTLA+/BTLA-)	fold change in BAL cDC2 (BTLA+/BTLA-)
BST1	-3.84	-2.81
CD163	-4.24	-1.08
CCR1	-4.58	-1.52
LAIR1	-5.16	-1.02
S100A9	-5.30	-1.13
LILRA6	-8.25	-2.63
LILRA6	-8.25	-2.63
S100A8	-11.14	-1.25
CLEC4E	-14.38	-2.91
CLEC4E	-14.38	-2.91
MRC1	-46.26	-1.44
CD14	-57.46	-1.9

Gene list associated with Figure 8.2.

D.2 Genes differentially expressed between GVH14 and CD14 MDM

Gene name	Fold change GVH14/CD14 MDM
SELPLG	2.18
PYCARD	2.13
SPP1	1.91
CD82	1.61
CD247	1.59
C2	1.57
CCL24	1.54
HAVCR2	1.54
LILRA2	1.53
TLR8	1.51
CLEC4E	1.45
TAP1	1.33
STAT5B	1.32
CCRL2	1.32
MAFF	1.31
PTAFR	1.29
CD80	1.28
TNFSF13B	1.26
GGT5	1.23
RAF1	1.22
HLA-A	1.20
IKBKG	1.20
PSMB9	1.19
HLA-C	1.19
GPI	1.17
TBK1	1.16
MAPK1	1.15
CXCR4	1.15
CD81	1.14
HLA-B	1.14
TRAF3	1.13
FCGRT	1.13
PML	1.12
FCER1G	1.11
LCP2	1.11
CCR7	1.10
NFKBIZ	1.09
JAK1	1.07
IL10	-1.16

Gene name	Fold change GVH14/CD14 MDM
IL10	-1.16
TFRC	-1.22
KCNJ2	-1.56
NFIL3	-1.72
MAP4K1	-2.25
TNFSF8	-2.58

Gene list associated with Figure 4.6.

D.3 Macrophage and DC signature genes

Macrophage genes	DC genes
CD14	FLT3
IRAK3	BTLA
FCGR2A	CIITA
CEBPB	BATF3
CD163	CD86
TLR4	CCR6
MERTK	GCSAM
TLR2	CXCR3
FCER1G	KIT
CCL13	TYK2
F13A1	
MAF	
KCNJ2	
LILRA5	
NOTCH1	
LAIR1	
CD53	
ATG7	
C1QA	

Gene lists associated with Figure 4.5

D.4 Gene signatures used in Figure 8.3 Gene Set Enrichment Analysis

moDC			**mono (classical)**			
ABL1	CLEC4A	MAP4K1	ARHGDIB	ITGAL	TNFRSF8	FCGR2A
AIRE	CLEC7A	MAP4K2	ATG7	ITGB2	TNFSF10	TNFRSF14
APP	CMKLR1	MAPK1	BCL10	LILRA1	TNFSF12	TYK2
ATG5	CSF1R	MBP	BST1	LILRA2	TNFSF8	CD44
B2M	CSF2RB	MIF	BTK	LILRA3	TRAF6	CD1D
BATF3	CTSC	MR1	CASP8	LILRA5	ZBTB16	LEF1
BAX	CXCL13	MRC1	CCND3	LILRA6	ATG12	TGFBR2
BCAP31	CXCR1	NFATC2	CD14	LILRB2	CASP2	TLR1
BCL2L11	CXCR2	NFATC3	CD244	LILRB3	CD163	TNFRSF1B
BCL6	EGR2	NFIL3	CD28	LTB4R	CD99	CTSG
BLNK	FCER1A	NOD1	CD36	LTBR	CMKLR1	CARD9
C1QA	GPI	PDCD1LG2	CD48	MAPK14	EGR1	NFATC1
C1QB	HLA-DMB	PECAM1	CD97	NCF4	FADD	HFE
C2	HLA-DPA1	PLA2G2E	CFD	NOD2	ITGA4	PSMB8
C4BPA	HLA-DRA	PLAU	CFP	NOTCH1	MBP	CUL9
CARD9	HLA-DRB1	PSMB5	CHUK	NOTCH2	MYD88	IL15
CASP10	HLA-DRB3	PSMB8	CLEC4E	PDCD2	PECAM1	LTF
CASP2	HRAS	PSMC2	CLEC6A	POU2F2	STAT2	MAPK1
CASP3	IFI16	PTPN2	CLEC7A	PRKCD	TGFBI	JAK2
CCL13	IFNGR1	RUNX1	CR1	PSMB10	C5	LY96
CCL23	IGF2R	SELPLG	CSF3R	PTAFR	CD45RB	LAIR1
CCL26	IKBKAP	SKI	CTSS	PTPN6	IKBKAP	C4A/B
CCR1	IKZF1	SLAMF1	CXCR2	PTPRC_all	IRAK4	CD4
CCR5	IKZF2	SMAD5	CYBB	PYCARD	IRF3	SELPLG
CD164	IL13RA1	SOCS1	FAS	RAF1	MAP4K2	IFNAR1
CD1A	IL1R1	SPP1	FCER1G	RARRES3	TBK1	CCR1
CD209	IL1R2	STAT5B	FCGRT	S100A8	APP	MR1
CD276	IL1RAP	TAL1	FYN	S100A9	ATM	CASP10
CD36	IL1RL2	TGFBI	HLA-A	SELL	CD46	XBP1
CD45R0	IL32	TIGIT	HLA-B	SIGIRR	IRF1	MCL1
CD46	IRF4	TIRAP	HLA-C	STAT5B	NLRP3	BAX
CD53	IRF5	TNFRSF11A	ICAM3	STAT6	PPBP	
CD59	ITGA2B	TNFRSF14	IFNAR2	SYK	TRAF3	
CD74	ITGAM	TOLLIP	IGF2R	TAGAP	IKBKB	
CD81	ITGAX	TP53	IKBKE	TIRAP	ITGAE	
CD8A	ITGB1	TRAF4	IKBKG	TLR2	NCR1	
CD99	KLRF1	TRAF5	IL10RA	TLR4	TGFB1	
CDKN1A	LTA	UBE2L3	IL11RA	TLR5	CD40LG	
CFH	LTBR		IL6R	TLR8	FCGR1A/B	
CFI	LY96		IRAK1	TMEM173	ITGAM	
CISH	MAF		IRAK3	TNFRSF10C	IL12RB1	

blood cDC2 LPS stim			**blood cDC2**	
ADA	ETS1	MUC1	C14orf166	CD79A
ATG10	GBP1	MX1	C1QBP	UBE2L3
B2M	GPR183	NFKB1	CASP1	BID
BATF	HAMP	NFKB2	CCR2	CFP
BCL3	ICAM1	NFKBIA	CD2	TYK2
C3	ICAM4	NFKBIZ	CD22	BTLA
C4BPA	ICAM5	NOTCH2	CD3EAP	IKBKAP
CASP1	IDO1	PDCD1	CD79B	SYK
CASP3	IFIH1	PDCD1LG2	CIITA	ITGAX
CCL19	IFNA1/13	PPBP	CX3CR1	CD45RA
CCL20	IL10	PRDM1	FCER1A	MIF
CCL22	IL12A	PSMB5	HLA-DMA	C1S
CCL24	IL12B	PTGS2	ICAM2	MR1
CCL3	IL15	PTPN2	ICAM3	
CCL4	IL19	S1PR1	IKZF1	
CCL5	IL1A	SLAMF1	IL16	
CCR7	IL1B	SLAMF7	ITGAE	
CD274	IL1R1	SOCS1	LTB4R2	
CD40	IL1RN	SOCS3	MAP4K1	
CD44	IL20	SRC	MYD88	
CD58	IL21R	STAT4	PTPN22	
CD59	IL23A	STAT5A	SELL	
CD70	IL23R	STAT5B	TP53	
CD80	IL27	TAP2	ABL1	
CD82	IL2RA	TBX21	ATG16L1	
CD83	IL2RG	TCF7	CD1D	
CD86	IL4R	TFRC	HLA-DMB	
CDKN1A	IL6	TICAM1	IL18	
CFB	IL7R	TNF	SIGIRR	
CLEC5A	IL8	TNFAIP3	CD244	
CRADD	IRAK2	TNFAIP6	PSMB7	
CSF1	KCNJ2	TNFRSF1B	TLR5	
CSF2	KIR_Activ 1	TNFRSF4	CCND3	
CTNNB1	LAMP3	TNFRSF9	IL6R	
CXCL1	LGALS3	TNFSF15	KIT	
CXCL13	LILRA3	TRAF1	PSMB8	
CXCL2	LILRB2	TRAF2	PTPN6	
CXCR3	LITAF	TRAF3	CD4	
DPP4	LTA	TRAF4	CUL9	
EBI3	MAP4K4	ZEB1	SMAD5	
EGR2	MAPKAPK2		ARHGDIB	